# Supramolecular polymer chemistry and the active role of solvents in the molecular assembly

# Supramolecular Polymer Chemistry and the Active Role of Solvents in the Molecular Assembly

PROEFSCHRIFT

ter verkrijging van de graad van doctor aan de Technische Universiteit Eindhoven, op gezag van de rector magnificus prof. dr. ir. F. P. R. Baaijens, voor een commissie aangewezen door het College voor Promoties, in het openbaar te verdedigen op 31 oktober 2019 om 13:30 uur

door

Marcin Leszek Ślęczkowski

geboren te Kędzierzyn-Koźle, Polen

Dit proefschrift is goedgekeurd door de promotoren en de samenstelling van de promotiecommissie als volgt:

| | |
|---|---|
| voorzitter: | prof. dr. ir. Emiel Hensen |
| 1e promotor: | prof. dr. E. W. Meijer |
| copromotor: | prof. dr. ir. A. R. A. Palmans |
| leden: | prof. dr. M. Suginome (Kyoto University) |
| | prof. dr. R. J. M. Nolte (Radboud Universiteit) |
| | prof. dr. R. P. Sijbesma |
| | dr. ir. M. M. J. Smulders (Wageningen University & Research) |
| adviseurs: | dr. S. Cantekin (SABIC) |

*Het onderzoek of ontwerp dat in dit proefschrift wordt beschreven is uitgevoerd in overeenstemming met de TU/e Gedragscode Wetenschapsbeoefening.*

Cover design: Marcin Ślęczkowski & Mathijs Mabesoone

Printed by: Gildeprint – the Netherlands

A catalogue record is available from the Eindhoven University of Technology Library

ISBN: 978-90-386-4874-3

This work has been financially supported by the European Union Horizon 2020 research and innovation programme under Marie Skłodowska-Curie grant agreement No 642083 (EUROSEQUENCES)

# *Table of contents*

# Chapter 1

# *The role of solvents in supramolecular polymer chemistry*

**Abstract**:

The active role of water as medium for supramolecular assembly of biomacromolecules is well acknowledged, yet not fully understood. The unique structures and thus function of the nucleic acids and proteins cannot be reproduced in other solvents. The fine balance between many interactions governs the functioning of the whole biosystem. Development of synthetic supramolecular systems offers an attractive way to create dynamic, functional materials with tunable properties. In recent years we developed the knowledge required in designing the supramolecular systems operating at, close-at, or far-from thermodynamic equilibrium. The next step in the quest of arriving at non-covalent synthesis is to understand and control weak interactions of the supramolecular assemblies with solvents. This introductory chapter addresses this fundamental property of some supramolecular systems. Herein, we aim to give insight into the active role of solvents in the wide field of supramolecular (polymer) chemistry.

## 1.1 Introduction

In early 1930s, William Astbury postulated the highly organized arrangement of peptides in wool,[1] which was followed in 1953 by the elucidation of the double helical structure of deoxyribonucleic acid (DNA) by Watson and Crick.[2] With these seminal works, a detailed understanding on how life is constructed on the molecular scale became possible. Ever since, it has become clear that Nature creates complex, functional architectures with help of much more than simple covalent bonds. In 1987, Cram, Lehn and Pedersen received the Nobel Prize for their pioneering research in molecular recognition.[3–5] Thereby, the importance of non-covalent interactions in synthetic systems was recognized, and nowadays, fundamental knowledge on the interactions between molecules is successfully transferred to material science. However, compared to Nature, these advances are still far from reflecting how multi-component supramolecular assemblies should be designed from scratch. The current molecular systems are still based on rather simple building blocks that employ a limited number of interactions. In contrast, natural systems introduce complexity using a plethora of interactions including hydrogen, ionic and coordination bonds as well as hydrophobic and Van der Waals interactions. These interactions together give rise to the formation of helical and β-sheet arrangements in nucleic acids and proteins – the most abundant structural motifs found in biomacromolecules. Unparalleled diversity of structure and function is ensured by a precisely controlled primary structure. Notably, Nature adapts its systems so they can operate in specific conditions and are responsive towards specific stimuli (pH, ionic strength, temperature). A vital role in the molecular assembly of these complex systems is played by solvent (water) molecules.

The genetic information of all living organisms is encoded in DNA. This polynucleotide normally exists in the form of a right-handed, antiparallel double helix, where two strains are connected via hydrogen bonds of the complementary nucleobases. Due to its complex structure, DNA can exist in multiple forms. One of biologically active forms is B-DNA, which has a pitch of 35 Å with 10 base pairs (bp) (Figure 1a). Other forms include A-DNA (28 Å, 11 bp) and Z-DNA (45 Å, 12 bp). The transition between the DNA polymorphs was showed to be driven by hydration.[6] At physiological pH and relative humidity above 90%, B-DNA is stabilized by a spanning water network and contains around 20 molecules of water per bp.[7] Its partial dehydration leads to the discontinuity of the spanning network and to a transition to the A-form, which is hydrated only by 15 water molecules per bp.[8] Further dehydration leads to a transition to the biologically inactive, D-form, where a significant role is already played by the counter ions interacting with negatively-charged oxygen atoms of the phosphate groups.[9] Thus the interactions of DNA with water and ions facilitate the stabilization of the electrostatic environment around the strands and enable specific interactions with other biologically important molecules.

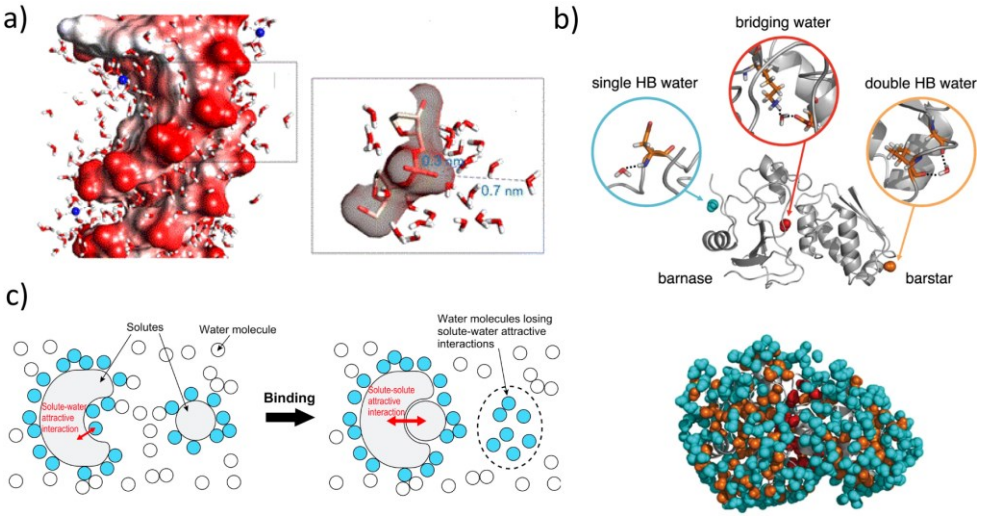


***Figure 1.1*** *a) Surface structure of hydrated B-DNA, inset on the right shows water molecules around a phosphate group in the deoxyribose-phosphodiester, adapted with permission from ref 6; b) top: illustration of water molecules incorporated in the barnase-barnstar complex, down: distribution of the water molecules in the barnase-barnstar complex: bridging water is depicted as red balls, adapted with permission from ref 10; c) cartoon illustrating the dehydration and the overlap of the excluded spaces accompanying the binding of two molecules, adapted with permission from ref 11.*

A similarly high importance of solvation by water is observed in proteins. Their three-dimensional structure and activity is highly dependent on the presence of the spanning hydration network. Protein recognition and binding often directly involves binding or removal of water molecules. Molecular dynamic simulations on, for example, barnase-barstar, an enzyme-inhibitor complex, showed participation of 20 bridging water molecules (Figure 1.1b).[10,11] In some cases, the removal of ordered water molecules causes a high gain in entropy that directs the binding of the proteins. Statistical thermodynamic methods revealed that such a process is operative in actomyosin, a molecular motor that is responsible for muscle contraction (Figure 1.1c). Release of water molecules from the interacting sites (dehydration) is a driving force for actin-myosin interactions that are crucial for the functionality of the motor.[12]

Nature teaches us that a profound understanding of the role of the solvent as a reaction medium for dynamic molecular assembly is indispensable. The ability of Nature to control macroscopic processes at the molecular level inspired chemists to search for synthetic molecules that can assemble in a controlled way. Therefore in the last thirty years, we witnessed a substantial development of supramolecular systems based on small molecules and macromolecules. Self-assembly of small molecules offers an attractive way to achieve

functional materials with highly-ordered structures at the mesoscopic scale.[13] However, its ultimate bottom-up characteristic encounters high sensitivity of the systems to small changes in temperature, solvent composition as well as the presence of minute amounts of impurities. On the other hand, self-assembly of macromolecules via supramolecular interactions is usually more robust as an effect of the covalent network reinforcing the structure. Recent progress in polymer chemistry allows to synthesize polymers with various topologies and structural motifs.[14] However, such systems become inherently more complex thus the interactions between all components including solvent often remain elusive.

This introductory chapter will briefly discuss the advances in supramolecular polymer chemistry. In the context of this thesis, it is important to underline the control of the supramolecular structure with solvents. Thus in the following sections self-assembly of covalent polymers via supramolecular interactions and the role of solvents therein will be addressed. Next, molecular assembly of small molecules with an emphasis on hydrogen-bonded supramolecular polymers along with the interactions and control of these with solvents will be outlined.

## 1.2 The role of solvents in controlling the global conformations of oligomers and macromolecules

Assembly of macromolecules into well-defined architectures can be achieved using different topologies and interactions. While the topology addresses the covalent structure of the polymer, the supramolecular interactions determine the secondary structure, and hereby the global tertiary conformation. Modern polymer chemistry developed methodologies to synthesize copolymers with various topologies such as block, graft, star, comb and brush copolymers. The structure of the monomer and the presence of the functional groups determines the lateral interactions that usually include phase segregation, hydrogen bonds, π-π stacking and solvophobic / solvophilic interactions. Thereby, macromolecules can adapt multiple morphologies, varying from nanoparticles of various shapes and sizes[15] to helical polymers[16] and foldamers[17]. Numerous studies addressed the influence of the solvent on the final structure of the polymeric assemblies. Following subsections will briefly discuss the examples dealing with the role of solvents in oligomeric and polymeric systems.

### 1.2.1 Solvent-controlled conformation in foldamers

An important class of synthetic structures with controlled conformations are foldamers. Foldamers are defined as oligomers that fold in solution into ordered structures stabilized via dynamic, non-covalent interactions. Two major classes of the foldamers are based on single- and multi-stranded foldamers.[17] Previous studies showed that helicity of foldamers could be switched with use of host-guest chemistry.[18,19] It was shown to be more difficult to achieve such transitions with solvents, because foldamers can be sensitive to denaturation by

changing the solvent parameters such as polarity[20] and pH[21]. More delicate function of solvents such as change in morphology in the folded states were rarely investigated.

Huc and coworkers used the solid state – solution equilibrium to investigate the influence of solvent on the crystallization of oligoamides of 8-amino-2-quinolinecarboxylic acid (**8OQ**), end-functionalized with (*R*)-phenylalanine.[22] When dissolved in non-polar organic solvents, the foldamer adapted helical conformation with *R-P* diastereomeric excess of 82%. Vapor-diffusion crystallization of the foldamers from toluene resulted in a 1/1 mixture of *R-P* and *R-M* diastereomers, showing that despite a helical preference in solution, crystallization of racemic crystals is favored. Upon crystallization from benzene, exclusively one diastereomer was obtained (Figure 1.2). The experiments showed that similarly to small molecules, solvation of the oligomer crystals is responsible for the changes in the morphology.

In solution, the regulation of the equilibrium between helical conformations with solvent was reported by Moore et al.[20,23–25] Hereto, discrete *m*-phenylene ethylene oligomers of varying lengths between eight and eighteen repeating units were studied. Stability of the helical conformation was highly dependent on the length of the oligomer and the nature of the solvent. UV-Vis spectroscopy revealed random-coil conformation present in pure chloroform in all oligomers. Upon titration with heptane, the sigmoidal transition towards helix was observed. In case of octadecamer, UV-Vis spectrum at 30 vol% of chloroform showed exclusively helical structures. Interestingly, despite high optical purity of the monomer, recorded CD spectrum revealed no optical activity of the solution, showing that no helical bias

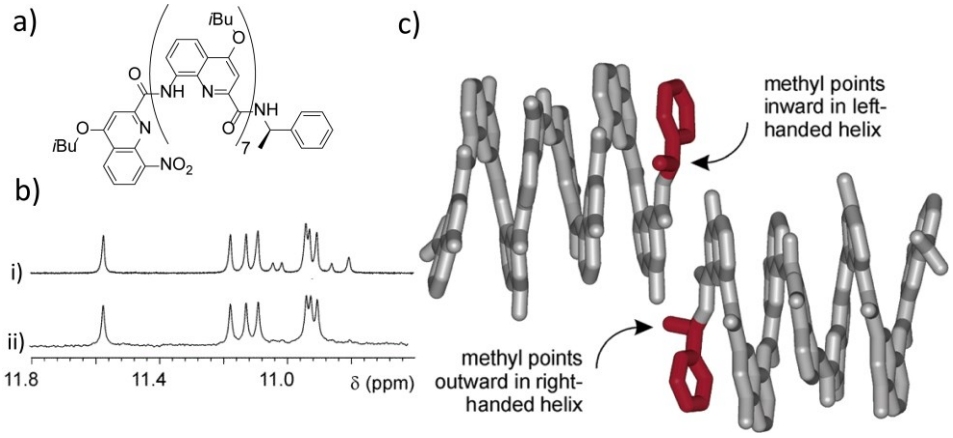


***Figure 1.2*** *a) structure of* ***8OQ****, b) 400 MHz 1H NMR spectra of* ***8OQ*** *in redissolved in* $CDCl_3$ *after crystallization in i) toluene, ii) benzene; showing the signals of intramolecularly hydrogen bonden amide protons; c) crystal structure of* ***8OQ*** *(asymmetric unit) showing diastereomeric right- and left-handed helices, adapted with permission from ref 21.*

was present in the structures. Only further addition of heptane resulted in drastic increase of the CD signal. Therefore the change in the solvent property facilitated two independent processes – the intramolecular conformation change from coil to helix and lateral aggregation of the helices into larger structures. The aggregation of multiple helices was necessary to create a bias within the helical organization.[24]

Lateral multi-chain aggregation of oligo(*m*-phenylene ethylenes) was further investigated in polar solvents with use of sergeants-and-soldiers principle (for sergeants-and-soldiers principle, *vide infra* section 1.2.2). In pure acetonitrile, no intermolecular aggregation of the helices was observed as evidenced by linear increase of the CD signal with respect to the sergeant fraction. In contrast, in presence of 20% of water in acetonitrile, 50% of enantiomerically pure oligomers could fully bias the helicity of the remaining optically inactive oligomers. Thereby solvent-induced amplification of supramolecular chirality confirmed intermolecular aggregation of the oligomers into higher-order structures.[25]

Sinkeldam *et al* studied poly(ureido-para-phthalimidyl) foldamers, in which folding of the polymer backbone was driven by intramolecular hydrogen bond between urea and imide groups.[26] Exchange of the alkyl solubilizing groups to oligo(ethylene glycol) permitted to study the folding of the oligomers in polar solvents. In water, the foldamers adapted a helical conformation of single handedness that was strongly stabilized by solvophobic interactions of the aromatic units of the backbone as reflected by UV-Vis spectrum with absorption bands at 315 and 394 nm and CD spectrum with positive Cotton effect at 331 nm. Interestingly UV-Vis spectrum of the foldamer in THF shows different helical conformation and the CD spectrum shows only low, negative Cotton effect at 331 nm, suggesting a small energetic difference between *P* and *M* helices in THF. The differences in the UV-Vis spectra suggested tight packing of the backbone in water as a result of hydrophobicity of the main chain. In THF such effect is not present, therefore the packing was proposed to be looser, resulting in a reduction of the helical preference. However, on the basis of the above examples, one cannot exclude intermolecular aggregation playing role in the equilibrium between *P* and *M* helical conformations.

### 1.2.2 The role of solvents in the assembly of helical polymers

The first reported synthetic helical polymer was highly isotactic polypropylene, synthesized with the use of Ziegler-Natta catalyst. In 1955, Natta found that such synthesized polypropylene yields an equal number of left- and right-handed helices in the crystalline state.[27] In the following years, helical polymers based on polyacetylenes[28], poly(isocyanide)[29], poly(isocyanate)[30,31], polysilanes[32] and more recently, poly(quinoxaline-2,3-diyl)[33] backbones were developed. Contrary to the isotactic polypropylene, helical conformations in the above systems are also adapted in solutions. The structure of the

polymers incorporate polar and bulky groups, thus the influence of the solvents on the helicity and other properties has been the subject of detailed investigations in the above polymers.

Poly(isocyanides) holding bulky substituents are static helical polymers. It means that the helical sense preference of the polymer is determined at the synthesis step as pioneered by Nolte[29,34] and Okamoto[35,36]. Yashima and co-workers showed that the helicity in poly(phenylisocyanide) synthesized from a single, enantiomerically pure monomer can be controlled by solvent and temperature applied for polymerization.[37] Polymerizations of L-alanine-functionalized phenyl isocyanide carried at ambient temperatures in apolar solvents such as $CCl_4$ and toluene yielded polymers of right-handed helical conformation. On the other hand, in polar solvent (THF) at room temperature or apolar solvent (toluene) at 100 °C, left-handed helices were synthesized. This remarkable sensitivity is an effect of hydrogen bond formation between the amide groups in the propagating polymer chain. In polar solvents or in toluene at high temperature, such hydrogen bonds cannot exist due to the interactions with the solvent, thus the opposite conformation, dictated solely by the steric effects of L-alanine unit, is favored. This observation was confirmed by replacing the amide substituents with esters. This structural change resulted in exclusively left-handed helices (such as in THF), regardless of the reaction conditions.[38]

Pioneering work of Green and co-workers on poly(isocyanate)s contributed significantly to the state-of-art knowledge in dynamic helical polymers. The helicity of poly(isocyanate)s is solely determined by the point chirality of the side chains.[30,39] Importantly, Green and co-workers discovered that the helicity of these polymers can be dictated by small excess of chiral monomers, thereby coining the "sergeants-and-soldiers"[40] and "majority-rules"[41] principles. Due to cooperativity within the polymers, enantioselective isotopic substitution of the side chains with deuterium resulted in a helical bias.[42,43] Subsequent studies showed that the helicity of poly(isocyanate)s can be controlled by temperature[44] as well as by chiral solvents[45] and circularly polarized light.[46]

Helicity in dynamic helical polymers can be controlled at any stage by solvent polarity and temperature. Masuda and coworkers reported solvent-driven conformational change in the helix of poly(*N*-propargylamide) which was accompanied with the change of the preferred helical handedness.[47] In chloroform, the helical conformation of the polymers gives rise to positive Cotton effect at 380 nm. Upon addition of methanol, hydrogen bonds are broken and the system gradually loses its helical conformation. However, when toluene is added instead, the polymers change the packing within the opposite helical assembly. This is reflected by the change of CD spectra, which show gradual disappearance of the positive band at 380 nm concomitant with the arising new, negative band at 305 nm in pure toluene. It is assumed that different solvation of the polymers leads to change in the hydrogen bonding pattern that is responsible for the packing alteration.

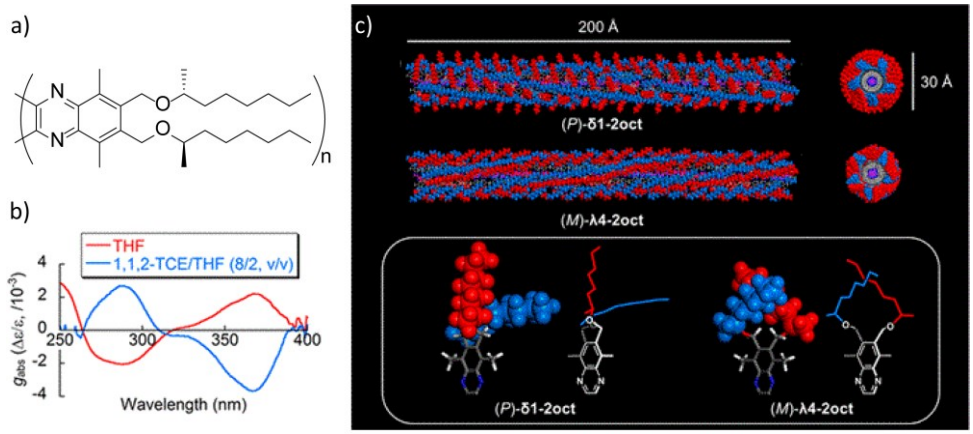


***Figure 1.3*** *a) structure of polyquinoxaline-2,3-diyl (**2-oct**); CD spectra of **2-oct** in THF and TCE/THF 8/2 vol% mixtures; c) molecular models of preferred conformations of **2-oct** in THF-$d_8$ and TCE-$d_3$ / THF-$d_8$ 8/2 vol%, adapted with permission from ref 46.*

More extensive and beautiful studies on the solvent nature that determines the helical packing of polymers were conducted by Suginome and co-workers. Hereto, a series of poly(quinoxaline-2,3-diyl)s (PQX) were decorated with chiral alkyl side chains (Figure 1.3a). The helical packing in chloroform was mirrored by the positive Cotton effect at 366 nm. Titration of the chloroform solutions with 1,1,2-trichloroethane (TCE) caused a helix inversion reflected by an almost mirror-imaged CD spectrum, showing the diastereomeric relationship between the two helices (Figure 1.3b).[48] In following studies, a detailed analysis of the solvent and side-chain influence on the helix stabilization energy was reported.[49] Small angle neutron scattering (SANS) measurements of PQX **2-oct** confirmed that the solvent-driven helix inversion was caused by the differential solvation of the chiral side chains by various solvents (Figure 1.3c).[50] Furthermore, in a recent report, the helicity of PQX was found to be dependent on the degree of polymerization.[51] The outstanding responsiveness of the PQX was utilized to obtain cholesteric structures of the polymers in the thin films upon solvent vapor annealing, yielding left- and right-handed helical assemblies depending on the solvent used.[52] Eventually, inherently chiral, dynamic structure of PQX was used as a scaffold for asymmetric catalysis, affording full control over stereoselectivity by adapting the reaction conditions.[53–55] Recently, achiral PQXs bearing phosphine ligands were found to adapt single helicity in (*S*)- and (*R*)-limonene thereby permitting enantioselective synthesis of binaphthyls via Suzuki Coupling.[56]

### 1.2.3 Solvent-controlled assembly of polymers into nanoparticles

The assembly of polymeric chains into nanoparticles can be done in a variety of ways including covalent and dynamic covalent chemistry as well as with supramolecular interactions.[15] In particular the last group was a subject of numerous studies due to their high

specific stimuli responsiveness and reversibility in the structure alteration. Therefore, polymeric nanoparticles are intensively investigated in terms of applications in, amongst others, the nanomedicine field.[57] Depending on the polymer topology and type of the structure, they can be divided into the subclasses of single-chain polymeric nanoparticles and polymersomes. Since strength of the interactions governing formation of the ordered structure is similar, both types of nanoparticles are susceptible to the changes in the environment.

Polymersomes are composed of amphiphilic block-copolymers, where the two blocks phase-segregate from each other to form vesicles that enclose solution in the core.[58] Depending on the nature and the ratio of the components, the nano-objects take spherical or non-spherical shapes such as cylinders.[59] The size and shape of the nano-objects comprising block copolymers can be controlled by solvent property. The group of Li reported the synthesis of poly(ethylene glycol)-*b*-polyacrylate via atom-transfer radical polymerization (ATRP). The acrylate block was functionalized with a mesogenic cholesterol unit.[60] Liquid-crystalline organization of the cholesterol-rich block yielded the formation of multi-chain aggregates in THF-water and dioxane-water solutions. It was found that critical water concentration, at which the aggregation occurs, is only 1% in mixtures with dioxane but 12% in mixtures with THF. Further studies by scanning electron microscopy (SEM) and cryogenic transmission electron microscopy (cryoTEM) showed that in THF-water mixtures, the block-copolymers form large, spherical aggregates up to 5 μm diameter, while in dioxane-water mixtures small vesicles no larger than 200 nm in diameter are present.

On the other hand, single-chain-polymeric nanoparticles are based on random, graft-copolymer topology. Graft-copolymers can be decorated with multiple side groups that govern the self-assembly of the polymer. Folding the polymer chains via non-covalent interactions in organic media can be achieved using few units of specific interactions such as metal complexation[61] and hydrogen-bonds[62–67]. The use of hydrogen-bonds as driving force for the polymer chain collapse has been studied by many groups. The most prominent examples of hydrogen-bonding units for are based on self-complementary units such as diaminotriazine[63] and ureidopyrimidinone[62,66] (UPy), complementary pairs such as cyanuric acid - Hamilton wedge[65] and thymine - diaminopyridine[64] and aggregation of benzene-1,3,5-tricarboxamides[67] (BTA) via three-fold hydrogen bond formation.

Extensive studies on the influence of the solvent and the rigidity of the polymer backbone on the folding properties via four-fold hydrogen bond-driven UPy dimerization were performed by Stals et al.[62] Hereto, 10 mol% of UPy units were attached onto polymers via post-functionalization strategy and the UPy dimerization was confirmed by $^{1}$H NMR. The morphology of the nanoparticles was evaluated using dynamic light scattering (DLS) and size-exclusion chromatography (SEC). In polar solvents such as THF, well-defined single-chain nanoparticles were observed. In chloroform, the interactions of UPy units were more

pronounced, which resulted in mixtures of small, single-chain nanoparticles with larger aggregates composed of multiple polymer chains. In this case, the stiffness of the polymeric backbone showed no substantial influence on the nanoparticle morphology.

Our group also investigated the role of solvent in polymer folding via BTA aggregation.[67] A specific advantage of using BTA as a supramolecular motif for polymer folding comes from its propensity to form helical aggregates. Enantiomerically pure BTAs assemble in the aggregates of preferred helicity, thereby making CD spectroscopy a useful and convenient method for characterization of the internal structure of the nanoparticles. First successful folding of the polymer chains via BTA aggregation was reported by Mes et al (Figure 1.4). Hereto, a polymethacrylate backbone was decorated with 10 mol% of *o*-nitrobenzyl protected BTA. The protecting group inhibited the assembly and was removed by the UV-irradiation at the final step of the synthesis. Notably, the functionalized polymer was found to be insoluble in methylcyclohexane (MCH) before and after deprotection. Therefore the deprotection was carried in 1,2-dichloroethane (DCE), a solvent in which free BTAs are normally molecularly dissolved. Interestingly, after deprotection in DCE, small, but a visible Cotton effect was measured thereby indicating the presence of BTAs aggregates with excess helicity. Addition of poor solvent, MCH, resulted in increase of the anisotropy *g* value which here is a measure of BTA aggregation. The highest Cotton effect was observed at 70 vol% of MCH and further addition resulted in decrease of the signal as a result of poor solubility of the polymers. The profiles of the Cotton effects with respect to temperature indicated

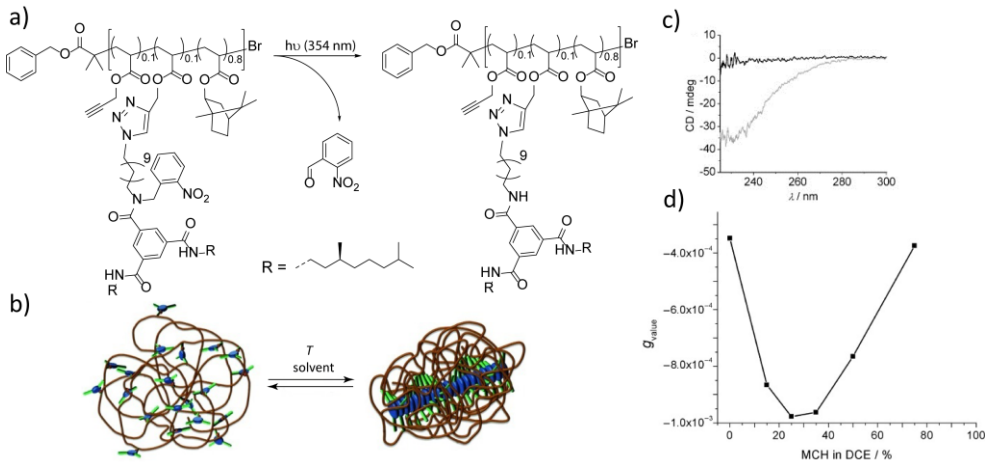


***Figure 1.4*** *a) structure of the polymer triggered to fold by BTA assembly; b) representation of the folding of random-coil polymer into nanoparticle via BTA assembly; c) CD spectra of the polymer before (black) and after (gray) the solution was heated to 80 °C and cooled to 20 °C; d) anisotropy g value of the polymer solution versus solvent composition, ($c_{BTA}$ = 75 μM). Adapted with permission from ref 63.*

isodesmic assembly of the BTA units, which is contrary to cooperative character of the free BTAs in alkanes.[68] These experiments show unambiguously that efficient assembly of the supramolecular motifs attached onto a polymer requires a balance in the interactions. Likewise in proteins, too strong interactions with solvents lead to denaturation of the structure. On the other hand, too weak interactions result in reduced solubility and therefore lack of the control over the assembly process.

## 1.3 The role of solvents in the synthesis of supramolecular assemblies of small molecules

To arrive at non-covalent synthesis from self-assembly of small molecules, it is important to develop the fundamental knowledge on how the interactions of the building blocks with the solvent influence the energetic landscape. Currently, we operate mostly with "rule-of-thumbs" approach and simplify the role of solvents wherever possible. As a consequence, we can overlook the complex function of solvent in these highly sensitive systems. The major difficulty in analysis is the concentration of the solvent, which prevents many analytical techniques to be useful in the probing of its role. Therefore, so far most of the systems showing peculiar behavior upon varying the nature and structure of the solvent were discovered empirically by using multiple solvents for the experiments. At this point it is important to discriminate between the solvents with respect to the strength of the interactions they form with the supramolecular assemblies. Thereby we can distinguish the solvents, which promote certain type of supramolecular structure due to the weak, non-specific interactions such as van der Waals forces and those, which form hydrogen bonds. As a result, the influence of the weakly interacting solvent is only observed, when it is present in bulk concentration, while very small amounts of strongly interacting solvent are enough to cause visible change in the structure. In this section, examples of solvent molecules playing important role in non-covalent assembly will be discussed.

### 1.3.1 Solvent-induced polymorphism in supramolecular assemblies at thermodynamic equilibrium

Polymorphism in crystals is a phenomenon known for a long time. Numerous examples show that polymorphism can be caused by different solvation of crystals.[69] The experiments revealed that the amount of water molecules in the crystal cell unit determines the molecular packing in the crystals of tartrate salts. How powerful these interactions can be, are illustrated by the example of racemic sodium ammonium tartrate. The tetrahydrate salt forms conglomerate crystals that could be separated by Pasteur in his seminal work.[70] Above 28 °C, a dehydration event takes place, thereby decreasing number of water molecules engaged in

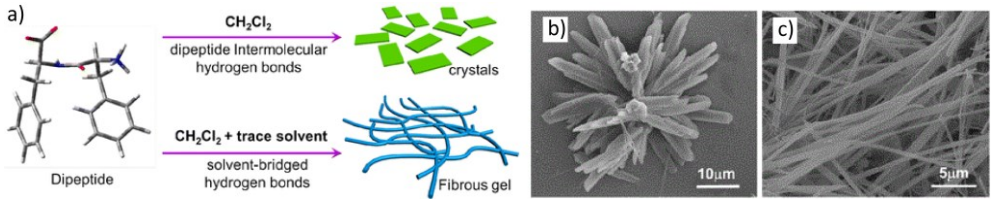


***Figure 1.5*** *a) Schematic depiction of a phase transition induced by trace amounts of solvents; SEM images of the dipeptide structure formed in b) DCM and c) DCM with 5% DMF, adapted with permission from ref 68.*

the crystal structure. Dehydration is accompanied by the transition to a racemic salt, which cannot be resolved physically.

Crystal science teaches us that it would be naive to not consider solvents as active players in the molecular assembly of small molecules. Synthetic supramolecular systems are at least equally sensitive and not surprisingly there are examples showing that even trace amounts of polar solvents, including water[71], can dramatically affect secondary structure. Such observations were reported by Yan and co-workers who studied the assembly of diphenylalanine in dichloromethane (DCM).[72] In pure DCM, intermolecular hydrogen bonds directed the assembly towards flower-like crystals. Addition of a trace amount of competing solvent (here DMF) resulted in an altered hydrogen bond pattern. In effect, with less than 1% of DMF, the dipeptide assembled into a fibrous organogel (Figure 1.5).

Polarity of the bulk solvent can be used to control the competition between halogen and hydrogen bond as showed by Hunter and coworkers.[73] Hereto, the influence of the solvent on the co-crystallization was investigated. Bifunctional 1,2-bis(4-pirydyl)ethane (**BisPy**) could form either hydrogen bond with a hydroquinone (**HQ**) derivative or halogen bond with 1,4-diodotetrafluorobenzene (**IFB**) (Figure 1.6). The hereby formed supramolecular copolymers crystallized by lateral interactions. In a mixture of the three components, the nature of the solvent determined the type of the dominating interactions that was the driving force for supramolecular copolymerization. Powder X-ray diffraction experiments revealed high selectivity in the co-crystallization. Polar solvents that effectively competed for the hydrogen bond with **HQ**, favored co-crystallization of the **BisPy** with **IFB** via halogen bonds. Conversely, non-polar solvent such as toluene and chloroform favored supramolecular copolymerization via hydrogen bond, yielding co-crystals of **BisPy** and **HQ**.

The solvent property was found to play a pronounced role in the hierarchical assembly of ferrocene-dipeptide conjugates.[74] In water – organic cosolvent mixtures, it formed a variety of superstructures, depending on cosolvent, temperature and counter-ion. With use of SEM, it was found that when 2-propanol was used as a cosolvent, right-handed helices of ca 100 nm diameter were formed. On the other hand, when acetonitrile or hexafluoroisopropanol were used, left-handed helices of diameters of, respectively, 200 and 300 nm were formed.

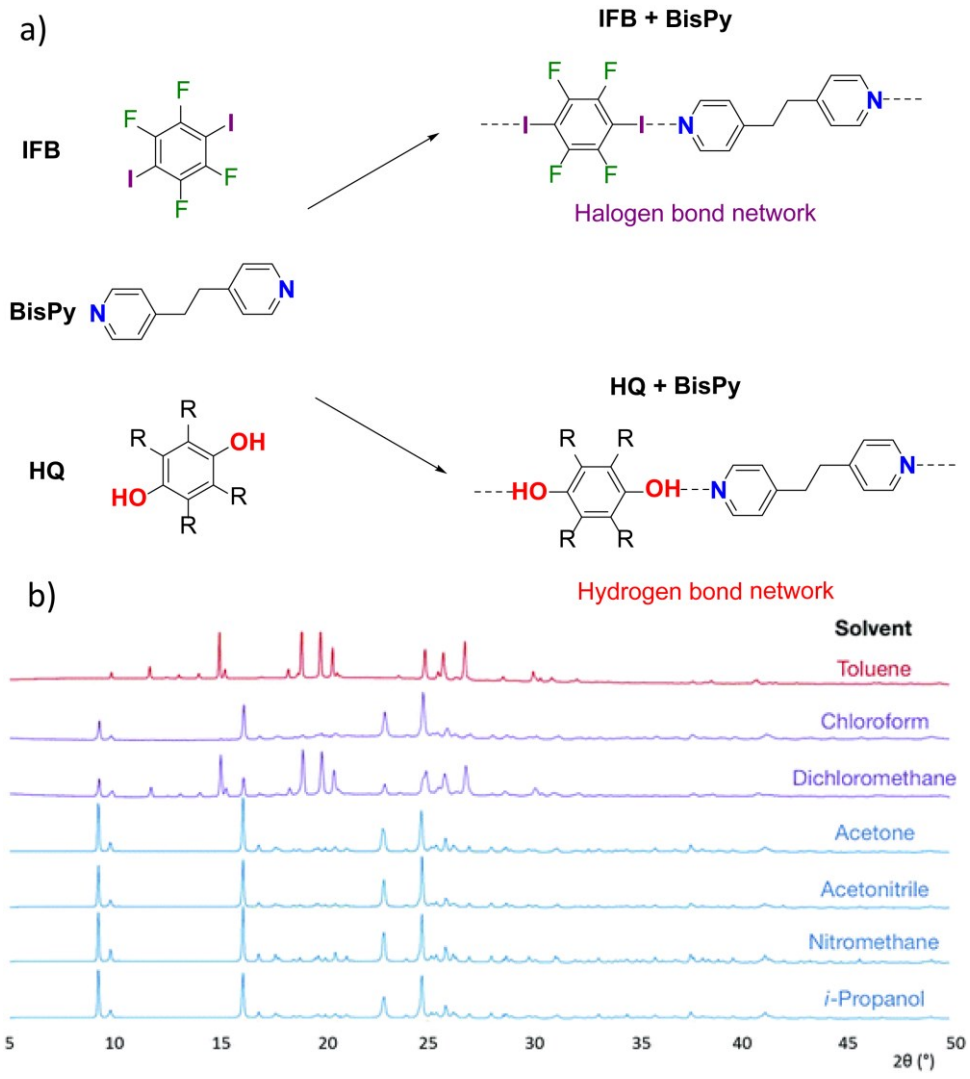


***Figure 1.6*** *Solvent regulates the competition between hydrogen and halogen bonds. a) Structures of monomers* ***IFB***, ***BisPy*** *and* ***HQ*** *and the dimers formed via non-covalent interactions; b) powder X-ray diffraction patterns for products of competitive cocrystallizations from various solvents. Adapted from with permission ref 69.*

Use of different counter-ions also resulted in a change of morphology and handedness. The increase in the helical pitch could be achieved by increasing the temperature. As such, the study shows that simple molecular building blocks can be responsive towards many factors, but one should always consider the effect of the given solvent on the supramolecular structure.

In competing supramolecular polymerization, small amounts of cosolvent can direct the polymerization towards otherwise unstable aggregates. Such behavior was observed in porphyrin-based supramolecular polymers.[75] At μM-range concentration in MCH, helical supramolecular polymers were formed via four-fold hydrogen bonds as evidenced by CD spectroscopy. Addition of chloroform resulted in a sharp decrease of the magnitude of the Cotton effect and already at 8% of chloroform, no excess helicity was present. A concomitant shift of the UV-Vis absorption spectra showed the morphology change from helically packed *H*-aggregates to less ordered *J*-aggregates. A further increase of the chloroform fraction increases the amount of free monomers in solution in an isodesmic fashion. Therefore the equilibrium between two competing types of aggregates – cooperative and isodesmic – is determined by the solvent. Below 8% of chloroform, long, helical polymers are formed via cooperative mechanism whereas above 8% of chloroform, disordered, short, *J*-type aggregates via isodesmic mechanism are favored.

Besides a major change in the morphology of the aggregates, the interactions between the aggregates and the solvent can also lead to helix inversion within the aggregates. Such changes are much more subtle, because they do not involve visible alteration in the molecular packing. Kulkarni et al showed a helical inversion of chiral coronene bisimide (**CBI**) that aggregate in alkane solvents (Figure 1.7).[76] The helicity inversion occurred upon decrease of the temperature. The transition temperature between the two helical states was solely

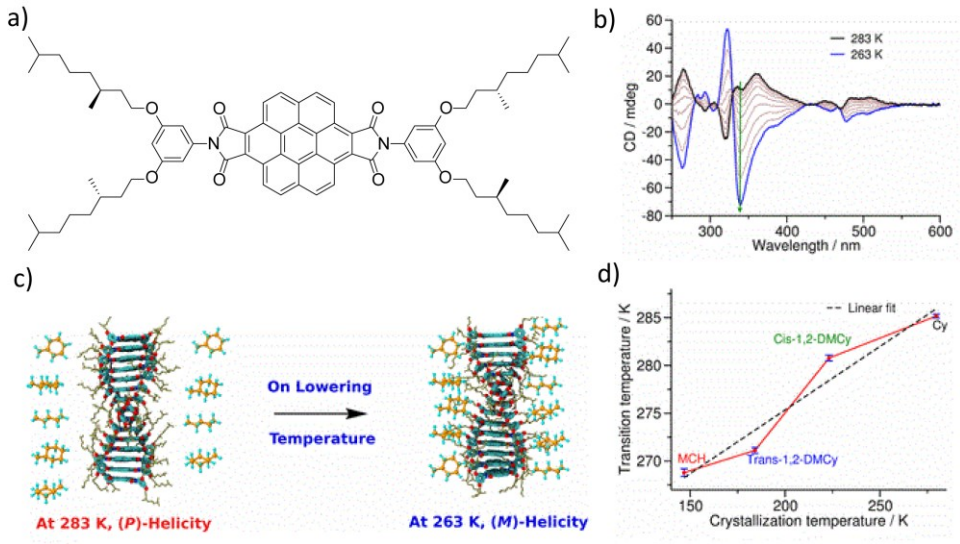


***Figure 1.7*** *a) structure of coronene bisimide (**CBI**); b) CD spectra of **CBI** in MCH at temperatures between 283 K and 263 K; c) a cartoon representing stereomutation process driven by solvation; d) plot of the transition temperature versus crystallization temperature of respective solvent, adapted with permission from ref 72.*

dependent on the structure of the solvent. The transition was fully reversible and independent of the free monomer concentration thereby confirming that both helical aggregates are in thermodynamic equilibrium at a given temperature. The linear increase of the transition temperature with respect to the crystallization temperature of a solvent was observed. From these experiments it was concluded that solvation event i.e. accommodation of solvent molecules in the pocket at the periphery of the aggregates was responsible for the helical inversion of the aggregates. Alteration of the side chains from 3,5-dialkoxyphenyl to 3,4,5-trialkoxydiphenyl substitution resulted in absence of the molecular pocket and a concomitant disappearance of the aggregates of higher solvation state at low temperatures.

### 1.3.2 The role of solvent in competition between kinetically and thermodynamically controlled molecular assembly

The solvent was found not only to influence the morphology of the thermodynamically stable state but also to induce competition between kinetic and thermodynamic control of the supramolecular assembly. Such dependency is reflected by presence of two different types of aggregates in different solvents whereby the kinetically controlled aggregate converts into thermodynamically stable state upon time. Solvent-induced kinetic control of the supramolecular polymerization can lead to interesting observations such as solvent-dependent helicity[77,78] or amplification of supramolecular chirality[79,80].

The group of Fenniri reported the helical inversion of hierarchically organized guanine-cytosine (**G-C**) rosette nanotubes via kinetic control.[78] Hereto, a six-membered supermacrocycle (the rosette) is critical for further assembly of the rosettes into helically assembled nanotubes (Figure 1.8). Strikingly, in pure methanol, exclusively left-handed helical nanotubes were observed, whereas with use of 1% of water in methanol, right-handed helices were formed. Experimental and computational analysis showed that left-handed helical nanotubes were formed as a kinetic product. The kinetic stability of the nanotubes was remarkably high: without heating the left-helical conformation was stable over months. In fact, the thermodynamically stable state could be obtained only when the solution was annealed within 72 hours. On the other hand, the right-handed helical conformation, formed readily with 1% of water was found to be thermodynamically stable. Such drastic difference between the stereoselectivity of the assembly of the rosettes was connected with difference in solvation energy of water and methanol.

Sánchez and co-workers studied the role of solvent in controlling pathway complexity in the supramolecular assembly of *N*-heterotriangulenes.[81] Kinetic versus thermodynamic control was achieved by appropriate solvent choice. In a mixture of MCH / toluene 1:2 vol%, only thermodynamically stable state could be spectroscopically detected. On the other hand, when $CCl_4$ was used instead, the emergence of a metastable off-pathway aggregate was observed. Off-pathway aggregates spontaneously converted into thermodynamically stable

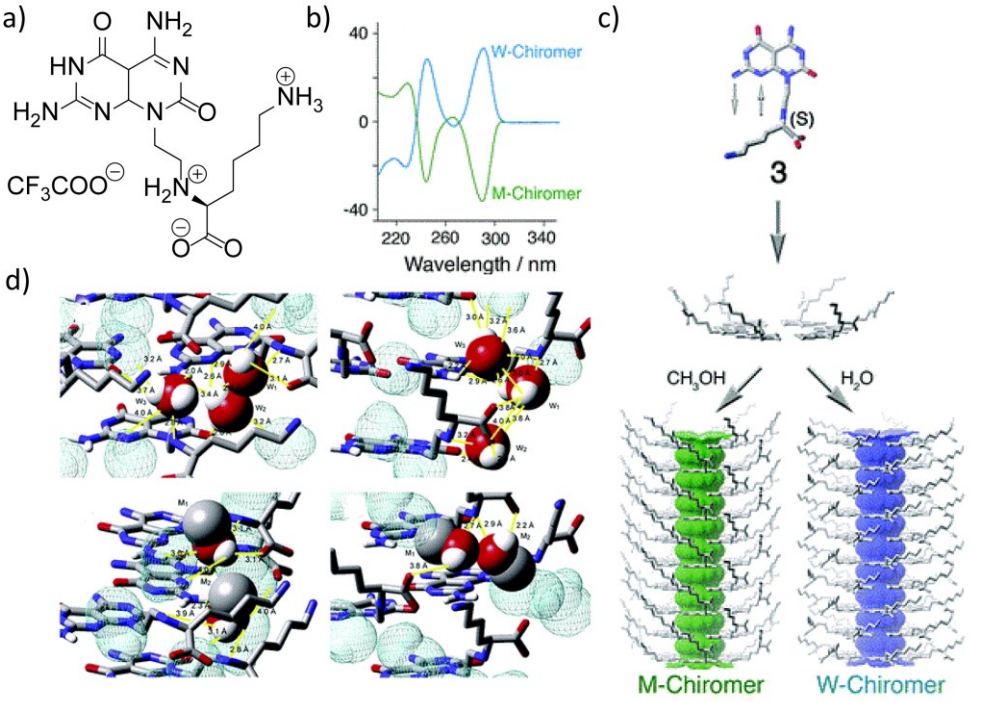


***Figure 1.8*** *a) Structure of guanine-cytosine monomer (**G-C**); b) CD spectra of **G-C** in water (blue) and methanol (green); c) schematic representation of hierarchical self-assembly of G-C into a rosette which in turn polymerizes into a nanotube. M- and W- notations stand for methanol and water chiromers; d) hydrogen bond network generated in the first solvation shell in water (top part) and in methanol (bottom part), adapted with permission from ref 74.*

*J*-type aggregates upon time. Similarly to the work of Takeuchi[82] and Würthner[83,84], metastable off-pathway aggregates could be used as a monomer pool for living supramolecular polymerization. This was achieved by adding a solution containing off-pathway aggregates to the aliquot of previously prepared, thermodynamically stable polymers. The living character of the polymerization was proven by showing that each addition of the off-pathway aggregates resulted in further elongation of the polymers. This study shows in an elegant way that new, emergent properties of supramolecular polymers can be obtained by simple alteration of the solvent, thereby controlling the energetic landscape of the assembly process.

## 1.4 Optically active solvents in supramolecular polymer chemistry

Interesting properties of optically active solvents were first proposed by van't Hoff in 1893.[85] Stereospecific solvation of optically active molecules was envisioned to be a powerful method for synthesis and resolution of enantiomers. Due to weak interactions, only specific

examples of stereoselective synthesis in cholesteric phase[86,87] and kinetic resolutions of enantiomers[88] could be achieved. The emergence of supramolecular polymer chemistry brought back the interest into the function of optically active solvents. Green and coworkers in their pioneering work recognized the potential of optically active solvents in the induction of single helicity in otherwise racemic mixture of *P* and *M* helices of achiral poly(isocyanates). Ever since, optically active solvents gained significant attention in polymer chemistry.[89]

In this context, the work of Green opened a field of asymmetric induction in helical polymers with solvents. Yashima and coworkers used carboxylic acid – amine interactions to bias the helicity in polyacetylenes.[90] Biased helicity could be kinetically trapped upon exchange of the chiral amine with achiral amine.[91] Following this, the group of Fujiki reported asymmetric induction in polysilylene aggregates by optically active alcohols.[92]

Consequently, asymmetric solvation was subject of study in conjugated polymers. Conjugated polymers are popular across the polymer science due to their tunable optical properties. Supramolecular structure is regulated by many weak, non-covalent interactions, with a dominant role of π-π stacking. Therefore the weak interactions with active solvents could effectively bias the helicity of the polyfluorene aggregates. Hereto, a series of optically active solvents such as (*R*)-(*α*)-pinene and (*R*)-(-)-carvone were employed. Due to the intrinsic emission properties of polyfluorenes, such aggregates emitted circularly polarized light.[93,94]

In supramolecular polymers, the choice of optically active solvents was limited due to the possible competing interactions for the hydrogen bonds with the monomers. First example of mirror-symmetry breaking in supramolecular polymers was reported by our group.[95] Hereto, (*S*)-2,6,-dimethyloctane induced helical bias of otherwise racemic helical aggregates based on disc-shaped monomer with the BTA core. The effect was referred to chiral solvation of the supramolecular polymers. Similarly, groups of Bouteiller[96] and Würthner[97] used (*R*)-limonene to induce single helicity in supramolecular polymers based on achiral monomers. Quantitative experiments by Bouteiller and coworkers showed that the equilibrium was established at the chiral induction of 33%. Full chiral induction by optically active solvents is proven to be difficult due to weak interactions between the aggregates and the solvents. We address this issue in further parts of this thesis.

## 1.5 Aim and outline of the thesis

The emergence of non-covalent synthesis as a new, exciting direction in molecular science has created a desire to fundamentally understand weak interactions between molecules. General knowledge about ionic, hydrogen and coordination bonds, van der Waals and hydrophobic interactions to name few, can be found in many chemical textbooks. While Nature is able to utilize all of the interactions in multi-component, non-covalent systems at and far from thermodynamic equilibrium, we still encounter difficulties in controlling the supramolecular structure of simple, synthetic molecules. In previous sections of this chapter it

was shown that a fundamental understanding of the interactions of the assemblies with solvents is required. Due to the intrinsic complexity of the supramolecular systems, most of the knowledge is still gathered empirically. Analogously to organic synthesis, in order to be able to regulate the interactions and control the structures in multi-component assemblies, we have to be able to predict the influence of the solvents as a reaction medium. However we still require a significant amount of experimental observations, before we can create the systems by design. The aim of this thesis is to further unravel the issue of (supramolecular) polymer – solvent interactions and the key role of the temperature and concentration in therein. To gain insight into these issues, $C_3$-symmetrical, hydrogen-bond-based assembling units are utilized. Firstly, the merger of extended aromatic cores with triple hydrogen bonds is exploited to improve the thermodynamic and kinetic stability of one-dimensional supramolecular polymers. The improved stability permits to study the effects of weak interactions with the solvents that were not observed before. Secondly, a covalent polymer is used as a scaffold to attach the well-studied BTA units. Hereby, the influence of additional interactions on usually strongly cooperative assembly of the BTA. Studies reveal that an optimized design of such system requires careful engineering of covalent and non-covalent characteristics such as sequence control, polymer – solvent and BTA – solvent interactions, which play a central role in the assembly process.

Chapter 2 introduces a new supramolecular motif: triphenylene-2,6,10-tricarboxamide (TTA). The synthetic approach towards the TTAs comprising alkyl, oligo(dimethylsiloxane) and oligo(ethylene glycol) chains is shown. This synthetic strategy is based on a versatile amide coupling method that facilitates activation of the carboxylate ion and subsequent nucleophilic substitution, leading to the formation of the amide. The core building block, triphenylene-2,6,10-tricarboxylic acid and the amine building blocks are prepared prior to the final coupling. The obtained materials are studied in solid state to confirm the presence helical aggregates stabilized by three-fold hydrogen bonds.

In Chapter 3, the influence of the solvent property on the thermodynamic and kinetic aspects of supramolecular polymerization in dilute solutions of alkyl substituted TTAs is discussed. Spectroscopic analysis reveals a significantly higher stability of the TTA-based assemblies compared to the analogous BTA aggregates. Amplification of supramolecular chirality experiments show that in decalin the TTA copolymers are under kinetic control and only upon addition of a cosolvent, the kinetic traps are released and strong amplification of supramolecular chirality is observed. Optically active, halogenated solvent effectively solvates the fibers of the achiral monomer, thereby inducing single helical handedness. Upon removal of the chiral solvent, the kinetically trapped homochiral helices in decalin persist and it takes months to racemize the helical superstructure.

Chapter 4 describes thermodynamic aspects of mirror-symmetry breaking in TTA-based supramolecular polymers by chiral solvent. Extensive studies by variable temperature circular

dichroism (VT-CD) spectroscopy shows that in chiral solvents, normally enantiomeric fibers of (*S*)-TTA and (*R*)-TTA are in diastereomeric relationship. Stereospecific solvation of the fibers with chiral solvent drives the co-assembly of a racemic mixture of the monomers towards single helicity, which coincides with the helicity preferred by the achiral monomer in the same chiral solvent. Majority-rules experiments in a chiral solvent shows the existence of a temperature, at which supramolecular copolymers have the same helicity, regardless of the monomer composition (*ee*).

In Chapter 5, the formation of covalent graft polymer aggregates via supramolecular interactions is described. The subtle interplay between the interactions of the components: PDMS, BTA and DCE as the solvent induces the unprecedentedly sharp transition between aggregated and non-aggregated state. The occurrence of an upper-critical solution temperature (UCST) of the PDMS in DCE causes the polymer backbone to collapse. In turn, the collapse of the backbone creates a pocket, wherein the BTAs can form helical aggregates. Phase segregation between the PDMS and the BTA together with inherently high flexibility of the PDMS backbone enables the assembly of the BTA to occur with cooperativity similar to the one observed for free BTAs in alkanes.

Chapter 6 discusses the limits of the synthesis of sequence-defined oligomers holding supramolecular motifs based on the BTA unit. Two synthetic approaches, based on iterative solution-phase synthesis and stepwise solid-phase synthesis, are presented. The iterative solution-phase protocol enables the synthesis of optically pure octa(L-γ-glutamamide) decorated with the BTA and alkyl chains in a sequence-defined fashion via post-functionalization strategy. The solid-phase synthesis protocol utilizes the thiolactone ring-opening chemistry to attach the functionality at each step of the repetitive elongation process. The strategies encounter problems characteristic for each technique such as low solubility in case of solution-phase and side reactions in case of solid-phase synthesis. These difficulties are believed to be overcome by the optimization of the synthesis. However, the first indications on how sequence control can influence folding are presented.

## 1.6 References


[1] W. T. Astbury, A. Street, *Philos. Trans. R. Soc. London* **1931**, *230*, 75–101.
[2] J. D. Watson, F. H. C. Crick, *Nature* **1953**, *173*, 737–738.
[3] J. Cram, Donald, *Angew. Chem. Int. Ed.* **1988**, *27*, 1009–1020.
[4] J. -M Lehn, *Angew. Chem. Int. Ed.* **1988**, *27*, 89–112.
[5] J. Pedersen, Charles, *Angew. Chem. Int. Ed.* **1988**, *27*, 1021–1027.
[6] M. Kulkarni, A. Mukherjee, *Prog. Biophys. Mol. Biol.* **2017**, *128*, 63–73.
[7] T. Siebert, B. Guchhait, Y. Liu, B. P. Fingerhut, T. Elsaesser, *J. Phys. Chem. Lett.* **2016**, *7*, 3131–3136.
[8] U. H. E. Hansmann, J. Meinke, S. Mohanty, O. Zimmermann, in *Proc. NIC Work.*, John Von Neumann Institute For Computing, Julich, **2007**, pp. 195–197.
[9] W. Fuller, T. Forsyth, A. Mahendrasingam, P. Ball, B. Halle, A. Kornyshev, *Philos. Trans. R. Soc. B Biol. Sci.* **2004**, *359*, 1237–1248.
[10] S. H. Chong, S. Ham, *J. Phys. Chem. Lett.* **2016**, *7*, 3967–3972.

[11] S. H. Chong, S. Ham, *Sci. Rep.* **2017**, *7*, 1–10.
[12] H. Oshima, T. Hayashi, M. Kinoshita, *Biophys. J.* **2016**, *110*, 2496–2506.
[13] T. F. A. De Greef, M. M. J. Smulders, M. Wolffs, A. P. H. J. Schenning, R. P. Sijbesma, E. W. Meijer, *Chem. Rev.* **2009**, *109*, 5687–5754.
[14] Y. Tezuka, H. Oike, *Prog. Polym. Sci.* **2002**, *27*, 1069–1122.
[15] S. Mavila, O. Eivgi, I. Berkovich, N. G. Lemcoff, *Chem. Rev.* **2016**, *116*, 878–961.
[16] E. Yashima, K. Maeda, H. Iida, Y. Furusho, K. Nagai, *Chem. Rev.* **2009**, *109*, 6102–6211.
[17] D. J. Hill, M. J. Mio, R. B. Prince, T. S. Hughes, J. S. Moore, *Chem. Rev.* **2001**, *101*, 3893–4011.
[18] R. M. Meudtner, S. Hecht, *Angew. Chem. Int. Ed.* **2008**, *47*, 4926–4930.
[19] M. Waki, H. Abe, M. Inouye, *Angew. Chem. Int. Ed.* **2007**, *46*, 3059–3061.
[20] J. C. Nelson, J. G. Saven, J. S. Moore, P. G. Wolynes, *Science* **1997**, *277*, 1793–1796.
[21] P. Doty, A. Wada, J. T. Yang, E. R. Blout, *J. Polym. Sci.* **1957**, *23*, 851–861.
[22] H. Jiang, C. Dolain, J. M. Léger, H. Gornitzka, I. Huc, *J. Am. Chem. Soc.* **2004**, *126*, 1034–1035.
[23] L. Brunsveld, E. W. Meijer, R. B. Prince, J. S. Moore, *J. Am. Chem. Soc.* **2001**, *123*, 7978–7984.
[24] L. Brunsveld, R. B. Prince, E. W. Meijer, J. S. Moore, *Org. Lett.* **2000**, *2*, 1525–1528.
[25] R. B. Prince, J. S. Moore, L. Brunsveld, E. W. Meijer, *Chem. Eur. J.* **2001**, *7*, 4150–4154.
[26] R. W. Sinkeldam, M. H. C. J. Van Houtem, K. Pieterse, J. A. J. M. Vekemans, E. W. Meijer, *Chem. Eur. J.* **2006**, *12*, 6129–6137.
[27] G. Natta, P. Pino, P. Corradini, F. Danusso, G. Moraglio, E. Mantica, G. Mazzanti, *J. Am. Chem. Soc.* **1955**, *77*, 1708–1710.
[28] E. Yashima, *Anal. Sci.* **2002**, *18*, 3–6.
[29] R. J. M. Nolte, A. J. M. van Beijnen, W. Drenth, *J. Am. Chem. Soc.* **1974**, *96*, 5932–5933.
[30] M. M. Green, K. S. Cheon, S. Y. Yang, J. W. Park, S. Swansburg, W. Liu, *Acc. Chem. Res.* **2001**, *34*, 672–680.
[31] M. M. Green, J. Park, T. Sato, A. Teramoto, S. Lifson, R. L. B. Selinger, J. V Selinger, *Angew. Chem. Int. Ed.* **1999**, *38*, 3138–3154.
[32] M. Fujiki, *Macromol. Rapid Commun.* **2001**, *22*, 539–563.
[33] M. Suginome, T. Yamamoto, Y. Nagata, *J. Synth. Org. Chem., Jpn.* **2015**, *73*, 1141–1155.
[34] A. J. M. van Beijnen, R. J. M. Nolte, W. Drenth, A. M. F. Hezemans, P. J. F. M. van de Coolwijk, *Macromolecules* **1980**, *13*, 1386–1391.
[35] T. Nakano, Y. Okamoto, K. Hatada, *J. Am. Chem. Soc.* **1992**, *114*, 1318–1329.
[36] Y. Okamoto, K. Suzuki, K. Ohta, K. Hatada, H. Yuki, *J. Am. Chem. Soc.* **1979**, *101*, 4763–4765.
[37] T. Kajitani, K. Okoshi, S. I. Sakurai, J. Kumaki, E. Yashima, *J. Am. Chem. Soc.* **2006**, *128*, 708–709.
[38] T. Kajitani, K. Okoshi, E. Yashima, *Macromolecules* **2008**, *41*, 1601–1611.
[39] R. Cook, A. Teramoto, S. Lifson, T. Sato, M. M. Green, N. C. Peterson, *Science* **2006**, *268*, 1860–1866.
[40] M. M. Green, M. P. Reidy, *J. Am. Chem. Soc.* **1989**, *111*, 6452–6454.
[41] M. M. Green, B. A. Garetz, B. Munoz, H. P. Chang, S. Hoke, R. G. Cooks, *J. Am. Chem. Soc.* **1995**, *117*, 4181–4182.
[42] S. Lifson, C. Andreola, N. C. Peterson, M. M. Green, *J. Am. Chem. Soc.* **1989**, *111*, 8850–8858.
[43] M. M. Green, C. Andreola, B. Muñoz, M. P. Reidy, K. Zero, *J. Am. Chem. Soc.* **1988**, *110*, 4063–4065.
[44] K. Tang, M. M. Green, K. S. Cheon, J. V. Selinger, B. A. Garetz, *J. Am. Chem. Soc.* **2003**, *125*, 7313–7323.
[45] M. M. Green, C. Khatri, N. C. Peterson, *J. Am. Chem. Soc.* **1993**, *115*, 4941–4942.
[46] G. B. Schuster, K.-S. Cheon, M. M. Green, J. Li, J. V. Selinger, *J. Am. Chem. Soc.* **2002**, *122*, 2603–2612.
[47] H. Zhao, F. Sanda, T. Masuda, *J. Polym. Sci. Part A Polym. Chem.* **2005**, *43*, 5168–5176.
[48] T. Yamada, Y. Nagata, M. Suginome, *Chem. Commun.* **2010**, *46*, 4914–4916.
[49] Y. Nagata, T. Yamada, T. Adachi, Y. Akai, T. Yamamoto, M. Suginome, *J. Am. Chem. Soc.* **2013**, *135*, 10104–10113.

[50] Y. Nagata, T. Nishikawa, M. Suginome, S. Sato, M. Sugiyama, L. Porcar, A. Martel, R. Inoue, N. Sato, *J. Am. Chem. Soc.* **2018**, *140*, 2722–2726.

[51] Y. Nagata, T. Nishikawa, K. Terao, H. Hasegawa, M. Suginome, *J. Polym. Sci. Part A Polym. Chem.* **2019**, *57*, 260–263.

[52] Y. Nagata, K. Takagi, M. Suginome, *J. Am. Chem. Soc.* **2014**, *136*, 9858–9861.

[53] T. Yamamoto, T. Yamada, Y. Nagata, M. Suginome, *J. Am. Chem. Soc.* **2010**, *132*, 7899–7901.

[54] Y. Yoshinaga, T. Yamamoto, M. Suginome, *ACS Macro Lett.* **2017**, *6*, 705–710.

[55] Y. Z. Ke, Y. Nagata, T. Yamada, M. Suginome, *Angew. Chem. Int. Ed.* **2015**, *54*, 9333–9337.

[56] Y. Nagata, R. Takeda, M. Suginome, *ACS Cent. Sci.* **2019**, *xxx*, xxx–xxx.

[57] B. L. Banik, P. Fattahi, J. L. Brown, *Wiley Interdiscip. Rev. Nanomedicine Nanobiotechnology* **2016**, *8*, 271–299.

[58] B. M. Discher, Y. Y. Won, D. S. Ege, J. C. M. Lee, F. S. Bates, D. E. Discher, D. A. Hammer, *Science* **1999**, *284*, 1143–1146.

[59] U. Tritschler, S. Pearce, J. Gwyther, G. R. Whittell, I. Manners, *Macromolecules* **2017**, *50*, 3439–3463.

[60] L. Jia, P. A. Albouy, A. Di Cicco, A. Cao, M. H. Li, *Polymer* **2011**, *52*, 2565–2575.

[61] J. Willenbacher, O. Altintas, W. Roesky, Peter, C. Barner-Kowollik, *Macromol. Rapid Commun.* **2014**, *35*, 45–51.

[62] P. J. M. Stals, M. A. J. Gillissen, R. Nicolaÿ, A. R. A. Palmans, E. W. Meijer, *Polym. Chem.* **2013**, *4*, 2584–2597.

[63] R. Deans, F. Ilhan, V. M. Rotello, *Macromolecules* **1999**, *32*, 4956–4960.

[64] O. Altintas, E. Lejeune, P. Gerstel, C. Barner-Kowollik, *Polym. Chem.* **2012**, *3*, 640–651.

[65] O. Altintas, P. Gerstel, N. Dingenouts, C. Barner-Kowollik, *Chem. Commun.* **2010**, *46*, 6291–6293.

[66] E. J. Foster, E. B. Berda, E. W. Meijer, *J. Am. Chem. Soc.* **2009**, *131*, 6964–6966.

[67] T. Mes, R. van der Weegen, A. R. A. Palmans, E. W. Meijer, *Angew. Chem. Int. Ed.* **2011**, *50*, 5085–5089.

[68] M. M. J. Smulders, A. P. H. J. Schenning, E. W. Meijer, *J. Am. Chem. Soc.* **2008**, *130*, 606–611.

[69] J. Jacques, A. Collet, S. H. Wilen, *Enantiomers, Racemates and Resolutions*, Krieger Publishing, Malabar, FL, **1991**.

[70] L. Pasteur, *Ann. Chim. Phys.* **1848**, *24*, 442–459.

[71] N. J. Van Zee, B. Adelizzi, M. F. J. Mabesoone, X. Meng, A. Aloi, R. H. Zha, M. Lutz, I. A. W. Filot, A. R. A. Palmans, E. W. Meijer, *Nature* **2018**, *558*, 100–103.

[72] J. Wang, K. Liu, L. Yan, A. Wang, S. Bai, X. Yan, *ACS Nano* **2016**, *10*, 2138–2143.

[73] C. C. Robertson, J. S. Wright, E. J. Carrington, R. N. Perutz, C. A. Hunter, L. Brammer, *Chem. Sci.* **2017**, *8*, 5392–5398.

[74] Y. Wang, W. Qi, R. Huang, X. Yang, M. Wang, R. Su, Z. He, *J. Am. Chem. Soc.* **2015**, *137*, 7869–7880.

[75] M. F. J. Mabesoone, A. J. Markvoort, M. Banno, T. Yamaguchi, F. Helmich, Y. Naito, E. Yashima, A. R. A. Palmans, E. W. Meijer, *J. Am. Chem. Soc.* **2018**, *140*, 7810–7819.

[76] C. Kulkarni, P. A. Korevaar, K. K. Bejagam, A. R. A. Palmans, E. W. Meijer, S. J. George, *J. Am. Chem. Soc.* **2017**, *139*, 13867–13875.

[77] J. S. Valera, R. Sánchez-Naya, F. J. Ramírez, J. L. Zafra, R. Gómez, J. Casado, L. Sánchez, *Chem. Eur. J.* **2017**, *23*, 11141–11146.

[78] R. S. Johnson, T. Yamazaki, A. Kovalenko, H. Fenniri, *J. Am. Chem. Soc.* **2007**, *129*, 5735–5743.

[79] N. Veling, R. van Hameren, A. M. van Buul, A. E. Rowan, R. J. M. Nolte, J. A. A. W. Elemans, *Chem. Commun.* **2012**, *48*, 4371.

[80] J. Buendía, F. García, B. Yélamos, L. Sánchez, *Chem. Commun.* **2016**, *52*, 8830–8833.

[81] J. S. Valera, R. Gómez, L. Sánchez, *Small* **2018**, *14*, 1702437.

[82] S. Ogi, K. Sugiyasu, S. Manna, S. Samitsu, M. Takeuchi, *Nat. Chem.* **2014**, *6*, 188–195.

[83] S. Ogi, V. Stepanenko, J. Thein, F. Würthner, *J. Am. Chem. Soc.* **2016**, *138*, 670–678.

[84] S. Ogi, V. Stepanenko, K. Sugiyasu, M. Takeuchi, F. Würthner, *J. Am. Chem. Soc.* **2015**, *137*, 3300–

3307.
[85] W. Meyerhoffer, J. H. van't Hoff, *Gleichgewichte Der Stereomeren*, B. G. Teubner, California, CA, **1906**.
[86] H. Goto, *Macromolecules* **2007**, *40*, 1377–1385.
[87] K. Kawabata, M. Takeguchi, H. Goto, *Macromolecules* **2013**, *46*, 2078–2091.
[88] M. B. Groen, H. Schadenberg, H. Wynberg, *J. Org. Chem.* **1971**, *36*, 2797–2809.
[89] M. Fujiki, *Symmetry* **2014**, *6*, 677–703.
[90] E. Yashima, T. Matsushima, Y. Okamoto, *J. Am. Chem. Soc.* **1995**, *117*, 11596–11597.
[91] E. Yashima, K. Maeda, Y. Okamoto, *Nature* **1999**, *399*, 449–451.
[92] H. Nakashima, J. R. Koe, K. Torimitsu, M. Fujiki, *J. Am. Chem. Soc.* **2001**, *123*, 4847–4848.
[93] Y. Kawagoe, M. Fujiki, Y. Nakano, *New J. Chem.* **2010**, *34*, 637–647.
[94] Y. Nakano, Y. Liu, M. Fujiki, *Polym. Chem.* **2010**, *1*, 460–469.
[95] A. R. A. Palmans, J. A. J. M. Vekemans, E. E. Havinga, E. W. Meijer, *Angew. Chem. Int. Ed.* **1997**, *36*, 2648–2651.
[96] B. Isare, M. Linares, L. Zargarian, S. Fermandjian, M. Miura, S. Motohashi, N. Vanthuyne, R. Lazzaroni, L. Bouteiller, *Chem. - A Eur. J.* **2009**, *16*, 173–177.
[97] V. Stepanenko, X. Q. Li, J. Gershberg, F. Würthner, *Chem. Eur. J.* **2013**, *19*, 4176–4183.

# Chapter 2

# *A modular approach to triphenylene-2,6,10-tricarboxamide-based supramolecular polymers*

**Abstract**:

The synthesis of a novel supramolecular motif based on a $C_3$-symmetrically substituted triphenylene core that is decorated with three amide groups is reported. The key intermediate, triphenylene-2,6,10-tricarboxylic acid, was prepared according to a modified literature procedure in an easy and scalable 3-step synthesis. Using a robust amide coupling strategy, we attached linear and branched aliphatic chains: *n*-octylamine, (*S*)- and (*R*)-3,7-dimethyloctyl as well as oligo(ethylene) glycol and homo- and heterotelechelic oligo(dimethyl)siloxane chains to the triacid core, affording a series of triphenylene-2,6,10-tricarboxamide (TTA) derivatives. Infrared spectroscopy of the synthesized TTAs showed that helical columnar structures stabilized by threefold intermolecular H-bonds were present in the bulk. Further studies of the solid phase properties indicated the presence of liquid crystalline mesophases and high clearing temperatures suggesting an increased stability of aggregates in comparison to their benzene-1,3,5-tricarboxyamide (BTA) analogues.

Part of this work will be published:
Supramolecular Chirality of Triphenylene-2,6,10-tricarboxamides: Kinetic and Thermodynamic Control by Solvent Engineering
M. L. Ślęczkowski, M. F. J. Mabesoone, Y. Post, A. R. A. Palmans, E. W. Meijer, *manuscript in preparation*

## 2.1. Introduction

The first report on the use of the triphenylene core in the field of liquid crystals dates back to 1978.[1] Since then, this unit has been thoroughly explored not only for liquid crystalline behavior[2] but also for crystalline coordination networks[3], liquid crystalline elastomers[4] and molecular glass properties[5]. As a result, multiple synthetic methodologies have been developed and now permit the synthesis of triphenylenes with a plethora of substituents that differ in nature and position of attachment. Synthetically the most easily accessible substituted triphenylenes are symmetrical 2,3,6,7,10,11-hexa alkoxy- (ether) and hexa alkoxycarbonyl- (ester) derivatives as well as hexa-substituted desymmetrized triphenylenes.[6,7] Functional wedges have been typically attached through an alkyl spacer. Depending on the desired mesomorphic properties and functions, various chemical moieties have been attached. Symmetrically substituted triphenylenes include ionic liquid pendants[8], dendrons[9], anthraquinone[10], azobenzene[11,12], cyanobiphenyl[13], naphthalene[14], thiophene[15,16] and carboxylate-ammonium salt conjugates[17] as pendant arms. Desymmetrized hexasubstituted triphenylenes comprise stable radicals (TEMPO and PROXYL)[18] as well as ferrocene[19], triazine[20], crown ether[21], cyclodextrin[22,23], cyanophenyl[24], dithiol[24], fullerene[25] and silsequioxane[26] groups. The strong affinity of triphenylene-based mesogens to assemble via π-π stacking induces the formation of liquid crystalline mesophases. Owing to the symmetry of the molecules, the motif has a tendency to form columnar hexagonal mesophases[2,6,7], but many other phases have also been obtained by appropriate molecular engineering including other columnar phases such as nematic[13,27–30], cubic[9], lamellar[21,26] and bicontinuous cubic[8] phases. Due to efficient charge transport within organized domains[31,32], triphenylene-based molecules have been extensively studied in terms of applications in optical compensation films for LCDs[33], organic light-emitting diodes (OLEDs)[24,34–36], organic field-effect transistors (OFETs)[15,16,37] and photovoltaic solar cells[38]. Despite many studies on triphenylene-based systems, only few examples of 2,6,10-trisubstituted triphenylenes have been reported. A notable exception is triphenylene-2,6,10-tricarboxylic acid which has been used as starting material for the preparation of triphenylene triesters by Bock and coworkers.[41] Via a three-step procedure, triphenylene-2,6,10-tricarboxylic acid was obtained in 43% yield and good purity. After esterification, several derivatives showed mesomorphic properties, exhibited electroluminescence, and were investigated in terms of applications in OLEDs.[39]

Inspired by the work of Bock and coworkers in combination with our knowledge on supramolecular polymerizations of BTA derivatives,[40] we here introduce a supramolecular motif based on triphenylene-2,6,10-tricarboxamide (TTA). This motif is analogous to the widely studied benzene-1,3,5-tricarboxyamides in the sense that it possesses a $C_3$-symmetrical core, has three amide units, and a variety of substituents can be easily attached via amide coupling procedures. In addition, both hydrogen bonding as well as π-π stacking can be operative to form supramolecular structures. In order to validate the modular approach for a

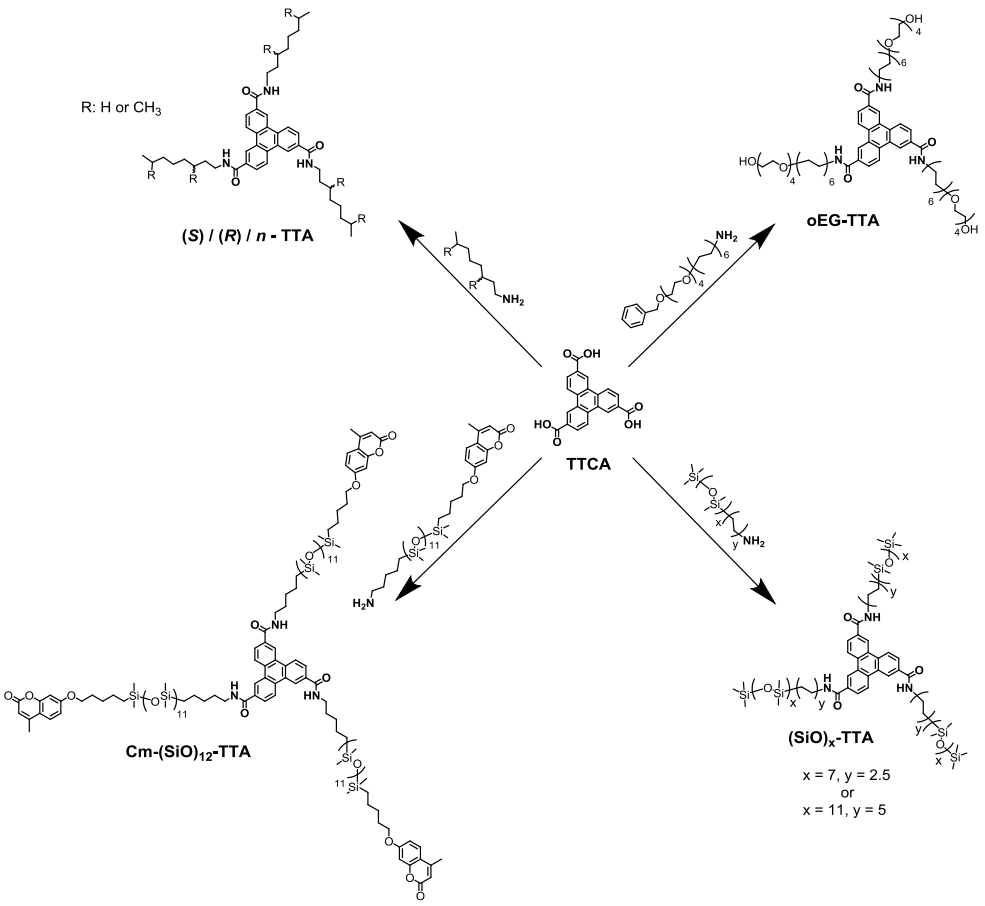


**Scheme 2.1** Modular approach for the synthesis of various TTAs from TTCA.

variety of TTA derivatives, we here report first on the optimized synthesis of triphenylene-2,6,10-tricarboxylic acid (TTCA) starting from the procedure developed by groups of Ogawa and Bock.[41,42] The synthesized TTCA serves as a key intermediate, and was subsequently converted into three families of TTAs that comprise alkyl, oligo(ethylene glycol)- or oligo(dimethylsiloxane)-based side chains (Scheme 2.1). These side chains were selected because of their inherently different chemical character, and the anticipated effects on the thermal and self-assembly behavior of TTAs. For the alkyl and oligo(ethylene glycol)-based side chains we selected (*R*)- and (*S*)-3,7-dimethyloctylamine and dodecyltetraethylene glycol, respectively, as the effect on self-assembly and thermal properties of these side chains has been studied in BTAs.[43–46] For the oligo(dimethylsiloxane)-based side chains, we here develop a synthesis of heterotelechelic, discrete oligo(dimethylsiloxane) with one amine end group and either a coumarin or methyl end group (Scheme 2.1). Those comprising the coumarin end group can be further crosslinked by UV.[47–49] All synthesized materials were fully characterized by NMR, IR and MALDI-TOF-MS. Their thermal properties were investigated by a combination

of X-ray scattering, differential scanning calorimetry (DSC), polarized optical microscopy (POM). Interestingly, a diversity of structures is revealed, hereby opening up new possibilities in controlling supramolecular structures.

## 2.2. Synthesis of triphenylene-2,6-10-tricarboxyamides

### 2.2.1. Synthesis of triphenylene-2,6,10-tricarboxylic acid

The synthesis of triphenylene-2,6,10-tricarboxylic acid (Scheme 2.2) was previously reported by Bock and coworkers in 2006[41]. The route was designed and optimized on the basis of the protocol of Ogawa for the synthesis of 2,6,10-trimethyltriphenylene.[42] The synthesis afforded the triphenylene-2,6,10-tricarboxylic acid in an overall yield of 43% in 3 steps starting from 4-methylcyclohexanone

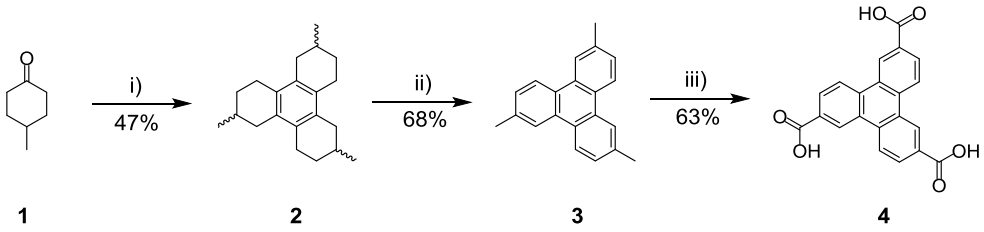


***Scheme 2.2*** *Synthetic route for key substrate triphenylene-2,6,10-tricarboxylic acid (**4**). Reagents and conditions: i) $ZrCl_4$, 170 °C; ii) Pd/C, triglyme, 220 °C; iii) $Na_2Cr_2O_7$, $H_2O$, 250 °C.*

The first step involves a double aldol condensation of 4-methylcyclohexanone (**1**). In solvent-free conditions at 170 °C, cyclodehydration of an intermediate enone occurs, affording 2,6,10-trimethyldodecahydrotriphenylene (**2**). After recrystallization from *n*-butanol **2** was obtained as a mixture of symmetrical and dissymmetrical diastereoisomers (*sym: S,S,S / R,R,R* + *dissymi: S,S,R / R,R,S*) in a yield of 47%. The diastereomer ratio (6/4 *sym/dissym*) was determined from the $^{13}C$ NMR spectrum and corresponds well to literature data.[42] In the original procedure, the synthesis of 2,6,10-trimethyltriphenylene (**3**) was accomplished by dehydrogenation of **2** in the melt in an autoclave to 280 °C in the presence of Pd/C.[42] To avoid working with such high temperatures, we followed the procedure reported by Bock et al, where the high boiling triethylene glycol dimethyl ether (triglyme) as a solvent was used.[41] This permitted to lower the reaction temperature to 220 °C and the reaction was complete in 12 hours. After workup, **3** was kept at 5 °C over the weekend which induced crystallization. Formed white crystals were isolated in 68% yield. Finally, **3** was oxidized at 250 °C in a stainless steel high-pressure reactor in aqueous $Na_2Cr_2O_7$ to yield sodium triphenylene-2,6,10-tricarboxylate. After removing the insoluble chromium salts, the carboxylate was acidified with concentrated HCl yielding **4** in a good yield (63%). This oxidation reaction was found to be very sensitive to the efficiency of stirring and proper dispersion of **3** in the aqueous phase during the reaction. If **3** was not sufficiently dispersed in

the water, no or only little amounts of product were isolated. To ensure good dispersion, **3** was poured in portions to a previously prepared, well-stirred solution of sodium dichromate in water in the stainless steel reactor. Unsurprisingly, we found that **4** was not soluble in any of the common NMR solvents at room temperature.[1] Therefore, we relied on the IR spectrum of **4**, which gave a broad absorption band centered at 3010 $cm^{-1}$ characteristic for $\upsilon_{O-H}$ in carboxylic acid. A strong band at 1679 $cm^{-1}$ corresponded to C=O stretching, and the C=C stretching in the aromatic ring was found at 1614 $cm^{-1}$. Finally, the O-H bending vibrations occurred at 1420 $cm^{-1}$. The total yield after 3 steps was 18%, which was lower than reported by Bock et al.[41] We observed visibly lower yields at first step of the synthesis (47% vs 69%). This could have been caused by trace impurities present in the 4-methylcyclohexanone that caused side reactions.

### 2.2.2. Synthesis of trisalkylated TTAs

Trisalkylated TTAs were synthesized by amide coupling between triphenylene-2,6,10-tricarboxylic acid and an alkyl amine of choice with the use of 2-(1H-benzotriazole-1-yl)-1,1,3,3-tetramethylaminium tetrafluoroborate (TBTU) as a coupling agent (Scheme 2.3). Chiral

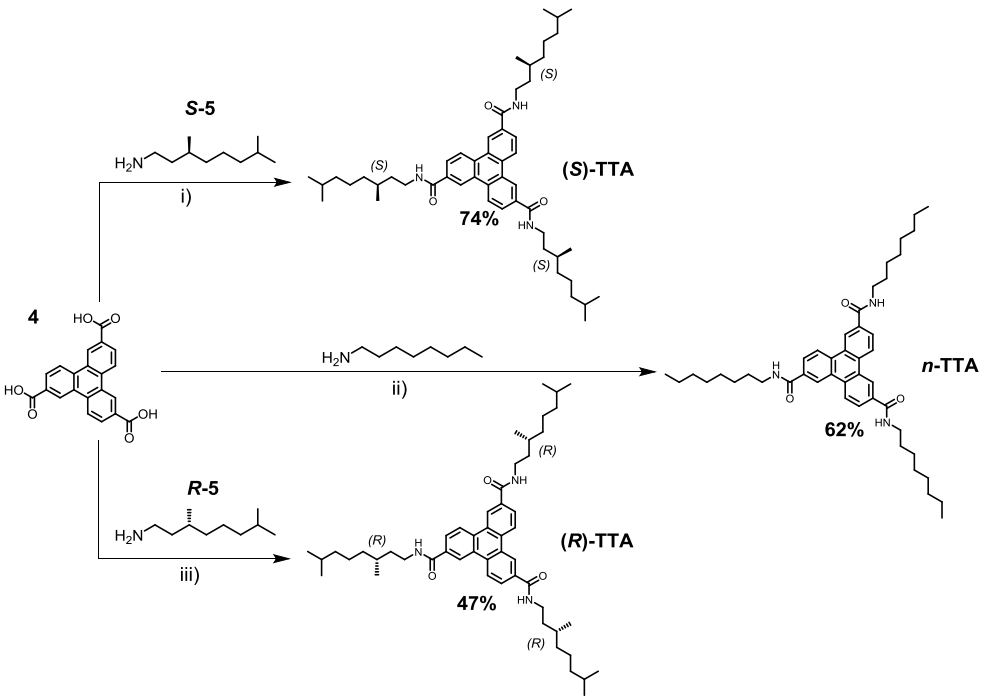


***Scheme 2.3*** *Synthesis of* ***(S)***, ***(R)*** *and* ***n-TTA****. Reagents and conditions: TBTU, DIPEA, DMF, 70 °C, i)* ***S-5****; ii) n-octylamine; iii)* ***R-5****.*

[1] **4** was found to be insoluble in deuterated chloroform, THF, DMSO and DMF.

(*R*)- and (*S*)-3,7-dimethyloctyl amine ***R*-5** and ***S*-5** were synthesized from commercially available D- and L-citronellol in 4 steps according to previously published procedures[50] in overall yields of 40% and 62%, respectively. The structure of both enantiomers was checked by $^1$H NMR spectroscopy. The amide coupling reactions towards TTAs were achieved by acid activation using TBTU in presence of *N,N*-diisopropylethylamine (DIPEA) as a base. Due to low solubility of **4** in solvents usually applied in this reaction, DMF at 70 °C had to be selected. Firstly, **4** was solubilized in dry DMF under argon atmosphere at 70 °C and then a solution of TBTU was added. Only when the carboxylic acid was well dissolved, DIPEA and the appropriate primary amine were added simultaneously, ensuring that an excess of DIPEA over primary amine was always present in the reaction mixture. After cooling to room temperature, the reaction mixture was worked up via extraction, affording a yellow / orange solid. Recrystallization from methanol gave the pure TTAs as white solids. The three compounds, (*S*)-, (*R*)-, and *n*–TTA were obtained in 74%, 47%, and 62% yield, respectively. It is worthy to note that the synthesized TTAs only readily dissolve in polar aprotic solvents such as DMF, THF or DMSO. They are also soluble in chloroform, but recording of the $^1$H NMR spectrum in $CDCl_3$ was not possible due to strong aggregation that occurred already at 1 mg mL$^{-1}$. In non-polar solvents such as toluene or alkanes, organogels were formed. Gelation was observed at 1 mg mL$^{-1}$ in decaline and 5 mg mL$^{-1}$ in toluene. TTAs were insoluble in alcohols and ethyl acetate in ambient conditions. The structure and purity of all obtained TTAs were confirmed by $^1$H, $^{13}$C NMR and MALDI-TOF-MS and IR (Figures 2.1 and 2.2). Due to strong aggregation

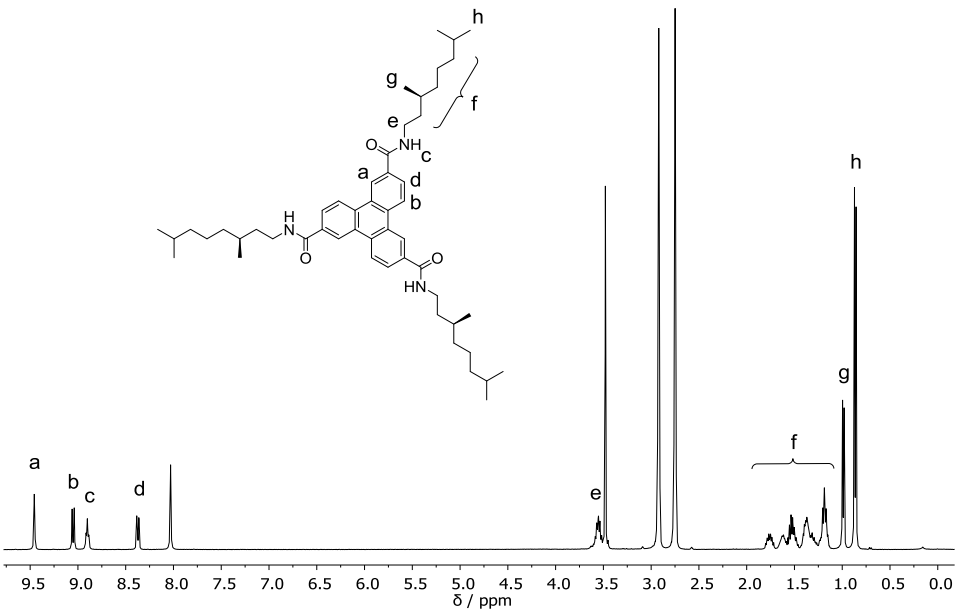


***Figure 2.1*** *$^1$H NMR spectrum of* ***(S)-TTA*** *(DMF-$d_7$, 400 MHz).*

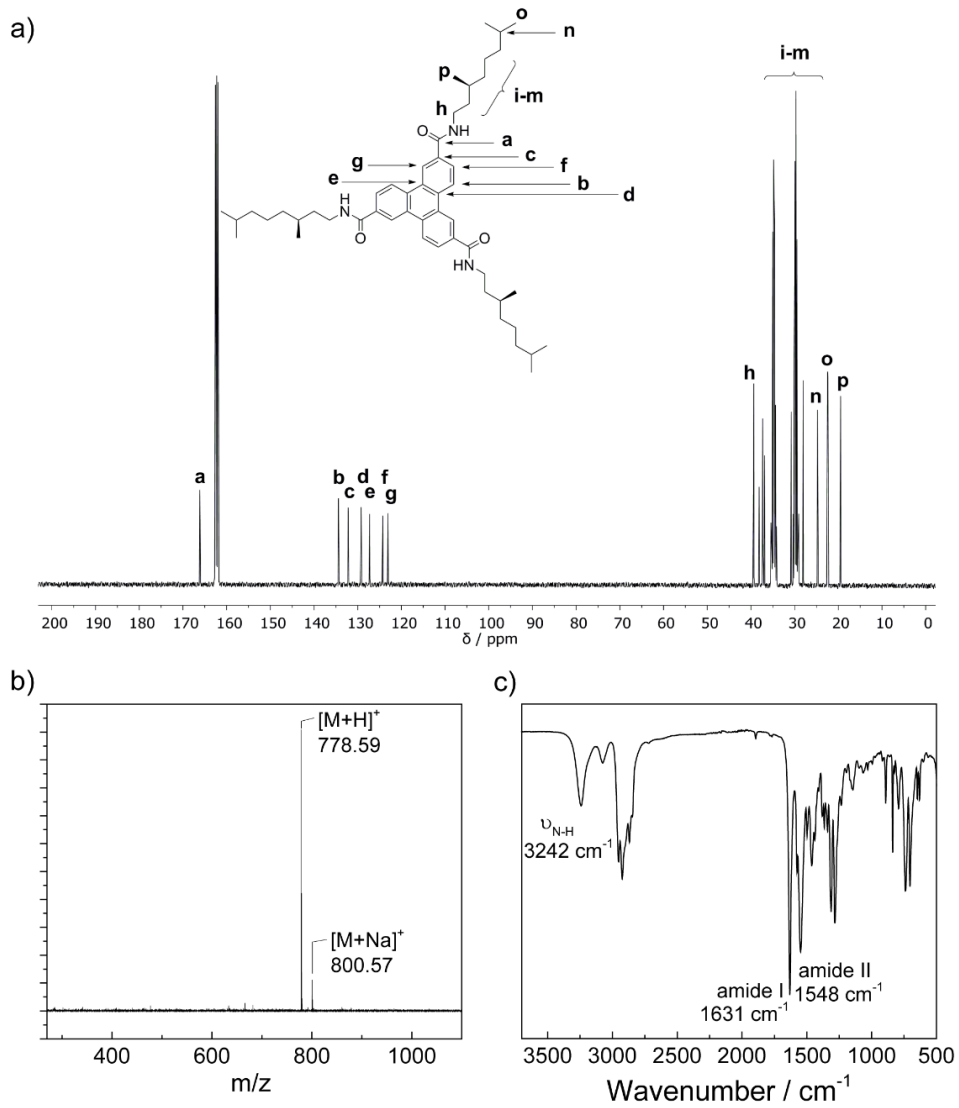


***Figure 2.2*** *a) $^{13}C$ NMR spectrum of* ***(S)-TTA*** *(DMF-$d_7$, 100 MHz); b) MALDI-TOF-MS and c) FT-IR spectra of* ***(S)-TTA***.

in $CDCl_3$, NMR spectra of TTA derivatives were recorded in DMF-$d_7$. In the low-field region of $^1H$ NMR spectrum of **(*S*)-TTA**, 4 groups of signals are visible. The singlet at 9.46 ppm (**a**), together with two doublets at 9.05 (**b**) and 8.37 (**d**) ppm ($J$ = 8.8 Hz) originate from the protons attached to the aromatic core. The triplet at 8.90 ppm ($J$ = 7 Hz) (**c**) is the signal from amide N-*H* proton. The signals below 3.55 ppm (multiplet of N-C$H_2$) (**e**) belong to the protons of the aliphatic chains (**f**). The characteristic doublets for the methyl end-groups in the 3,7-

dimethyloctyl chains are present at 0.99 ppm ($J$ = 6.4 Hz) (**g**) and 0.86 ppm ($J$ = 6.8 Hz) (**h**). The $^{13}C$ NMR spectrum in the low field region reveals peaks of $sp^2$-hybridized carbons from amide (**a**) and the aromatic core (**b-d**). High-field signals are caused by the resonance of aliphatic chain carbon atoms **e**-**h** with two terminal methyl groups being the most upfield at 23.26 and 20.34 ppm. The MALDI-TOF-MS spectrum shows a peak at 778.59 Da which corresponds well to protonated molecular ion $[M+H]^+$ of the product. Full functionalization of the acid is proven by the absence of $\upsilon_{O-H}$ at 3010 $cm^{-1}$, a shift of $\upsilon_{C=O}$ vibration from 1679 $cm^{-1}$ to 1631 $cm^{-1}$ typical for an amide I band. The presence of the amide group is further confirmed by vibrations at 3242 $cm^{-1}$ and 1548 $cm^{-1}$ that correspond to $\upsilon_{N-H}$ and amide II bands, respectively.

### 2.2.3. Synthesis of oligo(ethylene glycol)-functionalized TTA

On the basis of previous work done in our group using BTAs as the core[51], we anticipated that oligo(ethylene glycol) (oEG)-based TTAs could form supramolecular polymers in water. However, with the extension of the aromatic core from benzene to triphenylene, the hydrophobic effect is expected to be larger which may enhance the stability of the structures. In addition, the oligo(ethylene glycol) arms typically enhance solubility in organic media. The strategy for the synthesis for **oEG-TTA** is similar to that used for alkyl-TTAs (Scheme 2.4). Firstly, an amine precursor for the side chain was synthesized and subsequently attached to the core via amide coupling. Due to the presence of an alcohol functionality on the oEG chain we selected to use a benzyl-protected derivative to make the amide coupling more straightforward. The benzyl group can be cleaved in the final step.

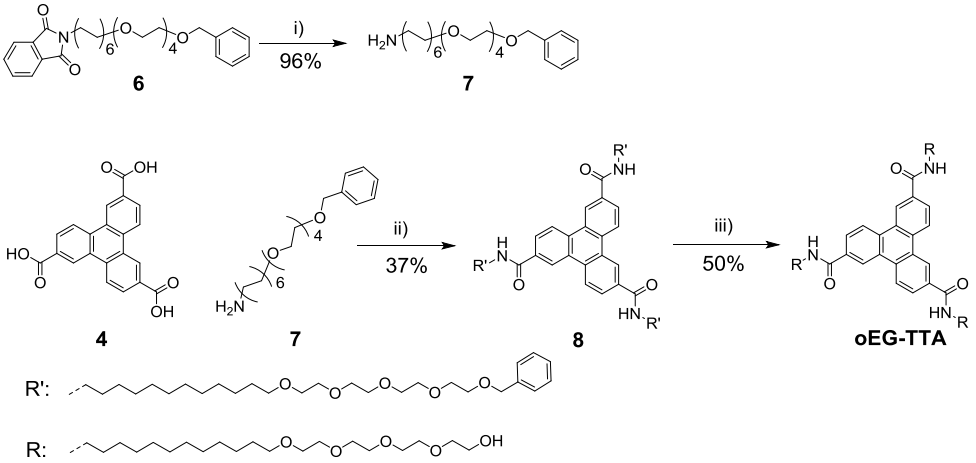


***Scheme 2.4*** *Synthesis of* ***oEG-TTA****. Reagents and conditions: i) hydrazine, EtOH, 70 °C; ii) TBTU, DIPEA, 70 °C; iii)* $H_2$*, Pd/C, EtOAc / MeOH 2:1 vol/vol, r.t.*

Amine precursor (**7**) was synthesized in one step from corresponding naphthalimidyl derivative (**6**) provided by Jolanda Spiering via Gabriel synthesis with hydrazine (96%). The amide coupling was performed in a similar manner as discussed in section 2.2.2. In this case, the workup was simplified due to significantly better solubility of the product. After purification by column chromatography, the benzyl-protected oEG-TTA (**8**) was isolated in relatively low purity. We assumed that deprotection of alcohol would increase the polarity of the molecule and therefore facilitate the separation between the product and the impurity. Therefore, the deprotection of the benzyl group with hydrogen gas and Pd/C as a catalyst was performed on the impure compound **8**. After workup, the crude product was purified by column chromatography. Gratifyingly, a good separation was achieved, facilitating the isolation of pure oEG-TTA as colorless sticky solid. The enhanced solubility of **oEG-TTA** in organic solvents in comparison to the alkylated TTAs enabled to measure NMR in acetone-$d_6$ with a drop of $CD_3OD$ (see Experimental Section for detailed analysis). The aromatic protons were shifted upfield for ca. 0.15 ppm, but the coupling constant remained the same ($J$ = 8.8 Hz). Due to fast exchange of protons in presence of MeOD, amide protons are not visible on the spectrum. The protons attached to the oligoethylene chains overlap with N-$CH_2$ protons adjacent to the amide at 3.50 ppm. Next, a clear triplet with $\delta$ = 3.39 ppm and $J$ = 6.4 HZ confirms the presence of the R-$CH_2$-O protons. MALDI-TOF-MS shows a single peak at 1461.80 Da, which corresponds well to $[M+Na]^+$ of **oEG-TTA**. The IR spectrum of **oEG-TTA** shows the presence of C=O stretch (amide I) at the same position as observed for **(S)-TTA**. The N-H bond gives rise to the absorption band at 3248 $cm^{-1}$, while amide I and amide II remain virtually the same (1632 and 1548 $cm^{-1}$, respectively). Additionally, a vibration for O-H stretching is observed at 3428 $cm^{-1}$.

As a result of the significant increase in the hydrophobicity of the core, we were not able to dissolve **oEG-TTA** in water. In oligo(ethylene glycol)-functionalized BTAs, water solubility was provided only by good ratio between hydrophobic and hydrophilic parts. In the current design of the TTA, we only changed the aromatic core, while the hydrophobic / hydrophilic chains composition remained the same. Therefore we infer that to solubilize TTAs in water, one must compensate for the core hydrophobicity. This issue is currently addressed in collaboration with Lu Su and Jesús Mosquera, where we aim to synthesize TTAs functionalized with carbohydrates and ionic groups.

### 2.2.4. Synthesis of oDMS-functionalized TTAs

The synthetic strategy for oDMS-functionalized TTAs required the preparation of alkyl-oDMS amines to be attached to the triphenylene core via the amide coupling methodology. We selected two sets of pendant arms which differed from each other in terms of alkyl and oDMS chains lengths as the changes in their length will affect the thermal behavior of these compounds. Alkyl-oDMS amines were synthesized in 3 steps starting from either 5-bromopent-1-ene or 10-bromodec-1-ene (Scheme 2.5).

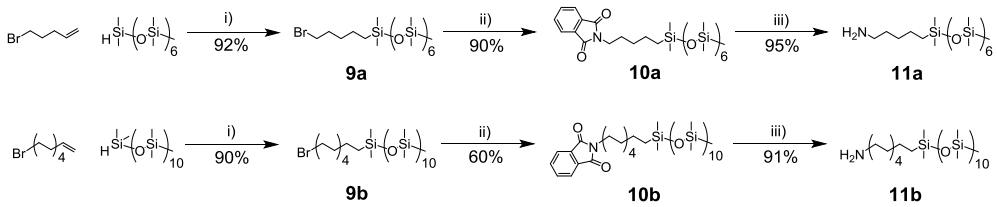


***Scheme 2.5*** *Synthetic routes for oDMS-alkylamines **11a** and **11b**. Reagents and conditions: i) Karstedt catalyst, DCM (**9a**) or toluene (**9b**), r.t.; ii) potassium phthalimide, DMF, 60 °C; iii) hydrazine, EtOH, 80 °C.*

The first step of the synthesis of oDMS-alkylamines **11a** and **11b** was a Pt(0)-catalyzed alkylation of discrete hydride-functionalized hepta- and undeca(dimethyl)siloxane, synthesized by Bas de Waal.[52] Although this reaction is considered as effective and robust, we found that precautions had to be taken in order to achieve good yields and high purity. We observed in multiple cases that poor solubility had a negative effect on the yields of the hydrosilylation. In fact, the longer siloxanes showed a reduced conversion in the Karstedt reaction presumably due to lower solubility in DCM. In contrast, short siloxanes gave excellent yields in this solvent. In several reports the hydrosilylation was carried out at elevated temperatures, but we found that the rate of double bond isomerization is increased at higher temperatures. The latter reaction converts the terminal olefin into an internal olefin which causes its deactivation and accumulation as a side product. In case of the synthesis of **9a**, starting material 5-bromopentene is a volatile liquid. Therefore, we used a 10% excess in the reaction to achieve 100% conversion of the hydride. Subsequently, unreacted or isomerized bromopentene was distilled off to yield pure **9a**. A similar procedure was applied for the synthesis of **9b**, even though 10-bromodecene is not volatile enough to be removed through rotary evaporation. Compound **9b** was readily purified by column chromatography. Next, the brominated compounds **9a** and **9b** were subjected to nucleophilic substitution reaction with potassium phthalimide to afford derivatives **10a** and **10b** in a yield of 90% and 60%, respectively, after column chromatography. The lower yield for **10b** was most likely due to low solubility of the siloxane part in polar DMF. The derivatives **10a** and **b** were reduced to hepta(dimethyl)siloxanyl-pentylamine **11a** and undeca(dimethyl)siloxanyl-decylamine **11b**. Both oDMS-TTA conjugates **$(SiO)_7$-TTA** and **$(SiO)_{11}$-TTA** were synthesized according to the earlier discussed amide-coupling strategy (Scheme 2.6). Dissolved tricarboxylic acid **4** was treated with TBTU and subsequently DIPEA together with the corresponding oDMS-alkylamines were added. In the case of **11b** a homogeneous solution in DMF was only formed at 110 °C, due to very low solubility of non-polar oDMS part.

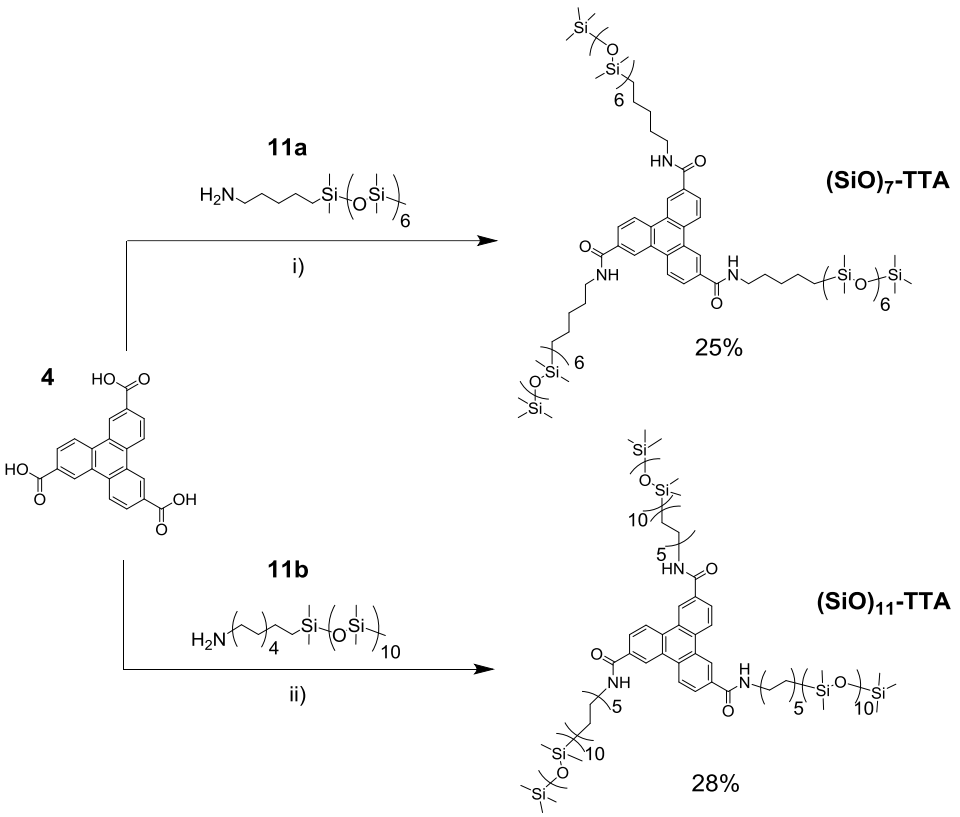


***Scheme 2.6*** *Synthesis of oDMS-TTA conjugates* ***(SiO)$_7$-TTA*** *and* ***(SiO)$_{11}$-TTA****. Reagents and conditions: TBTU, DIPEA, DMF i) 70 °C; ii) 110 °C.*

The final products were isolated with the use of column chromatography with yields of 25% and 28% for **(SiO)$_7$-TTA** and **(SiO)$_{11}$-TTA**, respectively. The final products showed paste-like appearances, indicative of liquid crystalline properties. The structures were confirmed by IR, $^1$H, $^{13}$C NMR, and MALDI-TOF-MS. $^1$H NMR spectra of **(SiO)$_7$-TTA** and **(SiO)$_{11}$-TTA** shows that no significant differences in comparison to previously discussed TTAs were observed. MALDI-TOF spectra show $[M+Na]^+$ signals of both **(SiO)$_7$-TTA** and **(SiO)$_{11}$-TTA** that appear at 2140.81 Da and 3241.30 Da, respectively. IR spectra of both **(SiO)$_x$-TTA** showed vibrations at 3245 cm$^{-1}$ ($\upsilon_{N-H}$) and 1552 cm$^{-1}$ (amide II). Presence of the oDMS chains was evidenced by strong absorption bands at 1257 cm$^{-1}$, 1020 cm$^{-1}$ and 790 cm$^{-1}$ are assigned to $\upsilon_{Si-C}$ and $\upsilon_{Si-O}$ stretching and correspond well with the literature.[53]

### 2.2.5 Synthesis of telechelic UV-crosslinkable oDMS-TTA conjugates

For the coumarin-functionalized TTAs, the proposed side chain comprises a coumarin attached through an ether bond to $C_5$-alkyl chain, which consecutively was connected to

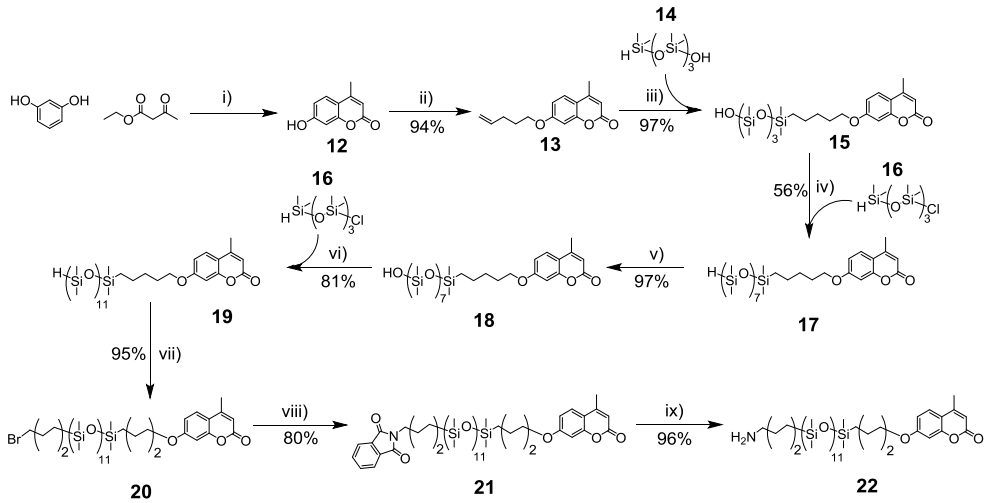


***Scheme 2.7*** *Synthetic route for $H_2N$-$C_5$-$Si_{12}$-$C_5$-Cm* ***22****. Reagents and conditions: i) TFA, 100 °C, microwave irradiation; ii) 5-bromopent-1-ene, ACN, 85 °C; iii) Karstedt catalyst, $CHCl_3$; r.t.; iv) pyridine, toluene, 0 °C; v) Pd/C, dioxane / aqueous phosphate buffer (pH 7) 4:3 vol/vol, r.t.; vi) pyridine, toluene, 0 °C; vii) 5-bromopent-1-ene, Karstedt catalyst, toluene, r.t.; viii) potassium phthalimide, DMF, 70 °C; ix) hydrazine monohydrate, EtOH, 80 °C.*

discrete dodeca(dimethyl)siloxane. The $C_5$-alkyl chain on the other side would be attached to the TTA via the amide linkage. In order to apply the amide coupling methodology, an amine-functionalized wedge had to be synthesized (Scheme 2.7). Retrosynthetic analysis indicated that a plausible route starts with a Pechmann condensation of resorcinol. We followed the procedure of Zak et al[54] who stirred resorcinol and ethylacetoacetate in trifluoroacetic acid under microwave irradiation. After aqueous work up and recrystallization from heptane / EtOAc 4:1, hydroxycoumarin (**12**) was obtained in a yield of 93%. The coumarin was converted into an ether through functionalization of the phenol with 5-bromopent-1-ene via a Williamson ether synthesis, affording **13** in a 94% yield. Next, tetra(dimethyl)siloxane arm was attached to **13** via a hydrosilylation reaction with freshly prepared octamethyltetrasiloxan-1-ol (**14**) in the presence of Karstedt catalyst affording silanol **15**. Owing to the silanol function, the synthesis of discrete oDMS chain could be continued according to the protocol developed by our group.[52] Herein coupling of **15** with 1-chlorooctamethyl siloxane **16** yielded hydride terminated octa(dimethyl)siloxane-coumarin conjugate **17** after aqueous work up and column in 56% yield. Corresponding silanol **18** was obtained in 97% yield after stirring **17** in a mixture of dioxane and aqueous phosphate buffer of pH = 7 with presence of Pd/C, which facilitates cleavage of Si-H bond and subsequent substitution of hydroxyl group. Removal of the catalyst by filtration and subsequent aqueous work-up facilitates the isolation of **18** with 97% yield, which was immediately used in a next step to avoid self-condensation of silanol groups. The next step was the oDMS-chain elongation via nucleophilic substitution of **16** furnishing

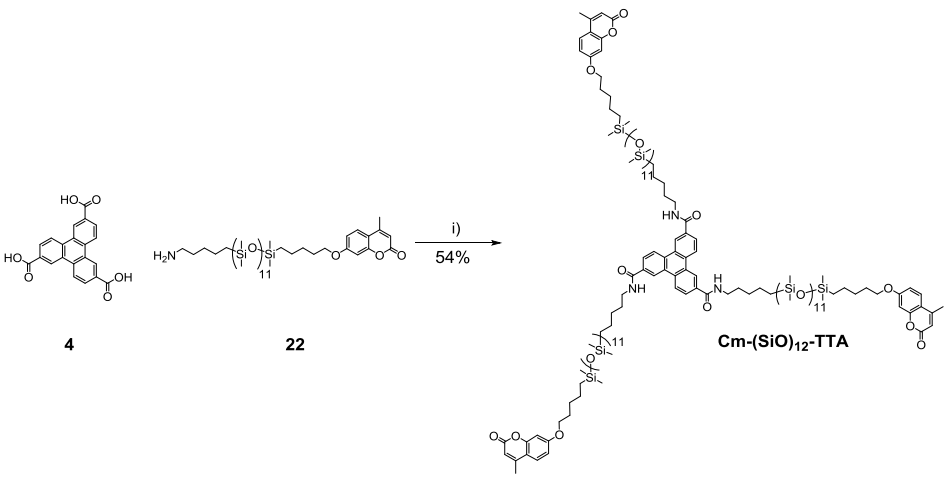


***Scheme 2.8*** *Synthesis of* ***Cm-(SiO)$_{12}$-TTA****. Reagents and conditions: i) TBTU, DIPEA, DMF, 70 °C.*

hydride-terminated dodeca(dimethyl)siloxane-coumarin **19** in 81% after purification via column chromatography. In the final phase of the synthesis, to an open end of dodeca(dimethyl)siloxane brominated alkyl chain was attached and later converted into a primary amine. The former step was achieved through Pt(0)-catalyzed hydrosilylation of 5-bromopent-1-ene with **19** to give bromo-functionalized **20** and through Gabriel synthesis final pentylamine holding coumarin-dodeca(dimethylsiloxane) tail (**22**) was obtained. The first step involving nucleophilic substitution of a phthalimide moiety was achieved with 80% yield. Using pure substrate for reduction of the amine is crucial to facilitate easy purification in the last step. Therefore, prior to the final reduction, **21** was purified via column chromatography. The last step involved reduction with hydrazine in ethanol at 80 °C. Aqueous work up resulted in isolation of **22** with 96% yield. The structure of **22** was confirmed by $^{1}$H NMR and MALDI-TOF-MS. $^{1}$H NMR spectrum of **22** shows signal characteristic for coumarin core, as well as for aliphatic and oDMS chains. MALDI-TOF was recorded with 2-[(2E)-3-(4-tert-butylphenyl)-2-methylprop-2-enylidene]malononitrile (DCTB) as a matrix and showed a single signal corresponding to $[M+184.1]^{+}$. Such behavior is consistent with the literature; it was previously shown that multiple amine derivatives show affinity towards adduct formation with the DCTB matrix.[55] Eventually, starting from 400 mg of hydroxycoumarin **15** we obtained 200 mg of final amine **22**. We produced 500 mg of intermediate **17** and used only 250 mg in the next step to keep remaining 250 mg as potential scaffold for further elongation of the oligodimethylsiloxane chain. In this way, we show that the synthetic route, despite number of steps, is scalable, robust and in this manner asymmetrically functionalized, discrete siloxanes can be synthesized with excellent yields, opening new possibilities in molecular engineering.

Finally, amine **22** was attached to the TTA core via TBTU amide coupling (Scheme 2.8). Triphenylene-2,6,10-tricarboxylic acid was dissolved in dry DMF at 70 °C. Subsequent addition

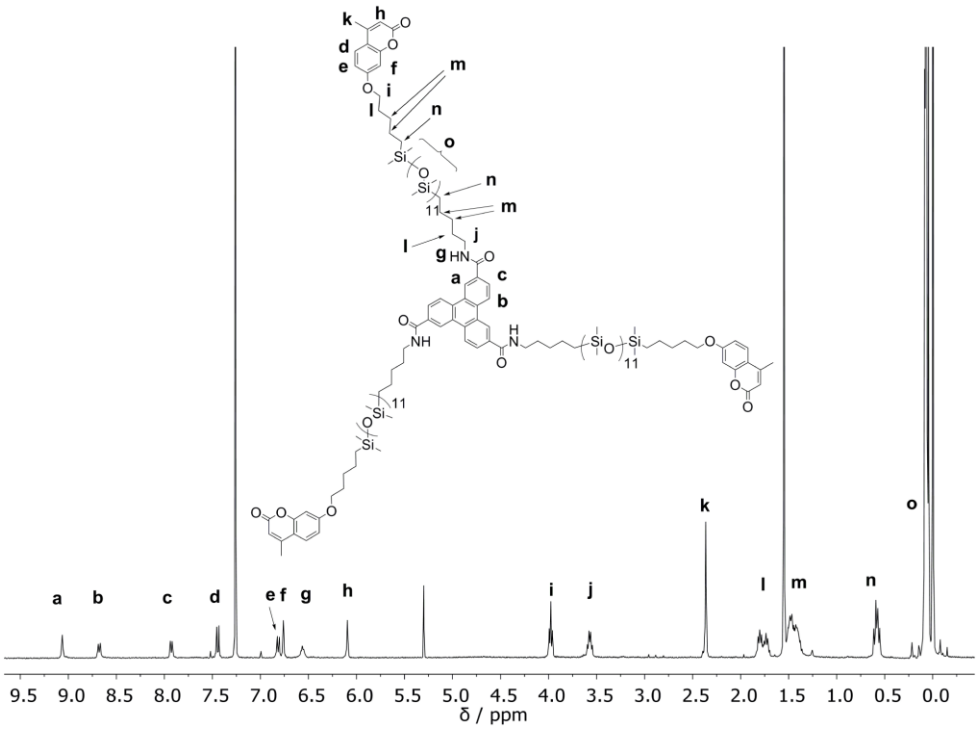


***Figure 2.3*** *$^{1}$H NMR spectrum of* ***Cm-(SiO)$_{12}$-TTA*** *($CDCl_3$, 400 MHz).*

of TBTU and DIPEA yielded the formation of the activated ester and upon addition of the amine **22**, conversion to **Cm-(SiO)$_{12}$-TTA** was achieved. The final product was obtained after aqueous work-up, followed by column chromatography in 54% yield. The structure and purity were confirmed by FT-IR, $^{1}$H, $^{13}$C NMR, MALDI-TOF-MS.. The $^{1}$H NMR spectrum of **Cm-(SiO)$_{12}$-TTA** shows 15 distinct groups of signals, with a high degree of similarity to previously discussed **(SiO)$_x$-TTA** and amine precursor **22** (Figure 2.3). Signals **a-c** and **g** belong to the protons of the aromatic core and the amide, respectively. No aggregation was observed as sharp peaks with clear multiplicity are visible. The chemical shifts and coupling constants of these protons remained unaffected by different amide substituents ($J_{ab}$ = 8.8 Hz). Similarly, protons attached to the coumarin system **d**-**f** and **h** showed no or very little changes in chemical shifts in comparison to the spectrum of **22**. The chemical shifts of the aliphatic protons adjacent to the ether and amide groups also remained virtually the same (3.98 ppm and 3.57 ppm, respectively). The methyl protons at the coumarin moiety **k** were shifted downfield to 2.36 ppm and lost their clear doublet multiplicity. Importantly, protons **o** are attached to the oDMS chains. MALDI-TOF shows a peak corresponding to the $Na^+$ adduct of the product. The FT-IR spectrum confirms the conversion of the TCTA (lack of the COOH $\upsilon_{O-H}$ vibration) to the amide by the presence of the functional groups: amide ($\upsilon_{N-H}$ = 3243 cm$^{-1}$ and

amide II = 1554 $cm^{-1}$), as well as triphenylene core and coumarin moiety: ($\upsilon_{C_{ar}-H}$ = 3075 $cm^{-1}$, $\upsilon_{C=C}$ = 1615 $cm^{-1}$), lactone ($\upsilon_{C=O}$ = 1733 $cm^{-1}$) and oDMS ($\upsilon_{Si-C}$ = 1257 $cm^{-1}$ and $\upsilon_{Si-O}$ = 1013 $cm^{-1}$).

## 2.3. Characterization of TTA derivatives in the solid state

In the following section, the organization of the TTA derivatives in the solid state is evaluated using IR spectroscopy. In addition, the thermal behavior of all derivatives using a combination of polarized optical microscopy (POM) and differential scanning calorimetry (DSC) is discussed. Finally, the morphology of microstructures is evaluated using X-ray scattering. On the basis of the presence of $C_3$ type of symmetry in all TTAs and in the previously studied BTAs, we assume the formation of supramolecular helices based on threefold hydrogen bonding will be favored.[46,56,57] Helical assembly of BTA derivatives is unambiguously confirmed by the presence of the bands at 3240 $cm^{-1}$ ($\upsilon_{N-H}$), 1640 $cm^{-1}$ ($\upsilon_{C=O}$, amide I) and 1560 $cm^{-1}$ (amide II) as combined with X-ray crystallography.[51] By comparing the IR spectrum of $N^1,N^3,N^5$-tris((*S*)-3,7-dimethyloctyl)benzene-1,3,5-tricarboxamide (**(*S*)-BTA**) (Figure 2.4) with that of **(*S*)-TTA** one can see the remarkable similarity in the absorption bands pattern. It is intuitive therefore to assign a helical structure of **(*S*)-TTA** in the solid state.

The IR data of synthesized TTAs are summarized in Table 2.1 and all show absorptions bands in close vicinity of above given vibrations. Therefore, we conclude that all synthesized TTAs assemble in helical fashion through threefold intermolecular hydrogen bonds. **(*S*)-TTA** showed vibrations at 3242 $cm^{-1}$ ($\upsilon_{N-H}$), 1631 $cm^{-1}$ ($\upsilon_{C=O}$) and 1548 $cm^{-1}$ (amide II). Interestingly, absorption bands of ***n*-TTA** are visible at 3244 $cm^{-1}$ ($\upsilon_{N-H}$), 1632 $cm^{-1}$ ($\upsilon_{C=O}$) and 1547 $cm^{-1}$

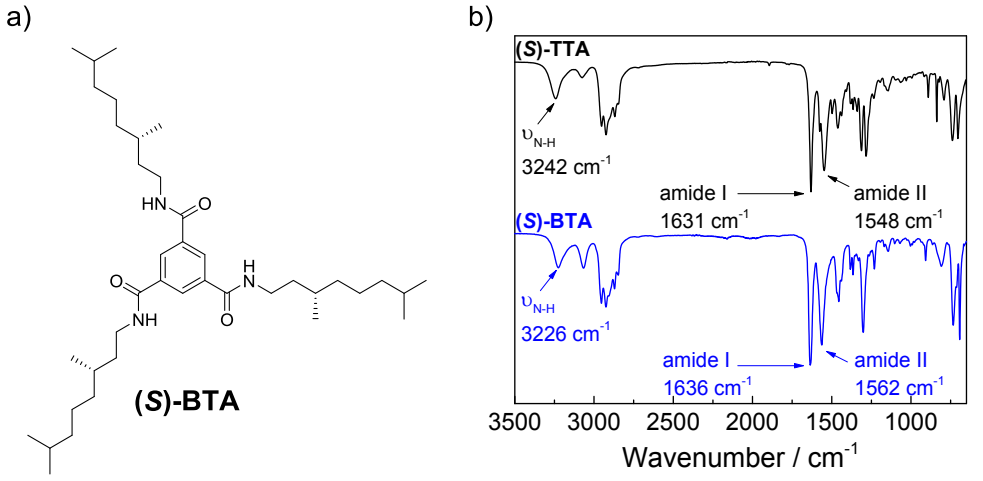


***Figure 2.4*** *a) Chemical structure of (S)-BTA, b) Overlayed IR spectra of (S)-TTA and (S)-BTA with amide absorption bands indicated.*

***Table 2.1*** *Summarized IR spectroscopy data of synthesized TTA derivatives.*

| Compound | Absorption band maximum [$cm^{-1}$] | | |
|---|---|---|---|
| | $\upsilon_{N-H}$ | Amide I | Amide II |
| **(*S*)-TTA** | 3242 | 1631 | 1548 |
| ***n*-TTA** | 3244 | 1632 | 1547 |
| **oEG-TTA** | 3248 | 1632 | 1548 |
| **$(SiO)_7$-TTA** | 3245 | 1635 | 1552 |
| **$(SiO)_{11}$-TTA** | 3245 | 1636 | 1555 |
| **Cm-$(SiO)_{12}$-TTA** | 3243 | not visible | 1554 |
| **(*S*)-BTA** | 3226 | 1636 | 1562 |

(amide II). This suggests that exchange of branched chiral to unbranched achiral side chains have no influence on the molecular packing, which is in contrast to to *$N^1$,$N^3$,$N^5$*-tris(octyl)benzene-1,3,5-tricarboxyamide (***n*-BTA**). The achiral BTA analogue shows a different crystal packing than the chiral **(*S*)-BTA** as evidenced by IR spectroscopy (vibrations at 3300 $cm^{-1}$, 1640 $cm^{-1}$ and 1531 $cm^{-1}$) in the solid state.[46] Therefore extension of the aromatic core significantly stabilizes the helical packing. This stabilization was also observed for **oEG-TTA** which shows vibrations at 3248 $cm^{-1}$ ($\upsilon_{N-H}$), 1632 $cm^{-1}$ (amide I) and 1548 $cm^{-1}$ (amide II). Analogously, IR absorption bands indicating helical structure were observed for both synthesized **$(SiO)_x$-TTA** derivatives. Vibrations assigned to N-H stretching is visible at 3245 $cm^{-1}$ for both derivatives, whereas amide I and amide II bands give maxima at 1635 $cm^{-1}$ and 1552 $cm^{-1}$ (**$(SiO)_7$-TTA**) and 1636 $cm^{-1}$ and 1555 $cm^{-1}$ (**$(SiO)_{11}$-TTA**). The IR spectrum of the last discussed molecule, namely the telechelic **Cm-$(SiO)_{12}$-TTA** also reveals the expected threefold hydrogen bond which is confirmed by the of presence of $\upsilon_{N-H}$ at 3243 $cm^{-1}$ and amide II at 1554 $cm^{-1}$. The amide I band overlaps with a stronger in intensity $\upsilon_{C=C}$ and therefore it is not possible to give the exact value.

Strong hydrogen bonds in alkyl-substituted BTAs were the driving force for the formation of liquid crystalline mesophases.[46] Knowing that threefold hydrogen bonds are also operating in all of the synthesized TTAs, we were interested, how the extension of the aromatic core from benzene to triphenylene would alter the solid state properties. Therefore we characterized the molecules further with use of POM and DSC. **(*S*)-TTA** appeared as a hard and brittle solid, suggesting lack of liquid crystalline properties at room temperature. No thermal transitions were observed by POM and DSC, showing the extraordinary stability of supramolecular structures formed by alkyl-TTAs. Most likely, short aliphatic chain do not have enough conformational freedom, therefore the TTAs remain crystalline. Liquid crystalline properties could be induced in all remaining synthesized TTA derivatives through functionalization of alkyl wedges with oligoethylene glycol (**oEG-TTA**) and oligodimethyl siloxane chains (**$(SiO)_x$-TTA** and **Cm-$(SiO)_{12}$-TTA**). POM micrographs of **$(SiO)_7$-TTA** obtained upon cooling from the isotropic melt showed two different focal textures (Figure 2.5a and b).

First, a LC mesophase appeared at 206 °C and remained unchanged upon further cooling to 149 °C, where transition to another LC mesophase was observed. The texture that appeared at 149 °C remained stable upon cooling to room temperature, indicating columnar packing of the triphenylene core. The thermal behavior of **$(SiO)_{11}$-TTA** was found to be slightly more complex, showing three thermal transitions located close to each other. A higher stability of the mesophase is evidenced by a higher isotropic – mesophase transition temperature, than

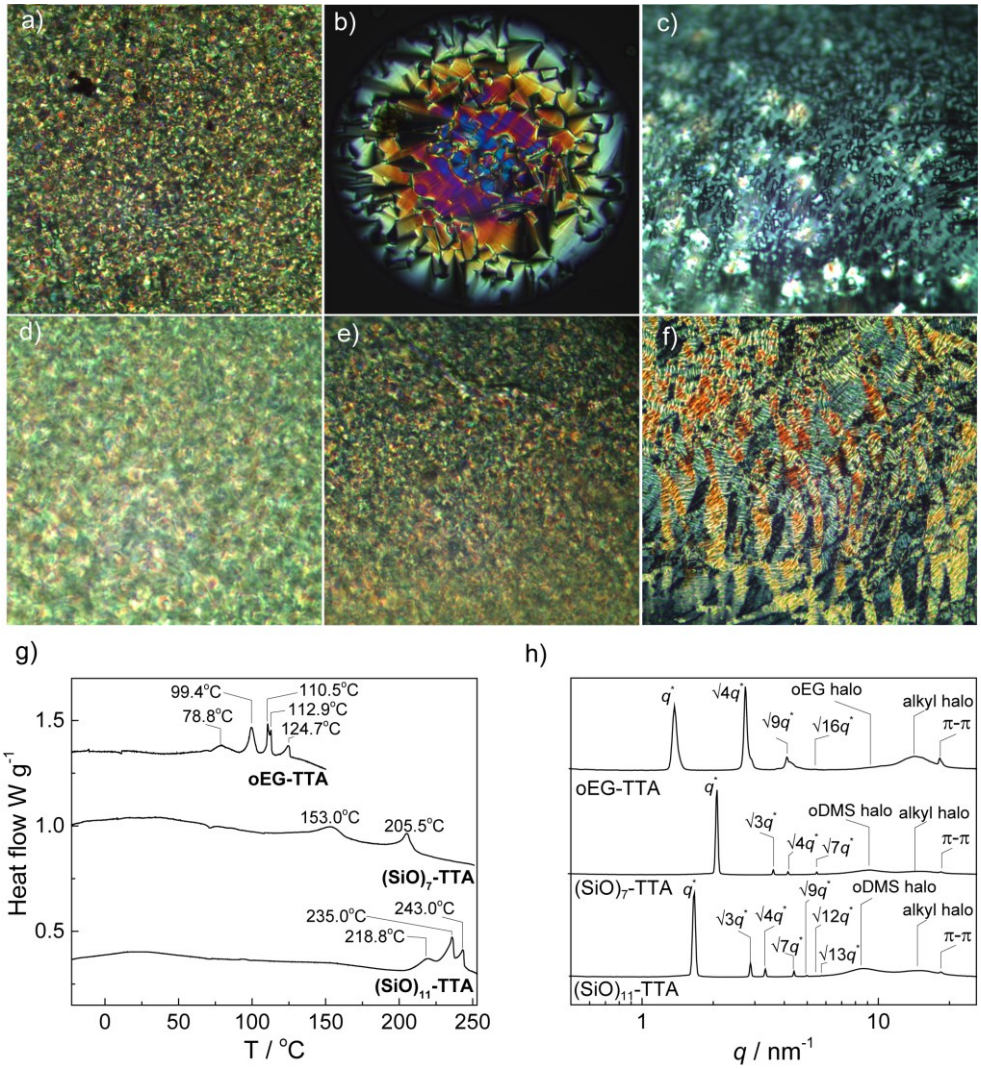


***Figure 2.5*** *POM micrographs of* ***$(SiO)_7$-TTA*** *at a) 205 °C, b) 25 °C;* ***$(SiO)_{11}$-TTA*** *at c) 240 °C, d) 230 °C, e) 25 °C and f)* ***oEG-TTA*** *at 25 °C obtained upon cooling materials from isotropic melt; g) DSC cooling traces (ramp: 10 K min$^{-1}$) and h) Reduced transmission-SAXS data of some TTA derivatives.*

in the case of **(SiO)$_7$-TTA**. This transition appeared at 243 °C and revealed a texture similar to the ones observed for nematic LCs (Figure 2.5c). Upon further cooling to 235 °C a texture characteristic for discotic LCs was obtained (Figure 2.5d). The third transition took place at 219 °C as evidenced by DSC but no visible change in the texture was seen by POM. No more transitions were observed upon cooling further to room temperature, indicating that the formed LC mesophase is stable across a wide temperature range (Figure 2.5e). Interestingly, despite the $C_3$-symmetry, a different POM texture was obtained for **oEG-TTA**, suggesting a different symmetry of packing (Figure 2.5f). A significantly lower stability of the formed mesophase was reflected by the transition to the liquid crystalline state at 125 °C upon cooling the isotropic melt. Further cooling revealed 4 consecutive transitions between 119 °C and 79 °C, which suggests the existence of multiple liquid crystalline mesophases and very narrow regimes in which they operate (Figure 2.5g).

The morphologies of the TTAs were evaluated with the use of SAXS (Figure 2.5h). **(*S*)-TTA** exhibited no long-range order in supramolecular polymers, indicating that to achieve well-organized structures, there must be a balance between ordering and disordering factors. Upon the addition of oDMS or oEG chains, well-defined morphologies were obtained. SAXS of annealed samples of both **(SiO)$_x$-TTA** analogues revealed that columnar hexagonal structure is favored in both cases. The intercolumnar spacing is determined by the length of the alkyl and oDMS chains and was found to be 3.03 nm for **(SiO)$_7$-TTA** and 3.78 nm for **(SiO)$_{11}$-TTA**. As evidenced by the relative intensities of higher-order scattering reflections, a better molecular organization is achieved for the latter analogue, where $1 : \sqrt{3} : \sqrt{4} : \sqrt{7} : \sqrt{9} : \sqrt{12} : \sqrt{13}$ pattern was observed whereas the former one shows only $1 : \sqrt{3} : \sqrt{4} : \sqrt{7}$ pattern. A smaller, in comparison to **oEG-TTA**, interdisc distance (0.34 nm versus 0.35 nm) is in agreement with the stronger hydrogen bonds in **oDMS-TTA** ($\upsilon_{N\text{-}H}$ = 3245 cm$^{-1}$ versus 3248 cm$^{-1}$). Interestingly, an annealed sample of **oEG-TTA** showed a scattering pattern characteristic for lamellar structures with spacings of 4.68 nm, 2.31 nm, 1.54 nm and 1.17 nm that correspond to ratio of spacing $1 : \frac{1}{2} : \frac{1}{3} : \frac{1}{4}$. The intense and sharp reflection at 0.35 nm shows a high regularity of the interdisc distance. This type of organization is unusual for a $C_3$-symmetrical discotic molecule. IR showed that threefold hydrogen bond is present, therefore one can confirm that helically packed triphenylenes are present. Besides lamellar organization, presumably an additional order can be seen, which is evidenced by particularly strong reflection at 2.31 nm and weak reflections visible as shoulders of 1.54 nm reflection. It has been previously reported that triphenylene discotics can self-assemble in lamellar-columnar superstructures with rectangular sub-lattice.[58–60] Also the POM texture obtained upon cooling from the isotropic melt could be assigned to rectangular ordering.[61] All together, the results confirm that the TTA cores are assembled into helical aggregates, which are further organized in layers. Most likely this feature is promoted by the phase segregation between stretched alkyl and oligoethylene glycol chains.

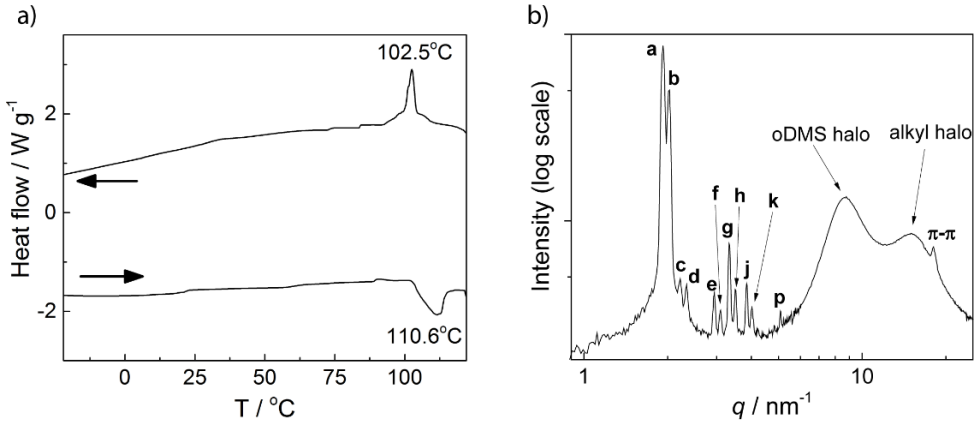


***Figure 2.6*** *a) DSC trace (second heating and cooling runs) of* ***Cm-(SiO)$_{12}$-TTA*** *at 10 K min$^{-1}$ ramp; b) reduced transmission-SAXS data for* ***Cm-(SiO)$_{12}$-TTA***.

On the contrary to the other TTAs, **Cm-(SiO)$_{12}$-TTA** showed one thermal transition at 102 °C as evidenced by DSC (Figure 2.6a). A significantly lower clearing temperature in comparison to both **oDMS-TTA** derivatives indicates that even though no difference in the strength of hydrogen bond was observed by IR, the coumarin units significantly destabilize the mesophase. Despite the simple thermal profile, **Cm-(SiO)$_{12}$-TTA** exhibited a complex phase behavior. As evidenced by SAXS, two distinct phases, each with two different domain spacings, were observed (Figure 2.6b). An annealed sample showed two primary scattering reflections at $q$ = 1.93 nm$^{-1}$ (**a**), and 2.03 nm$^{-1}$ (**b**). Both primary scattering peaks could be attributed to the columnar hexagonal $Col_h$ phases with $d$-spacing of 3.25 nm and 3.09 nm and cubic bicontinuous $Cub_{bi}$ (gyroid) phases. The appearance of a double columnar phase could be rationalized by the fact that two mesogens (triphenylene core and coumarin) units are present in the structure and they are separated by liquid siloxane block, which phase-seggregates from both mesogens. As shown by the IR spectrum, bands characteristic for threefold hydrogen bonded amides are present, which excludes the possibility of co-assembly of triphenylene and coumarin moieties. Such complex coexistence of four structures has not been reported for disc-like molecules. These results show, that it is difficult to predict the exact morphology of systems comprising subunits that significantly differ in their chemical nature.

Eventually we attempted to cross-link previously annealed sample of **Cm-(SiO)$_{12}$-TTA**. Photodimerization of the coumarin units follows the mechanism of 2+2 cycloaddition upon irradiation with the UV light of appropriate energy.[47–49] Hereby we anticipated that triple photodimerization of the coumarin units arms should result in the cross-linked network of the organized columnar assemblies of the TTAs. To realize this strategy, liquid-crystalline **Cm-(SiO)$_{12}$-TTA** was placed on a glass plate and was exposed to UV-A irradiation (λ = 310 – 400 nm) overnight. After irradiation with the UV light, the material became hard and brittle, which

suggested the presence of the cross-linked network. We were not able to dissolve it in any solvent in order to quantify the cross-linking process. Interestingly, SAXS experiments revealed that the complex structure stays unaffected during the cross-linking. The results show that preorganization of the assembly and lateral stabilization of the structure can be achieved via combination of the TTA-based columnar aggregates and the cross-linking via coumarin photodimerization. However, the structural complexity of the molecule results in coexistence of multiple morphologies. In following experiments we will focus on coassembly of **$(SiO)_x$-TTA** and **Cm-$(SiO)_{12}$-TTA** as a possible strategy to favor single supramolecular organization that can be covalently cross-linked.

## 2.4 Conclusions

We have introduced a new supramolecular motif based on a 2,6,10-substituted $C_3$-symmetrical triphenylene core. The key intermediate, triphenylene-2,6,10-tricarboxylic acid, was synthesized in three steps starting from commercially available 4-methylcyclohexanone in good yield. Furthermore, various wedges were attached to the triphenylene core through an amide coupling, leading to a diversity of synthesized materials that can be obtained in a single step (alkyl, oligo(dimethylsiloxane) and oligo(ethylene glycol)). Eventually, we developed a synthetic route for controlled iterative synthesis of two-end asymmetrically substituted oDMS, where one side can be a supramolecular / crosslinking motif (coumarin) and the other is coupling-reactive group (primary amine). At this stage, an oligomer of 12 repeating siloxane units and two $C_5$-alkyl linkers was synthesized. Longer, discrete oligomers with various functionalities can be accessed in this fashion. Coupling of this functional wedge resulted in a telechelic crosslinkable TTAs. Extension of the aromatic core from benzene to triphenylene resulted in reinforced threefold hydrogen bonding. All synthesized materials showed increased stability in comparison to their BTA analogues. Alkyl-substituted TTAs exhibited very strong interactions that hampered the formation of liquid crystalline mesophases, whereas oDMS-substituted TTAs have their clearing temperatures above 200 °C. Lower clearing temperatures together with an unexpected lamellar phase was observed for oligoethyleneglycol-substited TTA. Introduction of another functional unit also resulted in complex phase behavior. The results highlight that predicting stabilities and morphologies of systems comprising subunits that significantly differ in their chemical nature remains a challenge. Following chapters will discuss in detail supramolecular polymerizations of alkyl-TTAs in dilute solutions.

## 2.5 Experimental Section

### 2.5.1 Materials and methods

2-(1-Phenyl-2,5,8,11,14-pentaoxahexacosan-26-yl)isoindoline-1,3-dione (**9**) was synthesized by Jolanda Spiering according to a published procedure.[62] 1-Hydrohepta(dimethylsiloxane) and 1-Hydroundeca(dimethylsiloxane) were synthesized by Bas de Waal according to a published

procedure.[52] All other chemicals were purchased from commercial sources and used without further purification. Dry solvents were obtained with a MBRAUN Solvent Purification System (MB-SPS). Toluene was dried over 4 Å molecular sieves before use. Dried glassware was used for all reactions carried out under argon atmosphere. Reactions were followed by a thin-layer chromatography (TLC) using 60-F254 silica gel plates from Merck and visualized by UV light at 254 and 366 nm and/or stains: potassium permanganate ($KMnO_4$) and iodine. Automated column chromatography was conducted on a Biotage flash chromatography system and Grace Reveleris X2 Flash Chromatography System using 200-425 mesh silica gel (Type 60A Grade 633) and Reveleris silica flash cartridges. Elution gradients are specified in column volumes (CVs). NMR spectra were recorded on Bruker. The standard $^{1}H$ and $^{13}C$ NMR spectra were recorded using Bruker Mercury Vx 400 MHz (100 MHz for $^{13}C$) or Varian Unit Inova 500 MHz (125 MHz for $^{13}C$) NMR spectrometers. Variable temperature (VT) $^{1}H$ NMR spectra were recorded on a Varian Unit Inova 500 MHz NMR. Proton chemical shifts (δ) are reported in ppm downfield from tetramethylsilane (TMS). Carbon chemical shifts are reported using the resonance of $CDCl_3$ as internal standard. Peak multiplicity is abbreviated as s: singlet; d: doublet; t: triplet; p: pentet; hept: heptet; dd: doublet of doublets; m: multiplet; bs: broad singlet. Matrix assisted laser desorption/ionization time-of-flight (MALDI-TOF) mass spectra were obtained on a PerSeptive Biosystems Voyager DE-PRO spectrometer using α-cyano-4-hydroxycinnamic acid (CHCA) or *trans*-2-[3-(4-*tert*-butylphenyl)-2-methyl-2-propenylidene]-malononitrile (DCTB) as matrix. All standard infrared measurements were performed on a Perkin Elmer FT-IR Spectrum Two apparatus. Differential scanning calorimetry (DSC) data were collected on a DSC Q2000 from TA instruments, calibrated with an indium standard. The samples were weighed directly into aluminum pans and hermetically sealed. The presented data are second heating/cooling cycle unless otherwise stated. Polarized Optical Microscopy (POM) samples were placed on glass substrates and imaged using Nikon Xfinity1 Lumenera microscope with 10X magnification at room temperature. Bulk small-angle X-ray scattering (SAXS) was recorded on a Ganesha Lab instrument. The flight tube and sample holder were all under vacuum in a single housing, with a GeniX-Cu ultra-low divergence X-ray generator. The source produces X-rays with a wavelength (λ) of 0.154 nm and a flux of $1 \times 10^8$ ph $s^{-1}$. Samples were measured in glass capillaries. Scattered X-rays were captured on a 2-dimensional Pilatus 300K detector with 487 × 619 pixel resolution. Samples were measured in MAXS mode for 1200 seconds and WAXS mode for 300 seconds. The sample-to-detector distance was 0.084 m (WAXS mode) or 0.431 m (MAXS mode). The instrument was calibrated with diffraction patterns from silver behenate. The raw data files were calibrated and reduced to 1-D data with SAXSGui software provided by JJ X-Ray Systems ApS. MAXS and WAXS regions were merged into a single data file using the SAXS utilities software package provided by Michael Sztucki.

### 2.5.2 Synthetic procedures

Synthesis of triphenylene-2,6,10-tricarboxylic acid (**4**)[41,42]

*2,6,10-Trimethyldodecahydrotriphenylene* (**2**)[41,42]

4-Methylcyclohexanone (50 g, 450 mmol) was placed in a round-bottom flask equipped with a magnetic stirrer and a reflux condenser. Then $ZrCl_4$ (4 g, 20 mmol) was added and the mixture was stirred at 170 °C for 5 hours. The progress was monitored by TLC (heptane / EtOAc 9:1). On completion the reaction mixture was cooled down to room temperature. The resulting solid was redissolved in hot $CHCl_3$ (400 mL) and insoluble residue was filtered off at elevated temperature. The filtrate was concentrated under reduced

pressure to yield 41 g of orange solid. The product was recrystallized from *n*-butanol to yield 19.2 g of white crystals. The mother liquor was collected and concentrated under reduced pressure to give 18 g of a brown solid, which was divided into 2 parts of 9 grams and subjected to flash column chromatography using eluent gradient heptane – heptane / EtOAc 9:1. The resulting product was recrystallized from *n*-butanol and combined with previously recrystallized fraction to give 19.7 g of the title compound (47%). $^{1}$H NMR (400 MHz, $CDCl_3$): δ (ppm) = 2.82 (m, 3H); 2.74-2.43 (m, 6H); 2.22 – 2.01 (m, 3H); 1.93 (m, 3H); 1.77 (m, 3H); 1.35 (m, 3H); 1.11 (m, 9H). $^{13}$C NMR (100 MHz, $CDCl_3$): δ = *sym*: 132.52; 132.12; 36.16; 31.54; 29.21; 27.55; 22.66; *dissym*: 132.56; 132.30; 132.24; 132.23; 132.05; 132.02; 35.98; 35.50; 35.24; 31.41; 31.37; 30.94; 29.09; 28.94; 28;56; 27.28; 26.68; 26.07; 22.45; 22.41; 21.84.

*2,6,10-Trimethyltriphenylene* (**3**)[41,42]

2,6,10-Trimethyldodecahydrotriphenylene (3.5 g, 12 mmol) (**1**) and triglyme (35 mL) were placed in a round-bottom flask equipped with magnetic stirrer and reflux condenser. The resulting suspension was bubbled with argon for 15 minutes and then Pd/C (0.35 g) was added. Then the reaction mixture was heated up to 220 °C and stirred at this temperature overnight. Progress was monitored by TLC (heptane / EtOAc 9:1). The resulting mixture was cooled down to room temperature, diluted with $CHCl_3$ (100 mL) and heated up to reflux. The hot solution was filtered off through a celite pad, which was washed with hot chloroform until the filtrate contained no more product (checked by spotting a drop of filtrate on a TLC plate and visualizing the spot under UV light). The combined filtrates were concentrated *in vacuo* to yield an orange liquid which was placed in a fridge over the weekend to crystallize. The title compound was filtered off to give 2.28 g of white crystals (68%). $^{1}$H NMR (400 MHz, $CDCl_3$): δ (ppm) = 8.52 (d, *J* = 8.4 Hz, 3H); 8.40 (s, 3H); 7.44 (d, *J* = 8.4 Hz, 3H); 2.61 (s, 9H).

*Triphenylene-2,6,10-tricarboxylic acid* (**4**)[41]

In a 15 ml stainless steel reactor equipped with cross-shaped stirring bar, $Na_2Cr_2O_7$ (1.6 g, 3.9 mmol) was dissolved in water (6 mL) and the solution was vigorously stirred. Then 0.3 g (0.8 mmol) of 2,6,10-trimethyltriphenylene (**3**) was added in portions in order to create a well-stirred, homogeneous suspension. The suspension was stirred for 5 minutes and then tightly sealed. The reactor was then heated up in an oil bath with vigorous stirring to 250 °C and stirred at this temperature for 60 h. On completion the reaction mixture was cooled down to room temperature. The resulting green suspension was filtered off to give a yellow filtrate which was acidified with concentrated HCl. The formed precipitate was filtered off, washed with water until the filtrate had a neutral pH and dried in vacuum to yield triphenylene-2,6,10-tricarboxylic acid as yellow solid (0.25 g, 63%). FT-IR: $\tilde{\upsilon}_{max}$= 3010 ($\upsilon_{O-H}$, m, br); 1679 ($\upsilon_{C=O}$, s); 1614 ($\upsilon_{C=C}$, s); 1420 ($\delta_{O-H}$, m).

Synthesis of chiral (*S*)/(*R*)-3,7-dimethyloctylamine ***(S)/(R)*-5**[50]

*(S)-3,7-Dimethyloctan-1-ol*[50]

In the 500 mL Parr vessel (*S*)-3,7-dimethyloct-6-en-1-ol (150 g, 960 mmol) was dissolved in ethyl acetate (30 mL). The mixture was bubbled with argon for 10 minutes. Then Pd/C (1.5 g) was added to the mixture. The reactor was installed in Parr apparatus, filled with hydrogen and shaken until no more hydrogen consumption was observed. On completion the reaction mixture was filtered through celite, concentrated in vacuo and dried under high-vacuum to yield 152 g of (*S*)-3,7-dimethyloctan-1-ol (100%). $^{1}$H NMR (400

MHz, $CDCl_3$): δ (ppm) = 3.68 (m, 2H), 1.65 - 1.10 (m, 8H), 1.18 – 1.08 (m, 3H), 0.89 (d, *J* = 6.6 Hz, 3H), 0.86 (d, *J* = 6.6 Hz, 6H).

*(R)-3,7-Dimethyloctan-1-ol*[50]

In a round-bottom flask, (*R*)-3,7-dimethyloct-6-en-1-ol (3 g, 19.2 mmol) was dissolved in ethyl acetate (9 mL). The mixture was bubbled with argon for 10 minutes. Then Pd/C (0.1 g) was added to the mixture. The flask was then evacuated three times and refilled with hydrogen. Progress was monitored by TLC (*n*-heptane / EtOAc 1:1). On completion the reaction mixture was filtered through celite, concentrated *in vacuo* and dried under high-vacuum to yield 3 g of (*R*)-3,7-dimethyloctan-1-ol (100%). $^1$H NMR (400 MHz, $CDCl_3$): δ (ppm) = 3.68 (m, 2H), 1.65 - 1.10 (m, 8H), 1.18 – 1.08 (m, 3H), 0.89 (d, *J* = 6.6 Hz, 3H), 0.86 (d, *J* = 6.6 Hz, 6H).

*(S)-3,7-Dimethyloctyl 4-methylbenzenesulfonate*[50]

(*S*)-3,7-Dimethyloctan-1-ol (152 g, 960 mmol) and 4-methylbenzene-1-sulfonyl chloride (182 g, 960 mmol) were dissolved in dry dichloromethane (350 mL) and the solution was cooled down to 0 °C. Then pyridine (165 mL, 2 mol) was added dropwise and the mixture was stirred at 0 °C for another 30 minutes. Then the mixture was warmed up to room temperature and stirred overnight. The progress was monitored by TLC (*n*-heptane / EtOAc 1:1). Full conversion was observed after 24 hours. On completion the mixture was diluted with 800 mL of DCM and moved to a separatory funnel with 500 mL of 2 M HCl. The organic layer was washed then with 2 M NaOH, water and brine, dried over magnesium sulfate and filtered off. The solvent was removed under reduced pressure to give the title compound as orange oil (256 g, 80%). $^1$H NMR (400 MHz, $CDCl_3$): δ (ppm) = 7.79 (d, *J* = 8.3 Hz, 2H), 7.35 (d, *J* = 8.3 Hz, 2H), 4.06 (m, 2H), 2.45 (s, 3H), 1.70 – 1.05 (m, 10H) 0.84 (d, *J* = 6.6 Hz, 6H), 0.80 (d, *J* = 6.5 Hz, 3H).

*(R)-3,7-Dimethyloctyl 4-methylsulfonate*

(*R*)-3,7-Dimethyloctan-1-ol (3 g, 19.2 mmol) and methanesulfonyl chloride (2.6 g, 22.7 mmol) were dissolved in dry dichloromethane (30 mL) and the solution was cooled down to 0 °C. Then pyridine (3 mL, 37.9 mmol) was added dropwise and the mixure was stirred at 0 °C for another 30 minutes. Then the mixture was warmed up to room temperature and stirred overnight. The progress was monitored by TLC (*n*-heptane / EtOAc 1:1). Full conversion was observed after 24 hours. On completion the mixture was diluted with 60 mL of DCM and moved to a separatory funnel with 100 mL of 1 M HCl. Organic layer was washed then with 1 M NaOH, water and brine. The organic phase was dried over magnesium sulfate and filtered off. The solvent was removed under reduced pressure to give the title compound as orange oil (2.63 g, 60%). $^1$H NMR (400 MHz, $CDCl_3$): δ (ppm) = 7.79 (d, *J* = 8.3 Hz, 2H), 7.35 (d, *J* = 8.3 Hz, 2H), 4.06 (m, 2H), 2.45 (s, 3H), 1.70 – 1.05 (m, 10H) 0.84 (d, *J* = 6.6 Hz, 6H), 0.80 (d, *J* = 6.5 Hz, 3H).

*(S)-1-Azido-3,7-dimethyloctane*[50]

(*S*)-3,7-Dimethyloctyl 4-methylbenzenesulfonate (256 g, 819 mmol) was dissolved in DMF (550 mL). Then sodium azide (80 g, 1.2 mol) and potassium iodide (1.5 g, 8.2 mmol) were added and the mixture was stirred overnight at 50 °C. After full conversion was achieved (TLC: heptane / EtOAc 4:1), the reaction mixture was moved to a separatory funnel and washed with water (1 L). Upper phase was collected. The lower aqueous layer was basified with saturated $NaHCO_3$ to pH 10 and extracted with *n*-hexane until no more product was in the organic phase (4 x 700 ml of hexane). Then the combined organic layers were

washed with water, dried over magnesium sulfate and filtered. The organic solvent was removed *in vacuo* to give the (*S*)-1-azido-3,7-dimethyloctane (145 g, 97%). $^1$H NMR (400 MHz, $CDCl_3$): δ (ppm) = 3.30 (m, 2H), 1.67 – 1.10 (m, 10H), 0.90 (d, *J* = 6.6 Hz, 3H), 0.87 (d, *J* = 6.6 Hz, 6H).

*(R)-1-Azido-3,7-dimethyloctane*[50]

(*R*)-3,7-Dimethyloctyl 4-methylbenzenesulfonate (2.6 g, 14 mmol) was dissolved in DMF (4 mL). Then sodium azide (1.5 g, 22.7 mmol) and potassium iodide (0.16 g, 0.9 mmol) were added and the mixture was stirred overnight at 50 °C. After full conversion was achieved (TLC: heptane / EtOAc 4:1), the reaction mixture was moved to a separatory funnel and washed with water (10 mL). The upper phase was collected. The lower aqueous layer was basified with saturated $NaHCO_3$ to pH 10 and extracted with *n*-hexane until no more product was in the organic phase (3x 30 mL of hexane). Then the combined organic layers were washed with water, dried over magnesium sulfate and filtered. The organic solvent was removed *in vacuo* to give the (*R*)-1-azido-3,7-dimethyloctane (2.5 g, 95%). $^1$H NMR (400 MHz, $CDCl_3$): δ (ppm) = 3.30 (m, 2H), 1.67 – 1.10 (m, 10H), 0.90 (d, *J* = 6.6 Hz, 3H), 0.87 (d, *J* = 6.6 Hz, 6H).

*(S)-3,7-Dimethyloctan-1-amine* (***S*-5**)[50]

(*S*)-1-Azido-3,7-dimethyloctane (145 g, 791 mmol) was dissolved in THF (750 mL) and the resulting mixture was cooled down to 0 °C. Triphenylphosphine (218 g, 831 mmol) and water (21 mL, 1.2 mol) were added and the mixture was allowed to slowly warm up to 10 °C. Upon warming up to 10 °C the evolution of nitrogen gas was observed. Once no more gas was observed, the mixture was warmed to room temperature and stirred overnight. The progress was monitored by TLC (*n*-heptane / EtOAc 9:1). On completion the solvent was removed under reduced pressure, the white solid was triturated with *n*-pentane and washed until no product was observed in the filtrate (10 x 500 mL). Then the filtrate was concentrated to give an orange oil as the crude product. The title compound was isolated by vacuum distillation (bp: 51 °C, $2.5 \times 10^{-1}$ Torr) to yield 100 g (80%) of colorless liquid. $^1$H NMR (400 MHz, $CDCl_3$): δ (ppm) = 2.70 (m, 2H), 1.58 – 1.40 (m, 3H), 1.33 – 1.08 (m, 7H), 0.87 – 0.84 (m, 9H).

*(R)-3,7-Dimethyloctan-1-amine* (***R*-5**)[50]

(*R*)-1-Azido-3,7-dimethyloctane (2.5 g, 13.6 mmol) was dissolved in THF (10 mL) and the resulting mixture was cooled down to 0 °C. Triphenylphosphine (4.3 g, 16.4 mmol) and water (3 mL, 20.4 mmol) were added and the mixture was warmed to room temperature and stirred overnight. The progress was monitored by TLC (*n*-heptane / EtOAc 9:1). On completion the solvent was removed under reduced pressure, the white solid was triturated with *n*-pentane and washed until no product was observed in the filtrate (5 x 30 mL). Then the filtrate was concentrated to give an orange oil as the crude product. The title compound was isolated by vacuum distillation (bp: 51 °C, $2.5 \times 10^{-1}$ Torr) to yield 1.53 g (71%) of colorless liquid. $^1$H NMR (400 MHz, $CDCl_3$): δ (ppm) = 2.70 (m, 2H), 1.58 – 1.40 (m, 3H), 1.33 – 1.08 (m, 7H), 0.87 – 0.84 (m, 9H).

Synthesis of trisalkylated-TTAs (**(*S*), (*R*) and *n*-TTA**)

*N*$^2$,*N*$^6$,*N*$^{10}$-Tris((*S*)-3,7-dimethyloctyl)triphenylene-2,6,10-tricarboxamide (**(*S*)-TTA**)

Triphenylene-2,6,10-tricarboxylic acid (**4**) (0.05 g, 0.14 mmol) was dissolved in 0.5 mL of dry DMF at 70 °C under argon atmosphere. Then TBTU (0.147 g, 0.46 mmol) dissolved in 0.5 mL of DMF was added. Subsequently, DIPEA (0.145 ml, 0.83 mmol) followed by 0.07 g (0.44 mmol) of (*S*)-3,7-dimethyloctan-1-amine (***S*-5**) was added and the mixture was stirred for 30 minutes at 70 °C and

then let to cool down to room temperature. The resulting yellow solution was diluted with 100 mL of $CHCl_3$ and washed with water (50 mL), 1 M HCl (50 mL), 1 M NaOH (50 mL), water (50 mL) and brine (50 mL). The organic phase was then dried over magnesium sulfate, the drying agent was filtered off and crude compound was obtained by removing the solvent under reduced pressure. The title compound was isolated by precipitation from methanol to give 0.080 g of white solid with 74% yield. $^1$H NMR (500 MHz, DMF-$d_7$): δ (ppm) = 9.46 (s, 3H); 9.05 (d, *J* = 8.8 Hz, 3H); 8.90 (t, *J* = 7 Hz, 3H); 8.37 (d, *J* = 8.8 Hz, 3H); 3.55 (m, 6H); 1.76 (m, 3H); 1.62 (m, 3H); 1.52 (m, 6H); 1.34 (m, 9H); 1.19 (m, 9H); 0.99 (d, *J* = 6.4 Hz, 9H); 0.86 (d, *J* = 7 Hz, 18H). $^{13}$C NMR (125 MHz, DMF-$d_7$): δ = 167.02, 135.28, 133.07, 130.11, 128.15, 125.13, 123.98, 40.21, 38.17, 37.78, 28.88, 25.63, 23.33, 23.26, 20.34. FT-IR: $\tilde{\upsilon}_{max}$= 3242 ($\upsilon_{N\text{-}H}$, m); 1631 (amide I, s); 1548 (amide II, s). MS (MALDI-TOF): *m/z* calcd for $C_{51}H_{75}N_3O_3$ [M+H] = 778.58 found: 778.59.

$N^2$,$N^6$,$N^{10}$-Tris((*R*)-3,7-dimethyloctyl)triphenylene-2,6,10-tricarboxamide (**(*R*)-TTA**)

Triphenylene-2,6,10-tricarboxylic acid (**4**) (0.05 g, 0.14 mmol) was dissolved in 0.5 mL of dry DMF at 70°C under argon atmosphere. Then TBTU (0.147 g, 0.46 mmol) dissolved in 0.5 mL of DMF was added. Subsequently, DIPEA (0.145 ml, 0.83 mmol) followed by 0.07 g (0.44 mmol) of (*R*)-3,7-dimethyloctan-1-amine (***R*-5**) was added and the mixture was stirred for 30 minutes at 70 °C and then let to cool down to room temperature. The resulting yellow solution was diluted with 100 mL of $CHCl_3$ and washed with water (50 mL), 1 M HCl (50 mL), 1 M NaOH (50 mL), water (50 mL) and brine (50 mL). Organic phase was then dried over magnesium sulfate, drying agent was filtered off and crude compound was obtained up removing the solvent under reduced pressure. The title compound was isolated by precipitation from methanol to give 0.051 g of white solid with 47% yield. $^1$H NMR (500 MHz, DMF-$d_7$): δ (ppm) = 9.46 (s, 3H); 9.05 (d, *J* = 8.8 Hz, 3H); 8.90 (t, *J* = 7 Hz, 3H); 8.37 (d, *J* = 8.8 Hz, 3H); 3.55 (m, 6H); 1.76 (m, 3H); 1.62 (m, 3H); 1.52 (m, 6H); 1.34 (m, 9H); 1.19 (m, 9H); 0.99 (d, *J* = 6.4 Hz, 9H); 0.86 (d, *J* = 7 Hz, 18H). $^{13}$C NMR (125 MHz, DMF-$d_7$): δ = 167.02, 135.28, 133.07, 130.11, 128.15, 125.13, 123.98, 40.21, 38.17, 37.78, 28.88, 25.63, 23.33, 23.26, 20.34. FT-IR: $\tilde{\upsilon}_{max}$= 3242 ($\upsilon_{N\text{-}H}$, m); 1631 (amide I, s); 1548 (amide II, s). MS (MALDI-TOF): *m/z* calcd for $C_{51}H_{75}N_3O_3$ [M+H] = 778.58 found: 778.59.

$N^2$,$N^6$,$N^{10}$-Trioctyltriphenylene-2,6,10-tricarboxamide (***n*-TTA**)

Triphenylene-2,6,10-tricarboxylic acid (**4**) (0.05 g, 0.14 mmol) was dissolved in 0.5 mL of dry DMF at 70 °C under argon atmosphere. Then TBTU (0.147 g, 0.46 mmol) dissolved in 0.5 mL of DMF was added. Subsequently, DIPEA (0.145 mL, 0.83 mmol) followed by 0.057 g (0.44 mmol) of *n*-octylamine was added and the mixture was stirred for 30 minutes at 70 °C and then let to cool down to room temperature. The resulting yellow solution was diluted with 100 mL of $CHCl_3$ and washed with water (50 mL), 1 M HCl (50 mL), 1 M NaOH (50 mL), water (50 mL) and brine (50 mL). The organic phase was then dried over magnesium sulfate, drying agent was filtered off and crude compound was obtained up removing the solvent under reduced pressure. The title compound was isolated by precipitation from methanol to give 0.060 g of white solid with 62% yield. $^1$H NMR (500 MHz, DMF-$d_7$): δ (ppm) = 9.45 (s, 3H); 9.04 (d, *J* = 8.8 Hz, 3H); 8.95 (t, *J* = 5.5 Hz, 3H); 8.36 (d, *J* = 8.8 Hz, 3H); 3.50 (m, 6H); 1.69 (m, 6H); 1.43 (m, 6H); 1.38 – 1.22 (m, 24H); 0.87 (t, *J* = 7 Hz, 9H). $^{13}$C NMR (125 MHz, DMF-$d_7$): δ = 167.00, 135.21, 133.05, 130.08, 128.12, 125.11, 123.96, 40.89, 40.77, 32.76, 30.67, 30.21, 28.07, 23.51, 14.66. FT-IR: $\tilde{\upsilon}_{max}$= 3244 ($\upsilon_{N\text{-}H}$, m); 1632 (amide I, s); 1547 (amide II, s). MS (MALDI-TOF): *m/z* calcd for $C_{45}H_{63}N_3O_3$ [M+H] = 694.49; found: 694.49.

Synthesis of oligoethyleneglycol-functionalized TTA (**oEG-TTA**).

*1-Phenyl-2,5,8,11,14-pentaoxahexacosan-26-amine* (**7**)[62]

2-(1-Phenyl-2,5,8,11,14-pentaoxahexacosan-26-yl)isoindoline-1,3-dione (**6**) (0.3 g, 0.5 mmol) was dissolved in 4 mL of EtOH. Hydrazine monohydrate (0.25 mL, 5 mmol) was added and the mixture was stirred at 75 °C. After 1 hour the reaction mixture was cooled down to room temperature and diluted with EtOAc (50 mL). The resulting solution was washed with 50 mL of sat. $NaHCO_3$, 2 x 50 mL of 1 M NaOH, 50 mL of water, 50 mL of brine, dried over magnesium sulfate and solvent removed *in vacuo* to yield title compound (0.226 g, 96%) as colorless oil that crystallizes at room temperature. $^1$H NMR (400 MHz, $CDCl_3$): δ (ppm) = 7.34 – 7.28 (m, 5H), 4.58 (s, 2H), 3.71 – 3.63 (m, 14H), 3.58 (m, 2H); 3.45 (t, *J* = 5.6 Hz, 2H); 2.69 (t, *J* = 5.6 Hz, 2H); 1.60 (m, 2H); 1.44 (m, 2H); 1.29 (m, 16H).

*$N^2$,$N^6$,$N^{10}$-Tris(1-phenyl-2,5,8,11,14-pentaoxahexacosan-26-yl)triphenylene-2,6,10-tricarboxamide* (**8**)

Triphenylene-2,6,10-tricarboxylic acid (**4**) (0.04 g, 0.11 mmol) was dissolved in 0.5 mL of dry DMF at 70 °C under argon atmosphere. Then TBTU (0.124 g, 0.39 mmol) dissolved in 0.5 mL of DMF was added. Subsequently, DIPEA (0.1 mL, 0.67 mmol) followed by 0.18 g (0.39 mmol) of oEG-amine **7** was added and the mixture was stirred for 30 minutes at 70 °C and then let to cool down to room temperature. The resulting yellow solution was diluted with 50 mL of $CHCl_3$ and washed with water (30 mL), 1 M HCl (30 mL), 1 M NaOH (30 mL), water (30 mL) and brine (30 mL). The organic phase was then dried over magnesium sulfate, the drying agent was filtered off and the crude compound was obtained after removing the solvent under reduced pressure. The title compound was isolated by column chromatography using gradient $CHCl_3$ to $CHCl_3$ / EtOAc 7:3 vol/vol (0.07 g, 37%). $^1$H NMR (400 MHz, acetone-$d_6$): δ (ppm) = 9.15 (s, 3H); 8.74 (d, *J* = 8.8 Hz, 3H); 8.24 (t, *J* = 6 Hz, 3H); 8.18 (d, *J* = 8.8 Hz, 3H); 7.36 – 7.22 (m, 15H); 4.52 (s, 6H); 3.64 – 3.45 (m, 50H); 3.37 (t, *J* = 6.8 Hz, 6H); 1.72 (m, 6H); 1.48 (m, 9H); 1.43 – 1.24 (m, 45H).

*$N^2$,$N^6$,$N^{10}$-Tris(1-hydroxy-3,6,9,12-tetraoxatetracosan-24-yl)triphenylene-2,6,10-tricarboxamide* (**oEG-TTA**)

Benzyl-protected oEG-TTA **8** (0.07 g, 0.04 mmol) was dissolved in a mixture of 1 mL of EtOAc and 0.5 mL of MeOH. Solution was bubbled with argon for 15 minutes and then Pd/C (0.005 g) was added. Then reaction vessel was evacuated three times and refilled with argon. After the last evacuation, the reaction vessel was refilled with hydrogen and stirred under hydrogen atmosphere for 2 hours. On completion, reaction mixture was filtered through a celite pad and then the solvent was removed under reduced pressure. The title compound was isolated by column chromatography using gradient $CHCl_3$ to $CHCl_3$ / EtOAc 7:3 vol/vol affording 0.03 g of colorless paste (51%). $^1$H NMR (400 MHz, acetone-$d_6$): δ (ppm) = 9.24 (s, 3H); 8.84 (d, *J* = 8.8 Hz, 3H); 8.24 (m, 6H); 3.64 – 3.47 (m, 50H); 3.38 (t, *J* = 6.8 Hz, 6H); 1.72 (m, 6H); 1.48 (m, 9H); 1.43 – 1.24 (m, 45H). $^{13}$C NMR (100 MHz, acetone-$d_6$): δ = 168.15, 134.47, 131.80, 128.84, 126.84, 123.55, 123.00, 73.55, 71.74, 71.25, 71.23, 71.10, 70.86, 61.91, 40.75, 30.56, 30.47, 30.31, 27.93, 26.96. FT-IR: $\tilde{\upsilon}_{max}$= 3428 ($\upsilon_{O-H}$, m, br); 3248 ($\upsilon_{N-H}$, m); 1632 (amide I, s); 1548 (amide II, s). MS (MALDI-TOF): *m/z* calcd for $C_{81}H_{135}N_3O_{18}$ [M+Na] = 1461.96; found: 1461.80.

*Synthesis of oDMS-functionalized alkyl amines (**11a** and **11b**).*

*1-(5-Bromopentyl)-hepta(dimethylsiloxane)* (**9a**)

5-Bromopent-1-ene (0.11 g, 0.74 mmol) and 1-hydrohepta(dimethylsiloxane) (0.35 g, 0.67 mmol) were dissolved in 2 mL of DCM and then a drop of Karstedt catalyst solution in xylene was added. The resulting mixture was stirred for 1 hour. The progress was monitored by $^1$H NMR (disappearance of C*H*=C*H*$_2$ protons). On completion, title compound was isolated by removal of a solvent followed by three times coevaporation of added toluene and drying in vacuum (0.415 g, 92%). $^1$H NMR (400 MHz, $CDCl_3$): δ (ppm) = 3.40 (t, *J*= 6.9 Hz, 2H), 1.86 (dt, *J* = 14.5, 6.9 Hz, 2H), 1.51 – 1.30 (m, 4H), 0.60 – 0.50 (m, 2H), 0.15 – 0.02 (m, 45H).

*1-(10-Bromodecyl)-undeca(dimethylsiloxane)* (**9b**)

10-Bromodec-1-ene (0.2 g, 0.91 mmol) and 1-hydroundeca(dimethylsiloxane) (0.74g, 0.90 mmol) were dissolved in toluene and then a drop of Karstedt catalyst solution in xylene was added. The resulting mixture was stirred for 1 hour. The progress was monitored by $^1$H NMR (disappearance of Si-*H* protons). On completion, the solvent was removed under reduced pressure and crude product was subjected to column chromatography using gradient heptane to heptane / EtOAc 95:5 vol/vol affording 0.9 g (90%) of title compound as colorless liquid. $^1$H NMR (400 MHz, $CDCl_3$): δ (ppm) = 3.40 (t, *J* = 6.9 Hz, 2H), 1.85 (dt, *J* = 14, 6.8 Hz, 2H), 1.42 (m, 2H), 1.35 – 1.17 (m, 14H), 0.88 (m, 2H), 0.52 (m, 2H), 0.21 – 0.02 (m, 69H).

*2-(5-(Hepta(dimethylsiloxanyl))pentyl)isoindoline-1,3-dione* (**10a**)

Compound **9a** (0.415 g, 0.63 mmol) and potassium phthalimide (0.162 g, 0.87 mmol) were dissolved in 10 mL of DMF. The reaction mixture was heated up to 80 °C and stirred overnight. On completion, the solution was cooled down to room temperature and diluted with EtOAc. The resulting solution was washed with water, brine, dried over magnesium sulfate and filtered to give a 0.5 g of crude mixture of white solid and colorless liquid as a crude product. The title compound was isolated by column chromatography using gradient heptane to heptane / EtOAc 9:1 vol/vol to give 0.44 g of colorless liquid with 90% yield. $^1$H NMR (400 MHz, $CDCl_3$): δ (ppm) = 7.87 – 7.67 (m, 4H); 3.68 (m, 2H); 1.68 (p, *J* = 7.2 Hz, 2H); 1.36 (m, 4H); 0.53 (m, 2H); 0.10 – 0.02 (m, 45H).

*2-(10-(Undeca(dimethylsiloxanyl))decyl)isoindoline-1,3-dione* (**10b**)

Compound **9b** (0.9 g, 0.87 mmol) and potassium phthalimide (0.2 g, 1.1 mmol) were dissolved in 10 mL of DMF. The reaction mixture was heated up to 80 °C and stirred overnight. On completion, the solution was cooled down to room temperature and diluted with EtOAc. The resulting solution was washed with water, brine, dried over magnesium sulfate and filtered to give a 0.7 g of crude mixture of white solid and colorless liquid as a crude product. The title compound was isolated by column chromatography using gradient heptane to heptane / EtOAc 9:1 vol/vol to give 0.57 g of the title compound as colorless liquid with 60% yield. $^1$H NMR (400 MHz, $CDCl_3$): δ (ppm) = 7.88 – 7.66 (m, 4H); 3.67 (m, 2H); 1.65 (m, 2H); 1.38 – 1.20 (m, 16H); 0.88 (m, 2H); 0.52 (m, 2H); 0.10 – 0.02 (m, 69H).

*5-(Hepta(dimethyl)siloxanyl)pentan-1-amine* (**11a**)

Compound **10a** (0.44 g, 0.6 mmol) and hydrazine monohydrate (0.3 mL, 6 mmol) were dissolved in 4 mL of EtOH. The resulting mixture was heated up to 80 °C and after 10 minutes formation of white slurry was

observed. TLC (heptane / EtOAc 9:1) showed full conversion of the starting material. The reaction mixture was cooled to room temperature and partitioned between EtOAc (30 mL) and 1 M NaOH (30 mL). The organic phase was collected and washed with 1 M NaOH, water, brine, dried over magnesium sulfate, filtered and the solvent removed *in vacuo* to yield 0.34 g of the title compound as a colorless liquid in 95% yield. $^1$H NMR (400 MHz, $CDCl_3$): δ (ppm) = 2.69 (t, *J* = 7.0 Hz, 2H), 1.45 (m, 4H), 1.34 (m, 2H), 0.62 – 0.50 (m, 2H), 0.13 – 0.02 (m, 49H).

*10-(Undeca(dimethyl)siloxanyl)decan-1-amine* (**11b**)

Compound **10b** (0.57, 0.6 mmol) and hydrazine monohydrate (0.3 mL, 5.1 mmol) were dissolved in 6 mL of EtOH. Resulting mixture was heated up to 80 °C and after 10 minutes the formation of a white slurry was observed. TLC (heptane / EtOAc 9:1) showed full conversion of the starting material. The reaction mixture was cooled to room temperature and partitioned between EtOAc (40 mL) and 1 M NaOH (40 mL). The organic phase was collected and washed with 1 M NaOH (40 mL), water (40 mL), brine (40 mL), dried over magnesium sulfate, filtered and the solvent removed *in vacuo* to yield 0.457 g of title compound as a colorless liquid with 91% yield. $^1$H NMR (400 MHz, $CDCl_3$): δ (ppm) = 2.68 (t, *J* = 7.0 Hz, 2H), 1.43 (m, 2H), 1.28 (m, 14H), 0.52 (m, 2H), 0.15 – 0.01 (m, 69H).

*Synthesis of oDMS-functionalized TTAs* (**$(SiO)_7$-TTA** and **$(SiO)_{11}$-TTA**)

*$N^2$,$N^6$,$N^{10}$-Tris(5-(hepta(dimethyl)siloxanyl)pentyl)triphenylene-2,6,10-tricarboxamide* (**$(SiO)_7$-TTA**)

Triphenylene-2,6,10-tricarboxylic acid (**4**) (0.01 g 0.03 mmol) was dissolved in 0.3 mL of dry DMF at 70 °C under argon atmosphere. Then TBTU (0.03 g, 0.09 mmol) dissolved in 0.3 mL of DMF was added. Subsequently, DIPEA (0.05 mL, 0.2 mmol) followed by 0.05 g (0.09 mmol) of $(SiO)_7$-amine **11a** were added and the mixture was stirred for 30 minutes at 70 °C and then let to cool down to room temperature. The resulting yellow solution was diluted with 15 mL of EtOAc and washed with water (10 mL), 1 M HCl (10 mL), 1 M NaOH (10 mL), water (10 mL) and brine (10 mL). The organic phase was then dried over magnesium sulfate, the drying agent was filtered off and the crude compound was obtained by removing the solvent under reduced pressure. The title compound was isolated by column chromatography using gradient $CHCl_3$ to $CHCl_3$ / EtOAc / *i*-PrOH 90:9:1 vol/vol (0.015 g, 25%). $^1$H NMR (400 MHz, $CDCl_3$): δ (ppm) = 8.67 (s, 1H), 8.28 (d, *J* = 8.6 Hz, 1H), 7.74 (d, *J* = 8.6 Hz, 1H), 6.86 (s, 1H), 3.59 (q, *J* = 6.8 Hz, 2H), 1.78 (p, *J* = 7.5 Hz, 2H), 1.50 (m, 4H), 0.62 (m, 2H), 0.12 – 0.03 (m, 44H). $^{13}$C NMR (100 MHz, $CDCl_3$) δ (ppm) = 168.60, 133.39, 130.71, 127.84, 125.08, 122.46, 40.71, 31.23, 29.56, 23.35, 18.50, 1.94, 1.38, 1.30, 1.26, 1.23, 1.22. FT-IR: $\tilde{\upsilon}_{max}$= 3245 ($\upsilon_{N-H}$, m); 1635 (amide I, s); 1552 (amide II, s); 1257 ($\upsilon_{Si-C}$, s); 1020 ($\upsilon_{Si-O}$, s); 790 ($\delta_{Si-C}$, s). MS (MALDI-TOF): *m/z* calcd for $C_{81}H_{177}N_3O_{21}Si_{21}Na$ [M+Na] = 2138.79 found: 2140.81.

*$N^2$,$N^6$,$N^{10}$-Tris(10-(udeca(dimethyl)siloxanyl)decyll)triphenylene-2,6,10-tricarboxamide* (**$(SiO)_{11}$-TTA**)

Triphenylene-2,6,10-tricarboxylic acid (**4**) (0.02 g, 0.06 mmol) was dissolved in 0.3 mL of dry DMF at 110 °C under argon atmosphere. Then TBTU (0.06 g, 0.19 mmol) dissolved in 0.3 mL of DMF was added. Subsequently, DIPEA (0.08 mL, 0.33 mmol) followed by 0.19 g (0.19 mmol) of $(SiO)_{11}$-amine **11b** were added and the mixture was stirred for 30 minutes at 110 °C and then let to cool down to room temperature. The resulting yellow solution was diluted with 15 mL of EtOAc and washed with water (10 mL), 1 M HCl (10 mL), 1 M NaOH (10 mL), water (10 mL) and brine (10 mL). The organic phase was then dried over magnesium sulfate, the drying agent was filtered off and the crude compound was obtained by removing the solvent under reduced pressure. The title compound was isolated by column

chromatography using gradient $CHCl_3$ to $CHCl_3$ / EtOAc / *i*-PrOH 90:9:1 vol/vol (0.05 g, 28%). $^1$H NMR (400 MHz, $CDCl_3$): δ (ppm) = 8.53 (s, 1H); 8.14 (d, *J* = 8.3 Hz, 1H), 7.67 (d, *J* = 8.3 Hz, 1H), 6.99 (bs, 1H); 3.60 (q, *J* = 6.8 Hz, 2H), 1.78 (p, *J* = 7.4 Hz, 2H), 1.53 – 1.22 (m, 14H), 0.54 (s, 2H), 0.16 – 0.02 (m, 69H). $^{13}$C NMR (100 MHz, $CDC_3$) δ (ppm) = 168.34, 133.14, 130.32, 127.47, 124.79, 122.21, 122.01, 40.37, 33.42, 29.67, 29.60, 29.53, 29.43, 29.36, 27.19, 23.12, 18.13, 1.59, 0.98, 0.94, 0.88, 0.86. FT-IR: $\tilde{\upsilon}_{max}$= 3245 ($\upsilon_{N-H}$, m); 1636 (amide I, s); 1555 (amide II, s); 1257 ($\upsilon_{Si-C}$, s); 1020 ($\upsilon_{Si-O}$, s); 790 ($\delta_{Si-C}$, s). MS (MALDI-TOF): *m/z* calcd for $C_{120}H_{279}N_3O_{33}Si_{33}Na$ [M+Na] = 3241.25 found: 3241.30.

*Synthesis of $H_2N$-$C_5$-$Si_{12}$-$C_5$-Cm* (**22**)

*7-Hydroxy-4-methyl-2H-chromen-2-one* (**12**)[54]

Resorcinol (4 g, 36 mmol), ethyl acetoacetate (4.9 g, 38 mmol) and trifluoroacetic acid (8 mL) were placed in a microwave tube equipped with a stirring bar and subjected to microwave irradiation for 20 minutes at 100 °C. On completion, the solution was moved to a separatory funnel with 100 mL of EtOAc, washed with of water (100 mL) and brine (60 mL). The title compound was isolated via recrystallization from heptane / EtOAc 4:1 to yield 5.97 g of white crystals with 93% yield. $^1$H NMR (400 MHz, DMSO-$d_6$): δ (ppm) = 10.53 (bs, 1H), 7.60 (d, *J* = 8.7 Hz, 1H), 6.81 (dd, *J* = 8.7, 2.3 Hz, 1H), 6.71 (d, *J* = 2.3 Hz, 1H), 6.13 (d, *J* = 1.2 Hz, 1H), 2.37 (d, *J* = 1.2 Hz, 3H).

*4-Methyl-7-(pent-4-en-1-yloxy)-2H-chromen-2-one* (*$C_5$-Cm*) (**13**)

Compound **12** (0.2 g, 1.13 mmol), 5-bromopent-1-ene (0.19 g, 1.24 mmol) and $K_2CO_3$ (0.39 g, 2.83 mmol) together with 4 mL of acetonitrile were placed in a round-bottomed flask equipped with a magnetic stirrer and reflux condenser. The mixture was stirred at 80 °C overnight. The progress was controlled by TLC (heptane / EtOAc 1:1 vol/vol). On completion, the suspension was diluted with EtOAc (50 mL), washed with water (30 mL) and brine (30 mL). The organic phase was dried over magnesium sulfate, filtered off, the solvent removed under reduced pressure and coevaporated 3x with toluene to yield 260 mg of title compound as a viscous oil in 94% yield. $^1$H NMR (400 MHz, $CDCl_3$): δ (ppm) = 7.49 (d, *J* = 8.8 Hz, 1H), 6.86 (dd, *J* = 8.8, 2.5 Hz, 1H), 6.81 (d, *J* = 2.5 Hz, 1H), 6.13 (d, *J* = 1.2 Hz, 1H), 5.85 (ddt, *J* = 16.9, 10.1, 6.7 Hz, 1H), 5.15 – 4.97 (m, 2H), 4.03 (t, *J* = 6.4 Hz, 2H), 2.40 (d, *J* = 1.2 Hz, 3H), 2.26 (qt, J = 7.8, 1.4 Hz, 2H), 2.01 – 1.84 (m, 2H).

*7-((5-(7-Hydroxy(tetra(dimethyl)siloxanyl)pentyl)oxy)-4-methyl-2H-chromen-2-one (HO-$Si_4$-$C_5$-Cm)* (**15**)

Compound **13** (0.275 g, 1.12 mmol) and tetra(dimethyl)siloxan-1-ol (**14**) (0.34 g, 1.12 mmol) of were dissolved in 3 mL of $CHCl_3$. A drop of Karstedt catalyst solution in xylene was added and the mixture was stirred overnight at room temperature. The progress was monitored by $^1$H NMR (disappearance of Si-*H* signal) and IR (disappearance of Si-H stretching absorption band) spectroscopy. On completion, the solvent was removed under reduced pressure to get 0.6 g of crude product (98% yield) which was used without further purification in the following step. $^1$H NMR (400 MHz, $CDCl_3$): δ (ppm) = 7.48 (d, *J* = 8.8 Hz, 1H), 6.85 (dd, *J* = 8.8, 2.5 Hz, 1H), 6.81 (d, *J* = 2.5 Hz, 1H), 6.13 (d, *J* = 1.3 Hz, 1H), 4.01 (t, *J* = 6.6 Hz, 2H), 2.40 (d, *J* = 1.3 Hz, 3H), 1.82 (m, 2H), 1.54 – 1.29 (m, 4H), 0.85 – 0.52 (m, 2H), 0.16 – 0.03 (m, 24H).

*7-((5-(Octa(dimethyl)siloxanyl)pentyl)oxy)-4-methyl-2H-chromen-2-one (H-$Si_8$-$C_5$-Cm)* (**17**)

Crude *HO-$Si_4$-$C_5$-Cm* **(15)** (0.6 g, 1.1 mmol) of was dissolved in 6 mL of toluene and cooled down to 0 °C. Then 0.2 mL (2.5 mmol) of pyridine followed by 0.38 g (1.21 mmol) of 1-chlorotetra(dimethyl)siloxane (**16**)

were added. The formation of a white precipitate was observed. The suspension was allowed to warm up to room temperature and stirred for 1 hour. Progress was monitored by TLC (heptane / EtOAc 2:1 vol/vol). On completion the reaction mixture was diluted with 50 mL of EtOAc, washed with 30 mL of water, 30 mL of brine, dried over magnesium sulfate, filtered off and solvent removed *in vacuo* to yield 1.05 g of orange oil as crude product. The title compound was isolated by column chromatography with gradient elution (heptane to heptane / EtOAc 7:3 vol/vol) to yield 0.508 g of colorless liquid in 56% yield. $^1$H NMR (400 MHz, $CDCl_3$): δ (ppm) = 7.48 (d, *J* = 8.7 Hz, 1H), 6.85 (dd, *J* = 8.8, 2.5 Hz, 1H), 6.80 (d, *J* = 2.5 Hz, 1H), 6.13 (d, *J* = 1.2 Hz, 1H), 4.70 (hept, *J* = 2.8 Hz, 1H), 4.01 (t, *J* = 6.5 Hz, 2H), 2.40i (d, *J* = 1.2 Hz, 3H), 1.81 (p, *J* = 6.8 Hz, 2H), 1.53 – 1.30 (m, 4H), 0.58 (m, 2H), 0.26 – 0.03 (m, 48H).

*7-((5-(15-Hydroxy(octa(dimethyl)siloxanyl)pentyl)oxy)-4-methyl-2H-chromen-2-one (HO-$Si_8$-$C_5$-Cm)* (**18**)

*H-$Si_8$-$C_5$-Cm* (**17**) (0.5 g, 0.62 mmol) was dissolved in 20 mL of dioxane. Aqueous phosphate buffer (15 mL) of of pH 7 was added and the solution was degassed with argon for 5 minutes, followed by the addition of 0.05 g of Pd/C. The resulting mixture was stirred at room temperature for 1 hour. An evolution of hydrogen gas was observed. The progress was monitored by TLC (heptane / EtOAc 2:1). On completion, the mixture was filtered through a celite pad and diluted with 50 mL of EtOAc. The biphasic mixture was separated in a separatory funnel. The upper organic layer was collected, washed with water, brine, dried over magnesium sulfate, filtered off and solvent removed under reduced pressure to give 0.5 g of colorless oil (97%). $^1$H NMR (400 MHz, $CDCl_3$): δ (ppm) = 7.48 (d, *J* = 8.8 Hz, 1H), 6.85 (dd, *J* = 8.8, 2.5 Hz, 1H), 6.80 (d, *J* = 2.5 Hz, 1H), 6.13 (d, *J* = 1.1 Hz, 1H), 4.01 (t, *J* = 6.5 Hz, 2H), 2.40 (d, *J* = 1.1 Hz, 3H), 2.25 (s, 1H), 1.82 (p, J = 6.7 Hz, 2H), 1.53 – 1.35 (m, 4H), 0.58 (m, 2H), 0.14 (s, 6H), 0.11 – 0.04 (m, 42H).

*7-((5-(Dodeca(dimethyl)siloxanyl)pentyl)oxy)-4-methyl-2H-chromen-2-one (H-$Si_{12}$-$C_5$-Cm)* (**19**)

*HO-$Si_8$-$C_5$-Cm* (**18**) (0.5 g, 0.6 mmol) of was dissolved in 5 mL of toluene and cooled to 0 °C. Then 0.1 mL (1.2 mmol) of pyridine followed by 0.2 g (0.6 mmol) of 1-chlorotetra(dimethyl)siloxane (**16**) were added. The formation of a white precipitate was observed. The suspension was allowed to warm up to room temperature and stirred for 1 hour. Progress was monitored by TLC (heptane / EtOAc 2:1 vol/vol). On completion the reaction mixture was diluted with 50 mL of EtOAc, washed with 30 mL of water, 30 mL of brine, dried over magnesium sulfate, filtered off and solvent removed *in vacuo* to yield 0.7 g of orange oil as crude product. The title compound was isolated by column chromatography with gradient elution (heptane to heptane / EtOAc 4:1 vol/vol) to yield 0.543 g of colorless liquid in 81% yield. $^1$H NMR (400 MHz, $CDCl_3$): δ (ppm) = 7.48 (d, *J* = 8.8 Hz, 1H), 6.85 (dd, *J* = 8.8, 2.5 Hz, 1H), 6.80 (d, *J* = 2.5 Hz, 1H), 6.13 (d, *J* = 1.2 Hz, 1H), 4.70 (hept, *J* = 2.8 Hz, 1H), 4.01 (t, *J* = 6.5 Hz, 2H), 2.39 (d, *J* = 1.2 Hz, 3H), 1.82 (p, *J* = 6.7 Hz, 2H), 1.52 – 1.35 (m, 4H), 0.58 (m, 2H), 0.18 (d, *J* = 2.8 Hz, 6H), 0.07 (m, 60H), 0.05 (s, 6H).

7-((5-(23-(5-Bromopentyl)dodeca(dimethyl)dodecasiloxanyl)pentyl)oxy)-4-methyl-2H-chromen-2-one *Br-$C_5$-$Si_{12}$-$C_5$-Cm* (**20**)

*H-$Si_{12}$-$C_5$-Cm* (**19**) (0.25 g, 0.22 mmol) and 5-bromopent-1-ene (0.07 g, 0.45 mmol) were dissolved in 2 mL of toluene. A drop of Karstedt catalyst solution in xylene was added and the solution was stirred overnight at room temperature. The progress was monitored by $^1$H NMR spectroscopy (disappearance of Si-*H* signal). On completion, the solvent was removed to yield 0.27 g of crude product (95% yield) which was used in the next step without further purification. $^1$H NMR (400 MHz, $CDCl_3$): δ (ppm) = 7.48 (d, *J* = 8.8 Hz, 1H), 6.85 (dd, *J* = 8.8, 2.5 Hz, 1H), 6.80 (d, *J* = 2.5 Hz, 1H), 6.13 (d, *J* = 1.2 Hz, 1H), 4.01 (t, *J* = 6.6 Hz,

2H), 3.40 (t, *J* = 6.9 Hz, 2H), 2.39 (d, *J* = 1.2 Hz, 3H), 1.84 (m, 4H), 1.52 – 1.28 (m, 8H), 0.56 (m, 4H), 0.07 (m, 60H), 0.05 (d, *J* = 1.6 Hz, 12H).

*2-(5-(23-(5-((4-Methyl-2-oxo-2H-chromen-7-yl)oxy)pentyl)dodeca(dimethyl)siloxanyl)pentyl)isoindoline-1,3-dione Nph-$C_5$-$Si_{12}$-$C_5$-Cm* (**21**)

*Br-$C_5$-$Si_{12}$-$C_5$-Cm* (**20**) (0.27 g, 0.21 mmol) of was dissolved in 3 mL of DMF. Then potassium phthalimide (0.05 g, 0.26 mmol) was added and the mixture was stirred overnight at 70 °C. The progress was monitored by TLC (heptane / EtOAc 2:1 vol/vol). On completion, the suspension was cooled down to room temperature, diluted with 30 mL of EtOAc, washed with water (20 mL), brine (20 mL), dried over magnesium sulfate, filtered off and the solvent removed under reduced pressure to give 0.27 g of crude product as an orange oil. The title compound was isolated by column chromatography with gradient elution (heptane to heptane / EtOAc 4:1 vol/vol) to yield 0.225 g (80%) of a colorless oil. $^1$H NMR (400 MHz, $CDCl_3$): δ (ppm) = 7.84 (m, 2H), 7.70 (m, 2H), 7.48 (d, *J* = 8.8 Hz, 1H), 6.85 (dd, *J* = 8.8, 2.5 Hz, 1H), 6.80 (d, *J* = 2.5 Hz, 1H), 6.12 (d, *J* = 1.3 Hz, 1H), 4.01 (t, *J* = 6.5 Hz, 2H), 3.67 (m, 2H), 2.39 (d, *J* = 1.3 Hz, 3H), 1.82 (p, *J* = 6.7 Hz, 2H), 1.67 (p, *J* = 7.2 Hz, 2H), 1.53 – 1.28 (m, 8H), 0.73 – 0.43 (m, 4H), 0.10 – 0.02 (m, 72H).

7-((5-(23-(5-Aminopentyl)dodeca(dimethyl)dodecasiloxanyl)pentyl)oxy)-4-methyl-2H-chromen-2-one *$H_2N$-$C_5$-$Si_{12}$-$C_5$-Cm* (**22**)

*Nph-$C_5$-$Si_{12}$-$C_5$-Cm* (**21**) (0.225 g, 0.17 mmol) and hydrazine monohydrate (0.1 mL) were dissolved in 3 mL of EtOH. The resulting solution was stirred at 70 °C and the formation of white suspension was observed. The progress was monitored by TLC (heptane / EtOAc 2:1 vol/vol) and full consumption of the starting material was achieved after 2 hours. On completion, the suspension was cooled to room temperature and partitioned between EtOAc (30 mL) and 1 M NaOH (20 mL). The organic phase was collected and washed with 1 M NaOH (20 mL), water (20 mL), brine (20 mL), dried over magnesium sulfate, filtered and solvent removed *in vacuo* to yield 0.196 g of the title compound as a colorless liquid in 96% yield. $^1$H NMR (400 MHz, $CDCl_3$): δ (ppm) = 7.48 (d, *J* = 8.8 Hz, 1H), 6.85 (dd, *J* = 8.8, 2.5 Hz, 1H), 6.80 (d, *J* = 2.5 Hz, 1H), 6.13 (d, *J* = 1.3 Hz, 1H), 4.01 (t, *J* = 6.5 Hz, 2H), 2.71 (t, *J* = 7.1 Hz, 2H), 2.39 (d, *J* = 1.3 Hz, 3H), 1.96 (bs, 2H), 1.82 (m, 2H), 1.59 – 1.28 (m, 10H), 0.64 – 0.48 (m, 4H), 0.07 (m, 60H), 0.04 (d, *J* = 2.7 Hz, 12H). MS (MALDI-TOF): *m/z* calcd for $C_{44}H_{102}NO_{14}Si_{12}$ [M+H] = 1203.45; found: 1204.49.

*Synthesis of telechelic comarin-oDMS-TTA* (**Cm-$(SiO)_{12}$-TTA**)

*$N^2$,$N^6$,$N^{10}$-Tris(5-(23-(5-((4-methyl-2-oxo-2H-chromen-7-yl)oxy)pentyl)dodeca(dimethyl)siloxanyl)pentyl)triphenylene-2,6,10-tricarboxamide* (**Cm-$(SiO)_{12}$-TTA**)

Triphenylene-2,6,10-tricarboxylic acid (**4**) (0.023 g, 0.06 mmol) was dissolved in 0.5 mL of dry DMF at 70 °C under argon atmosphere. Then TBTU (0.072 g, 0.22 mmol) dissolved in 0.5 mL of DMF was added. Subsequently, DIPEA (0.1 mL, 0.6 mmol) followed by 0.26 g (0.22 mmol) of *$H_2N$-$C_5$-$Si_{12}$-$C_5$-Cm* (**22**) was added and the mixture was stirred for 30 minutes at 70 °C and then let to cool down to room temperature. The resulting yellow solution was diluted with 40 mL of EtOAc and washed with water (30 mL), 1 M HCl (30 mL), 1 M NaOH (30 mL), water (30 mL) and brine (30 mL). The organic phase was dried over magnesium sulfate, the drying agent was filtered off and the crude product was obtained by removing the solvent under reduced pressure (0.290 g of orange paste). The title compound was isolated by column chromatography with gradient elution (DCM to DCM / EtOAc / *i*-PrOH 90:9:1 vol/vol/vol) to give 0.135 g

of a colorless paste with 54% yield. $^{1}$H NMR (400 MHz, $CDCl_3$): δ (ppm) = 9.06 (s, 3H), 8.68 (d, *J* = 8.6 Hz, 3H), 7.93 (d, *J* = 8.6 Hz, 3H), 7.44 (d, J = 8.8 Hz, 3H), 6.82 (dd, J = 8.8, 2.5 Hz, 3H), 6.76 (d, *J* = 2.5 Hz, 3H), 6.56 (s, 3H), 6.09 (d, *J* = 1.3 Hz, 1H), 3.98 (t, *J* = 6.5 Hz, 6H), 3.57 (q, *J* = 6.8 Hz, 6H), 2.36 (d, *J* = 1.3 Hz, 9H), 1.77 (m, 4H), 1.47 (m, 8H), 0.58 (m, 4H), 0.13 – 0.03 (m, 216H). $^{13}$C NMR (400 MHz, $CDCl_3$): δ (ppm) = 168.09, 162.36, 161.56, 155.38, 152.75, 133.72, 131.38, 128.52, 125.53, 125.37 123.29, 122.99, 113.47, 112.79, 111.87, 101.40, 68.72, 40.68, 31.15, 29.78, 29.63, 28.88, 23.29, 23.19, 18.77, 18.46, 18.31, 1.36, 1.32, 1.24, 1.22, 1.20, 0.36, 0.33. FT-IR: $\tilde{\upsilon}_{max}$= 3243 ($\upsilon_{N-H}$, w); 1734 ($\upsilon_{C=O}$, m); 1614 ($\upsilon_{C=C}$, m); 1554 (amide II, m); 1257 ($\upsilon_{Si-C}$, s); 1020 ($\upsilon_{Si-O}$, s); 790 ($\delta_{Si-C}$, s). MS (MALDI-TOF): *m/z* calcd for $C_{153}H_{309}N_3O_{45}Si_{36}Na$ [M+Na] = 3943.36 found: 3944.37.

## 2.6 References


[1] J. Billard, J. C. Dubois, J. C. Tinh, N. H. Zann, *Nouv J Chim.* **1978**, *2*, 535–540.
[2] S. Kumar, *Chem. Soc. Rev.* **2006**, *35*, 83–109.
[3] M. Kawano, M. Fujita, *Coord. Chem. Rev.* **2007**, *251*, 2592–2605.
[4] T. Ikeda, J. I. Mamiya, Y. Yu, *Angew. Chem. Int. Ed.* **2007**, *46*, 506–528.
[5] N. Boden, R. J. Bushby, A. N. Cammidge, P. S. Martin, *J. Mater. Chem.* **1995**, *5*, 1857–1860.
[6] S. Kumar, *Liq. Cryst.* **2004**, *31*, 1037–1059.
[7] S. K. Pal, S. Setia, B. S. Avinash, S. Kumar, *Liq. Cryst.* **2013**, *40*, 1769–1816.
[8] M. A. Alam, J. Motoyanagi, Y. Yamamoto, T. Fukushima, J. Kim, K. Kato, M. Takata, A. Saeki, S. Seki, S. Tagawa, T. Aida, *J. Am. Chem. Soc.* **2009**, *131*, 17722–17723.
[9] V. Percec, M. R. Imam, M. Peterca, D. A. Wilson, R. Graf, H. W. Spiess, V. S. K. Balagurusamy, P. A. Heiney, *J. Am. Chem. Soc.* **2009**, *131*, 7662–7677.
[10] G. Cooke, N. Kaushal, N. Boden, R. J. Bushby, Z. Lu, O. Lozman, *Tetrahedron Lett.* **2000**, *41*, 7955–7959.
[11] Y. Shimizu, A. Kurobe, H. Monobe, N. Terasawa, K. Kiyohara, K. Uchida, *Chem. Comm.* **2003**, 1676–1677.
[12] M. L. Rahman, C. Tschierske, M. Yusoff, S. Silong, *Tetrahedron Lett.* **2005**, *46*, 2303–2306.
[13] C. T. Imrie, Z. Lu, S. J. Picken, Z. Yildirim, *Chem. Commun.* **2007**, 1245–1247.
[14] L. H. Wu, N. Janarthanan, C. S. Hsu, *Liq. Cryst.* **2001**, *28*, 17–24.
[15] M. H. Hoang, D. N. Nguyen, T. T. Ngo, M. J. Cho, S. J. Lee, D. H. Choi, *Synth. Met.* **2015**, *209*, 434–440.
[16] M. H. Hoang, M. J. Cho, K. H. Kim, M. Y. Cho, J.-S. Joo, D. H. Choi, *Thin Solid Films* **2009**, *518*, 501–506.
[17] K. Tao, T. Wu, D. Lu, R. Bai, H. Li, L. An, *J. Mol. Liq.* **2008**, *142*, 118–123.
[18] C. V. Yelamaggad, A. S. Achalkumar, D. S. S. Rao, M. Nobusawa, H. Akutsu, J. I. Yamada, S. Nakatsuji, *J. Mater. Chem.* **2008**, *18*, 3433–3437.
[19] Z.-B. Jian, K.-Q. Zhao, P. Hu, B.-Q. Wang, *Acta Chim. Sin.* **2008**, *66*, 1353–1360.
[20] F. Yang, J. Xie, H. Guo, B. Xu, C. Li, *Liq. Cryst.* **2012**, *39*, 1368–1374.
[21] R. J. Bushby, Q. Liu, O. R. Lozman, Z. Lu, S. R. McLaren, *Mol. Cryst. Liq. Cryst.* **2004**, *411*, 293–304.
[22] F. Yang, Y. Zhang, H. Guo, J. Lin, *Tetrahedron Lett.* **2013**, *54*, 4953–4956.
[23] F. Yang, Y. Zhang, H. Guo, *New J. Chem.* **2013**, *37*, 2275–2279.
[24] T. Christ, B. Glüsen, A. Greiner, A. Kettner, R. Sander, V. Stümpflen, V. V. Tsukruk, J. H. Wendorff, *Adv. Mater.* **1997**, *9*, 48–52.
[25] F. Yang, H.-Y. Guo, J.-W. Xie, Z.-Q. Liu, B.-T. Xu, *Chem. Res. Chin. Univ.* **2012**, *28*, 358–360.
[26] L. Cui, J. P. Collet, G. Xu, L. Zhu, *Chem. Mater.* **2006**, *18*, 3503–3512.
[27] M. Ukon, T. Sugino, T. Watanabe, H. Monobe, Y. Shimizu, *Macromol. Mater. Eng.* **2002**, *287*, 698–705.
[28] T. J. Phillips, J. C. Jones, D. G. McDonnell, *Liq. Cryst.* **1993**, *15*, 203–215.
[29] H. Monobe, S. Mima, T. Sugino, Y. Shimizu, M. Ukon, *Liq. Cryst.* **2001**, *28*, 1253–1258.

[30] N. H. Tinh, C. Destrade, H. Gasparoux, *Phys. Lett.* **1979**, *72A*, 251–254.

[31] J. M. Warman, P. G. Schouten, *J. Phys. Chem.* **1995**, *99*, 17181–17185.

[32] D. Adam, P. Schuhmacher, J. Simmerer, L. Häussling, K. Siemensmeyer, K. H. Etzbachi, H. Ringsdorf, D. Haarer, *Nature* **1994**, *371*, 141–143.

[33] M. Okazaki, U.S. Patent 5,730,903, **1998**

[34] R. Freudenmann, B. Behnisch, M. Hanack, *J. Mater. Chem.* **2001**, *11*, 1618–1624.

[35] Y. Wang, M. Zhu, J. Deng, G. Xie, E. Baranoff, *New J. Chem.* **2017**, *41*, 1773–1780.

[36] I. Seguy, P. Jolinat, P. Destruel, J. Farenc, R. Mamy, H. Bock, J. Ip, T. P. Nguyen, *J. Appl. Phys.* **2001**, *89*, 5442–5448.

[37] P. Staffeld, M. Kaller, S. J. Beardsworth, K. Tremel, S. Ludwigs, S. Laschat, F. Giesselmann, *J. Mater. Chem. C,* **2013**, *1*, 892–901.

[38] X. Chen, L. Chen, Y. Chen, *RSC Adv.* **2014**, *4*, 3627–3632.

[39] T. Hassheider, S. A. Benning, H. S. Kitzerow, M. F. Achard, H. Bock, *Angew. Chem. Int. Ed.* **2001**, *40*, 2060–2063.

[40] S. Cantekin, T. F. A. de Greef, A. R. A. Palmans, *Chem. Soc. Rev.* **2012**, *41*, 6125–6137.

[41] H. Bock, M. Rajaoarivelo, S. Clavaguera, E. Grelet, *Eur. J. Org. Chem.* **2006**, 2889–2893.

[42] H. Shirai, N. Amano, Y. Hashimoto, E. Fukui, Y. Ishii, M. Ogawa, *J. Org. Chem.* **1991**, *56*, 2253–2256.

[43] Y. Matsunaga, Y. Nakayasu, S. Sakai, M. Yonenaga, *Mol. Cryst. Liq. Cryst.* **1986**, *141*, 327–333.

[44] Y. Matsunaga, N. Miyajima, Y. Nakayasu, S. Sakai, M. Yonenaga, *Bull. Chem. Soc. Jpn.* **1988**, *61*, 207–210.

[45] P. J. M. Stals, J. F. Haveman, R. Martín-Rapún, C. F. C. Fitié, A. R. A. Palmans, E. W. Meijer, *J. Mater. Chem.* **2009**, *19*, 124–130.

[46] P. J. M. Stals, M. M. J. Smulders, R. Martín-Rapún, A. R. A. Palmans, E. W. Meijer, *Chem. Eur. J.* **2009**, *15*, 2071–2080.

[47] G. S. Hammond, C. A. Stout, A. A. Lamola, *J. Am. Chem. Soc.* **1964**, *86*, 3103–3106.

[48] G. O. Schenck, I. von Wilucki, C. H. Krauch, *Chem. Ber.* **1962**, *95*, 1409–1412.

[49] R. Anet, *Can. J. Chem.* **1962**, *40*, 1249–1257.

[50] M. L. Ślęczkowski, E. W. Meijer, A. R. A. Palmans, *Macromol. Rapid Commun.* **2017**, *38*, 1700566.

[51] M. P. Lightfoot, F. S. Mair, R. G. Pritchard, J. E. Warren, *Chem. Commun.* **1999**, 1945–1946.

[52] B. Van Genabeek, B. F. M. de Waal, M. M. J. Gosens, L. M. Pitet, A. R. A. Palmans, E. W. Meijer, *J. Am. Chem. Soc.* **2016**, *138*, 4210–4218.

[53] P. J. Launer, *Silicon Compounds: Silanes & Silicones*, Gelest Inc., Morisville, **2013**.

[54] J. Zak, D. Ron, E. Riva, H. P. Harding, B. C. S. Cross, I. R. Baxendale, *Chem. Eur. J.* **2012**, *18*, 9901–9910.

[55] X. Lou, B. F. M. de Waal, J. L. J. Van Dongen, J. A. J. M. Vekemans, E. W. Meijer, *J. Mass Spectrom.* **2010**, *45*, 1195–1202.

[56] T. F. A. de Greef, M. M. L. Nieuwenhuizen, P. J. M. Stals, C. F. C. Fitié, A. R. A. Palmans, R. P. Sijbesma, E. W. Meijer, *Chem. Commun.* **2008**, 4306–4308.

[57] M. García-Iglesias, B. F. M. de Waal, I. de Feijter, A. R. A. Palmans, E. W. Meijer, *Chemistry* **2015**, *21*, 377–385.

[58] D. Zeng, I. Tahar-Djebbar, Y. Xiao, F. Kameche, N. Kayunkid, M. Brinkmann, D. Guillon, B. Heinrich, B. Donnio, D. A. Ivanov, E. Lacaze, D. Kreher, F. Mathevet, A.-J. Attias, *Macromolecules* **2014**, *47*, 1715–1731.

[59] M. Gupta, S. P. Gupta, S. K. Pal, *J. Phys. Chem. B* **2017**, *121*, 8593–8602.

[60] S. Pan, B. Mu, Y. Zhou, Q. Li, B. Wu, J. Fang, D. Chen, *RSC Adv.* **2016**, *6*, 49556–49566.

[61] K. Nickmans, J. N. Murphy, B. de Waal, P. Leclère, J. Doise, R. Gronheid, D. J. Broer, A. P. H. J. Schenning, *Adv. Mater.* **2016**, *28*, 10068–10072.

[62] C. M. A. Leenders, L. Albertazzi, T. Mes, M. M. E. Koenigs, A. R. A. Palmans, E. W. Meijer, *Chem. Commun.* **2013**, *49*, 1963–1965.

# Chapter 3

# *Supramolecular chirality of triphenylene-2,6,10-tricarboxamides: kinetic and thermodynamic control by solvent engineering*

**Abstract**:

Triphenylene is a well-established motif in the field of liquid crystals but has attracted remarkably little attention in the field of supramolecular polymerizations. We here introduce $C_3$-symmetrical trialkyl-substituted triphenylene-2,6,10-tricarboxamides (TTAs) as a novel motif for supramolecular polymerizations. We show that the TTA-based supramolecular polymers are stabilized by intermolecular hydrogen-bond formation in addition to π-π stacking. Because of this, at μM concentrations, the supramolecular polymers remain stable when chloroform is added (up to 40%). The strong intermolecular hydrogen-bond formation in combination with π-π stacking leads to strongly cooperative character of the aggregation. Sergeants-and-soldiers and majority-rules experiments reveal that the quality of the solvent determines the degree of amplification of supramolecular chirality. In alkanes, no amplification is observed whereas the addition of chloroform, results in strong amplification of supramolecular chirality by increasing the dynamic behavior of the system. The reduced dynamic behavior of the TTAs in alkanes leads to kinetically trapped aggregates in a controlled way. When (*S*)-1-chloro-2-methylbutane is added as a co-solvent, the mirror symmetry in racemic supramolecular polymers based on the achiral monomers is broken. Subsequent removal of the chiral cosolvent yields kinetically trapped supramolecular polymers of a single helicity.

This work has been performed in close collaboration with Mathijs Mabesoone.

Part of this work will be published:
Supramolecular Chirality of Triphenylene-2,6,10-tricarboxamides: Kinetic and Thermodynamic Control by Solvent Engineering
M. L. Ślęczkowski, M. F. J. Mabesoone, Y. Post, A. R. A. Palmans, E. W. Meijer, *manuscript in preparation*

## 3.1 Introduction

The versatility, robustness and responsiveness of biomacromolecules have served as a source of inspiration to develop synthetic equivalents that form helical superstructures through covalent bonds.[1,2] Examples range from polymeric systems[3–12] and foldamers[13–17] to supramolecular complexes[18–21] and polymers based on non-covalent interactions.[2,22–30] Interestingly, in these synthetic systems, a helical bias is not only induced by the use of chiral, non-racemic monomers, but also by applying chiral, non-racemic solvents,[31–36] chiral guest molecules,[37–42] a chiral initiator[30] or even circularly polarized (CP) light.[43] The sergeants-and-soldiers and majority-rules principles —pioneered by Green[44,45]—were found to operate in many systems that show dynamic helicity, based on both covalent[12,46–49] and non-covalent bonds.[28,32,50–52] When these principles are operative, a bias is induced in the helical preference, which is non-proportional to the amount of chiral compound added to an achiral compound (the sergeants-and-soldiers experiment) or to the enantiomeric excess of the monomers applied (the majority-rules experiment). These effects are commonly referred to as "amplification of supramolecular chirality"[53]

In recent years, our group focused on the use of $C_3$-symmetrical systems to explore the limits of amplification of supramolecular chirality.[53–55] Owing to their directionality, hydrogen bonds are a perfect scaffold for the transfer of helical handedness.[56,57] The use of intermolecular hydrogen-bonding interactions as the dominant force results in cooperative growth of the helical aggregates, in many cases giving rise to strong amplification of supramolecular chirality.[58] The development of mathematical models has permitted to quantify the energies involved in both the cooperative growth of the systems as well as the energies involved in the amplification of supramolecular chirality.[28,53,59,60] Systematic, quantitative studies on amplification of supramolecular chirality in alkyl substituted benzene-1,3,5-tricarboxamides (BTAs) showed that the mismatch penalty - the parameter that denotes the energetic penalty for a monomer to reside in a non-preferred helical superstructure - is affected by several variables. The number,[61] position[61] and nature of the stereogenic centra[62] as well as the temperature[63,64] all affect the mismatch penalty. The excellent correspondence between the mathematical models and the experimental findings is largely a result of the highly dynamic nature of the BTAs, which always operate at thermodynamic equilibrium. Aside from the benefits that a system operating under thermodynamic control brings, many systems that show kinetic traps[29,30,65–68] or aggregate along different pathways[69–71] also express interesting behavior when amplification of supramolecular chirality studies are performed.[54] For example, as elegantly shown by the groups of Elemans[72] and Sanchez[54,72,73] sergeants-and-soldiers studies can be used to assess the system's dynamic behavior, and in case of slow dynamics, it becomes a tool to control the extent of the chiral amplification of the system. In addition, by using chiral guest molecules that create helical bias by specific interactions with the supramolecular polymer followed by removal of the guest molecule, chiral memory effects result. This chiral memory only persists

on reasonable times scales when the supramolecular polymer can be kinetically trapped.[41,42,74,75]

In this chapter, we explore the merger of the structural features of the BTA core (amide functionality, cooperative aggregation, strong amplification of supramolecular chirality) and the triphenylene core (large aromatic core). Triphenylene is a well-established motif in the field of liquid crystals,[76] yet has been rarely applied in supramolecular polymerizations.[77] We study, the supramolecular polymerization of the TTAs in dilute decalin solutions and in mixtures of decalin and chloroform by $^{1}$H-NMR, UV-spectroscopy, circular dichroism (CD) spectroscopy and fluorescence spectroscopy. Sergeants-and-soldiers and majority-rules experiments were conducted in pure decalin and decalin mixed with chloroform to obtain information of the dynamic exchange between monomers and polymers as a function of solvent composition. Finally, (*S*)-1-chloro-2-methylbutane was synthesized to serve as a volatile co-solvent, with the aim to break the symmetry in racemic helical supramolecular polymers based on achiral TTA, and to investigate the kinetic stability after removal of the chiral solvent (Scheme 3.1).

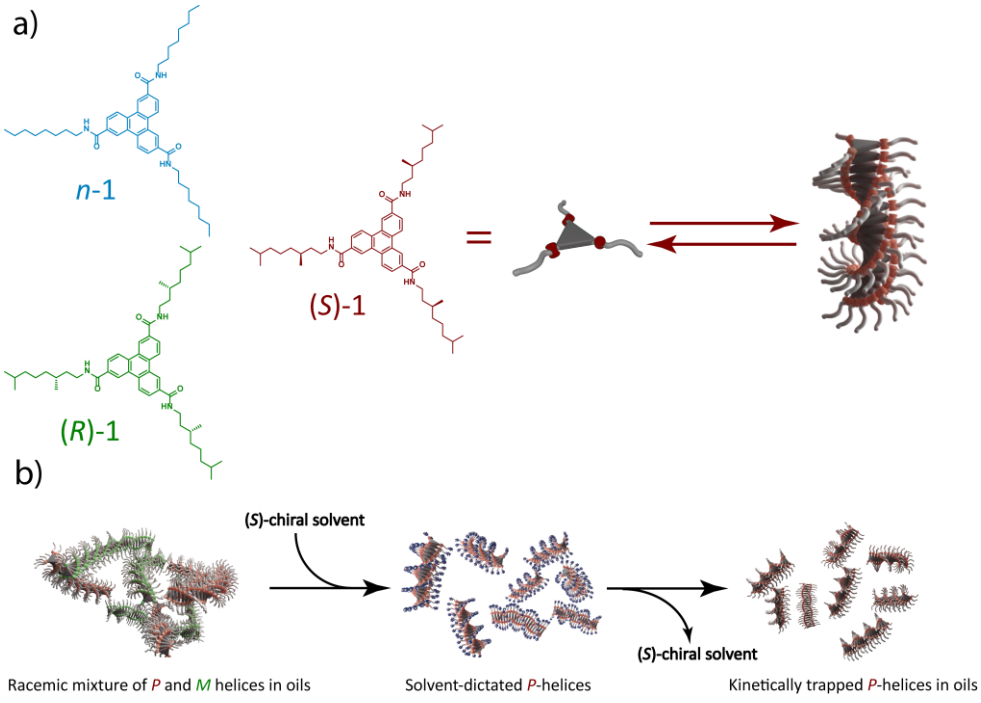


***Scheme 3.1.*** *a) Structures of studied triphenylene-2,6,10-tricarboxamides* ***1*** *and schematic representation of helical self-assembly; b) chiral induction in aggregates of* ***n-1*** *with chiral solvent followed by its removal to yield kinetically trapped helices of single handedness.*

## 3.2 Supramolecular polymerization of TTAs studied in chloroform

In the previous chapter we studied the assembly of TTAs **1** in bulk and showed unambiguously the presence of three-fold hydrogen bonding that gives rise to aggregation of the monomers in a helical fashion. Due to the high structural similarity between TTAs **1** and alkyl substituted BTAs, we anticipated that the formation of supramolecular polymers in solution will also occur through threefold hydrogen bonding, resulting in the cooperative formation of helical aggregates. FT-IR spectroscopy in chloroform at 2 mM (Figure 3.1a) shows the absorption bands at 3254 $cm^{-1}$, 1627 $cm^{-1}$ and 1554 $cm^{-1}$ which resembles the spectrum recorded in solid state and confirms the presence of intermolecular hydrogen bonds between TTAs.[78] The UV spectrum of ***(S)*-1** dissolved in chloroform at 512 μM at -5 °C shows a broad absorption band at 260 nm (Figure 3.1b). When increasing the temperature, a bathochromic shift to 276 nm occurs, coinciding with a sharpening of the band and the formation of two

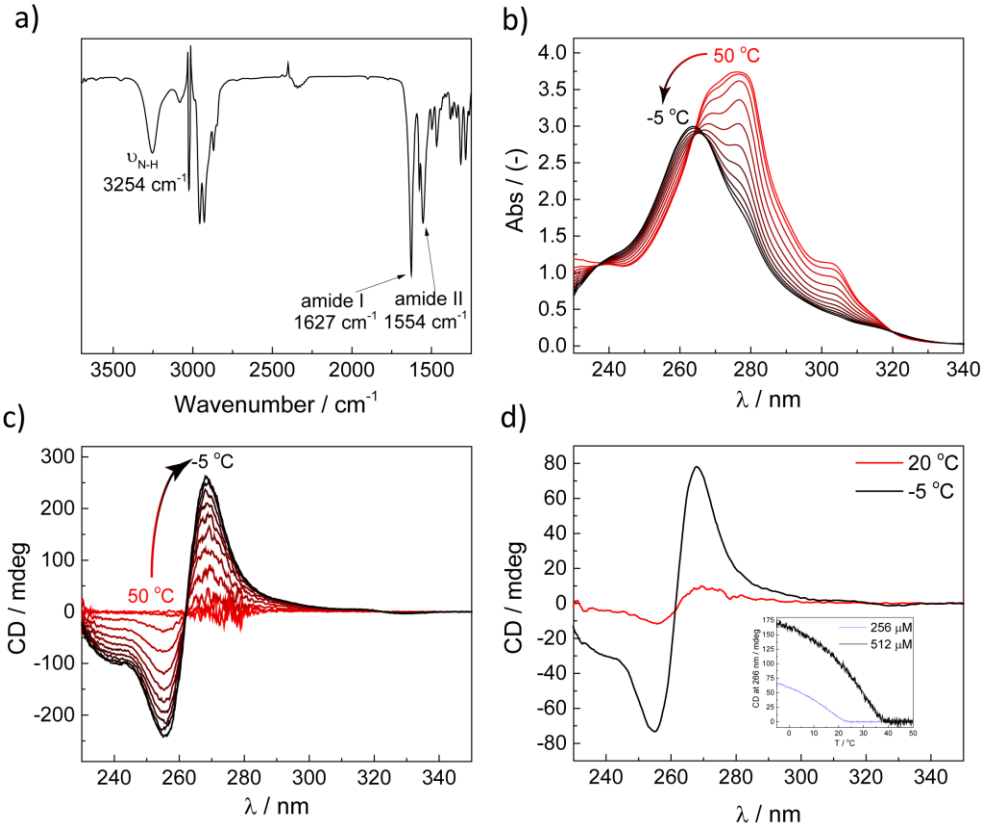


***Figure 3.1.*** *a) FT-IR spectrum of **(S)-1** in chloroform at 2 mM; b) UV and c) CD spectra of **(S)-1** at variable temperatures in chloroform at 512 μM; d) CD spectra of **(S)-1** in chloroform at 256 μM at 20 °C and -5 °C. Inset: VT-CD of **(S)-1** in chloroform at 256 μM and 512 μM (k = 1 K·min$^{-1}$).*

shoulders at 267 nm and 303 nm. Circular dichroism (CD) spectroscopy at the same conditions in chloroform reveals a bisignate Cotton effect (Figure 3.1 c and d), highlighting the presence of a helical bias within the aggregates formed. When the CD signal is followed at 266 nm while cooling the sample at rate of 1 K $min^{-1}$, a non-sigmoidal curve, characteristic for the cooperative aggregation, is observed.[79] Above 40 °C no Cotton effect is observed, whereas decreasing the temperature leads to rapid increase in the Cotton effect. Lowering the concentration to 256 µM results in the loss of the CD signal at room temperature, indicating that the ordered aggregates are lost.

Despite the loss of the CD effect when lowering the concentration, $^1$H NMR spectroscopy at 256 µM reveals the presence of broad peaks only, indicating that ***(S)*-1** is not molecularly dissolved at 20 °C (Figure 3.2a). By plotting the chemical shifts corresponding to the N-*H* and C-$H_{ar}$ peaks of ***(S)*-1** in $CDCl_3$ at 256 µM upon heating from 20 °C to 60 °C, we observe a clear sigmoidal trend, characteristic for isodesmic aggregation together with the peak sharpening (Figure 3.2b). Since we see this behavior for N-*H* protons, we assume that the formation of hydrogen bonds is also involved in the isodesmic process. However lower degree of ordering of the aggregates formed via isodesmic pathway results in no helical packing and lack of the CD signal of these species. The combined results of FT-IR, CD/UV and NMR spectroscopy confirm the assembly of ***(S)*-1** into helical, supramolecular polymers stabilized by threefold intermolecular hydrogen bonds in chloroform above 0.5 mM concentrations, a solvent in which the previously studied BTAs do not aggregate.[80] This indicates that also in solution, the aggregation of TTAs is much stronger than the aggregation of BTAs. However, high concentrations are required for helical aggregation stabilized by intermolecular hydrogen-bond interactions. $^1$H NMR spectroscopy at 256 µM showed that the isodesmic pathway is a

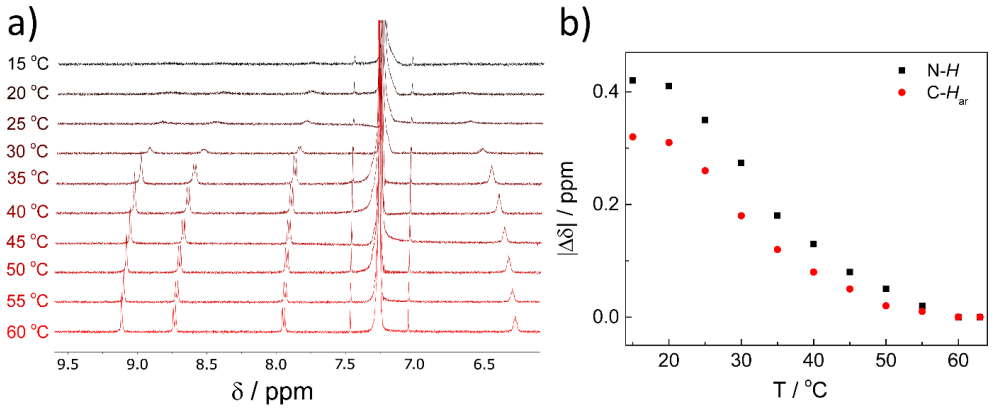


***Figure 3.2.*** *a) Partial $^1$H NMR spectra of **(S)-1** at temperatures between 15 °C to 60 °C ($c_{TTA}$ = 256 µM, $CDCl_3$, 500 MHz); b) absolute change in chemical shift of the **(S)-1** amide N-H and aromatic proton C-$H_{ar}$ protons with respect to the chemical shits at 60 °C as function of temperature.*

result of weak hydrogen bonds and π-π stacking. Lack of the CD signal suggests that these short aggregates are of low supramolecular order.[1]

The presence of two types of aggregates – isodesmic and cooperative – staying in thermodynamic equilibrium with each other can be mechanistically regarded in two ways.[81] In the first mechanism the formation of aggregate of the critical length – the nucleus – is isodesmic. The energetically unfavored isodesmic nucleation is followed by elongation with much higher association constant $K_{ass}$.[82] According to the alternative mechanism, disordered aggregates are in competition with cooperative aggregates.[83] The competition between the aggregates implies important difference between the two mechanism. Whereas in the first case, there is globally one pathway that converts monomers into the polymers, in the second case isodesmic pathway consumes the monomers thereby decreasing the free monomer concentration available for cooperative polymerization. This can have pronounced consequences in case, when energetic difference between the two types of aggregates is small. To distinguish between the two mechanisms, detailed kinetic experiments are required that are out of the scope of this thesis.

## 3.3 Supramolecular polymerization of TTAs studied in decalin

Knowing that **(*S*)-1** can form helical aggregates, we continued detailed studies of ***n*-1**, **(*S*)-1** and **(*R*)-1** in decalin, a solvent that promotes hydrogen-bonding interactions stronger than chloroform and which permits performing assembly-disassembly studies in a broad temperature range. In addition, with the use of the apolar decalin the polymerization can be studied at concentration as low as 5 μM. In decalin at 5 μM, **(*S*)-1** shows identical CD and UV spectra both in shape and intensity to the spectra observed at -5 °C in chloroform at 512 μM, indicating that the nature of the helical aggregates formed in decalin at a 100x lower concentration than in chloroform are the same. Accordingly, **(*R*)-1** showed the mirror-image CD spectrum and ***n*-1** formed a racemic mixture of *P* and *M* helices, giving rise to no net CD signal (Figure 3.3a). Analogously, at temperatures above 97 °C no Cotton effect was observed for **(*S*)-1** and **(*R*)-1**, and the UV spectrum indicated the presence of a molecularly dissolved state with $\lambda_{max}$ = 276 nm. Variable temperature (VT) UV and CD spectra were measured for **(*S*)-1** to probe the nature of the assembly mechanism in dilute decalin solutions (Figure 3.3 b and c). To confirm this, we simultaneously measured UV at the absorption maximum for the monomer (λ = 276 nm) and CD at the maximum of the Cotton effect of the helical aggregate (λ = 266 nm) upon cooling from 105 °C to 20 °C. Initially, a small but noticeable decrease in absorption is observed, while the CD signal remains at zero (Figure 3.3d). This is an indication that also at high temperatures in decalin, disordered aggregates are formed, presumably caused by the absence of directional hydrogen bonding at these high temperatures. Upon reaching the elongation temperature ($T_e$) of 97 °C, a sharp increase in the CD signal is

[1] Weak Cotton effect visible on Figure 3.1d originates from cooperative aggregates.

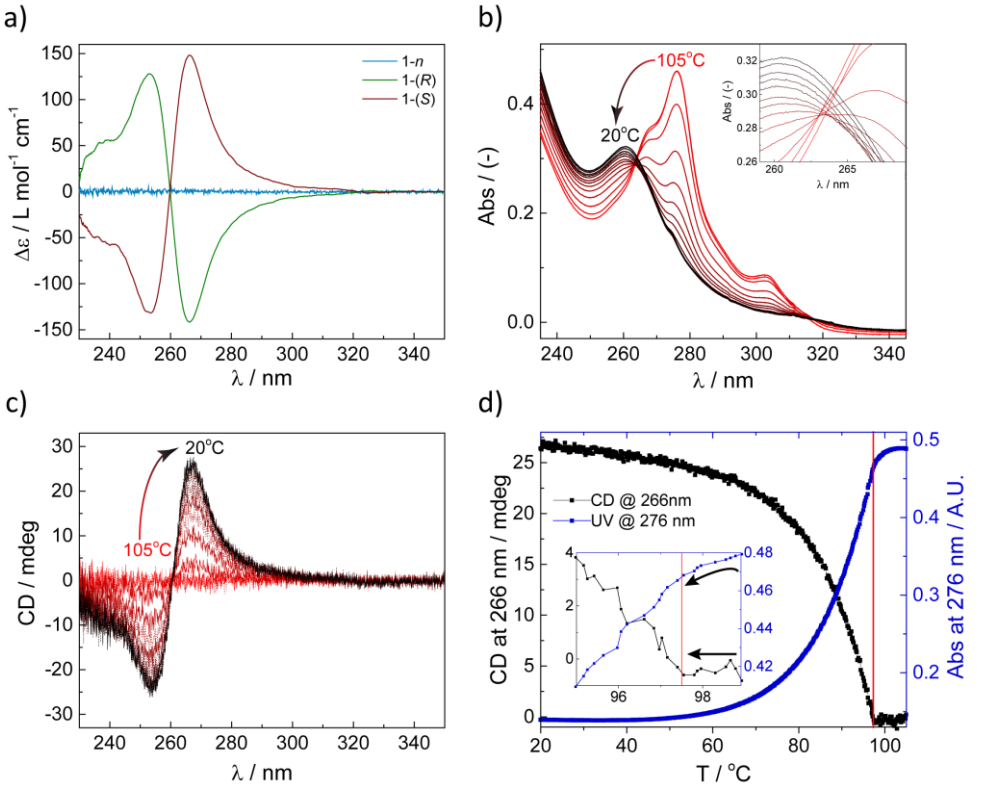


***Figure 3.3*** *a) CD spectra of* ***(S)-1*** */* ***(R)-1*** */* ***n-1****; b) UV and c) CD spectra of* ***(S)-1****; at variable temperatures. Concentration: 5 μM, solvent: decalin; d) CD and UV cooling curves of* ***(S)-1*** *(inset: b) zoom of the temperature-dependent UV-Vis spectra showing lack of a single isosbestic point; d) CD and UV around elongation temperature* $T_e$*, the arrow indicates constant CD signal while UV signal is already decreasing).*

observed; a hallmark of cooperative aggregation. At $T_e$ stable nuclei are formed and the CD-silent, short aggregates are converted into CD-active cooperative aggregates (*vide supra*). These become more prevalent as the system is cooled further and the degree of polymerization increases.

## 3.4 The importance of the sample preparation protocol in TTAs

The high stability of the assemblies formed by TTAs in decalin has important consequences on their energy landscape. Alkyl BTAs always operate at thermodynamic equilibrium, which means that the way the solutions are prepared does not affect the outcome of the measurements.[84] In contrast, in the initial experiments we observed that the CD measurements for TTA solutions suffered from a lack of reproducibility. Due to poor solubility, initially the protocol for sample preparation involved preparing a stock solution of ca 500 μM

of TTA in decalin by heating the solution with a heat gun and simultaneous fast vortex stirring. After fast cooling down, this concentrated solution was diluted to 5 μM and measured in the CD spectrometer. However, preparing a concentrated solution of ***n*-1** according to this protocol resulted sometimes in spontaneous symmetry breaking of otherwise racemic mixture of left- and right-handed helices, similarly to previously reported organogelators.[85,86] In case of ***(S)*-1** mirror image Cotton effects were sometimes observed. In both cases, the thermodynamically controlled states could only be obtained when the 5 μM solutions were subsequently heated to 100 °C and slowly cooled down (1 $K \cdot min^{-1}$) from the molecularly dissolved state. To avoid issues with kinetic traps, we therefore devised a well-defined and reproducible sample preparation protocol. In the protocol, ***(S)*-1** is stirred in decalin at 150 °C for 2 hours to yield a stock solution of 50 μM. This solution is subsequently slowly cooled to room temperature and diluted to 5 μM. This protocol was applied for all measurements reported here, as it affords reproducible results in the homopolymerizations. For copolymerizations, reproducibility in pure decalin could not be achieved (*vide infra* in section Amplification of supramolecular chirality). Importantly, preparation of the solution ($c_{TTA}$ = 500 μM) in chloroform was significantly less troublesome. Such prepared sample showed identical CD spectrum before and after heating (*vide supra* Figure 3.1). We inferred that in chloroform TTA-aggregates are more dynamic than in decalin thus chloroform can be used as a cosolvent to release the kinetic traps.

## 3.5 The influence of cosolvent on the homopolymerization of TTAs

Since TTAs **1** in chloroform form supramolecular polymers at a concentration of 500 μM, but are molecularly dissolved at 5 μM, we can use this solvent as denaturant (cosolvent) for the supramolecular polymers and investigate the effect of the presence of chloroform on the dynamic exchange between monomers and the supramolecular polymers formed. Therefore, we prepared 5 μM solutions of **(*R*)-1** in decalin / chloroform mixtures and recorded UV cooling curves at λ = 276 nm to follow monomerically dissolved **1** and CD cooling curves and at λ = 266 nm to track the cooperative polymer formation (Figure 3.4a and b). The addition of increasing amounts of chloroform reduces linearly the elongation temperature $T_e$ (Figure 3.4c) while the shape of the CD curves remains the same. UV melting curves, however, show that although the cooperative region, similarly to the CD, stays unaffected by the addition of the cosolvent, the isodesmic pathway operates at broader temperature regime with increasing chloroform content. However, the large amount of chloroform required to fully depolymerize stacks of **1** suggests that there is no preferential solvation of chloroform and that chloroform is able to effectively compete for the hydrogen bonds only at high concentrations (Figure 3.4d). Characteristically for cooperative aggregation, below critical chloroform fraction at given concentration (here 40%), the sharp increase in the signal is observed. Interestingly, all samples prepared by dilution of concentrated stock solution in chloroform with decalin do not suffer from the kinetic traps.

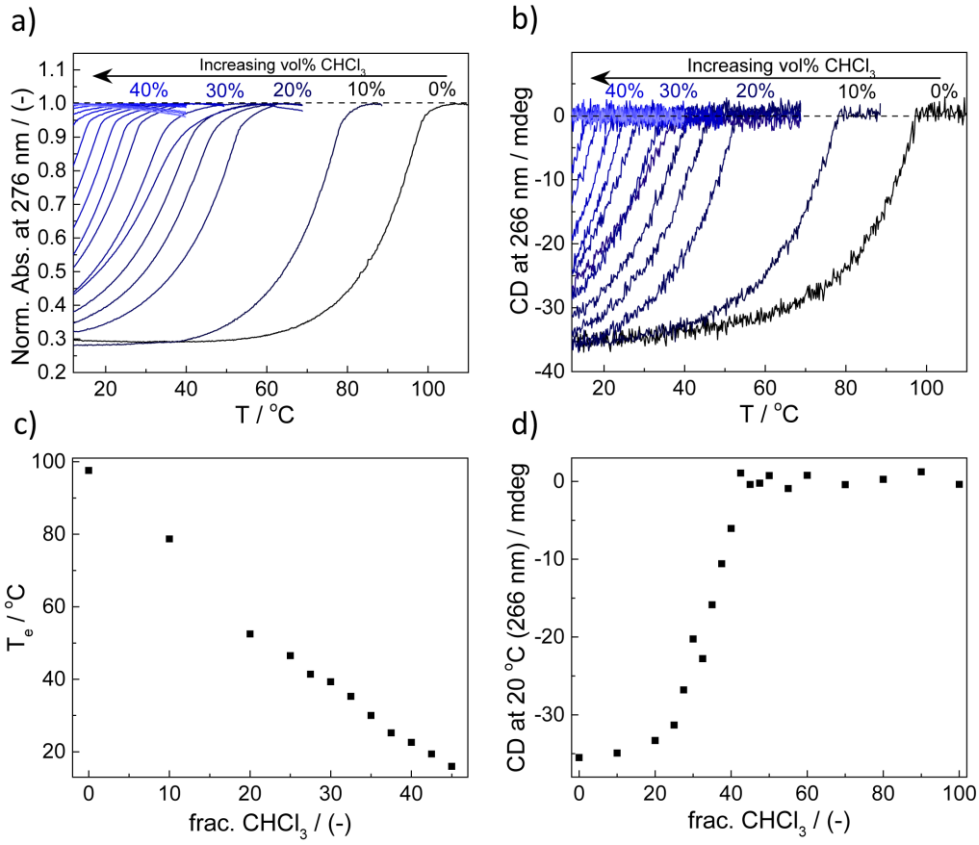


***Figure 3.4*** *a) Normalized absorbance measured at λ = 276 nm and b) CD effect measured as λ = 266 nm as a function of temperature for cooling curves of* ***(R)-1****; c) $T_e$ as a function of fraction of chloroform; d) CD at 266 nm at 20 °C as a function of fraction of chloroform. Concentration = 5 μM, solvent: decalin / chloroform mixtures, cooling rate: 0.5 K·min$^{-1}$.*

To shed more light on the solvent-polymer interactions, we investigated the excited-state properties of ***(S)*-1** by means of VT fluorescence measurements in decalin and decalin / chloroform solutions ($c$ = 5 μM). We selected the excitation wavelength $\lambda_{ex}$ corresponding to the absorption maximum of the monomerically dissolved species ($\lambda_{ex}$ = 276 nm, Figures 3.5a, b and c). At high temperatures and/or high chloroform content (red curves in Figure 3.5a, b and c), all spectra show a strong and narrow emission band at 380 nm corresponding to the emission of the monomerically dissolved species. When lowering the temperature, a new, broad band between 450 nm and 500 nm, corresponding to the aggregated species, appears. The relatively large Stokes shift and band broadening were observed before for aggregated triphenylene derivatives and were rationalized by the formation of an excimer state.[87,88] When following the intensity of the emission maxima at 380 nm, upon cooling the solutions, the initial gradual decrease of monomer emission is followed by a steep decrease (Figures 3.5d).

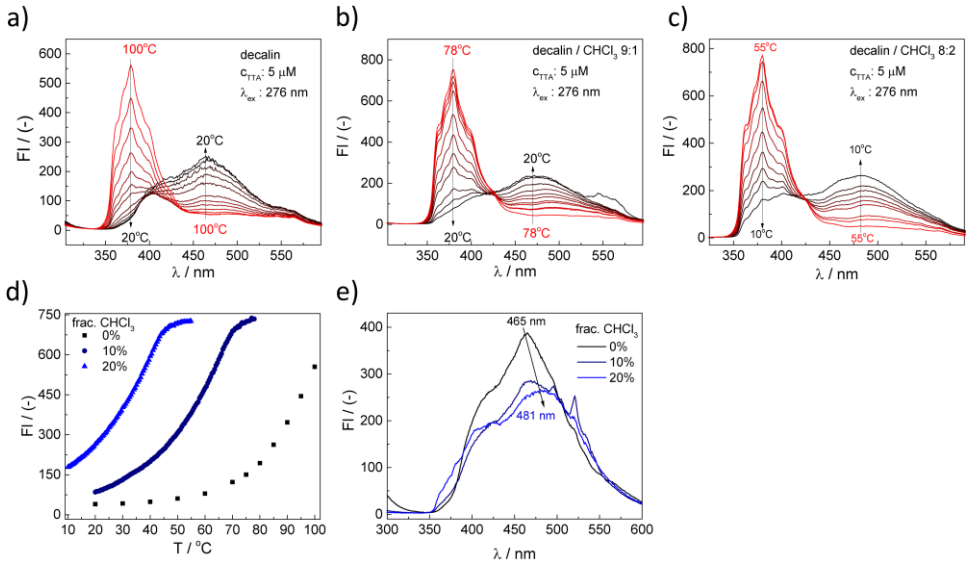


***Figure 3.5*** *Fluorescence spectroscopy in solution of* ***(S)-1.*** *The excitation wavelength $\lambda_{ex}$ was adjusted to the emission maximum of the monomer ($\lambda_{ex}$ = 276 nm, spectra a, b and c); d) VT-fluorescence of* ***(S)-1*** *in decalin / $CHCl_3$ mixtures at rate 1 K $min^{-1}$; e) Fluorescence spectra of the polymer ($\lambda_{ex}$ = 260 nm) at variable content of $CHCl_3$. Upon addition of $CHCl_3$ red shift and the decrease in intensity is observed.*

This suggests that the initial isodesmic aggregation followed by a cooperative aggregation can also be probed by fluorescence spectroscopy. Interestingly, the wavelength of the maxima of the broad emission band increases with increasing the fraction of chloroform (Figure 3.5.e). This shift shows that, although solvent property has no impact on the excited state properties of the monomer, it does affect the excimer state in the aggregates. All experiments performed in chloroform, decalin and their mixtures show the presence of the two aggregation pathways – isodesmic and cooperative. Earlier investigations by van der Zwaag et al show that multiple aggregates can belong to a single nucleation-elongation pathway or to two distinct competing pathways (*vide supra,* section 3.2).[81] Fitting of the experimental data for TTAs **1** obtained at the thermodynamic equilibrium to models describing both types of the energetic landscape yielded reasonable fits for both. To ultimately unravel the mechanism governing the assembly of a system showing such polymorphism, kinetic experiments together with a descriptive kinetic model have to be employed.

The kinetic experiments and modelling we did not address in this chapter. Alternatively, preliminary fitting of the data obtained at thermodynamic equilibrium was performed by Mathijs Mabesoone. Herein the model that describes the isodesmic nucleation within a single-cooperative pathway (Figure 3.6a), was applied. The results permit to qualitatively estimate higher stability of the TTAs **1** than the alkyl BTAs (Figure 3.6b). Significantly lower ΔG (-54 kJ

a)

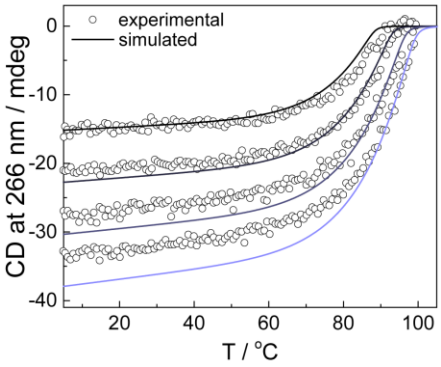


b)

| | ***(R)*-1** | ***R*-BTA**[b] |
|---|---|---|
| $\Delta H$ (kJ·mol$^{-1}$) | –96 | –72 |
| $\Delta S$ (kJ·mol$^{-1}$) | –142 | –128 |
| $\Delta G$ (kJ·mol$^{-1}$)[a] | –54 | –35[c] |
| $\sigma$[a] | 1.6x10$^{-4}$ | 4.6x10$^{-6}$ |

***Figure 3.6*** *a) Experimental and simulated CD cooling curves of* ***(R)-1*** *in decalin at variable concentrations (rate: 0.5 K min$^{-1}$); b) thermodynamic parameters obtained from the simulations. [a] The cooperativity parameter σ and Gibbs free energies are determined at 293 K. [b]Data obtained from ref 59. [c] calculated from the ΔH and ΔS using equation ΔG = ΔH-TΔS.*

mol$^{-1}$ for 1 versus -35 kJ mol$^{-1}$ for **S-BTA**) meets our expectations as even at very low concentrations, supramolecular polymers of **1** form very stable aggregates. The differences in the cooperativity parameter σ arise from a difference in assumed size of nucleus, which in turn affects the nucleation penalty. While for the BTA, a nucleus size of 2 was assumed, in case of TTAs, the best fits were obtained for the nucleus size 4. Qualititatively, the results can be treated as constraints for the kinetic model. Quantitative results can be obtained only after kinetic experiments are done.

## 3.6 Amplification of supramolecular chirality in TTAs: the sergeants-and-soldiers and majority-rules principle

For the "sergeants-and-soldiers" and "majority-rules" experiments, we mixed chiral **(*S*)-1** with achiral ***n*-1** or its enantiomer **(*R*)-1** in decalin or decalin - chloroform keeping the total monomer concentration constant at 5 μM. We hypothesized that due to structural similarity to the BTAs, TTAs should also manifest strong amplification of supramolecular chirality.[53] On the other hand, the low solubility of the TTAs in alkanes could lead to kinetically controlled states, in which transfer of supramolecular chirality could be hampered.

The sergeants-and-soldiers experiment was conducted by copolymerizing **(*S*)-1** with ***n*-1**. In order to examine the role of cosolvent in copolymerization, we applied the same protocol for solutions prepared in decalin and decalin / chloroform mixtures. After mixing, the CD cooling curves were obtained by slowly cooling from molecularly dissolved state (Figure 3.7a). In pure decalin a linear dependence of the CD signal with respect to the fraction of **(*S*)-1** was observed at 20 °C after cooling down with a rate of 0.5 K min$^{-1}$. Such prepared sample of 10% sergeants **(*S*)-1** in pure decalin standing on the bench shows 40% of chiral

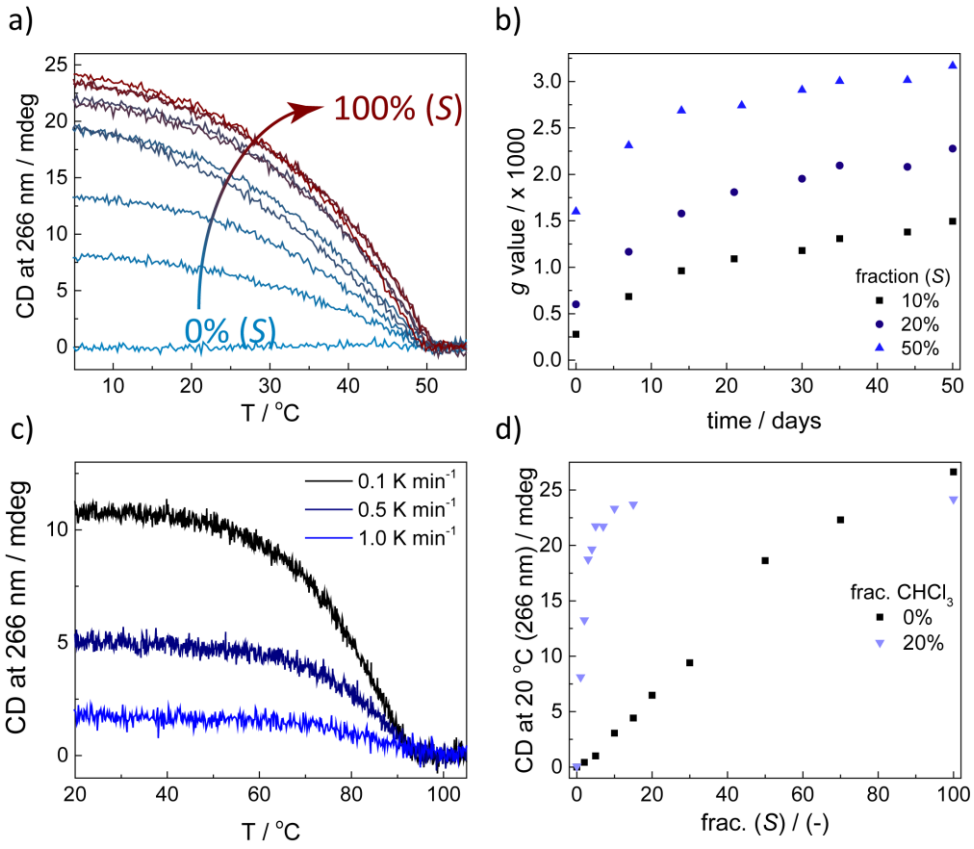


***Figure 3.7*** *a) CD cooling curves of* ***(S)-1*** *copolymerized with* ***n-1*** *at variable fractions of* ***(S)-1*** *in decalin / chloroform 8:2; b) anisotropy g value as a function of time of* ***(S)-1*** */* ***n-1*** *solutions in decalin at fraction sergeant of 10%, 20% and 50%; c) CD-cooling curves of* ***(S)-1*** */* ***n-1*** *at fraction sergeant 10% in decalin at different cooling rates; d) CD effect as a function of the fraction of* ***(S)-1*** *in decalin / chloroform solutions at* $c_{total}$ *= 5 µM.*

amplification after 50 days (Figure 3.7b). This suggests that in decalin the supramolecular chirality transfer is kinetically controlled. To confirm this statement, we performed the VT-CD experiment of the 10% of sergeants **(*S*)-1** at variable cooling rates. Interestingly, the degree of chiral amplification was enlarged by applying very slow cooling rate (0.1 K $min^{-1}$), while little to no amplification was observed at the rates of 0.5 K $min^{-1}$ and 1 K $min^{-1}$ (Figure 3.7c). On the other hand, in the presence of chloroform only 10% of chiral sergeant **(*S*)-1** is necessary to yield full chiral expression (Figure 3.7d). Subsequent removal of chloroform results in no change in the CD signal over days, confirming the presence of thermodynamically controlled states. These results imply that in decalin the system is kinetically controlled and only addition of aliquots of good solvent (chloroform) enable formation of thermodynamically stable fibers with high degree of chiral amplification. Similar solvent-dependent chiral amplification was

observed previously. The origin of this phenomenon was ascribed to the frozen dynamics of the system in "bad" solvent that results in a lack of monomer exchange between the fibers and subsequent kinetic traps. The "good" solvent releases the kinetic traps by inducing exchange of monomers between polymers.[72,73]

To perform the majority-rules experiment, we start with a racemic mixture of **(*S*)-1** and **(*R*)-1** in decalin, and titrate small amounts of **(*R*)-1** into this mixture ($c_{tot,TTA}$ = 5 µM). After mixing, the CD cooling curves were obtained by slowly cooling from the molecularly dissolved state (Figure 3.8a). VT-CD experiments revealed that the majority-rules experiment is equally sensitive towards the solvent composition. The CD signal at the assembled state plotted as a function of the enantiomeric excess shows a clear difference in the strength of the effect in the mixtures with and without chloroform. A strong deviation from linearity is only observed when chloroform is present. An *ee* of only 15% is required to obtain fibers of one helical sense in the presence of 20% chloroform, which implies that the mismatch penalty (MMP) in the TTAs is considerably lower than the MMP of BTAs where an *ee* of 40% is needed to fully dictate the supramolecular chirality at room temperature.[53] In contrast, when using pure decalin as the solvent the increase of the CD effect is much more gradual as a function of *ee* (Figure 3.8b). This is readily explained by hampered dynamics of the system without chloroform. It is therefore impossible to arrive at thermodynamic equilibrium at reasonable time scale even at high temperatures. Fitting the experimental data into a two-component mass balance model[59] was performed by Mathijs Mabesoone and yielded a mismatch penalty of 0.46 kJ·mol$^{-1}$ for the TTAs when 20% chloroform is present. This value is 4 times lower than the one of BTAs (2.1 kJ·mol$^{-1}$) in pure methylcyclohexane. The results indicate that a higher fraction of

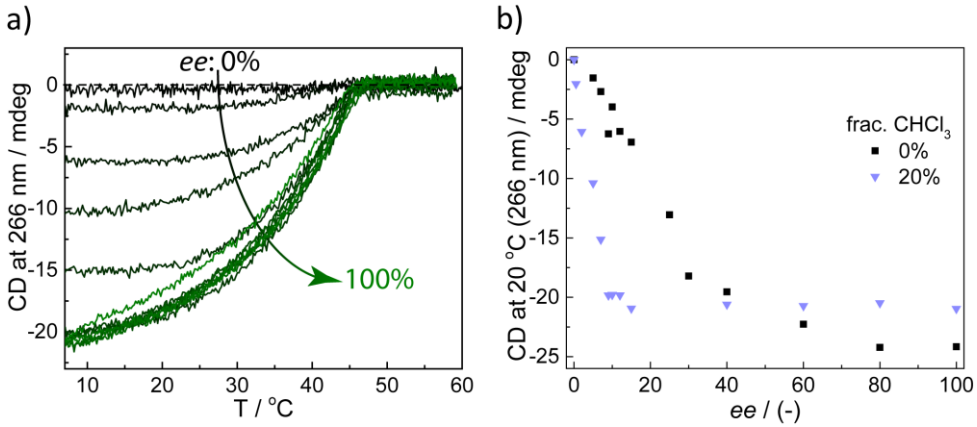


***Figure 3.8.*** *a) CD cooling curves of* ***(S)-1*** *and* ***(R)-1*** *mixtures with varying ee values in decalin / chloroform 8:2 at* $c_{total}$ *= 5 µM; b) CD effect versus ee in decalin / chloroform solutions* $c_{total}$ *= 5 µM at 20°C (decalin) and 10 °C (decalin / chloroform 8:2).*

the other enantiomer is tolerated in a *P* or *M* helical stacks before the opposite helical sense starts to form.

## 3.7 The origin of solvent-dependent amplification of supramolecular chirality

On the basis of the above experiments we conclude that the exchange of the monomers between the aggregates in pure decalin is very slow, while this is not the case when chloroform in small amounts is present. A reason for this behavior could be in differences in structure of the fibers. Although we assumed that the helical aggregates in both decalin and decalin / chloroform mixtures consist of a fiber with 1 molecule in the cross section, previous studies have revealed that poor solvents can result in bundling of fibers, which reduces the dynamic exchange.[89,90] The slow exchange between monomer and polymers could be explained by bundle formation, which in turn may trap monomers in their respective fibers due to the solvophobic effects. The presence of slow exchange in decalin may enable the selective trapping of a kinetic product on long time scales as long as no cosolvent is present in the system. On the other hand, the thermodynamic product can be easily obtained by using the cosolvent, therefore the cosolvent can be considered as a lever for the choice between kinetic and thermodynamic pathway. In a kinetically hindered system, even at the temperatures of the nucleation, the dynamics of the system are slow enough to promote kinetically controlled states. Only complete equilibration, which happens on relatively long time scales, enables the formation of the nuclei that leads to the formation of thermodynamically favored fibers. Obviously, in presence of chloroform, such a long equilibration time for the nuclei is not a prerequisite to obtain full chiral amplification.

## 3.8 Induction of supramolecular chirality with a volatile chiral solvent

It was previously shown that small, chiral molecules can bias the helicity of the supramolecular polymers through specific interactions in the case of chiral dopants[38–42] or non-specific interactions in the case of chiral solvents.[32,34–36] The group of Green described effective chiral induction in achiral, dynamic helical polyisocyanates with a series of chiral chloroalkanes.[31] Following this work, we selected (*S*)-1-chloro-2-methylbutane ((*S*)-ClMeBu) as a cosolvent for the decalin solutions of ***n*-1**. Upon increasing the amount of (*S*)-ClMeBu we observe that 60% of (*S*)-ClMeBu in decalin is enough to yield a CD spectrum reminiscent of ***(S)*-1** in decalin / chloroform 8:2 (Figure 3.8a). Besides chiral induction, (*S*)-ClMeBu also destabilizes polymers, which is reflected in the gradual decrease in the CD signal at higher fractions of (*S*)-ClMeBu. A plot of the CD intensity at 20 °C at various chiral solvent fractions shows that the chiral induction increases linearly to 40% of (*S*)-ClMeBu, where it reaches a maximum (Figure 3.8b). Above 80% of the (*S*)-ClMeBu the solvent effectively competes with the hydrogen bonds thereby causing depolymerization. To estimate the degree of chiral induction, we calculated the anisotropy value ($g_{value}$) of the solutions based on ***n*-1** and

compared to the one obtained by ***(S)*-1** in decalin. Remarkably, the $g_{value}$ of any solution between 40% and 80% of (*S*)-ClMeBu is equivalent to the $g_{value}$ measured for ***(S)*-1** in decalin at thermodynamic equilibrium ($g_{value}$ = 0.0035). This result highlights that full chiral induction is achieved in ***n*-1** in the presence of 40% of (*S*)-ClMeBu.

Next, to realize our strategy for obtaining optically pure fibers in an achiral solvent with an achiral TTA, we prepared a 7.5 µM solution of ***n*-1** in decalin / (*S*)-ClMeBu 1:1 (vv), equilibrated the sample by slow cooling from 80 °C to room temperature and measured the CD spectrum, which showed full chiral induction. After this, the chiral cosolvent was removed. This could be achieved by bubbling of the solution with argon overnight as shown the $^1$H NMR spectroscopy, which showed no signals corresponding to (*S*)-ClMeBu. On completion, the

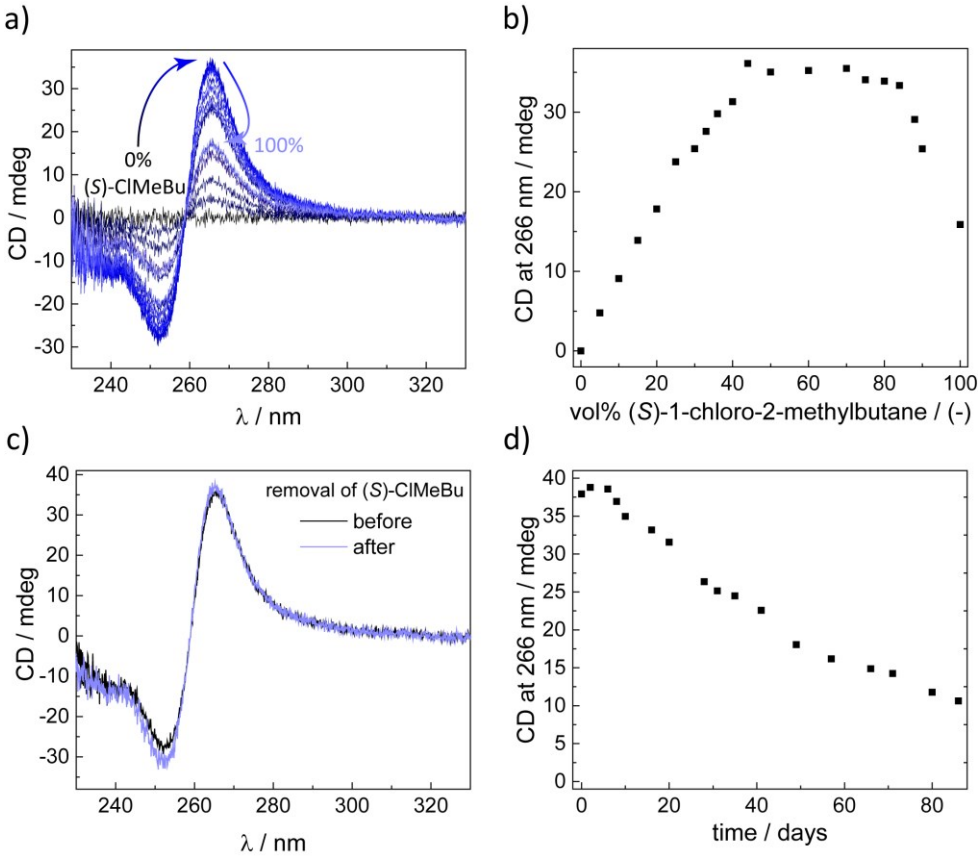


***Figure 3.9.*** *a) CD spectra of **n-1** at various decalin / (S)-ClMeBu compositions; b) CD effect at 266 nm of **n-1** solutions in decalin / (S)-ClMeBu as a function of fraction of (S)-ClMeBu; c) CD spectra of **n-1** before and after removal of (S)-ClMeBu; d) CD effect at 266 nm of **n-1** solutions after removal of (S)-ClMeBu as a function of time.* $c_{TTA}$ *= 7.5 µM.*

concentration of the solution was readjusted to 7.5 μM by adding the appropriate amount of decalin. The measured CD spectrum showed an identical strength of the CD effect, indicative of the chiral memory of the system (Figure 3.8c). To measure the kinetic stability of these polymers, we collected a CD spectrum every few days and measured the strength of the CD effect at 266 nm as a function of time (Figure 3.8d). The extraordinary high kinetic stability of the polymers was confirmed by a racemization half-life, $\tau_{1/2}$, of over 40 days, which is, to the best of our knowledge, one of the highest reported for supramolecular polymers.

## 3.9 Conclusions

In this chapter, we have shown that a simple extension of an aromatic benzene core to a triphenylene core on the one hand increases significantly the thermodynamic stability of the formed supramolecular polymers and on the other makes the system more prone to kinetic traps when poor solvents are used. By applying a combination of spectroscopic techniques and mathematical models, we showed that TTA-based supramolecular polymers are formed via isodesmic and cooperative nucleation-elongation mechanism staying in thermodynamic equilibrium with each other. Interestingly, adding more chloroform results in the isodesmic pathway operating at broader temperature regime, whereas the cooperativity of the process is hardly affected. By using "majority-rules" and "sergeants-and-soldiers" principles we found that strong amplification of supramolecular chirality can be achieved only in presence of chloroform. In decalin, the copolymerizations suffer from kinetic traps, resulting in very slow exchange of monomer between polymers, and consequently low amplification of supramolecular chirality. The presence of kinetic traps also presented the opportunity to achieve cosolvent-controlled pathway selection. In this way, homochiral fibers were formed from an achiral monomer with use of a chiral cosolvent. Due to monomer-solvent interactions, full induction of chirality was obtained. As long as the chiral solvent was present, the chirality of the fibers was under thermodynamic control. Upon removal of the chiral solvent and "freezing" the fibers in decalin, a kinetically trapped state was obtained, which showed a very slow racemization profile. Such high kinetic stability of the supramolecular fibers might be interesting for applications in optoelectronic devices, where kinetic and thermodynamic stability of the supramolecular structures constitute an important issue in the fabrication process. In addition, the control over kinetic and thermodynamic stability that TTAs display, may have implications for the non-covalent synthesis of increasingly complex supramolecular architectures. The successful isolation of kinetically trapped structures are reminiscent of some of the early steps in the synthetic methodology of classical covalent organic chemistry.

## 3.10 Experimental Section

### 3.10.1 Materials and methods

All standard solvents were obtained from Biosolve, Acros or Aldrich and used as received. *(S)*-1-Chloro-2-methylbutane ((*S*)-ClMeBu) was synthesized according to modified protocol of previously

described procedure.[90] Variable temperature (VT) $^1$H NMR spectra were recorded on a Varian Unit Inova 500 MHz NMR. Proton chemical shifts (δ) are reported in ppm downfield from tetramethylsilane (TMS). All infrared measurements were performed on a Perkin Elmer FT-IR Spectrum Two apparatus. Circular dichroism and UV-Vis absorption spectroscopy was performed on a JASCO J-815 CD spectrometer with either a JASCO Peltier MPTC-490S temperature controller with a range of 278 – 373 K or a JASCO Peltier PFD-425S/15 with a range of 263 – 383 K. Separate UV/Vis spectra were obtained from a Perkin–Elmer UV/Vis spectrometer Lambda 40. Fluorescence spectra were measured with Varian Cary Eclipse fluorescence spectrometer. For all spectroscopic measurements, cells with an optical path length of 1 cm were employed and spectroscopic grade solvents were employed. Stock solutions (75 µM) were prepared by weighing the necessary amount of compound for the given concentration and transferring it to a screw-capped vial that was filled up to the proper volume using Gilson™ MICROMAN™ Positive-Displacement Pipets. The stock solutions were heated up and stirred until the solid material was completely dissolved every time before the preparation of diluted sample solutions. All the spectroscopic measurement were performed with freshly prepared solutions (max. 1 week after the preparation of the stock solution). The molar dichroism is defined as Δε = CD effect/(32980·c·l) in which c is the concentration in mol·L$^{-1}$ and l is the optical path length in cm. Anisotropy value *g*: *g* = CD effect / (absorbance·32980).

### 3.10.2 Synthetic procedures

(*S*)-1-Chloro-2-methylbutane ((*S*)-ClMeBu)[91]

(*S*)-2-Methylbutan-1-ol (247 mL, 2.27 mol) and freshly distilled pyridine (183 mL, 2.27 mol) were placed in a 1 L 3-neck round-bottomed flask equipped with a mechanical stirrer and dropping funnel. The mixture was heated up to 60 °C and subsequently, freshly distilled thionyl chloride (246 mL, 3.40 mol) was added dropwise within 4 hours. Upon addition of c.a. 1 eq. of $SOCl_2$, the reaction mixture became a slurry (crystallization of pyridinium chloride). Upon subsequent addition of the remaining $SOCl_2$, the brown biphasic mixture was obtained. The progress of the reaction was monitored by $^1$H NMR. The reaction was regarded as complete, when a characteristic quartet of doubles at 3.47 ppm is the only group of signals between 5 ppm and 3 ppm (other intermediates corresponding to possible sulfite were present during the course of the reaction). On completion, the biphasic mixture was moved to the separatory funnel without cooling (bottom, inorganic phase crystallizes at low temperatures, making separation not possible) and quickly separated. The upper, organic layer was subsequently washed with water, saturated $NaHCO_3$, water and brine (emulsion formation possible), dried over magnesium sulfate, which was filtered off to yield 150 mL of brown liquid. In order to yield the solvent in suitable quality for spectroscopic measurements, three fractional distillations under reduced pressure (p = 190 mbar, b.p. = 60 °C) were carried out. After the first distillation, the distillate was collected and redistilled twice from over the activated charcoal. Finally the liquid was stirred overnight with a mixture containing activated charcoal, silicagel, neutral aluminum and potassium carbonate (ca 1 gram each) and subsequently filtered off to yield 135 mL (56%) of (*S*)-ClMeBu, which was stored over 3Å molecular sieves.

$^1$H NMR (500 MHz, $CDCl_3$,): δ = 3.47 (qd, J = 10.7, 5 Hz, 2H), 1.75 (m, 1H), 1.53 (m, 1H), 1.28 (m, 1H), 1.02 (d, *J* = 6.7 Hz, 3H), 0.93 (t, J = 7.5 Hz, 3H)

## 3.11 References

[1] E. Yashima, K. Maeda, H. Iida, Y. Furusho, K. Nagai, *Chem. Rev.* **2009**, *109*, 6102–6211.

[2] E. Yashima, N. Ousaka, D. Taura, K. Shimomura, T. Ikai, K. Maeda, *Chem. Rev.* **2016**, *116*, 13752–

13990.
[3] R. J. M. Nolte, A. J. M. van Beijnen, W. Drenth, *J. Am. Chem. Soc.* **1974**, *96*, 5932–5933.
[4] M. M. Green, K. S. Cheon, S. Y. Yang, J. W. Park, S. Swansburg, W. Liu, *Acc. Chem. Res.* **2001**, *34*, 672–680.
[5] M. Suginome, T. Yamamoto, Y. Nagata, *J. Synth. Org. Chem., Jpn.* **2015**, *73*, 1141–1155.
[6] E. Yashima, *Anal. Sci.* **2002**, *18*, 3–6.
[7] M. Fujiki, J. R. Koe, K. Terao, T. Sato, A. Teramoto, J. Watanabe, *Polym. J.* **2003**, *35*, 297–344.
[8] Y. Okamoto, M. Nishikawa, T. Nakano, E. Yashima, K. Hatada, *Macromolecules* **1995**, *28*, 5135–5138.
[9] D. S. Schlitzer, B. M. Novak, *J. Am. Chem. Soc.* **1998**, *120*, 2196–2197.
[10] R. Nomura, J. Tabei, T. Masuda, *Macromolecules* **2002**, *35*, 2955–2961.
[11] J. Deng, X. Luo, W. Zhao, W. Yang, *J. Polym. Sci. Part A Polym. Chem.* **2008**, *46*, 4112–4121.
[12] V. Percec, M. Obata, J. G. Rudick, B. B. De, M. Glodde, T. K. Bera, S. N. Magonov, V. S. K. Balagurusamy, P. A. Heiney, *J. Polym. Sci. Part A Polym. Chem.* **2002**, *40*, 3509–3533.
[13] J. C. Nelson, J. G. Saven, J. S. Moore, P. G. Wolynes, *Science* **1997**, *277*, 1793–1796.
[14] R. B. Prince, S. A. Barnes, J. S. Moore, *J. Am. Chem. Soc.* **2000**, *122*, 2758–2762.
[15] V. Berl, I. Huc, R. G. Khoury, M. J. Krische, J. M. Lehn, *Nature* **2000**, *407*, 720–723.
[16] A. Tanatani, M. J. Mio, J. S. Moore, *J. Am. Chem. Soc.* **2001**, *123*, 1792–1793.
[17] V. Maurizot, C. Dolain, I. Huc, *European J. Org. Chem.* **2005**, 1293–1301.
[18] G. Yuan, C. Zhu, Y. Liu, W. Xuan, Y. Cui, *J. Am. Chem. Soc.* **2009**, *131*, 10452–10460.
[19] M. A. Alam, A. Tsuda, Y. Sei, K. Yamaguchi, T. Aida, *Tetrahedron* **2008**, *64*, 8264–8270.
[20] J. F. Modder, K. Vrieze, A. L. Spek, G. Challa, G. van Koten, *Inorg. Chem.* **1992**, *31*, 1238–1247.
[21] L. J. Prins, F. De Jong, P. Timmerman, D. N. Reinhoudt, *Nature* **2000**, *408*, 181–184.
[22] H. Engelkamp, S. Middelbeek, R. J. M. Nolte, *Science* **1999**, *284*, 785–789.
[23] J. H. K. K. Hirschberg, L. Brunsveld, A. Ramzi, J. A. J. M. Vekemans, R. P. Sijbesma, E. W. Meijer, *Nature* **2000**, *407*, 167–170.
[24] C. Thalacker, F. Würthner, *Adv. Funct. Mater.* **2002**, *12*, 209–218.
[25] V. Percec, A. E. Dulcey, V. S. K. Balagurusamy, Y. Miura, J. Smidrkal, M. Peterca, S. Nummelin, U. Edlund, S. D. Hudson, P. A. Heiney, H. Duan, S. N. Magonov, S. A. Vinogradov, *Nature* **2004**, *430*, 764–768.
[26] G. D. Pantoş, P. Pengo, J. K. M. Sanders, *Angew. Chem. Int. Ed.* **2007**, *46*, 194–197.
[27] S. Pense, N. Nouvel, A. Guilleman, C. Creton, F. Boue, L. Bouteiller, *Macromolecules* **2010**, *43*, 2529–2534.
[28] F. García, L. Sánchez, *J. Am. Chem. Soc.* **2012**, *134*, 734–742.
[29] S. Ogi, K. Sugiyasu, S. Manna, S. Samitsu, M. Takeuchi, *Nat. Chem.* **2014**, *6*, 188–195.
[30] J. Kang, D. Miyajima, T. Mori, Y. Inoue, Y. Itoh, T. Aida, *Science* **2015**, *347*, 646–651.
[31] M. M. Green, C. Khatri, N. C. Peterson, *J. Am. Chem. Soc.* **1993**, *115*, 4941–4942.
[32] A. R. A. Palmans, J. A. J. M. Vekemans, E. E. Havinga, E. W. Meijer, *Angew. Chem. Int. Ed.* **1997**, *36*, 2648–2651.
[33] Y. Nakano, Y. Liu, M. Fujiki, *Polym. Chem.* **2010**, *1*, 460–469.
[34] Y. Kawagoe, M. Fujiki, Y. Nakano, *New J. Chem.* **2010**, *34*, 637–647.
[35] B. Isare, M. Linares, L. Zargarian, S. Fermandjian, M. Miura, S. Motohashi, N. Vanthuyne, R. Lazzaroni, L. Bouteiller, *Chem. Eur. J.* **2009**, *16*, 173–177.
[36] V. Stepanenko, X. Q. Li, J. Gershberg, F. Würthner, *Chem. Eur. J.* **2013**, *19*, 4176–4183.
[37] E. Yashima, T. Matsushima, Y. Okamoto, *J. Am. Chem. Soc.* **1997**, *119*, 6345–6359.
[38] R. Oda, I. Huc, S. J. Candau, *Angew. Chem. Int. Ed.* **1998**, *37*, 2689–2691.
[39] R. Oda, I. Huc, M. Schmutz, S. J. Candau, F. C. MacKintosh, *Nature* **1999**, *399*, 566–569.
[40] A. A. Sobczuk, Y. Tsuchiya, T. Shiraki, S. I. Tamaru, S. Shinkai, *Chem. Eur. J.* **2012**, *18*, 2832–2838.

[41] S. J. George, R. de Bruijn, Ž. Tomović, B. Van Averbeke, D. Beljonne, R. Lazzaroni, A. P. H. J. Schenning, E. W. Meijer, *J. Am. Chem. Soc.* **2012**, *134*, 17789–17796.
[42] W. Zhang, W. Jin, T. Fukushima, N. Ishii, T. Aida, *J. Am. Chem. Soc.* **2012**, *135*, 114–117.
[43] J. Kim, J. Lee, W. Y. Kim, H. Kim, S. Lee, H. C. Lee, Y. S. Lee, M. Seo, S. Y. Kim, *Nat. Commun.* **2015**, *6*, 1–8.
[44] M. M. Green, M. P. Reidy, *J. Am. Chem. Soc.* **1989**, *111*, 6452–6454.
[45] M. M. Green, B. A. Garetz, B. Munoz, H. P. Chang, S. Hoke, R. G. Cooks, *J. Am. Chem. Soc.* **1995**, *117*, 4181–4182.
[46] K. Maeda, Y. Okamoto, *Macromolecules* **2002**, *31*, 1046–1052.
[47] R. B. Prince, J. S. Moore, L. Brunsveld, E. W. Meijer, *Chem. Eur. J.* **2001**, *7*, 4150–4154.
[48] F. Takei, K. Onitsuka, S. Takashashi, *Polym. J.* **2000**, *32*, 524–526.
[49] M. Fujiki, *Macromol. Rapid Commun.* **2001**, *22*, 539–563.
[50] T. W. Anderson, J. K. M. Sanders, G. D. Pantoş, *Org. Biomol. Chem.* **2010**, *8*, 4274–4280.
[51] W. Jin, T. Fukushima, M. Niki, A. Kosaka, N. Ishii, T. Aida, *Proc. Natl. Acad. Sci.* **2005**, *102*, 10801–10806.
[52] L. J. Prins, P. Timmerman, D. N. Reinhoudt, *J. Am. Chem. Soc.* **2001**, *123*, 10153–10163.
[53] M. M. J. Smulders, I. A. W. Filot, J. M. A. Leenders, P. van der Schoot, A. R. A. Palmans, A. P. H. J. Schenning, E. W. Meijer, *J. Am. Chem. Soc.* **2010**, *132*, 611–619.
[54] J. S. Valera, R. Gómez, L. Sánchez, *Angew. Chem. Int. Ed.* **2019**, *58*, 510–514.
[55] T. Kim, T. Mori, T. Aida, D. Miyajima, *Chem. Sci.* **2016**, *7*, 6689–6694.
[56] M. Liu, L. Zhang, T. Wang, *Chem. Rev.* **2015**, *115*, 7304–7397.
[57] L. J. Prins, D. N. Reinhoudt, P. Timmerman, *Angew. Chem. Int. Ed.* **2001**, *40*, 2382–2426.
[58] A. R. A. Palmans, E. W. Meijer, *Angew. Chem. Int. Ed.* **2007**, *46*, 8948–8968.
[59] A. J. Markvoort, H. M. M. ten Eikelder, P. a. J. Hilbers, T. F. A. de Greef, E. W. Meijer, *Nat. Commun.* **2011**, *2*, 509.
[60] J. Van Gestel, P. Van der Schoot, M. A. J. Michels, *J. Chem. Phys.* **2004**, *120*, 8253–8261.
[61] M. M. J. Smulders, P. J. M. Stals, T. Mes, T. F. E. Paffen, A. P. H. J. Schenning, A. R. A. Palmans, E. W. Meijer, *J. Am. Chem. Soc.* **2010**, *132*, 620–626.
[62] S. Cantekin, D. W. R. Balkenende, M. M. J. Smulders, A. R. A. Palmans, E. W. Meijer, *Nat. Chem.* **2011**, *3*, 42–46.
[63] Y. Nakano, A. J. Markvoort, S. Cantekin, I. A. W. Filot, H. M. M. Ten Eikelder, E. W. Meijer, A. R. A. Palmans, *J. Am. Chem. Soc.* **2013**, *135*, 16497–16506.
[64] S. Cantekin, Y. Nakano, J. C. Everts, P. Van Der Schoot, E. W. Meijer, A. R. A. Palmans, *Chem. Commun.* **2012**, *48*, 3803–3805.
[65] M. Endo, T. Fukui, S. H. Jung, S. Yagai, M. Takeuchi, K. Sugiyasu, *J. Am. Chem. Soc.* **2016**, *138*, 14347–14353.
[66] S. Ogi, V. Stepanenko, K. Sugiyasu, M. Takeuchi, F. Würthner, *J. Am. Chem. Soc.* **2015**, *137*, 3300–3307.
[67] M. E. Robinson, D. J. Lunn, A. Nazemi, G. R. Whittell, L. De Cola, I. Manners, *Chem. Commun.* **2015**, *51*, 15921–15924.
[68] J. S. Valera, R. Gómez, L. Sánchez, *Small* **2018**, *14*, 1702437.
[69] P. A. Korevaar, S. J. George, A. J. Markvoort, M. M. J. Smulders, P. A. J. Hilbers, A. P. H. J. Schenning, T. F. A. De Greef, E. W. Meijer, *Nature* **2012**, *481*, 492–496.
[70] A. T. Haedler, S. C. J. Meskers, R. H. Zha, M. Kivala, H. W. Schmidt, E. W. Meijer, *J. Am. Chem. Soc.* **2016**, *138*, 10539–10545.
[71] T. Fukui, S. Kawai, S. Fujinuma, Y. Matsushita, T. Yasuda, T. Sakurai, S. Seki, M. Takeuchi, K. Sugiyasu, *Nat. Chem.* **2017**, *9*, 493–499.
[72] N. Veling, R. van Hameren, A. M. van Buul, A. E. Rowan, R. J. M. Nolte, J. A. A. W. Elemans, *Chem.*

*Commun.* **2012**, *48*, 4371.
[73] J. Buendía, F. García, B. Yélamos, L. Sánchez, *Chem. Commun.* **2016**, *52*, 8830–8833.
[74] J. S. Zhao, Y. Bin Ruan, R. Zhou, Y. B. Jiang, *Chem. Sci.* **2011**, *2*, 937–944.
[75] E. Bellacchio, R. Lauceri, S. Gurrieri, L. M. Scolaro, A. Romeo, R. Purrello, *J. Am. Chem. Soc.* **1998**, *120*, 12353–12354.
[76] S. K. Pal, S. Setia, B. S. Avinash, S. Kumar, *Liq. Cryst.* **2013**, *40*, 1769–1816.
[77] L. Brunsveld, B. J. B. Folmer, E. W. Meijer, R. P. Sijbesma, *Chem. Rev.* **2001**, *101*, 4071–4097.
[78] P. J. M. Stals, M. M. J. Smulders, R. Martín-Rapún, A. R. A. Palmans, E. W. Meijer, *Chem. Eur. J.* **2009**, *15*, 2071–2080.
[79] J. F. Douglas, J. Dudowicz, K. F. Freed, *J. Chem. Phys.* **2008**, *128*, 224901
[80] L. Brunsveld, A. P. H. J. Schenning, M. A. C. Broeren, H. M. Janssen, J. A. J. M. Vekemans, E. W. Meijer, *Chem. Lett.* **2000**, 292–293.
[81] D. Van Der Zwaag, P. A. Pieters, P. A. Korevaar, A. J. Markvoort, A. J. H. Spiering, T. F. A. De Greef, E. W. Meijer, *J. Am. Chem. Soc.* **2015**, *137*, 12677–12688.
[82] P. Jonkheijm, P. Van Der Schoot, A. P. H. J. Schenning, E. W. Meijer, *Science* **2006**, *313*, 80–84.
[83] M. F. J. Mabesoone, A. J. Markvoort, M. Banno, T. Yamaguchi, F. Helmich, Y. Naito, E. Yashima, A. R. A. Palmans, E. W. Meijer, *J. Am. Chem. Soc.* **2018**, *140*, 7810–7819.
[84] M. M. J. Smulders, A. P. H. J. Schenning, E. W. Meijer, *J. Am. Chem. Soc.* **2008**, *130*, 606–611.
[85] Z. Shen, Y. Jiang, T. Wang, M. Liu, *J. Am. Chem. Soc.* **2015**, *137*, 16109–16115.
[86] Z. Shen, T. Wang, M. Liu, *Angew. Chem. Int. Ed.* **2014**, *53*, 13424–13428.
[87] R. Nandy, S. Sankararaman, *Org. Biomol. Chem.* **2010**, *8*, 2260–2266.
[88] M. Ikeda, M. Takeuchi, S. Shinkai, *Chem. Commun.* **2003**, *3*, 1354–1355.
[89] P. J. M. Stals, P. A. Korevaar, M. A. J. Gillissen, T. F. A. De Greef, C. F. C. Fitié, R. P. Sijbesma, A. R. A. Palmans, E. W. Meijer, *Angew. Chem. Int. Ed.* **2012**, *51*, 11297–11301.
[90] M. C. T. Fyfe, J. N. Lowe, J. F. Stoddart, D. J. Williams, *Org. Lett.* **2000**, *2*, 1221–1224.
[91] F. C. Whitmore, J. H. Olewine, *J. Am. Chem. Soc.* **1938**, *60*, 2570–2571.

# Chapter 4

# *A tribute to Jacobus van't Hoff: enantiomers become diastereomers in optically active solvents.*

**Abstract**:

Mirror-symmetry breaking with an optically active solvent was first proposed by van't Hoff in 1893. Despite multiple trials, it has been only showed that in optically active solvents under thermodynamic equilibrium, enantiomers have identical physical properties. As a result, no systematic study tackling solvation of chiral supramolecular polymers with optically active solvents has been published. In this chapter, we show that chiral, halogenated alkanes can break the mirror symmetry in helical, hydrogen-bonded supramolecular polymers based on triphenylene-2,6,10-tricarboxamide. The key feature of the system is the presence of competing polymorphic states, which stability is determined by the energy of solvation. In optically inactive solvents, the polymers based on *R* and *S* monomers behave as enantiomers. On the other hand, the use of an optically active solvent results in differential solvation energy of the corresponding polymorphic states. In consequence, the optically active solvent favors the formation of one helix over the other. Remarkably, the stabilization of one helicity over the other is reflected by a temperature at which any mixture of the enantiomers, regardless of the enantiomeric excess, always polymerizes with excess of the same helicity. The co-assembly of a racemic mixture of the two monomers in an optically active solvent yields supramolecular polymers of single helicity, showing that the small energetic difference can be amplified due to the cooperative nature of the copolymerization.

This work has been performed in close collaboration with Mathijs Mabesoone.

Part of this work will be published:
Cooperativity as a Missing Element in van't Hoff's Puzzle to Find a Difference Between Enantiomers in Optically Active Solvents
M. L. Ślęczkowski, M. F. J. Mabesoone, A. R. A. Palmans, E. W. Meijer, *To be submitted*

## 4.1 Introduction

Ever since the physical separation of the enantiomers of tartaric acid salt was accomplished by Pasteur in 1848,[1] the capability to separate enantiomers and control interactions between chiral molecules has been actively pursued in the field of organic chemistry. Despite their physical and chemical equivalence, two enantiomers of a single compound interact differently with other chiral molecules as a result of diastereomeric relations between the formed complexes.[2] This results in different physical properties of diastereomers such as solubility,[3] and different chemical reactivities.[4] Already in 1893, van't Hoff in a letter to his coworker Meyerhoffer[5] proposed that enantiomers may also show different solubilities in chiral solvents as a result of induced diastereomeric relationships.[6] However, most ternary phase diagrams of racemic mixtures in chiral solvents are symmetric, suggesting no difference in solubility under thermodynamic equilibrium.[7] However, there are notable exceptions. For example, when a high structural similarity between a (molecularly dissolved) solute and optically active solvent is present, strong interactions can be observed: the two enantiomers of mandelic acid show different solubilities in (*S*)-propyl mandelate.[8] In addition, when optically active solvents were used as a medium for crystallizations,[9] in rare cases the kinetic resolution of conglomerate-forming crystals has been achieved.[10,11] Moreover, cholesteric liquid crystals were successfully applied as chiral reaction media to induce the chirality at molecular and supramolecular scale.[12–14]

So far the conclusion is that in most cases in chiral solvent the molecular interactions are too small to induce an energetic difference between the two enantiomers. But, when molecules are aggregated in large structures, differences can be observed. As a result, one should take into consideration not only the interactions between *molecules* and the solvent but also of the formed *supermolecules* (ultimately crystals) and the solvent. In fact, numerous examples of crystals showing polymorphism due to interactions with the solvent have been reported.[15–18] The most important work from a historical point of view has been carried out on sodium ammonium tartrate crystals. At room temperature, sodium ammonium tartrate forms conglomerate crystals, while above 28 °C a racemic salt is formed. The change from the low temperature polymorph to the higher temperature polymorph is accompanied by a loss of water: in the conglomerate crystal state, the crystals comprise four molecules of water in the unit cell whereas only one molecule of water is present in the racemate crystals.[19] This extremely important property of solvation of any supramolecular system is often overlooked. Apart from crystals, solvent molecules also play explicit roles in supramolecular polymerizations.[20] For example, the self-assembly of α-deuterated benzene-1,3,5-tricarboxamides (BTAs) in heptane and methylcyclohexane (MCH) resulted in two different helical structures, even though the driving force for the assembly process remained the same.[21] It was found that both structures are in competition and that the shape of the solvent in combination with temperature determines the thermodynamic equilibrium between them. In another example, solvation of MCH molecules within the pocket of the supramolecular

fibers of coronene bismide resulted in the competition between two types of helical aggregates of the opposite helicity.[22] Chiral solvation by optically active solvents was observed in several examples, in the induction of single helicity in covalent[23–25] and supramolecular[26–29] helical polymers built of achiral monomers. However, up to date no report addressing the interactions of biased[1] helical superstructures with optically active solvents was published.[30] Due to their inherent chirality, helical supramolecular polymers based on one-dimensional aggregates could serve as an ideal model system for a detailed study on the induction of the diastereomeric relationships between a pair of enantiomers in a chiral solvent.

After analyzing the examples discussed above, we inferred that an ideal system would comprise two competing, cooperative types of aggregates of the opposite helicity and different solvation states, which stay in thermodynamic equilibrium with each other. Thus the competition between the two pathways will be driven explicitly by a different degree of solvation. This different degree of solvation can be controlled by the solvent composition and the temperature. In achiral solvents, the corresponding morphologies of the enantiomers should adopt an enantiomeric relationship. However, the use of a chiral solvent should result in an induction of a diastereomeric relationship, because solvation by the chiral solvent molecules breaks the mirror symmetry due to inherently different stability of the diastereomeric solvates. We here use TTAs as a model for supramolecular polymerization under thermodynamic control and explore the induction of diastereomeric relationships with the use of chiral, chlorinated alkanes as a solvent. We used ultraviolet-visible (UV-Vis) and circular dichroism (CD) spectroscopy to study the influence of the solute concentration, the solvent and the temperature on single- and multi-component mixtures. The results indicate that the chiral solvents can indeed induce a diastereomeric relationship in supramolecular polymers that are susceptible to polymorphism caused by solvation.

## 4.2 Supramolecular homopolymerization of (*R*)-TTA in chiral solvents

In Chapter 3, we studied in detail the supramolecular polymerization of TTAs **1** (Figure 4.1) in mixtures of decalin and chloroform. We showed that small amounts of chloroform as a cosolvent were necessary to avoid kinetic traps, and that enantiomerically pure (*S*)-1-chloro-2-methylbutane biases the helicity of otherwise racemic mixture of *P*- and *M*-helical aggregates of achiral TTA ***n*-1**. To our surprise, only 40% of the chiral solvent was necessary to fully bias the helicity. We deduced from those experiments, that chlorinated solvents can improve the dynamics of the TTAs **1**, as well as the (chiral) solvation of the polymers.

Because of the sensitivity of ***n*-1** towards the presence of (*S*)-ClMeBu, we start by studying the influence of (*S*)-ClMeBu on the assembly of chiral TTA monomers. We first focus on the supramolecular polymerization of **(*R*)-1**, which shows a single preferred helicity in

[1] based on chiral monomers

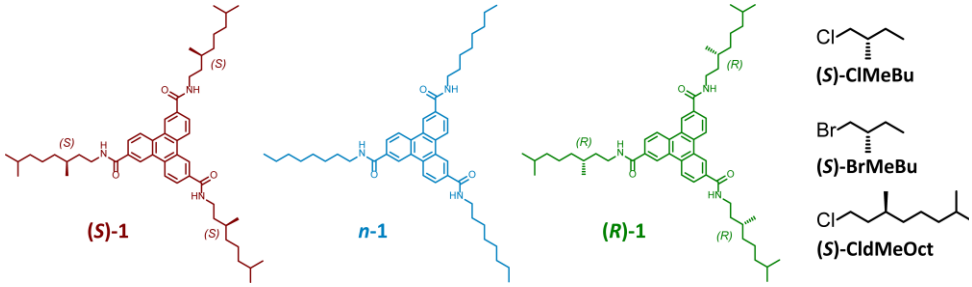


***Figure 4.1*** *Structures of TTAs* ***1*** *and chiral solvents used in this chapter.*

decalin / chloroform mixtures, which is opposite to the one of ***n*-1** induced by (*S*)-ClMeBu (*vide* Chapter 3). Variable temperature (VT)-CD spectroscopic measurements were conducted at concentrations between 20 and 200 µM of **(*R*)-1** in (*S*)-ClMeBu (Figure 4.2a). An unusual concentration dependency was observed in the temperature-dependent measurements. At concentrations below 30 µM, a single cooperative pathway, endorsed by an exclusively negative Cotton effect at 266 nm across the whole temperature regime, is observed (Figure 4.2b). When the concentration is increased, so is the temperature at which aggregations starts, the elongation temperature, $T_e$. Above 30 µM, we first observe the appearance positive CD signal at 266 nm upon cooling. Further cooling results in a sharp change of the CD signal from positive to negative. The temperature at which the sign switches is at 69 °C. The switching temperature appears to be monomer-concentration independent. The temperature region where the CD effect is positive indicates the presence of another type of aggregate at that temperature and is followed by the formation of the "normally" observed aggregates, i.e. those that show a negative CD effect at 266 nm. The rate of cooling has no influence on the temperature of the transition, suggesting that the two competing aggregates are in thermodynamic equilibrium. The sharpness of the transition between the aggregates forming superstructures of positive and negative Cotton effects indicates that both aggregates are cooperatively formed.

To unravel the relationship between the two types of aggregates, we recorded the full CD spectra at 20 °C and 75 °C, where the opposite states dominate (Figure 4.2c). Besides different signs for all transitions, and a different amplitude of the signal no spectral differences are observed. This implies that no change in the supramolecular structure of the chromophore takes place and that the aggregates differ only by means of their preferred helicity. Hence the relationship between the two states is diastereomeric in nature. In further discussions, the aggregate that is stable at high temperatures will be denoted as **A**, while the state that dominates at low temperatures will be denoted as **B**.

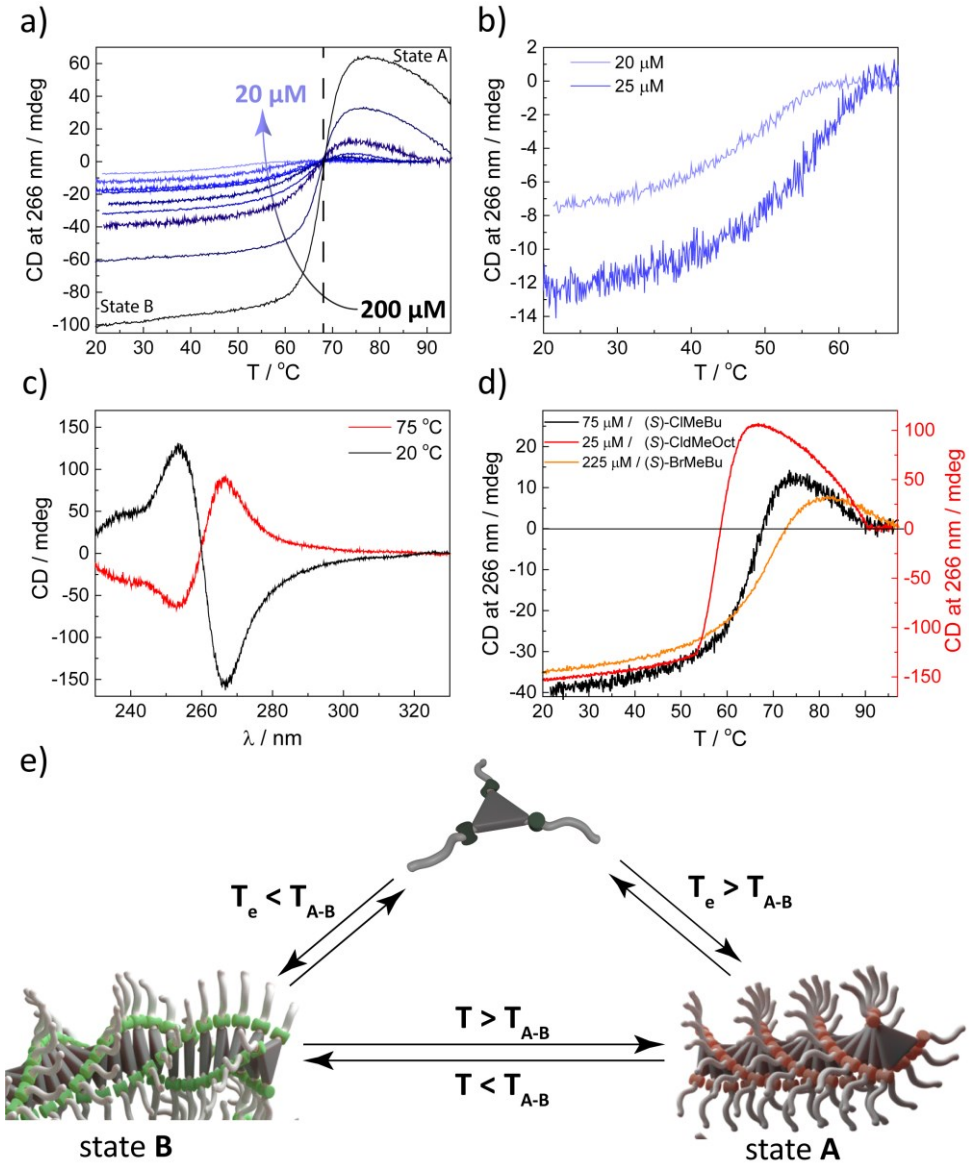


***Figure 4.2*** *a) VT-CD of* ***(R)-1*** *in (S)-ClMeBu at variable concentrations (0.5 K min$^{-1}$, l = 0.1 cm); b) VT-CD of (****R****)-****1*** *in (S)-ClMeBu at 20 µM and 25 µM (0.5 K min$^{-1}$, l = 0.1 cm); c) CD spectra of* ***(R)-1*** *in (S)-ClMeBu at 20 °C and 75 °C (200 µM, l = 0.1 cm); d) VT-CD of* ***(R)-1*** *in different chiral solvents (cooling rate: 0.5 K min$^{-1}$); e) a cartoon depicting two helical states of TTA* ***1***, ***A*** *and* ***B***, *in thermodynamic equilibrium with free monomer.*

Prompted by the unexpected outcomes of dissolving **(*R*)-1** in (*S*)-ClMeBu, we subsequently investigated the role of the structure of the solvent in the stereomutation in **(*R*)-1** polymers. We selected (*S*)-1-bromo-2-methylbutane ((*S*)-BrMeBu) and (*S*)-1-chloro-3,7-dimethyloctane ((*S*)-CldMeOct) as solvents with similar structure to (*S*)-ClMeBu. Similarly, VT-CD of **(*R*)-1** reveals the competition between two types of aggregates, **A** and **B** (Figure 4.2d) above a critical concentration. Because of the higher polarity of (*S*)-BrMeBu compared to (*S*)-ClMeBu and (*S*)-CldMeOct, the critical concentration was above 150 μM, so a monomer concentration of 225 μM, was used. Similarly, because of the lower polarity of (*S*)-CldMeOct compared to (*S*)-ClMeBu the critical concentration was below 5 μM and measurements could be conducted at 25 μM. Interestingly, the **A**→**B** transition temperature ($T_{A\text{-}B}$) varied with the nature of the solvent. The $T_{A\text{-}B}$ was the highest for the most polar (*S*)-BrMeBu (73 °C), whereas $T_{A\text{-}B}$ in (*S*)-ClMeBu and (*S*)-ClMeOct took place at 69 °C and 61 °C, respectively. The solvent dependency on the transition temperature suggests that the nature of the solvent determines the strength of the polymer – solvent interactions thereby governing the change in relative thermodynamic stability of the diastereomeric states **A** and **B** (Figure 4.2e).

## 4.3 The role of optical purity of the solvent in the competition between two types of aggregates

Until now we confirmed that the competition between aggregates **A** and **B** is under thermodynamic control and is driven by the interactions of the polymers with (chiral) solvent. Therefore, the equilibrium between **A** and **B** is determined by the nature of the solvent and the temperature. Thus another question is if and in how far the optical purity the solvent affects the equilibrium between **A** and **B**. At the time of the experiment, we expected that if the optical activity of the solvent is necessary to stabilize the alternative pathway **A** in TTAs **1**, the use of a racemic mixture of ClMeBu will result in the formation of the aggregates of type **B** exclusively. Thus, we recorded VT-CD of **(*R*)-1** in racemic ClMeBu at 75 μM (Figure 4.3a). Interestingly, in racemic ClMeBu, the aggregates **A** are still observed, but the $T_{A\text{-}B}$ shifted from 69 °C (*ee* = 100%) to 73 °C (*ee* = 0%). The increase of the *ee* to 40% and 80% resulted in the decrease of $T_{A\text{-}B}$ in a linear manner (Figure 4.3b). The results suggest that optical activity of the solvent is *not* a prerequisite for the stabilization of state **A**. However, since $T_{A\text{-}B}$ is sensitive towards enantiopurity of the solvent, the polymer-solvent interactions are stereosensitive and in this example, (*S*)-ClMeBu stabilizes the state **A** better than (*R*)-ClMeBu.

Consequently, if the opposite helicity state **A** can be formed in *racemic* ClMeBu, it should also be possible to observe state **A** in halogenated, *achiral* solvents. In order to confirm this, we prepared a 200 μM solution of **(*R*)-1** in 1-chlorooctane. We selected high concentration to ensure that we can observe stable optically active polymers in the whole temperature regime permitted by the Peltier cell (up to 110 °C). At this concentration, stable aggregates are present already at 110 °C. As evidenced by the positive CD signature at 266 nm, between 110 °C and 100 °C, aggregates of state **A** dominate. Upon cooling below 100 °C, aggregates **A** were

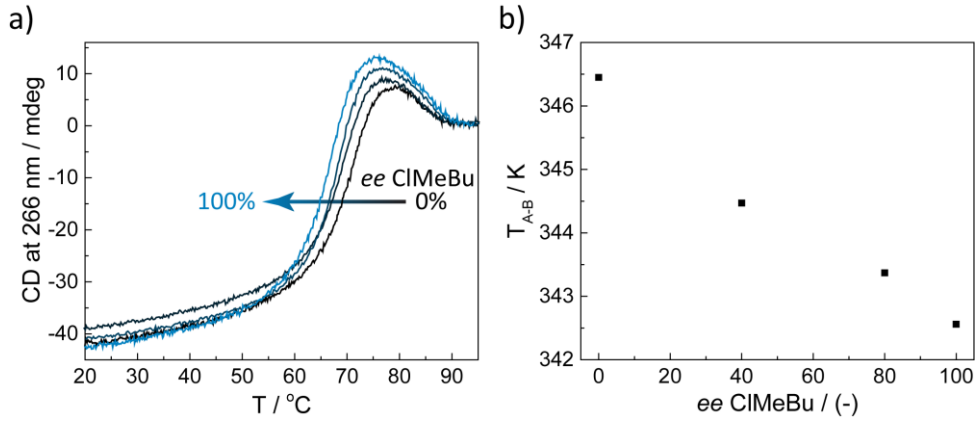


***Figure 4.3*** *a) VT-CD of* ***(R)-1*** *in ClMeBu at variable ee ($c_{TTA}$ = 75 µM, 0.5 K min$^{-1}$, l = 0.1 cm); b)* ***A*** *→* ***B*** *transition temperature versus ee of ClMeBu.*

converted into aggregates **B** with negative CD signature at 266 nm with concomitant further elongation of the fibers (Figure 4.4a). For ***(S)*-1** in 1-chlorooctane, a mirror-image VT-CD was recorded, which is in agreement with the enantiomeric relationship between the two monomers. The transition temperature $T_{A-B}$ was significantly higher in 1-chlorooctane than any of the chiral solvents. Geometrically, 1-chlorooctane is a linear, halogenated alkane with no tertiary carbon atoms (no branching). The chiral solvents have either one ((*S*)-ClMeBu) and ((*S*)-BrMeBu)) or two ((*S*)-CldMeOCt) tertiary carbon atoms, which results in branching of the structure. The lowest $T_{A-B}$, thus highest stabilization of aggregate **A**, was observed for (*S*)-ClMeOct, which is the largest from the studied solvents and has two tertiary carbon atoms.

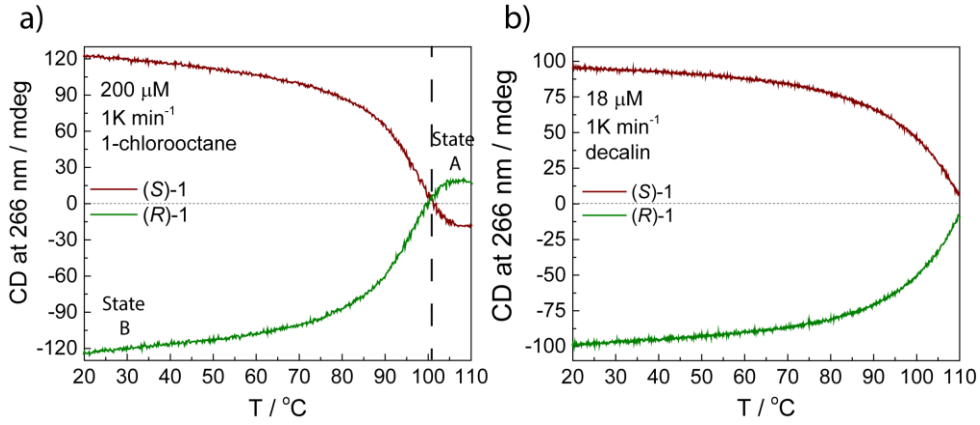


***Figure 4.4*** *a) VT-CD of* ***(R)-1*** *and* ***(S)-1*** *in 1-chlorooctane (200 µM, 1 K min$^{-1}$); b) VT-CD of* ***(R)-1*** *and* ***(S)-1*** *in decalin (18 µM, 1 K min$^{-1}$).*

As discussed earlier, we observed no difference in the CD spectra profiles of aggregates **A** and **B**. Therefore, both are helical aggregates of opposite helicity with respect to each other and are regarded as diastereomers. The optical activity of the solvent is not required to enable the formation of **A** at high temperatures. When we connect this with the observed $T_{A\text{-}B}$ in each solvent, we can conclude that the competition between **A** and **B** is driven by the solvation of the fibers. Hereto, we refer to other 1D supramolecular polymers, where different solvation states, leading to the stereomutation, were observed.[21,22] In a cooperative system with multiple competing pathways, minute differences in $\Delta G$ result in sharp transitions between competing polymorphs. Hence in case of TTAs **1**, a small difference in the energy of solvation can affect a global change in the helical preference. Since there is no experimental or theoretical proof at the moment, which state, **A** or **B**, is better solvated, we cannot directly define the solvation states.

The last question to be addressed is the nature of the solvent that permits the presence of the second solvation state, **A**. In Chapter 3, we presented supramolecular polymerizations of TTAs **1** in decalin. We never observed stereomutation during any of the variable temperature experiments (Figure 4.4b). There could be two reasons for such behavior. Either TTAs **1** cannot form two different solvation states in decalin at all, or the **A**→**B** transition temperature is higher than the upper limit of the Peltier cell (110 °C). Due to technical limitations, we cannot perform VT-CD experiment above 110 °C, thus in all experiments described in Chapter 3 we selected concentrations so that the $T_e$'s were below 100 °C. Possibly, the concentrations were below the critical concentration required to observed state **A**. However, from Chapter 3 we also know that in decalin TTAs **1** can be easily frozen far from thermodynamic equilibrium. We used this property to design an experiment that could

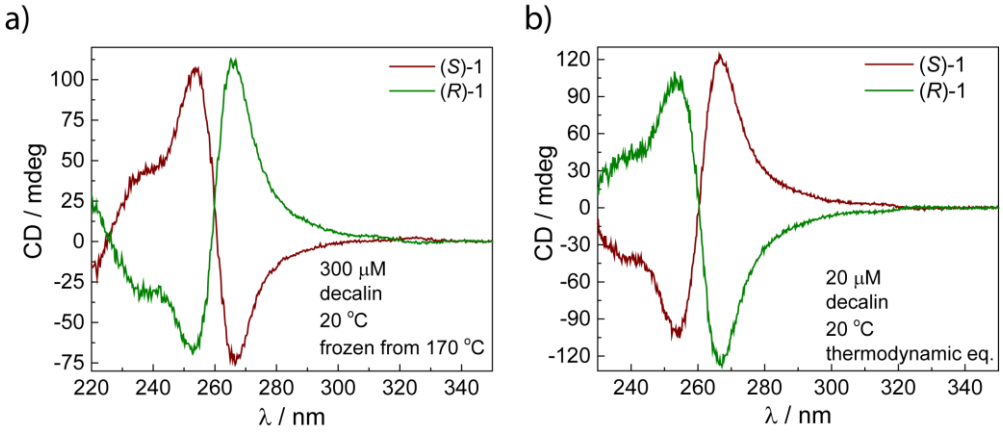


***Figure 4.5*** *a) CD spectra of* ***(R)-1*** *and* ***(S)-1*** *in decalin at 20 °C after fast cooling of the solutions from 170 °C (300 μM, kinetically trapped state* ***A****, l = 0.1 cm); b) CD spectra of* ***(R)-1*** *and* ***(S)-1*** *in decalin at 20 °C (20 μM, thermodynamic equilibrium, state* ***B****, l = 1 cm).*

indirectly indicate, whether in decalin state **A** can also be present. We prepared highly concentrated solutions ($c_{TTA}$ = 300 μM) of **(*R*)-1** and **(*S*)-1** to ensure high degree of aggregation at high temperature. The solutions were equilibrated at 170 °C and subsequently "frozen" by direct immersion in water at room temperature. The CD spectrum of such prepared sample of **(*R*)-1** showed positive Cotton effect at 266 nm, while **(*S*)-1** showed negative Cotton effect, being the mirror image of its enantiomer (Figure 4.5a). Both spectra are opposite to what is expected at state **B** (Figure 4.5b), thereby indicating that also in decalin the competition between the states **A** and **B** occurs.

## 4.4 Induction of diastereomeric relationship by optically active solvent

In the previous paragraphs, we demonstrated that competing diastereomeric states **A** and **B** are the result of differential solvation of the aggregates formed by TTAs, and depend on the temperature and solvent structure. The shift of $T_{A\text{-}B}$ caused by the change in *ee* of ClMeBu suggested that the solvation is stereosensitive. Therefore, next to **(*R*)-1**, we measured VT-CD of **(*S*)-1** in (*S*)-CldMeOct. VT-CD curves of 30 μM solutions of **(*R*)-1** and **(*S*)-1** in (*S*)-ClddMeOct showed first formation of aggregates of state **A** at 90 °C, which was followed by the transition to state **B** at lower temperatures (Figure 4.6a). Unlike in achiral 1-chlorooctane, in chiral (*S*)-ClddMeOct, the **A**→**B** transition of **(*R*)-1** and **(*S*)-1** did not occur at the same temperature. Instead, $\mathbf{A}_{(S)}\rightarrow\mathbf{B}_{(S)}$ transition occurred at 77 °C, while $\mathbf{A}_{(R)}\rightarrow\mathbf{B}_{(R)}$ transition occurred at 61 °C. The differences in the transition temperature indicate a lower relative stability of $\mathbf{B}_{(R)}$ than $\mathbf{B}_{(S)}$ and / or a higher relative stability of $\mathbf{A}_{(R)}$ than $\mathbf{A}_{(S)}$ in (*S*)-ClddMeOct (Figure 4.6a). This difference in temperature also shows that the interactions between the aggregates and the solvent are sensitive towards the absolute configuration of all components. In the optically pure (*S*)-ClddMeOct, both types of aggregates, **A** and **B**, formed by **(*S*)-1** and **(*R*)-1** are not enantiomers, but diastereomers and show visible differences in their thermal behavior. Because such a phenomenon is visible only in chiral solvents, the difference in the transition points of $\mathbf{A}_{(R)}$, $\mathbf{A}_{(S)}$, $\mathbf{B}_{(R)}$ and $\mathbf{B}_{(S)}$ is solely determined by the energies of the diastereomeric solvates. No spectral difference between the corresponding states besides the maximum CD value is observed (Figure 4.6b). All normalized CD spectra are completely superimposable, which shows that the structure of the chromophore remains unaffected (Figure 4.6c). This result highlights the subtleties involved and how delicate the energetic differences between the corresponding states are.

To compare in more detail the profiles of the CD cooling curves of **(*R*)-1** and **(*S*)-1** in (*S*)-ClddMeOct, we inverted the cooling curve of **(*S*)-1** and superimposed it with the cooling curve of **(*R*)-1** (Figure 4.6d). In achiral solvents, such curves are superimposable within the entire elongation regime. However, in the optically active solvent, there are significant differences in the expression of supramolecular chirality with respect to temperature due to diastereomeric relationships. At high temperatures the curves overlap, showing a single elongation temperature for both **(*R*)-1** and **(*S*)-1** in (*S*)-ClddMeOct. In this temperature regime

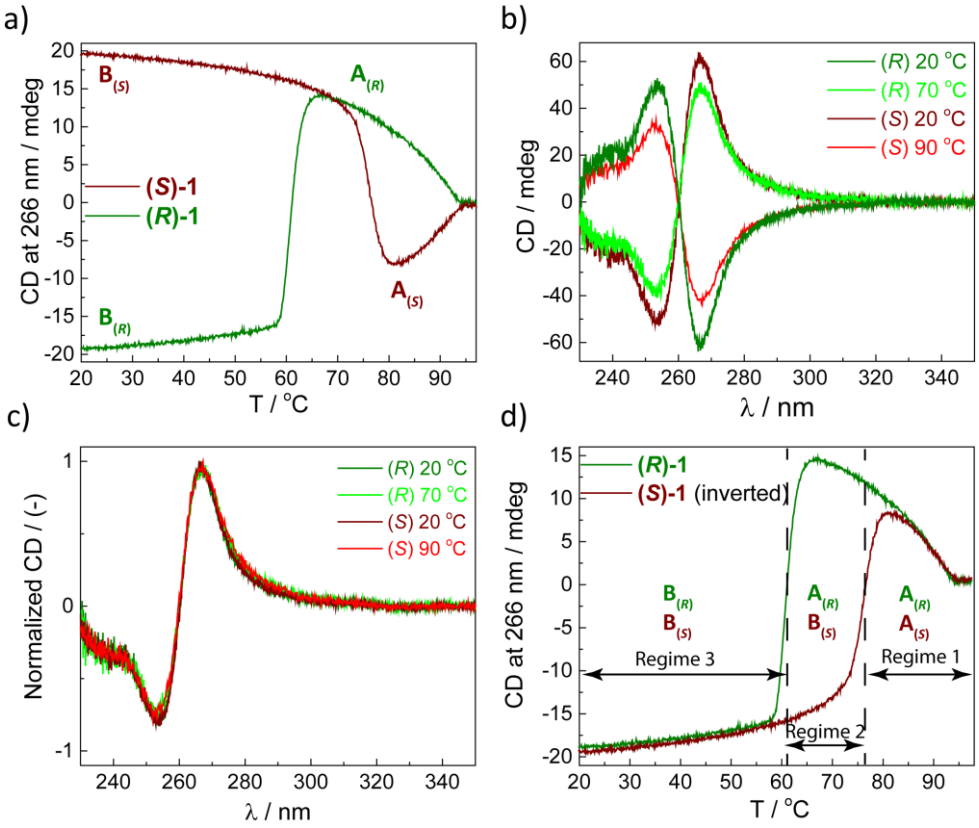


***Figure 4.6*** *a) VT-CD of* ***(R)-1*** *and* ***(S)-1*** *in (S)-CldMeOct (30 µM, 0.1 K min-1); b) CD spectra of* ***(R)-1*** *and* ***(S)-1*** *in (S)-CldMeOct at states* ***A*** *and* ***B*** *(100 µM); c) normalized CD spectra as in* ***Fig c*** *(spectra of* ***(S)-1*** *at state* ***A*** *and of* ***(R)-1*** *at state* ***B*** *were inverted);* d) *VT-CD of* ***(R)-1*** *and inverted VT-CD of* ***(S)-1****, the dominative states for each regime are indicated.*

(regime 1), states $\mathbf{A}_{(R)}$ and $\mathbf{A}_{(S)}$ are the most thermodynamically stable. Once the temperature reaches 76 °C, the two curves start to deviate. This is due to the competition between $\mathbf{A}_{(S)}$ and $\mathbf{B}_{(S)}$ that pushes the equilibrium towards $\mathbf{B}_{(S)}$ at 76 °C. At this temperature, the system enters regime 2. While state $\mathbf{B}_{(S)}$ is now favored for **(*S*)-1**, state $\mathbf{A}_{(R)}$ still dominates the elongation of **(*R*)-1**. Regime 2 ends at the transition temperature, where **(*R*)-1** elongates with excess of state $\mathbf{B}_{(R)}$, which takes place at 61 °C. Below 61 °C, states $\mathbf{B}_{(R)}$ and $\mathbf{B}_{(S)}$ are the most thermodynamically stable and the curves overlap again (regime 3).

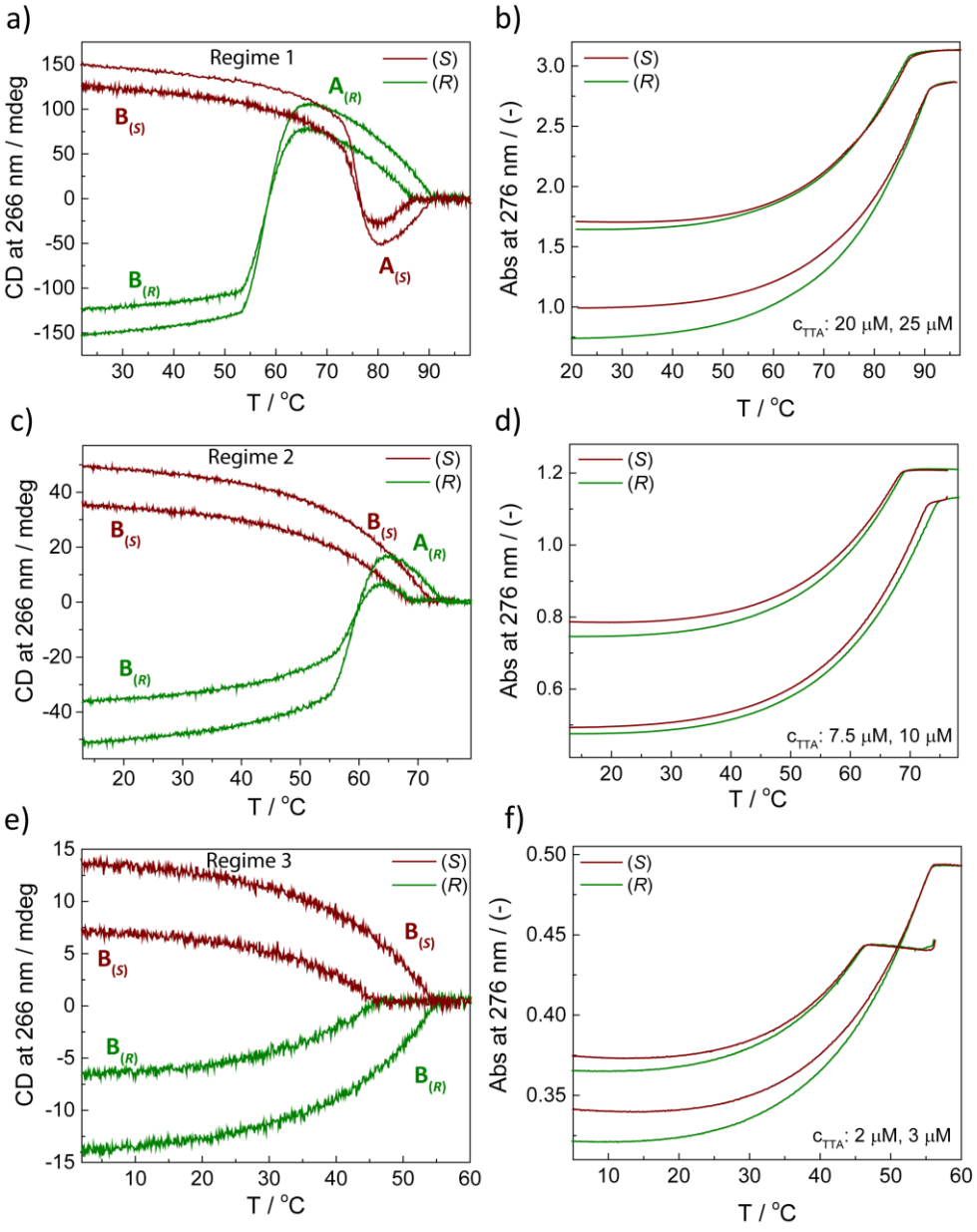


***Figure 4.7*** *VT-CD (a, c, e) and VT-UV (b, d, f) of* ***(R)-1*** *and* ***(S)-1*** *solutions in (S)-CldMeOct at variable concentrations (0.5 K min$^{-1}$). The experiments were carried in three regimes. Regime 1: Mon→**A**$_{(R)}$→**B**$_{(R)}$ and Mon→**A**$_{(S)}$→**B**$_{(S)}$, Regime 2: Mon→**A**$_{(R)}$→**B**$_{(R)}$ and Mon→**B**$_{(S)}$, Regime 3: Mon→**B**$_{(R)}$ and Mon→**B**$_{(S)}$.*

Subsequently, we studied the homopolymerizations of **(*R*)-1** and **(*S*)-1** in (*S*)-CldMeOct at various concentrations. We selected the concentrations in such way, that the elongation temperature $T_e$ at a given concentration would be found in one of the previously discussed temperature regimes 1, 2 or 3. Consequently, we measured VT-CD of **(*R*)-1** and **(*S*)-1** at six different concentrations (two per regime). In regime 1, $T_e$ is higher than 76 °C, thus the concentrations of **(*R*)-1** and **(*S*)-1** were selected as 20 and 25 μM. In regime 2, the concentrations had to be selected to fulfill the following condition: (76 °C > $T_e$ > 61 °C). This was observed for solutions with concentrations of 10 and 7.5 μM. To meet the condition 61 °C > $T_e$, valid for regime 3, we prepared solutions with concentrations of 3 and 2 μM. During the analysis of the CD and VT cooling curves, we focused mostly on the elongation temperatures of **(*R*)-1** and **(*S*)-1**, to asses if here are measurable differences in the $T_e$.

In regime 1, we observe no difference in the $T_e$ between **(*R*)-1** and **(*S*)-1** in both the UV and CD cooling curves. From this we infer that there is no appreciable difference in $\Delta G_A$ between $\mathbf{A}_{(S)}$ and $\mathbf{A}_{(R)}$ (Figure 4.7a, b). Interestingly, in regime 2, where upon cooling below the $T_e$ states $\mathbf{A}_{(R)}$ and $\mathbf{B}_{(S)}$ are dominating, the absolute stability of $\mathbf{A}_{(R)}$ is higher than of $\mathbf{B}_{(S)}$, as reflected by the higher elongation temperature of **(*R*)-1** in this regime (Figure 4.7c, d). This implies a measurable difference in the solvation energy between $\mathbf{A}_{(R)}$ and $\mathbf{B}_{(S)}$. In regime 3 only states $\mathbf{B}_{(S)}$ and $\mathbf{B}_{(R)}$ are observed and no significant difference between the elongation temperature and the polymerization profile was recorded by the VT-CD and VT-UV (Figure 4.7e, f). These results show that the energetic differences between corresponding solvated states $\mathbf{A}_{(R)} \leftrightarrow \mathbf{A}_{(S)}$ and $\mathbf{B}_{(R)} \leftrightarrow \mathbf{B}_{(S)}$ are very small, but globally can give rise to high dissimilarities due to the strongly cooperative nature of the supramolecular polymerization of **1**.

## 4.5 Effect of an achiral solvent on diastereomeric relationship

Since the solvent molecules play an implicit role in the supramolecular polymerization, we can treat it as an active participant in the supramolecular polymerization process. Our group previously reported the hydration of biphenyl-based supramolecular aggregates in oils that lead to the competition between high and low hydrated states.[31] The therein applied model indicated that a change in the concentration of water results in the equilibrium shift between two states, which is reflected by different $T_{A\text{-}B}$. The current example is little bit more complex, due to the fact that any solvent studied permits the formation of state **A**. Because in decalin such transition occurs at very high temperature, we can assume that decalin strongly stabilizes state **B**. Therefore, we performed VT-CD curves of the solutions of **(*R*)-1** in (*S*)-CldMeOct / decalin mixtures to assess how the presence of decalin affects the transition from state **A** to state **B**. Figure 4.8a shows that a decrease of the concentration of (*S*)-CldMeOct by dilution with decalin results in the concomitant increase of the $T_{A\text{-}B}$. This is in excellent agreement with our expectation, as decalin should stabilize state $\mathbf{B}_{(R)}$ with respect to $\mathbf{A}_{(R)}$. The same experiment performed on **(*S*)-1** showed an analogous trend upon dilution of the (*S*)-CldMeOct (Figure 4.8b). Remarkably, the shift of the equilibrium between $\mathbf{A}_{(S)}$ and $\mathbf{B}_{(S)}$ was

significantly less affected by the concentration of (*S*)-CldMeOct (Figure 4.8c). The higher dependency of the equilibrium between $\mathbf{A}_{(R)}$ and $\mathbf{B}_{(R)}$ suggests that $\mathbf{B}_{(R)}$ is more sensitive towards the change of the solvent composition than $\mathbf{B}_{(S)}$. Indeed, the less stable state $\mathbf{B}_{(R)}$ should be more susceptible to the solvation by the achiral solvent than the more stable $\mathbf{B}_{(S)}$. Extrapolated linear fits of the temperatures of **A**→**B** transition versus the concentration of (*S*)-CldMeOct intercept each other at x = 3.09, y = 375, which corresponds to the molar concentration of (*S*)-CldMeOct, where ***(R)*-1** and ***(S)*-1** should behave as enantiomers and the temperature of **A**→**B** transition at that particular concentration of (*S*)-CldMeOct.

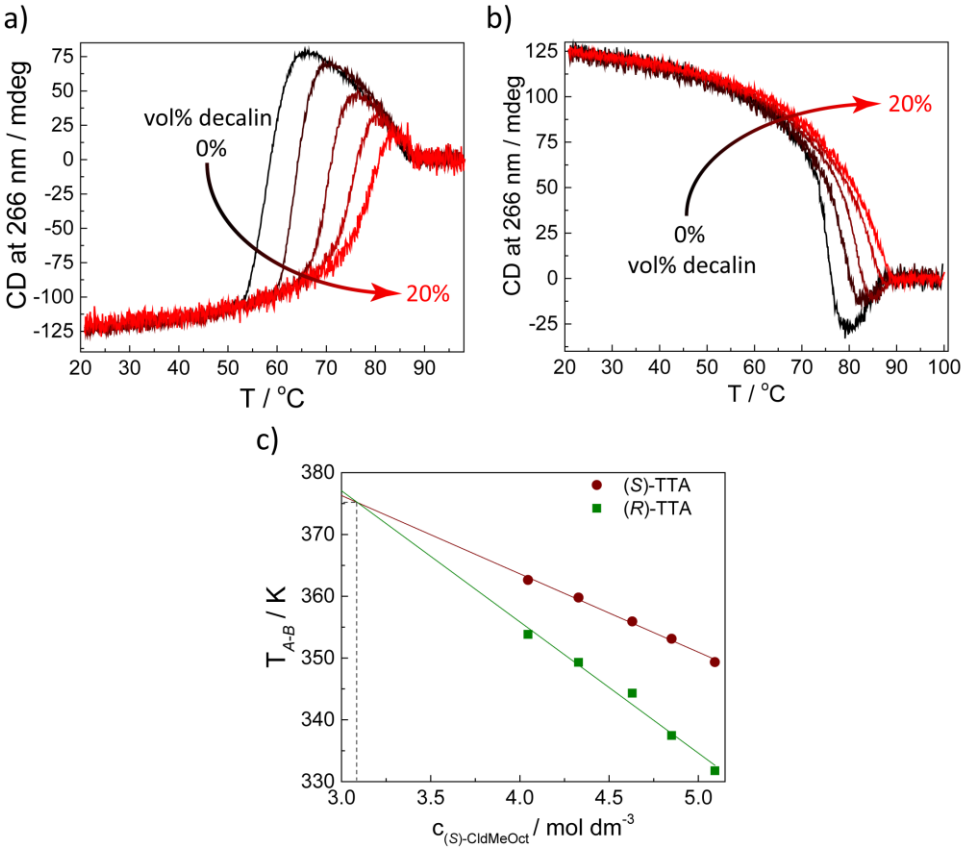


***Figure 4.8*** *VT-CD of a)* ***(R)*-1** *and b)* ***(S)*-1** *in (S)-CldMeOct / decalin solutions (20 µM, 0.5 K min$^{-1}$); c)* ***A*→*B*** *transition temperature versus concentration of (S)-CldMeOct, the lines correspond to the calculated linear fits.*

## 4.6 Preliminary mathematical simulations of supramolecular polymerization of TTAs in optically active solvents

Mathematical modelling methods can be very useful tool in the thermodynamic description of supramolecular (co)polymerization process as well as the competition between multiple pathways. As mentioned above, our group investigated competition in supramolecular polymerization of biphenyl tetracarboxamides (BPTA) in alkane solvents.[31] In that case, the presence of the competing pathways was determined by minute amounts of water present in ambient conditions in methylcyclohexane. The absolute concentration of water dictated the equilibrium between the three polymorphs. Therefore the transition temperature between the states was solely dependent on water concentration. The free monomer concentration determined only the absolute stability of the polymers. On the basis of the spectroscopic and calorimetric data, therein applied mathematical model accurately described the thermodynamic parameters of the system and the number of water molecules involved in hydrated polymorphs.

VT-CD spectroscopy of TTAs **1** shows similar behavior to the one observed for BPTA. The transition temperature between the competing polymorphs is governed by the solvent composition, while free monomer concentration regulates only the absolute stability of the polymers in both states. Therefore, we inferred that supramolecular polymerization of **1** can be mathematically described in a similar way to BPTAs. Preliminary calculations were performed by Mathijs Mabesoone. As discussed before, the polymerization of **1** can be described through the competition between cooperative and isodesmic pathways or through the elongation of a single cooperative polymerization mechanism that involves CD-silent pre-nuclei. To describe the supramolecular polymerization of **1** in chiral solvent, we simplified our model to only consider the competition between the two cooperative pathways in the

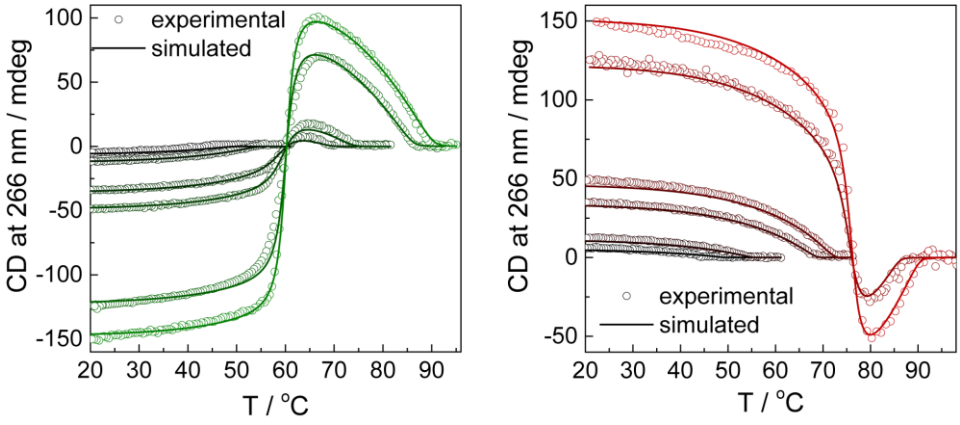


***Figure 4.9*** *Experimental data (circles) and simulated (lines) VT-CD curves of a)* ***(R)-1*** *and b)* ***(S)-1*** *in (S)-CldMeOct at variable concentrations (rate: 0.5 K min$^{-1}$).*

supramolecular polymerization of **1**. Since only a small fraction of the monomers goes into isodesmic aggregates or pre-nuclei at high temperatures, this simplification leads only to minor deviations and therefore, the model still describes the solvent-dependent supramolecular polymerization of **1** in an accurate manner (Figure 4.9). The preliminary simulations show that similar features i.e. solvation of the polymers control the competition between the two observed polymorphs.

## 4.7 Deracemization via diastereomeric relationships: copolymerization

TTAs **(*R*)-1** and **(*S*)-1** are enantiomers and only in the presence of a chiral solvent they become diastereomers. We suspected that the diastereomeric relationship could give rise to stabilization of one helicity over the other. Hence we investigated, how the energetic difference of **(*R*)-1** and **(*S*)-1** in a chiral environment will be reflect in a copolymerization of the two enantiomers. This experiment is normally referred to a majority-rules[32] experiment. In case of TTA **1** dissolved in decalin / chloroform mixtures, we observed full helical expression provided by an *ee* of 15% of *R* or *S* enantiomer and no net helicity in case of racemic mixture (*vide* Chapter 3).

At this point we make a division between homo- and copolymers. Until now we used **A** and **B** to denote homopolymeric states, which are connected to the helicity and the solvation. To discuss the copolymeric states we use notation of **A'** and **B'**. We do not refer states **A'** and **B'** to the solvation, but only to the helicity. The lack of the **A'**→**B'** transition does not mean, that the solvation or desolvation event does not occur. Due to the complexity of the interactions and the competition, it can simply not affect the change of the chiral superstructure. This division is done to avoid simplification which could lead to incorrect conclusions.

To access full insight into the copolymerization thermodynamics, we recorded VT-CD of **(*R*)-1** and **(*S*)-1** mixed at different *ee* in (*S*)-CldMeOct at the rate of cooling of 0.1 K $min^{-1}$. Between the *ee* of 100% and 50% of **(*R*)-1**, first a cooperative supramolecular polymerization towards $\mathbf{A'_{(R)}}$ is observed, which is followed by sharp $\mathbf{A'_{(R)}}$→$\mathbf{B'_{(R)}}$ transition (Figure 4.10a). Notably, in this regime, the reduction of the *ee* caused concomitant decrease in the temperature of $\mathbf{A'_{(R)}}$→$\mathbf{B'_{(R)}}$ transition and its sharpness. This reflects the copolymerization process, where the excess of (*R*) enantiomer is being diluted in the aggregates by increasing amounts of (*S*) enantiomer. Due to the cooperativity of the copolymerization and low mismatch penalty, **(*S*)-1** can efficiently enter the stacks of its non-preferred helicity. At the same time, the $\mathbf{B'_{(R)}}$ state gradually is destabilized in favor of $\mathbf{A'_{(R)}}$. A further decrease of the *ee* from 50% to 20% *ee* **(*R*)-1** drastically changes the copolymerization profile. Already at 45% *ee* the **A'**→**B'** transition loses its sharpness visibly and the Cotton effect at 20 °C is no longer -20 mdeg. As more **(*S*)-1** is added, the **A'**→**B'** transition diminishes and at *ee* of 20% (*R*) a CD cooling curve showing single cooperative pathway ($\mathbf{A'_{(R)}}$→$\mathbf{B'_{(S)}}$) is observed (Figure 4.10b). This particular behavior is maintained until an *ee* for 20% (*S*) is reached, which means

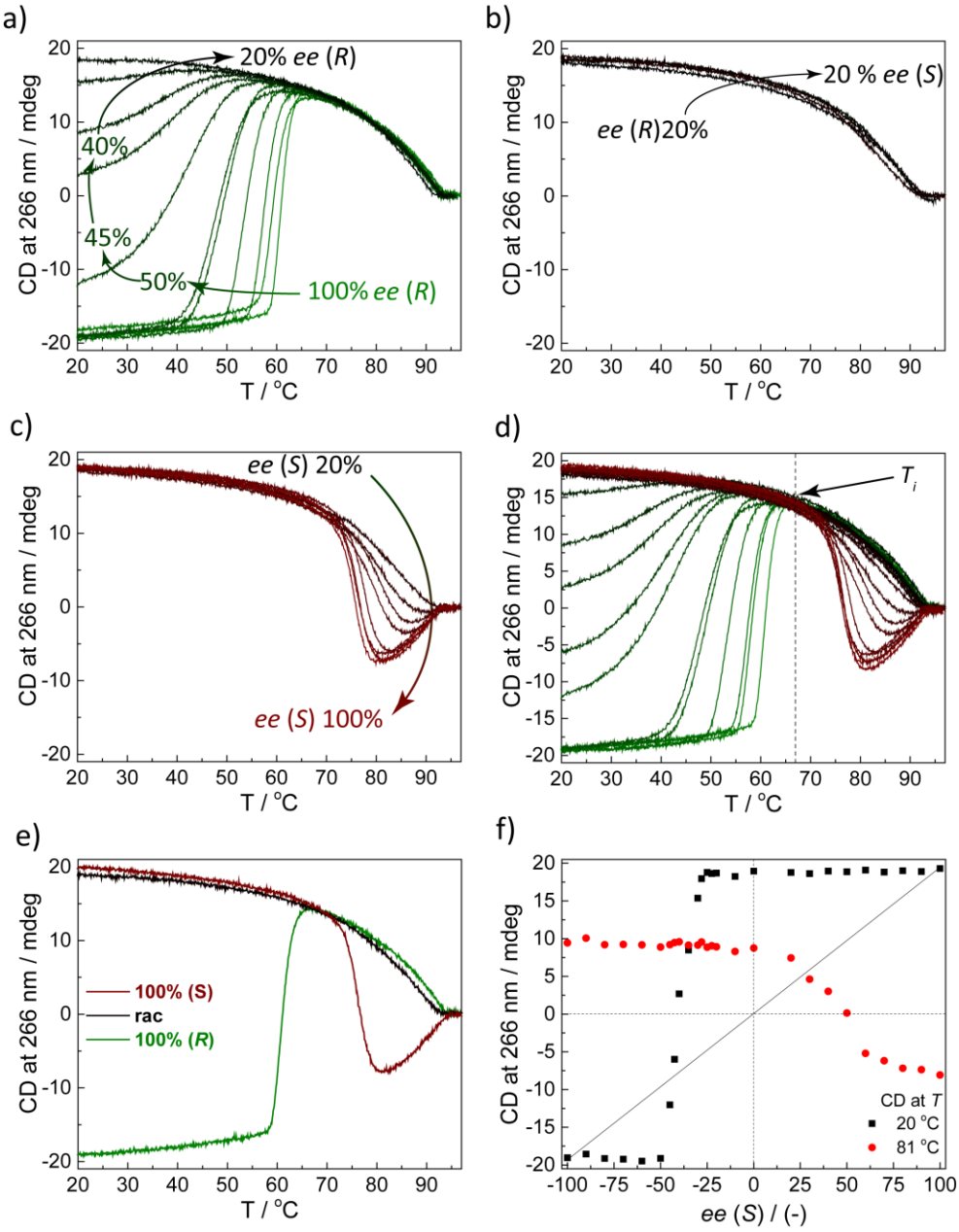


***Figure 4.10*** *Copolymerization of* ***(R)-1*** *and* ***(S)-1*** *in (S)-CldMeOct; a) curves of ee 20% to 100%* ***(R)-1****; b) curves of 20%* ***(R)-1*** *to 20%* ***(S)-1****; c) curves of ee 20% to 100%* ***(S)-1****; d) overview of the VT-CD curves showing $T_i$ at 67 °C; e) curves of* ***(R)-1****,* ***(S)-1*** *and racemic mixture; f) CD at 266 nm at 20 °C and 81 °C versus ee of* ***(S)-1*** *(-100% = 100%* ***(R)-1****).*

that between *ee* 20% (*R*) and 20% (*S*), similarly to ***n*-1**, a single helicity is favored across the whole polymerization regime. In consequence, the racemic mixture of **(*S*)-1** and **(*R*)-1** polymerizes with a single helicity preferred across the whole elongation regime – a remarkable signature of the mirror symmetry breaking by chiral solvent. At 30% *ee* of (*S*), we observe the appearance of state $\mathbf{A'}_{(S)}$ at high temperatures. Upon further increase of the *ee* towards (*S*), the $\mathbf{A'}_{(S)}$ is continuously stabilized at the expense of $\mathbf{B'}_{(S)}$ and the $\mathbf{A'}\rightarrow\mathbf{B'}$ transition becomes sharp again (Figure 4.10c). Interestingly, no significant difference is visible between the CD cooling curves of 70% and 100% *ee* (*S*). This 30% *ee* difference (100% - 70%) coincides with the 30% *ee* of (*R*), which is the minimum *ee* of **(*R*)-1** necessary to induce the $\mathbf{A'}_{(R)}\rightarrow\mathbf{B'}_{(R)}$ transition. The value constitutes an energetic difference between **(*R*)-1** and **(*S*)-1** introduced by the interactions with chiral solvent. A peculiar feature of this diastereomeric system is that all cooling curves have an intersection point ($T_i$) at 67 °C, which accompanies the temperature, where **(*R*)-1** is still at its $\mathbf{A}_{(R)}$ (just about to undergo the $\mathbf{A}_{(R)}\rightarrow\mathbf{B}_{(R)}$ transition) and **(*S*)-1** is already at $\mathbf{B}_{(S)}$ (just left the transition regime) (Figure 4.10d, e). In consequence, regardless of the *ee*, at this temperature, a single helicity with positive CD signature at 266 nm is favored. The energetic difference between **(*R*)-1** and **(*S*)-1** in (*S*)-CldMeOct can be visualized by plotting the Cotton effect at 266 nm recorded for each composition at room temperature (Fig 4.10f). It shows that only around *ee* of 40% (*R*), the equilibrium between *P* and *M* helices is obtained. The same plot obtained at 81 °C shows that positive Cotton effect at 266 nm is present up to *ee* of 40% (*S*). This confirms that the helicity of the TTA aggregates plays central role in the interactions with chiral solvents.

## 4.8 Rebellion-in-the-army: achiral monomers dictate the helicity

The solvation of the chiral **(*R*)-1** and **(*S*)-1** aggregates by the chiral, halogenated solvent can promote the formation of state **A**. Our idea was to combine the competition between two states with a single preferred helicity of ***n*-1** in (*S*)-ClMeBu. In this way, we can investigate, how achiral monomers ***n*-1** with a strong helical preference in the chiral solvent will drive the equilibrium between states **A** and **B** of supramolecular polymers built of chiral monomers. Therefore we designed an alternative sergeants-and-soldiers experiment[33], which comprised the supramolecular copolymerization of the sergeant **(*R*)-1** and the soldiers ***n*-1** in (*S*)-ClMeBu. The choice of **(*R*)-1** as chiral comonomer was dictated by the preferred helicity of ***n*-1** and the helicity of $\mathbf{A}_{(R)}$ and $\mathbf{B}_{(R)}$ of **(*R*)-1**. In (*S*)-ClMeBu, $\mathbf{A}_{(R)}$ adapts the same helicity as ***n*-1**, while $\mathbf{B}_{(R)}$ adapts the opposite helicity (Figure 4.11a). Therefore we envisioned that mixing of the two components in (*S*)-ClMeBu can lead to a *rebellion* which is referred to the situation, where achiral soldiers - through interactions with chiral solvent - will dictate their helical preference to the chiral sergeants. Similarly to the majority-rules experiment, when discussing the helicity of the ***n*-1** and **(*R*)-1** copolymers, we abbreviate these as $\mathbf{A'}_{(R)}$ and $\mathbf{B'}_{(R)}$, which refer only to the helicity of the polymer at given temperature and not to the solvation state.

VT-CD cooling curves of mixed ***n*-1** and **(*R*)-1** in (*S*)-ClMeBu show that at high temperatures ***n*-1** and **(*R*)-1** have the same preferred helicity (**A'**$_{(R)}$). In case of pure **(*R*)-1**, the transition **A'**$_{(R)}$→**B'**$_{(R)}$ occurs at 67 °C. When **(*R*)-1** is diluted with ***n*-1**, its preference to undergo the transition to the **B'**$_{(R)}$ at 67 °C is inhibited by the presence of the soldiers, who follow the solvent and not the chiral sergeant (Figure 4.11b). Therefore, the increase in the fraction of ***n*-1** results in the concomitant shift of the transition to **B'**$_{(R)}$ towards lower temperatures. Eventually, addition of 65% of soldier ***n*-1** is sufficient to dictate the helicity of the remaining 35% sergeants **(*R*)-1** at room temperature (Figure 4.11c). As a consequence of the high cooperativity of the system, the transition between **A'**$_{(R)}$ and **B'**$_{(R)}$ remains sharp regardless of the composition of the copolymers. The **A'**$_{(R)}$→**B'**$_{(R)}$ transition temperature shows a linear decrease as a function of **(*R*)-1** fraction, which says that the relative stability of the competing states changes proportionally to the monomeric pool composition (Figure 4.11d). Since

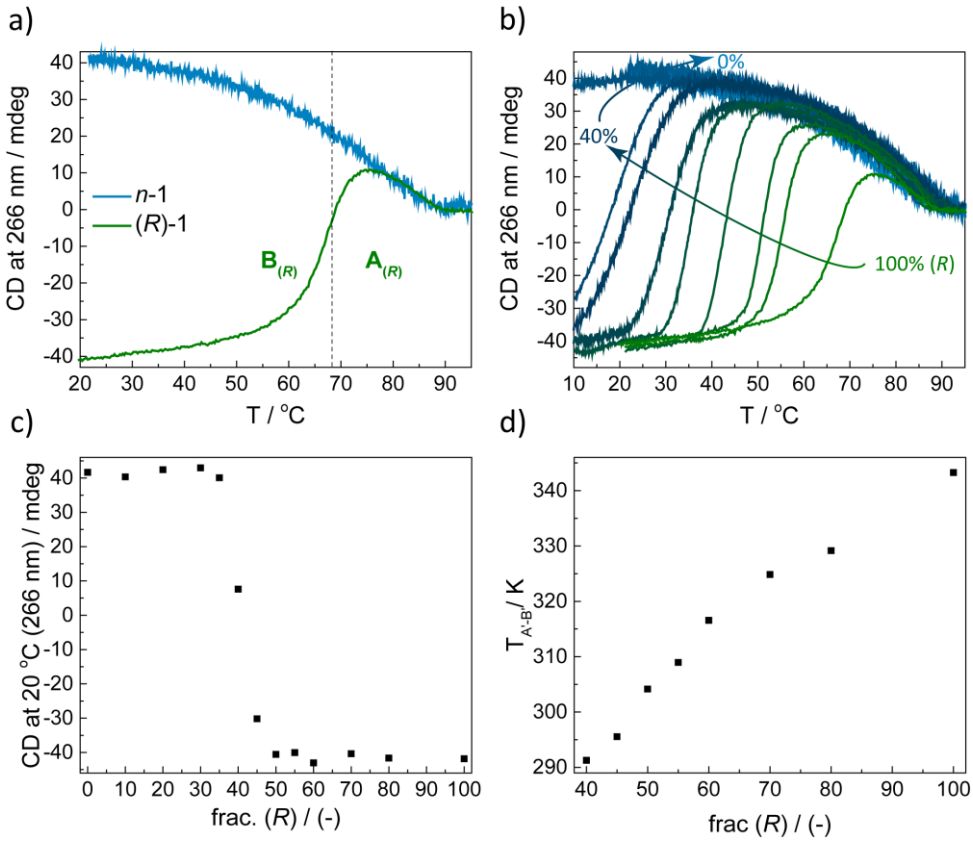


***Figure 4.11*** *Sergeants-and-soldiers experiment in (S)-ClMeBu; a) VT-CD of pure* ***(R)-1*** *and* ***n-1*** *in (S)-ClMeBu; b) VT-CD curves of the* ***(R)-1*** *copolymerized with* ***n-1****; c) CD signal at 20 °C versus fraction of* ***(R)-1****; d)* $T_{A'-B'}$ *versus fraction of* ***(R)-1*** *(*$c_{TTA}$ *= 75 µM, rate: 0.5 to 0.1 K min*$^{-1}$*).*

already little quantities of ***n*-1** soldier affect the supramolecular chirality of **(*R*)-1** sergeants, no effects such as buffering take place. Hence the phenomenon can be treated as *rebellion*, because increase of the *rebelling soldiers* constantly destabilizes the preferred helicity of the sergeants. As such, the concept of *rebellion* constitutes another remarkable feature of the supramolecular copolymerization in chiral solvent.

## 4.9 Conclusions

We showed that supramolecular polymers formed by enantiomerically pure monomers behave like diastereomers in chiral solvents due to specific solvent-polymer interactions. The key to this remarkable phenomenon lies in the presence of the two competing supramolecular morphologies in the TTAs. The morphologies differ from each other only in terms of solvation and helicity, thus are diastereomers. In achiral solvents, **(*R*)-1** and **(*S*)-1** behave like enantiomers – the VT-CD curves are mirror image of each other, showing that the polymorphic states $\mathbf{A}_{(R)}$ and $\mathbf{A}_{(S)}$ as well as $\mathbf{B}_{(R)}$ and $\mathbf{B}_{(S)}$ are of degenerate energy. Characteristically for a cooperative system, the transition between the two competing states of similar energies remaining in a dynamic equilibrium with free monomer is very sharp. The competition between the two morphologies induced by different solvation states of **A** and **B** can be exploited to induce diastereomeric relationship between **(*R*)-1** and **(*S*)-1** by using chiral solvents. Even though we found no significant differences between the elongation temperatures of $\mathbf{A}_{(R)}$ and $\mathbf{A}_{(S)}$ as well as $\mathbf{B}_{(R)}$ and $\mathbf{B}_{(S)}$, the temperatures of **A**→**B** transition were remarkably different for **(*R*)-1** and **(*S*)-1**. Interestingly, we observed the difference in the elongation temperature of aggregates $\mathbf{A}_{(R)}$ and $\mathbf{B}_{(S)}$, which are of the same helicity, while are composed of the enantiomers (therefore are diastereomers). The titration of the solutions of enantiomerically pure **(*R*)-1** and **(*S*)-1** in (*S*)-CldMeOct with decalin showed that the less stable state $\mathbf{B}_{(R)}$ is more responsive upon addition of the achiral solvent than more stable state $\mathbf{B}_{(S)}$. We further exploited the diastereomeric relationship between **(*R*)-1** and **(*S*)-1** in the chiral solvent in the multi-component assembly. VT-CD curves showed that even at the composition with a significant excess of **(*R*)-1**, supramolecular helicity preferred by the minor component **(*S*)-1** is dominant at room temperature. Only, when the *ee* was increased above 30% of **(*R*)-1**, the transition to $\mathbf{B'}_{(R)}$ is favored.

Eventually, we investigated the copolymerization of the chiral **(*R*)-1**, with achiral ***n*-1**. At high temperatures, in (*S*)-ClMeBu, sergeants **(*R*)-1**, and soldiers ***n*-1** have identical helical preference, but at low temperatures they have the opposite. Remarkably, copolymerization of the two monomers resulted in a *rebellion* effect. Small amounts of achiral soldiers could control the supramolecular helicity of chiral sergeants at high temperatures and 65% of the soldiers dictated the helicity to the 35% of the sergeants at room temperature. To the best of our knowledge, such influences of the chiral solvents on the supramolecular (co)polymerizations of chiral monomers have not been observed before. These results contribute to the fundamental understanding of weak, but stereospecific interactions in

supramolecular polymers. Moreover, this work constitutes a connection between supramolecular polymers and crystals. Many principles present in crystallization appear to be valid supramolecular polymerization. The results show, that it should be possible to crystallize pseudoracemates in a highly stereoselective fashion in chiral solvents. This could be achieved by stereoselective solvation of the crystals. Therefore, if we consider supramolecular assemblies, we confirm that van't Hoff thesis was right, but the discussed properties are non-trivial. Since crystals have been an object of thorough study in the last century, they can be a valuable source of the knowledge and inspiration, when designing new supramolecular materials

## 4.10 Experimental Section

### 4.10.1 Materials and methods

All standard solvents were obtained from Biosolve, Acros or Aldrich. All other chemicals were obtained from Aldrich. Thionyl chloride and pyridine were distilled before use. All other chemicals were used as received. (*S*)-1-bromo-2-methylbutane ((*S*)-BrMeBu) was purchased from Aldrich and used as received. *(S)*-1-Chloro-3,7-dimethyloctane ((S)-CldMeOct) was synthesized according to modified protocol of the procedure described for (*S*)-1-chloro-2-methylbutane in Chapter 3. $^{1}$H NMR spectra were recorded on a Varian Unit Inova 500 MHz NMR. Proton chemical shifts (δ) are reported in ppm downfield from tetramethylsilane (TMS). Circular dichroism and UV-Vis absorption spectroscopy was performed on a JASCO J-815 CD spectrometer with either a JASCO Peltier MPTC-490S temperature controller with a range of 278 – 373 K or a JASCO Peltier PFD-425S/15 with a range of 263 – 383 K. For all spectroscopic measurements, cells with an optical path length of 1 cm or 1 mm were employed and spectroscopic grade solvents were employed. Stock solutions were prepared by weighing the necessary amount of compound for the given concentration and transferring it to a screw-capped vial that was filled up to the proper volume using Gilson™ MICROMAN™ Positive-Displacement Pipets. The stock solutions were heated up and stirred until the solid material was completely dissolved. All the spectroscopic measurement were performed with freshly prepared solutions (max. 1 week after the preparation of the stock solution).

### 4.10.2 Synthetic procedures

(*S*)-1-Chloro-3,7-dimethyloctane was prepared in a two-step synthesis starting from commercially available (*S*)-3,7-dimethyloct-6-en-1-ol. The first step comprised a hydrogenation to the (S)-3,7-dimethyloctan-1-ol, according to the procedure reported in Chapter 2. In the second step the hydroxyl group was replaced with chlorine in a nucleophilic substitution reaction using $SOCl_2$ using protocol to synthesize (*S*)-ClMeBu as reported in Chapter 3.

*(S)-1-Chloro-3,7-dimethyloctane (**(S)-CldMeOct**)*

(*S*)-3,7-Dimethyloctan-1-ol (95 g, 120 mL, 0.6 mol) and freshly distilled pyridine (48 mL, 0.6 mol) were placed in a 0.5 L 3-neck round-bottomed flask equipped with a mechanical stirrer and dropping funnel. The mixture was heated up to 60 °C and subsequently, freshly distilled thionyl chloride (65 mL, 0.9 mol) was added dropwise within 4 hours. Upon addition of c.a. 1 eq. of $SOCl_2$, the reaction mixture became a slurry (crystallization of pyridinium chloride). Upon subsequent addition of the remaining $SOCl_2$, the brown

biphasic mixture was obtained. The progress of the reaction was controlled by $^1$H NMR. The reaction was regarded as complete only, when a characteristic quartet of doubles is the only group of signals between 5 ppm and 3 ppm (other intermediates corresponding to an organic sulfite were present during the course of the reaction). On completion, the biphasic mixture was moved to the separatory funnel without cooling down (bottom, inorganic phase crystallizes at low temperatures, making separation not possible) and quickly separated. The upper, organic layer was subsequently washed with water, saturated $NaHCO_3$, water and brine (emulsion formation possible), dried over magnesium sulfate, which was filtered off to yield 150 mL of brown liquid. In order to yield the solvent of suitable quality for spectroscopic measurements, three fractional distillations under reduced pressure (p = 2.8 mbar, b.p. = 59 °C) were carried out. After the first distillation, the distillate was collected and redistilled twice from over the activated charcoal. Finally the liquid was stirred overnight with a mixture containing activated charcoal, silicagel, neutral aluminum and potassium carbonate (ca 1 gram each) and subsequently filtered off to yield 74 mL (80%) of (*S*)-CldMeOct, which was stored over molecular sieves (3Å).

$^1$H NMR (400 MHz, $CDCl_3$): δ (ppm) = 3.57 (m, 2H), 1.80 (m, 1H), 1.68 – 1.47 (m, 3H), 1.32 – 1.23 (m, 3H), 1.19 – 1.09 (m, 3H), 0.89 (d, *J* = 6.6 Hz, 3H), 0.86 (d, *J* = 6.7 Hz, 6H)

### 4.10.3 Details on the thermodynamic mass balance model of polymerization

The supramolecular polymerization of **TTA** is modelled with thermodynamic mass balance expressions. In the model, the influence of solvent stabilization of the two polymer types is introduced in a way similar to a previous report[1] by describing the interaction of the supramolecular polymer as if the solvent is part of the supramolecular polymer. Thus, the polymerization is described with a series of sequential equilibria that describe the solvent influenced addition of a monomer, X, to the chain ends of a supramolecular polymer:

$$\begin{aligned} &X + X + \nu_P S \longleftarrow \\ &P_2 + X + \nu_P S \longleftarrow \\ &P_3 + X + \nu_P S \longleftarrow \\ &\quad\vdots \\ &P_i + X + \nu_P S \longleftarrow \\ &\quad\vdots \end{aligned} \tag{E1}$$

with $K_{2,P}$ the equilibrium constant of dimerization and $K_P$ the equilibrium constant of polymerization beyond the dimer in the *P*-type polymer, $\nu_P$ a temperature independent constant that captures the degree of interaction between the polymeric *P*-aggregates and the solvent and S the solvent.

As such, the equilibrium constant expresses the solvent dependent equilibrium between the polymeric aggregates with:

$$K_P = \frac{[P_{i+1}]}{[P_i]\cdot[X]\cdot[S]^{\nu_P}} \tag{E2}$$

with $[P_{i+1}]$ the chemical activity of the polymers of length $i$+1, $[P_i]$ the chemical activity of polymers of length $i$, [X] the chemical activity of the free monomers and [S] the chemical activity of the solvent.

In this expression, the solvent term can be isolated together with the equilibrium constant, to yield:

$$K'_{\mathrm{P}} = K_{\mathrm{P}} \cdot [\mathrm{S}]^{\nu_{\mathrm{P}}} = \frac{[\mathrm{P}]_{i+1}}{\mathrm{P}_i \cdot [\mathrm{X}]} \cdot \tag{E3}$$

Eq. (E3) shows that in our model, the solvent interaction with the supramolecular polymer can be isolated and an equilibrium constant that is modified by a solvent dependency, $K'_P$, can be used to describe the supramolecular polymerization. This modification eliminates the solvent from the equilibrium expression and enables the description of the supramolecular polymerization with well described methods that have been developed for solvents in which no solvent influence is taken into account.

Following the deduction outlined by Zhao and Moore, the concentration of monomers in *i*-mers of the *P*-type polymer can be expressed as a function of the free monomer concentration with:

$$[\mathrm{P}_i] = i \cdot \sigma'_{\mathrm{P}} \cdot K'_{\mathrm{P}}{}^{i-1} \cdot [\mathrm{X}]^i \text{ for } i \geq 2 \tag{E4}$$

where $\sigma'_P$ is the solvent modified cooperativity parameter: $\sigma'_{\mathrm{P}} = K'_{2,\mathrm{P}} / K'_{\mathrm{P}}$.

The formation of the *M*-type polymer is described in a similar way, giving the concentration of *i*-mers of the *M* polymer as a function the free monomer concentration through:

$$[\mathrm{M}_i] = i \cdot \sigma'_{\mathrm{M}} \cdot K'_{\mathrm{M}}{}^{i-1} \cdot [\mathrm{X}]^i \text{ for } i \geq 2 \tag{E5}$$

where $\sigma'_M$ is the cooperativity parameter: $\sigma'_{\mathrm{M}} = K'_{2,\mathrm{M}} / K'_{\mathrm{M}}$, in which $K'_{2,M}$ is the solvent modified equilibrium constants for dimerization to form the nucleus, and $K_M$ is the solvent modified equilibrium constant of elongation beyond the dimer.

The total concentration of M in the system can thus be expressed with:

$$\begin{aligned} [\mathrm{X}]_{\mathrm{tot}} &= [\mathrm{P}]_{\mathrm{tot}} + [\mathrm{M}]_{\mathrm{tot}} + [\mathrm{X}] = \left( \sum_{i=2}^{\infty} [\mathrm{P}_i] \right) + \left( \sum_{i=2}^{\infty} [\mathrm{M}_i] \right) + [\mathrm{X}] \\ &= \left( \sum_{i=1}^{\infty} i \cdot \sigma'_{\mathrm{P}} \cdot K'_{\mathrm{P}}{}^{i-1} [\mathrm{X}]^i \right) + \left( \sum_{i=1}^{\infty} i \cdot \sigma'_{\mathrm{M}} \cdot K'_{\mathrm{M}}{}^{i-1} [\mathrm{X}]^i \right) - [\mathrm{X}] \end{aligned} \tag{E6}$$

Using standard expression for converging series, Eq. (E6) can be solved to obtain the mass-balance equation for the polymerization into one supramolecular polymer:

$$[\mathrm{X}]_{\mathrm{tot}} = (1 - \sigma'_{\mathrm{P}}) \cdot [\mathrm{X}] + \frac{\sigma'_{\mathrm{P}} \cdot [\mathrm{X}]}{(1 - K'_{\mathrm{P}} \cdot [\mathrm{X}])^2} + \frac{\sigma'_{\mathrm{M}} \cdot [\mathrm{X}]}{(1 - K'_{\mathrm{M}} \cdot [\mathrm{X}])^2} - \sigma'_{\mathrm{M}} \cdot [\mathrm{X}] \tag{E7}$$

In the simulation, the temperature dependence of the various equilibrium constants is introduced via the Van 't Hoff equation:

$$K_i = \frac{K'_i}{[\mathrm{S}]^{\nu_i}} = \exp\left( \frac{-\Delta G_i}{R \cdot T} \right) = \exp\left( \frac{-\Delta H_i}{R \cdot T} + \frac{\Delta S_i}{R} \right) \tag{E8}$$

with $\Delta G_i$ the Gibbs free energy of monomer addition in aggregation process *i*, *R* the gas constant, *T* the absolute temperature, $\Delta H_i$ the enthalpy of monomer addition in aggregation process *i* and $\Delta S_i$ the entropy of monomer addition in aggregation process *i*.

For the nucleation step, an enthalpic nucleation penalty is introduced to offset the Gibbs free energy of elongation and nucleation via:

$$\Delta H_2 = \Delta H + NP \tag{E9}$$

with $\Delta H_2$ the enthalpy of dimerization, $\Delta H$ the enthalpy of monomer addition to dimers and larger aggregates and $NP$ the nucleation penalty.

In the simulations of the experiments, the mass balance equation (E7) is solved using a binary search algorithm.

## 4.11 References


[1] L. Pasteur, *Ann. Chim. Phys.* **1848**, *24*, 442–459.
[2] E. L. Eliel, S. H. Wilen, L. N. Mander, *Stereochemistry of Organic Compounds*, John Wiley & Sons, Inc., New York, NY, **1994**.
[3] L. A. Nguyen, H. He, C. Pham-Huy, *Int. J. Biomed. Sci.* **2006**, *2*, 85–100.
[4] H. Wynberg, B. Feringa, *Tetrahedron* **1976**, *32*, 2831–2834.
[5] W. Meyerhoffer, J. H. van't Hoff, *Gleichgewichte Der Stereomeren*, B. G. Teubner, California, CA, **1906**.
[6] J. H. van't Hoff, *Die Lagerung Der Atome Im Raume*, F. Vieweg, Braunschweig, DE, **1894**.
[7] J. Jacques, A. Collet, S. H. Wilen, *Enantiomers, Racemates and Resolutions*, Krieger Publishing, Malabar, FL, **1991**.
[8] S. K. Tulashie, The Potential of Chiral Solvents in Enantioselective Crystallization, Otto-von-Guericke Universität Magdeburg, **2010**.
[9] F. S. Kipping, W. J. Pope, *J. Chem. Soc. Trans.* **1909**, *95*, 103–108.
[10] A. Lüttringhaus, D. Berrer, *Tetrahedron Lett.* **1959**, *10*, 10–12.
[11] M. B. Groen, H. Schadenberg, H. Wynberg, *J. Org. Chem.* **1971**, *36*, 2797–2809.
[12] H. Goto, *Macromolecules* **2007**, *40*, 1377–1385.
[13] K. Kawabata, M. Takeguchi, H. Goto, *Macromolecules* **2013**, *46*, 2078–2091.
[14] C. Eskenazi, J. F. Nicoud, H. B. Kagan, *J. Org. Chem.* **1979**, *44*, 995–999.
[15] J. H. van't Hoff, W. Muller, *Ber.* **1898**, *31*, 2206.
[16] F. B. Kenrick, *Ber.* **1897**, *30*, 1749.
[17] P. Vieles, *C. R. Acad. Sci.* **1934**, *198*, 2102.
[18] J. H. van't Hoff, H. M. Dawson, *Ber.* **1898**, *31*, 528.
[19] J. H. van't Hoff, H. Goldschmidt, W. P. Tommsen, *Z. Phys. Chem.* **1895**, *17*, 49.
[20] S. Xue, P. Xing, J. Zhang, Y. Zeng, Y. Zhao, *Chem. Eur. J.* **2019**, 7426–7437.
[21] S. Cantekin, Y. Nakano, J. C. Everts, P. Van Der Schoot, E. W. Meijer, A. R. A. Palmans, *Chem. Commun.* **2012**, *48*, 3803–3805.
[22] C. Kulkarni, P. A. Korevaar, K. K. Bejagam, A. R. A. Palmans, E. W. Meijer, S. J. George, *J. Am. Chem. Soc.* **2017**, *139*, 13867–13875.
[23] H. Nakashima, M. Fujiki, J. R. Koe, M. Motonaga, *J. Am. Chem. Soc.* **2001**, *123*, 1963–1969.
[24] M. M. Green, C. Khatri, N. C. Peterson, *J. Am. Chem. Soc.* **1993**, *115*, 4941–4942.
[25] Y. Nakano, Y. Liu, M. Fujiki, *Polym. Chem.* **2010**, *1*, 460–469.
[26] V. Stepanenko, X. Q. Li, J. Gershberg, F. Würthner, *Chem. Eur. J.* **2013**, *19*, 4176–4183.
[27] A. R. A. Palmans, J. A. J. M. Vekemans, E. E. Havinga, E. W. Meijer, *Angew. Chem. Int. Ed.* **1997**, *36*, 2648–2651.
[28] Y. Kawagoe, M. Fujiki, Y. Nakano, *New J. Chem.* **2010**, *34*, 637–647.
[29] B. Isare, M. Linares, L. Zargarian, S. Fermandjian, M. Miura, S. Motohashi, N. Vanthuyne, R. Lazzaroni, L. Bouteiller, *Chem. Eur. J.* **2009**, *16*, 173–177.
[30] M. Fujiki, *Symmetry,* **2014**, *6*, 677–703.
[31] N. J. Van Zee, B. Adelizzi, M. F. J. Mabesoone, X. Meng, A. Aloi, R. H. Zha, M. Lutz, I. A. W. Filot, A.

R. A. Palmans, E. W. Meijer, *Nature* **2018**, *558*, 100–103.
[32] M. M. Green, B. A. Garetz, B. Munoz, H. P. Chang, S. Hoke, R. G. Cooks, *J. Am. Chem. Soc.* **1995**, *117*, 4181–4182.
[33] M. M. Green, M. P. Reidy, *J. Am. Chem. Soc.* **1989**, *111*, 6452–6454.

# Chapter 5

# *Phase segregation-driven synthesis of polymeric nanoparticles*

**Abstract**:

We report the synthesis and characterization of graft copolymers based on linear poly(dimethyl siloxane) (PDMS) and pendant benzene-1,3,5-tricarboxamides (BTAs). The copolymers differ in degree of polymerization (DP) and BTA graft density. Characterization of the bulk materials at room temperature reveals that the BTAs aggregate in a helical fashion via threefold hydrogen-bond formation within the PDMS matrix. A significant degree of hydrogen bonding persists up to 180 °C, regardless of DP and BTA content. Analysis of the solution behavior by $^{1}$H NMR spectroscopy indicates that BTA aggregation occurs in $CDCl_3$, a solvent normally suppressing aggregation. Circular dichroism spectroscopy in 1,2-dichloroethane shows strong CD effects and reveals that increasing the DP and decreasing the BTA graft density results in an increase in the cooperativity of the BTA aggregation. Dynamic light scattering indicates the formation of particles with sizes of 400 nm. This is the first time that polymers with pendant BTAs show a sharp transition between a non-aggregated and aggregated state, a behavior similar to the one observed for "free" BTAs. The cooperative aggregation is attributed to the strong phase-segregation between the PDMS backbone and the BTAs, in combination with a high propensity of these polymers to form multi-chain aggregates.

Part of this work has been published:
Cooperative Folding of Linear Poly(dimethyl siloxane)s via Supramolecular Interactions
M. L. Ślęczkowski, E. W. Meijer, A. R. A. Palmans, *Macromol. Rapid. Commun*. **2017**, 1700566

## 5.1 Introduction

Poly(dimethyl siloxane)s (PDMS) are a highly interesting and versatile class of polymers.[1–3] Their simple chemistry combined with the propensity to phase segregate[4] as well as the unique flexibility of the siloxane backbone[5–7] provide outstanding possibilities in the bottom-up synthesis of functional materials that found applications in microfluidic devices[8], actuators[9] and as dielectric insulators in electronic devices[10]. Their biocompatibility with human tissue[11] and living cells[12] can potentially extend the applications towards biomaterials. Previous studies showed strong phase-segregation is a powerful force that can drive the self-assembly of (macro)molecules in bulk. Covalent block copolymers of poly(dimethyl siloxane) and poly(ethylene oxide)[13,14], poly(lactic acid)[15–17], poly(methacrylate)[18], poly(styrene)[19–21] and poly(2-vinylpyridine)[22] phase segregate to form well-ordered morphologies in the bulk. In addition, oligo- and poly(dimethyl siloxanes) have been combined with supramolecular hydrogen-bonding motifs to afford supramolecular block copolymers[23], thermoplastic elastomers[24–26], self-healing elastomers[27,28] and liquid crystalline materials[29]. The introduction of functionality in supramolecular phase segregating systems has been achieved by direct symmetrical end-functionalization of oligo(dimethyl siloxane) (oDMS) of discrete lengths with ureidopyrimidinone (UPy) units that are able to dimerize via fourfold hydrogen-bond formation.[30] Protected UPy-oDMS conjugates exhibited liquid crystalline properties whereas deprotection caused a sharp transition towards block copolymer-like behavior.

In recent years, we and others have evaluated in detail the folding of single polymer chains driven by pendant hydrogen-bonding units in water[31–36] and organic media.[37–43] Notably, benzene-1,3,5-tricarboxamides (BTAs) have been found to efficiently fold polymer chains into compartmentalized structures in water.[44] In organic media, in contrast, there is a propensity for multichain aggregation when dynamic hydrogen-bonding motifs are applied.[35] Often, these studies used poly(methacrylate)- or poly(norbornene)-based backbones in poor solvents, in which the conformational flexibility of the polymer backbone is reduced. We wondered in how far the high flexibility of the PDMS backbone, in combination with helical self-assembling BTAs, could enhance effective chain folding in organic media. In addition, we previously established that the folding of polymers with BTA pendants is non-cooperative,[45] which is in sharp contrast to the highly cooperative nature of the self-assembly of free BTAs.[46] The origin of the non-cooperative behavior was attributed to the formation of several domains in which BTAs were aggregated within one polymer particle. This lack of ability of all BTAs to aggregate into one helical stack was associated with the high entropic penalty of the polymeric backbone to fold around a BTA stack.[31] The entropic penalty of the folding of the polymeric backbone off-sets the normal cooperative behavior of BTAs, which

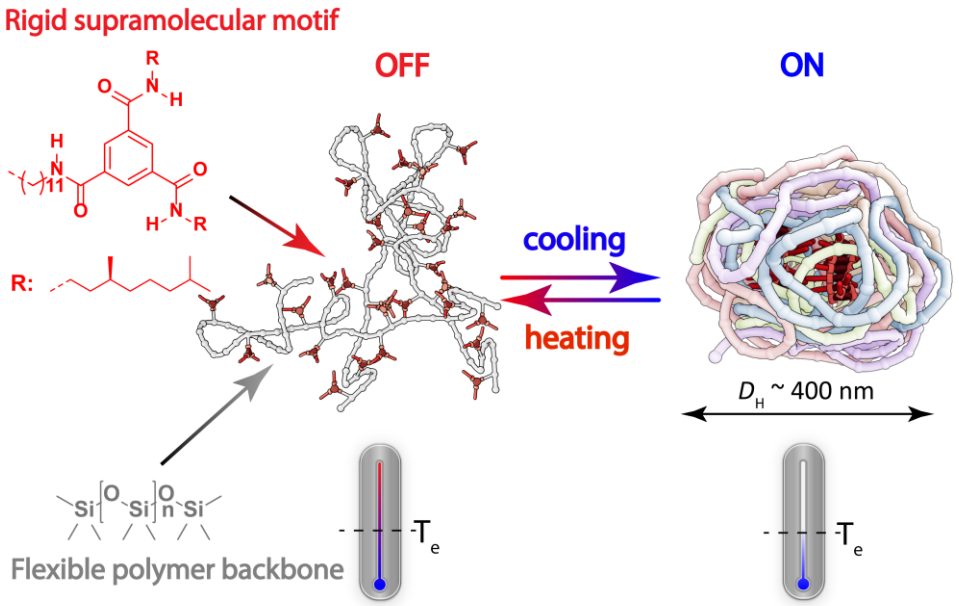


***Scheme 5.1*** *Nanoparticles are the thermodynamic product of self-assembly driven collapse of the polymers.*

has an enthalpic origin. The use of a highly flexible backbone, in contrast, could result in cooperative folding of the polymer chains.

Inspired by the work of Bouteiller and coworkers,[47] we here decorate a PDMS backbone with BTA units affording graft copolymers, encoded as **PDMS-*g*-BTA**. We vary the polymer length and BTA density along the backbone. The materials obtained are studied in detail in bulk using infrared spectroscopy (IR) and circular dichroism (CD) spectroscopy, whereas in dilute solution CD and dynamic light scattering (DLS) are used. Here, we show that strong phase segregation between the BTAs and the PDMS backbone in solution results in unparalleled cooperativity in the assembly of the BTA-pendants, but at the same time also in the formation of large particles (Scheme 5.1).

## 5.2 Synthesis of the PDMS-*g*-BTA copolymers

The synthesis of **PDMS-*g*-BTA** copolymers required two building blocks, namely poly(dimethyl siloxane)-*co*-poly(hydromethyl siloxane) **PDMS-*co*-PHMS** copolymers and (*S*)-BTA-olefin (**9**) or *n*-BTA-olefin (**10**). **PDMS-*co*-PHMS** is commercially available with different average degrees of polymerization (DP) and molar PHMS content, which determines the

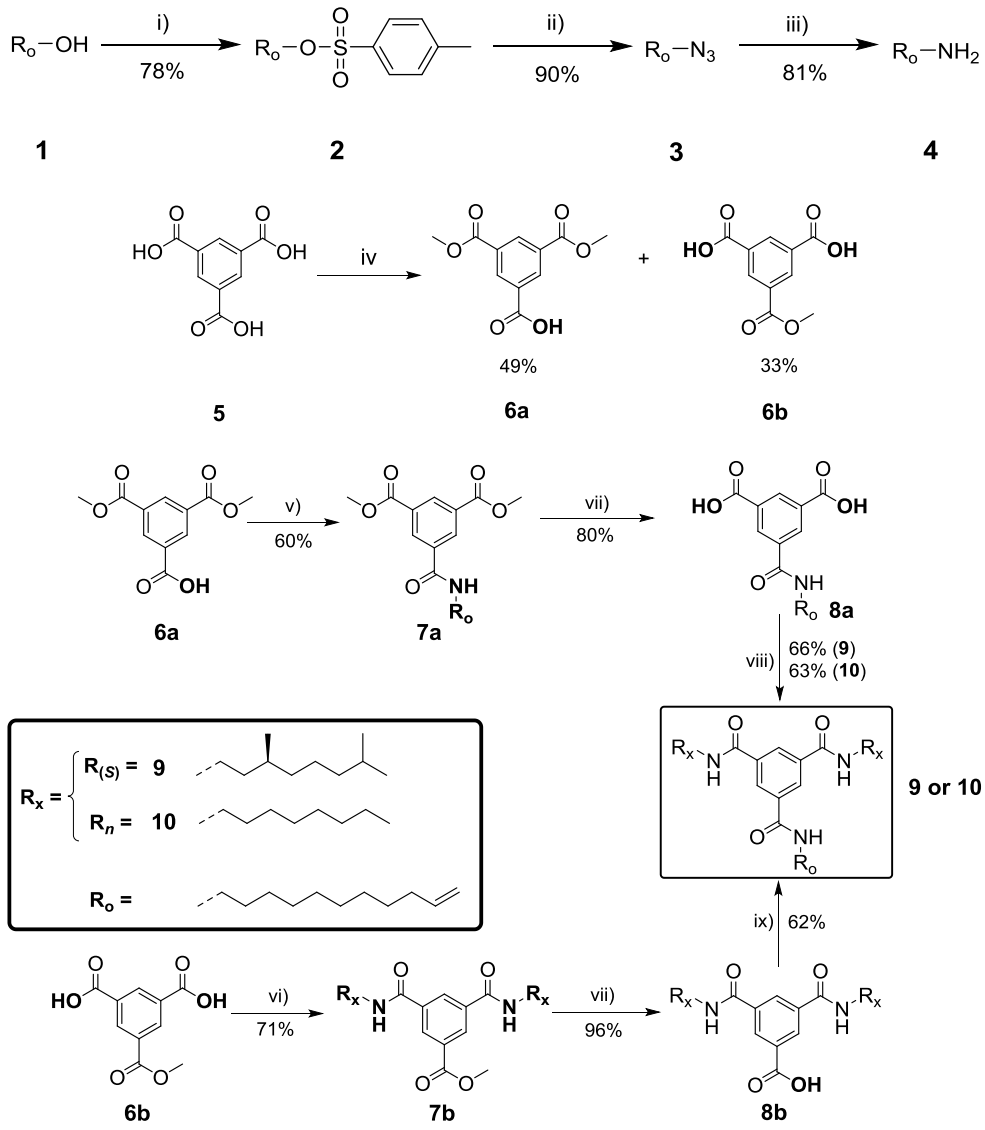


***Scheme 5.2*** *Synthetic route for (S)- / n-BTA-olefin* ***9*** *and* ***10*** *. Reagents and conditions: i) tosyl chloride, pyridine, DCM, 0 °C-r.t.; ii) sodium azide, DMF, 50 °C; iii) $PPh_3$, $H_2O$, THF, 50 °C; iv) MeOH, $H_2SO_4$, 55 °C; v) oxalyl chloride, DCM, 0 °C-r.t. then DIPEA, undec-10-en-1-amine (****4****), DCM, 0 °C-R.T.; vi) oxalyl chloride, DCM, 0 °C-r.t. then DIPEA, (S)-3,7-dimethyloctylamine, DCM, 0 °C-r.t.; vii) LiOH, MeOH, r.t. viii) DIPEA, (S)-3,7-dimethyloctylamine or octylamine, DMF, 0 °C; ix) DIPEA, undec-10-en-1-amine (****4****), DMF, 0 °C.*

degree of functionalization. The enantiomerically pure (*S*)-BTA-olefin (**9**) and *n*-BTA-olefin (**10**) were synthesized in 4 steps via a parallel synthesis starting from trimesic acid (Scheme 5.2).

Undec-10-en-1-amine (**4**) was synthesized starting from undec-10-en-1-ol (**1**). Starting alcohol was converted into the corresponding tosylate (**2**) with use of tosyl chloride and pyridine. The tosylate subsequently readily reacted with sodium azide thereby forming 11-azidoundec-1-ene (**3**). Staudinger reduction of the azide intermediates yielded after distillation undec-10-en-1-amine **4** in an overall yield of 56%. In the first step of the BTA-olefin synthesis, trimesic acid (**5**) was converted into a mixture of 3,5-bis(methoxycarbonyl)benzoic acid **6a** and 5-(methoxycarbonyl)isophthalic acid **6b** via Fischer esterification with methanol. The products were separated by column chromatography using mixture of dichloromethane (DCM), methanol (MeOH) and acetic acid (AcOH) with a slowly increasing gradient to afford good separation of both acids. Both **6a** and **6b** were subsequently converted into the corresponding chlorides by oxalyl chloride in presence of a catalytic amount of DMF. Subsequent nucleophilic substitution with undec-10-en-1-amine and (*S*)-3,7-dimethyloctylamine yielded amides **7a** and **7b** with one or two methoxycarbonyl groups remaining, respectively. Treatment of the methyl ester-protected amides with methanol / water solution of LiOH at room temperature afforded free acids **8a** and **8b**, which were subsequently activated with 2-(1H-benzotriazole-1-yl)-1,1,3,3-tetramethylaminium tetrafluoroborate (TBTU) and converted into the final (*S*)-BTA-olefin **9** by addition of (*S*)-3,7-dimethyloctylamine (**8a**) or undec-10-en-1-amine (**8b**). The combined yield of the parallel routes was 29%. *n*-BTA-olefin (**10**) was synthesized using **8a** and *n*-octylamine according to the same protocol as (*S*)-BTA-olefin (**9**). **PDMS-*g*-BTA** copolymers were synthesized via direct hydrosilylation of three commercially available PDMS-*co*-PHMS with average molecular weights of 25 kg mol$^{-1}$ (5% PHMS), 6 kg mol$^{-1}$ (8% PHMS) and 2 kg mol$^{-1}$ (16% PHMS). The (*S*)-BTA olefin (**9**) was coupled to the three polymers while *n*-BTA-olefin (**10**) was coupled only to one PDMS-*co*-PHMS backbone (**P1-*g*-*n*-BTA**) applying a platinum(0)-1,3-divinyl-1,1,3,3-tetramethyldisiloxane complex (the Karstedt catalyst) (Scheme 5.3). All polymers were purified by means of BioBeads$^{TM}$ in THF, which afforded a good separation between final product and the residual BTA-olefin impurities.

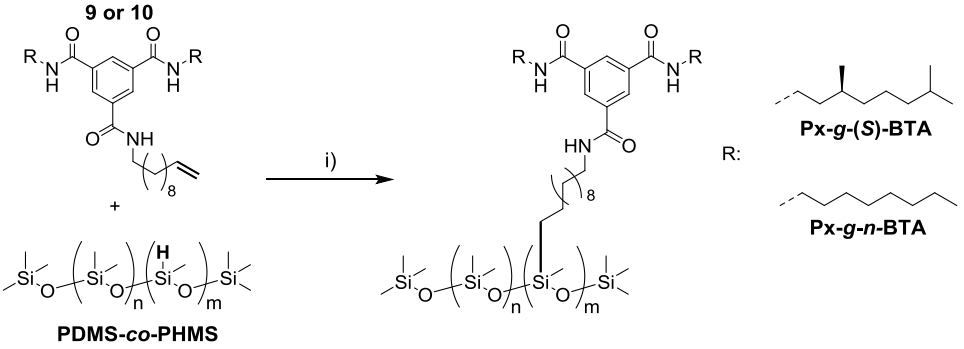


***Scheme 5.3*** *Synthetic route for **PDMS-g-BTA**. Reagents and conditions: i) Karstedt catalyst solution, THF, R.T.*

**Table 5.1.** Characterization data of polymers **PDMS-g-BTA**.

| polymer | $M_n$[a] (kg mol$^{-1}$) | $Đ$ [a] (-) | mol % BTA[b] | $n$[c] | $m$[d] | $g$[e] |
|---|---|---|---|---|---|---|
| **P1-*g*-(*S*)-BTA** | 42.1 | 2.05 | 3 | 439 | 14 | 0.0012 |
| **P2-*g*-(*S*)-BTA** | 17.6 | 1.66 | 9 | 123 | 12 | 0.0019 |
| **P3-*g*-(*S*)-BTA** | 10.7 | 3.08 | 14 | 57 | 9 | 0.0023 |
| **P1-*g*-*n*-BTA** | 40.3 | 2.34 | 3 | 429 | 13 | n/a |

[a] Determined by SEC in THF, calibrated with polystyrene standards. [b] Determined by $^1$H NMR. [c] $n$ is the number of siloxane units within the polymer backbone, which was calculated using the HMS content provided by the supplier and $M_n$. [d] $m$ is the number of BTA units within the polymer backbone, which was calculated using $M_n$ and mol% BTA. [e] The anisotropy $g$ value was determined using CD spectroscopy of a film spin coated on a quartz substrate.

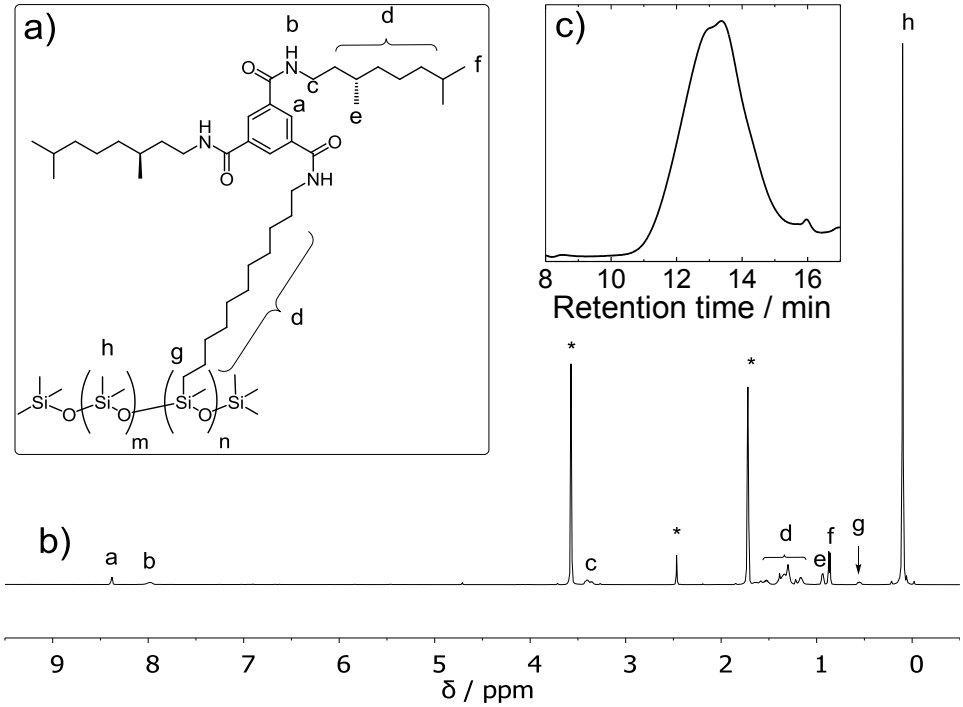


***Figure 5.1**: a) Chemical structure of **PDMS-g-BTA**; b) $^1$H NMR spectrum of **P1-g-BTA** in THF-$d_8$. * peaks at 1.73 and 3.57 correspond to THF, peak at 2.46 ppm corresponds to water; c) SEC trace of **P1-g-BTA** in THF.*

The four polymers were fully characterized by $^1$H NMR and size exclusion chromatography (SEC) in THF (Table 5.1). The $^1$H NMR spectrum of **P1-*g*-(*S*)-BTA** in THF-$d_8$ showed characteristic signals of the BTA core at 8.38 (Ph-H) and 7.98 ppm (NH) as well as the aliphatic protons (between 3.40 and 0.80 ppm) (Figure 5.1b). The largest peak at 0.10 ppm corresponds to the PDMS methyl protons. The BTA functionalization of PDMS is unambiguously confirmed by presence of a triplet at 0.5 ppm which corresponds to the methylene group attached to the PDMS backbone. The degree of BTA functionalization was quantified by comparing the integrals of the signals at 0.1 ppm and 0.5 ppm. Both **P1-*g*-(*S*)-BTA** and **P1-*g*-*n*-BTA** show a BTA graft density of 3%. **P2-*g*-(*S*)-BTA** and **P3-*g*-(*S*)-BTA** show higher graft densities of 9% and 14%, respectively. The SEC trace of **P1-*g*-(*S*)-BTA** in THF shows a unimodal peak, corresponding to an $M_n$ of 42.1 kg mol$^{-1}$ and a molar mass dispersity $Đ$ of 2.05 (Figure 5.1c). The measured $M_n$ is higher than expected (38 kg mol$^{-1}$ based on the SEC data of PDMS-*co*-PHMS and calculated degree of functionalization), presumably a result of the graft polymer topology in combination with the fact that the SEC column is calibrated with polystyrene standards. Analogously, all remaining copolymers show also higher $M_n$ values than expected.

## 5.3. Self-assembly of PDMS-*g*-(*S*)-BTA in bulk

In the FT-IR spectrum of **P1-*g*-(*S*)-BTA** (Figure 5.2a) absorptions bands characteristic for helically aggregated BTAs[48] at 3238 cm$^{-1}$, 1641 cm$^{-1}$ and 1562 cm$^{-1}$, are observed as well as bands corresponding to the siloxane backbone (1250 cm$^{-1}$, 1010 cm$^{-1}$, 790 cm$^{-1}$).[49] Bands at similar positions were found for **P2-*g*-(*S*)-BTA** and **P3-*g*-(*S*)-BTA** indicating that irrespective of the physical appearance of the polymers, aggregated BTAs are present in the bulk samples. The helical aggregation was confirmed with CD spectroscopy (Figure 5.2b). Since the chiral BTA grafts all possess (*S*)-stereogenic centra, we expect that a *M*-helical sense is favored in the

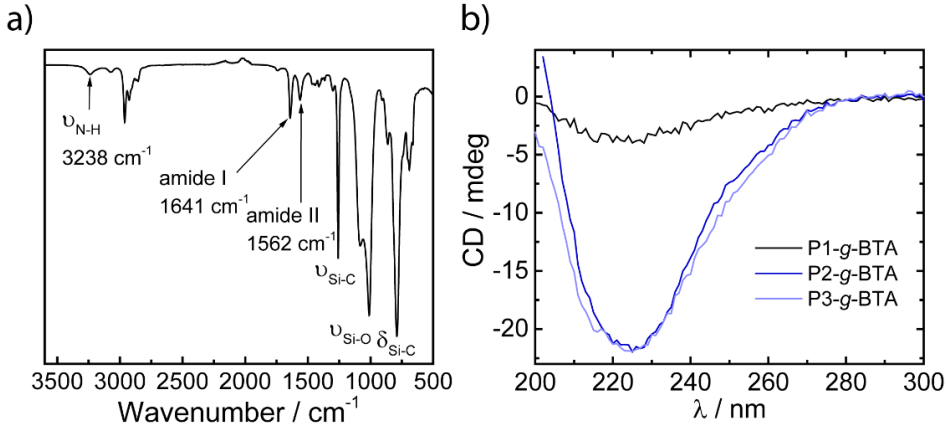


***Figure 5.2**. a) FT-IR spectrum of **P1-g-(S)-BTA**; b) CD spectra of spin coated **PDMS-g-(S)-BTA** polymers, anisotropy values are given in Table 1.*

formed aggregates, which is characterized by a negative CD effect.[50] Films of all polymers were spin coated on quartz and all **PDMS-*g*-(*S*)-BTA** polymers exhibited a negative CD effect with an extremum at 225 nm. The anisotropy value (*g*) was calculated and the absolute values increases in the series **P1-*g*-(*S*)-BTA** to **P3-*g*-(*S*)-BTA**. This suggests that although helical aggregation is present in all graft copolymers, the degree to which this occurs depends on the density of the BTA grafts. High stability of the BTA aggregates formed within the PDMS matrix was reflected by lack of the thermal transitions up to 250 °C as showed by DSC. Additionally, variable-temperature IR did not show significant changes in the BTA absorption bands, showing that also no change in the structure is observed at the supramolecular level.

## 5.4 Self-assembly of PDMS-*g*-BTA in dilute solution

We followed the assembly of the polymers in solution by investigating the effect of solvent on BTA-grafts association in **PDMS-*g*-(*S*)-BTA** systems. Previous studies of BTA-grafted polymers showed that these can form globular particles comprising single polymer chains in organic solvents and water via self-assembly of by polymeric chain folding. However, the interplay between the backbone solubility in the solvent and BTA aggregation can also result in multi-chain aggregation and since the PDMS backbone is exceptionally flexible, the question is in how far this promotes or impedes single chain folding. Dilute solution characterization of **PDMS-*g*-(*S*)-BTA** was performed with CD spectroscopy. For this, 1,2-dichloroethane (DCE), which has a better optical transparency in the BTA absorption region than chloroform, was selected. In contrast to "free BTA" molecules that do not aggregate in chloroform and DCE, **PDMS-*g*-(*S*)-BTA** solutions in DCE ($c_{BTA}$ = 50 µM) all showed negative CD effects with extrema at 225 nm. In all examples, a single-maximum CD spectrum is observed, which is characteristic for helically aggregated (*S*)-BTA with a dihedral angle of θ = 45° between the planes of the benzene ring and the C=O bond.[51] Interestingly, in sharp

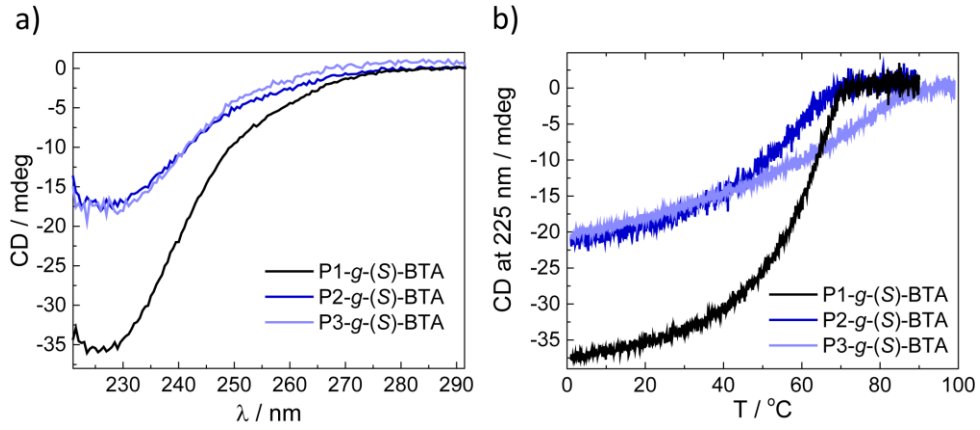


***Figure 5.3*** *a) CD spectra of* ***PDMS-g-(S)-BTA*** *in 1,2-dichloroethane ($c_{BTA}$ = 50 µM, 20 °C), CD cooling curves of PDMS-g-BTA in 1,2-dichloroethane (rate: 1 K min$^{-1}$, $c_{BTA}$ = 50 µM).*

contrast to the CD spectra in bulk, the molar circular dichroism (|Δε|) of **P1-*g*-(*S*)-BTA** is now the highest of the three polymers (|Δε| = 43 L mol$^{-1}$, 20 L mol$^{-1}$ and 22 L mol$^{-1}$ for **P1-*g*-(*S*)-BTA**, **P2-*g*-(*S*)-BTA** and **P3-*g*-(*S*)-BTA**, respectively) (Figure 5.3a). This remarkable difference highlights the importance of BTA-solvent and PDMS-solvent interactions which promote the aggregation of BTAs to the magnitude of "free BTA" in heptane (|Δε| = 43 L mol$^{-1}$ for "free BTA" in heptane).[46] This indicates that nearly all BTAs in **P1-*g*-(*S*)-BTA** are present in helical aggregates. On the other hand, values of |Δε| for **P2-*g*-(*S*)-BTA** and **P3-*g*-(*S*)-BTA** are close to the ones reported for PMMA-BTA polymers.[38,39,45] This suggests that a number of BTA units does not participate in helical assemblies in **P2-*g*-(*S*)-BTA** and **P3-*g*-(*S*)-BTA** whereas nearly all BTAs do in **P1-*g*-(*S*)-BTA**. Possibly, the higher local concentration of the BTA pendants in **P2-*g*-(*S*)-BTA** and **P3-*g*-(*S*)-BTA** reduce their conformational freedom preventing remaining BTAs to aggregate as effectively as in the case of **P1-*g*-(*S*)-BTA**.

Temperature-dependent CD measurements were conducted by cooling the dilute solutions of **PDMS-*g*-(*S*)-BTA** from 100 °C to 0 °C (Figure 5.3b). At 90 °C, no CD effect is visible, indicating that the BTAs are not aggregated. Upon cooling, an abrupt increase in the CD effect is observed for **P1-*g*-(*S*)-BTA** at 72 °C, a less abrupt increase takes place in case of **P2-*g*-(*S*)-BTA** at 70 °C, and **P3-*g*-(*S*)-BTA** exhibits a cooling curve similar to previously reported for carbon-based polymers with BTA pendants, which all exhibited a gradual increase of the CD effect.[31,32,36,38,39,52] The shapes of the cooling curves are connected to the increase of the density of BTA pendants. Despite the differences in the sharpness of the transition between **P2-*g*-(*S*)-BTA** and **P3-*g*-(*S*)-BTA**, the values of |Δε| are similar. **P1-*g*-(*S*)- BTA** shows a cooling curve similar to the ones recorded for free BTAs in alkane solvents, which is indicative

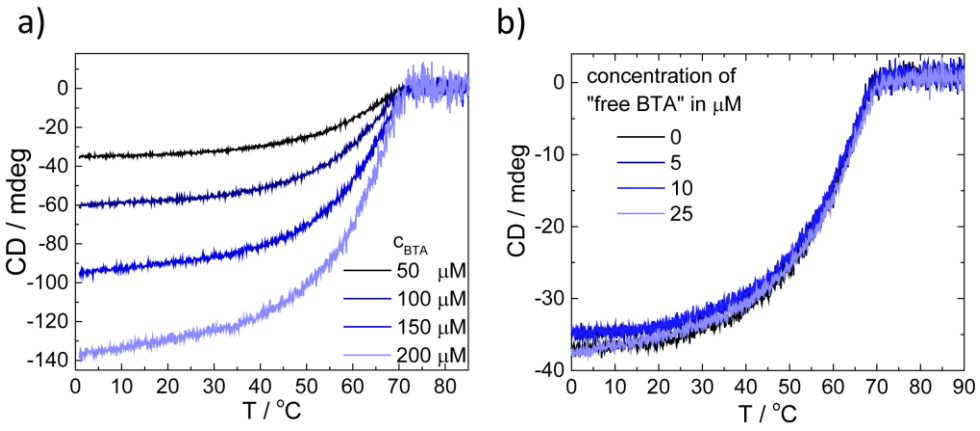


***Figure 5.4**. a) CD cooling curves of **P1-g-(S)-BTA** in 1,2-dichloroethane recorded at different BTA concentrations, (cooling rate = 1 K min$^{-1}$); b) CD cooling curves of **P1-g-(S)-BTA** in 1,2-dichloroethane with varying concentration of added "free BTA" while the concentration of the BTA attached covalently onto a polymeric backbone was kept constant at 50 µM.*

for highly cooperative BTA aggregation.[46] As the degree of functionalization is increased, the sharpness in the transition, and therefore the cooperativity diminishes. Interestingly, increasing the BTA concentration of **P1-*g*-(*S*)-BTA** from 50 to 200 µM shows that the $T_e$ remains at 72 °C and that the cooperativity of the transition remains very high (Figure 5.4a). In addition, the CD effect increases proportionally with the BTA concentration. This suggests that the stability of the aggregates is polymer concentration independent and therefore is solely dependent on the interactions of the individual polymers with the solvent. Addition of (*S*)- BTA-olefin (**9**, "free BTA"), which is normally molecularly dissolved in DCE to the solution did not result in the copolymerization of free and grafted BTAs (Figure 5.4b). The lack of the

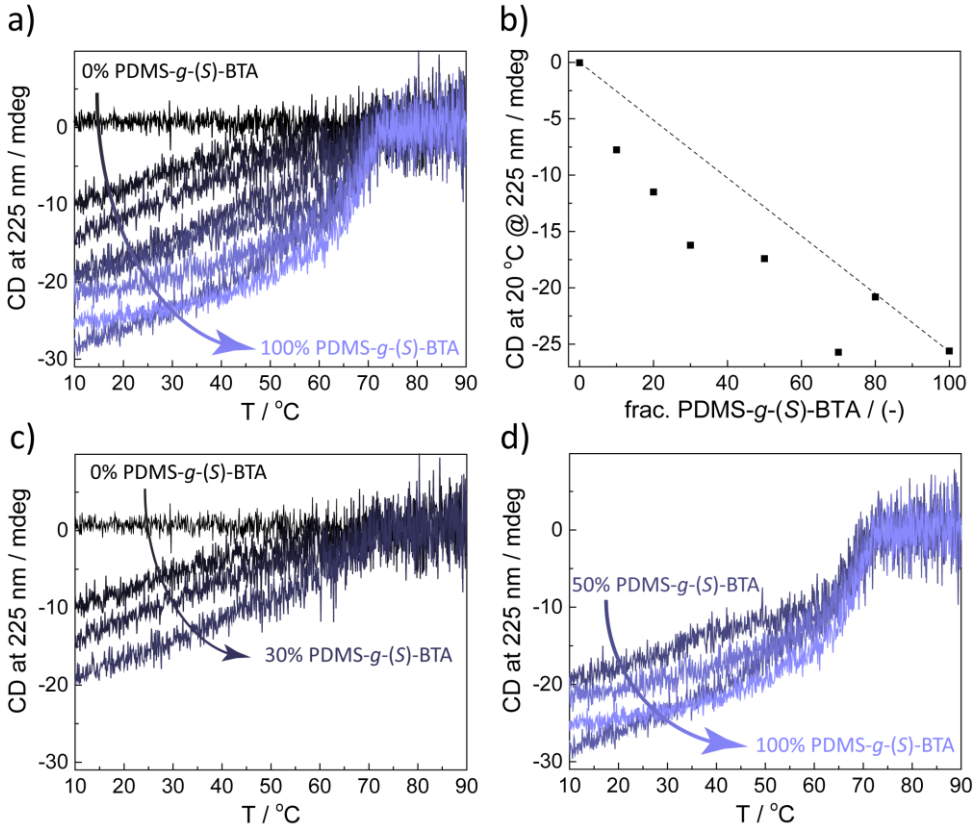


***Figure 5.5*** *a) overview of the CD cooling curves of sergeants-and-soldiers experiment (mixed* ***P1-g-n-BTA*** *and* ***P1-g-(S)-BTA****) in 1,2-dichloroethane ($c_{BTA}$ = 30 µM, cooling rate: 1 K min$^{-1}$); b) CD signal at 20 °C at λ = 225 nm as function of fraction of sergeant* ***P1-g-(S)-BTA****; CD cooling curves of sergeants-and-soldiers experiment at c) 0% to 30%* ***P1-g-(S)-BTA****; d) 50% to 100%* ***P1-g-(S)-BTA****.*

(co)assembly of "free BTAs" further confirmed that the aggregation of the BTAs is driven by the polymeric backbone collapse and not vice versa.

To investigate the nucleation of the BTA aggregates and collapse of the polymers, we performed sergeants and soldiers experiment by mixing **P1-*g*-BTA** containing (*S*)-BTA or *n*-BTA pendants. In case of "free BTA", typically strong amplification of supramolecular chirality is observed which is manifested by full helical bias of *n*-soldiers (*n*-BTA) by only 5% of (*S*)-sergeants ((*S*)-BTA).[46] According to our expectations, CD cooling curves of mixed **P1-*g*-(*S*)-BTA** and **P1-*g*-*n*-BTA** show that aggregation of the BTA starts at the same temperature regardless of the fraction of sergeant, further confirming that nucleation of the stacks takes place at the level of single polymer (Figure 5.5a). Further elongation of the aggregates is connected to the coassembly of polymers containing (*S*)-sergeants and *n*-soldiers as we observe a certain degree of chiral amplification (Figure 5.5b). Careful analysis of the CD cooling curves between 50% and 100% of **P1-*g*-(*S*)-BTA** suggests that at the temperatures between $T_e$ (72 °C) and 65 °C supramolecular polymerization of the BTAs occurs in highly stereoselective fashion (Figure 5.5d). High helical bias in this regime means, that even though the nucleation of the assemblies occurs at the single-chain level, subsequent formation of aggregates formed by more than one polymer chain overrules the assembly. Another transition is visible at 65 °C, where the CD cooling curves level off. A plausible explanation for this observation is another aggregation process, in which previously formed small aggregates of polymers again collapse to form larger particles. Since the process is purely stochastic, there is significant probability of recombination of non- or poorly biased stacks, therefore the increase of the CD signal at lower fractions of sergeants is hampered.

The formation of the large aggregates was confirmed by atomic force microscopy (AFM) and dynamic light scattering (DLS) (Figure 5.6a and b). Spin-coated sample of **P1-*g*-(*S*)-BTA** (1 mg $mL^{-1}$) in DCE showed presence of aggregates with sizes between 200 nm and 400 nm. DLS experiments performed on **P1-*g*-BTA** in DCE at 20 °C show the presence of particles with sizes of around 400 nm hydrodynamic diameter with a low dispersity. Interestingly, the size of the particles formed at room temperature remains unaffected after heating-cooling cycles, indicating that the formation of the particles is thermodynamically controlled. Rate-dependent CD cooling curves of **P1-*g*-BTA** show that the transition between aggregated and non-aggregated state is under full thermodynamic control, showing that it is highly connected to the solubility of the polymeric backbone (Figure 5.6c).

Based on the results above, we propose that the remarkable, cooperative BTA aggregation observed in **P1-*g*-BTA** is related to the highly incompatible nature of PDMS and the covalently attached BTAs combined with the formation of helical BTA aggregates. In addition to the phase segregation process, there is also the intrinsic flexibility of the PDMS backbone[4,7] which significantly reduces the entropic penalty of backbone folding in comparison to the more stiff PMMA backbones, permitting a high degree of aggregation

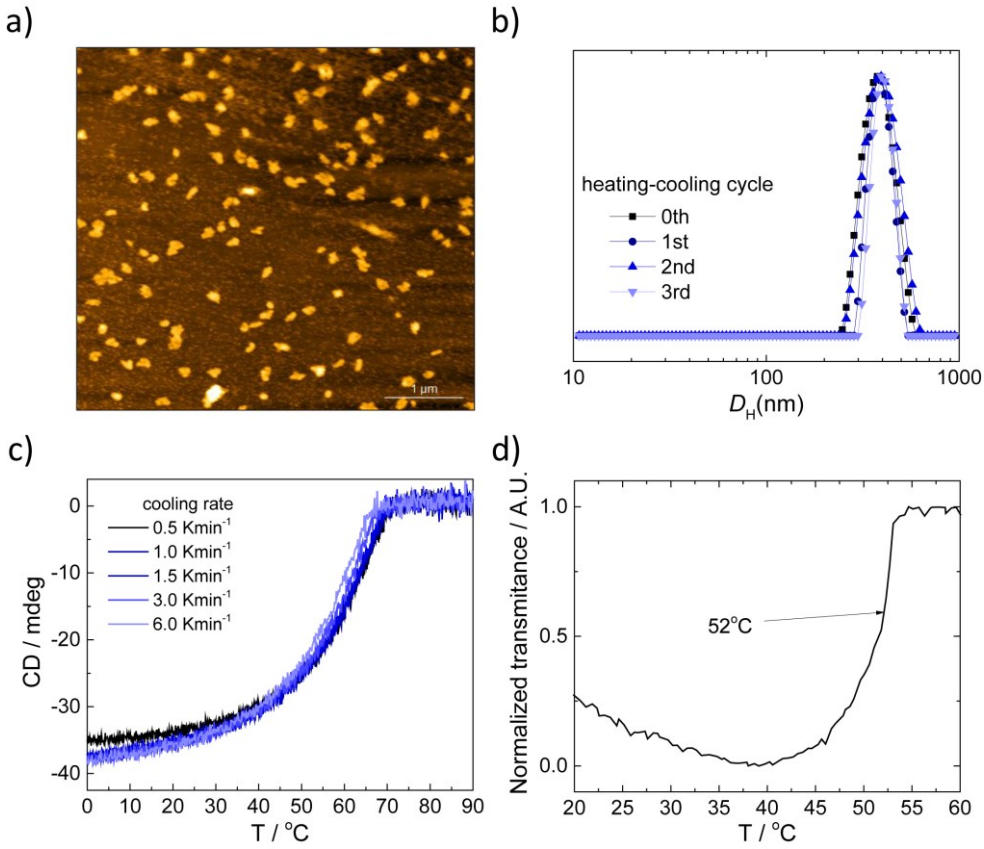


***Figure. 5.6*** *a) AFM phase image of* ***P1-g-(S)-BTA*** *film on a silicon wafer obtained by spin-coating from a DCE solution (1 mg mL$^{-1}$); b) DLS profiles of* ***P1-g-(S)-BTA*** *in DCE at 1 mg mL$^{-1}$ and 20 °C after heating-cooling cycles in the temperature interval of 20–75 °C; c) CD cooling curves of* ***P1-g-(S)-BTA*** *in 1,2-dichloroethane recorded at variable cooling rates ($c_{BTA}$ = 50 µM); d) UV cooling curve of PDMS-co-PHMS (P1) in 1,2-dichloroethane at 1 mg mL$^{-1}$.*

between pendant BTAs. Also, the poor solubility of PDMS in DCE at lower temperatures could play an important role. At room temperature, the mixture of the pure precursor polymer PDMS-*co*-PHMS in DCE is turbid at 10 mg mL$^{-1}$ whereas the mixture becomes clear when heated above 50 °C, as evidenced by VT-UV recorded at 600 nm (Figure 5.6d). Covalently attaching the BTAs changes the solvent compatibility of the graft copolymer. At the same time, the PDMS backbone may shield the BTAs from the solvent, hereby enhancing hydrogen-bonding interactions. Although it appears from the above results that the collapse of the PDMS backbone in DCE creates a confined space that promotes BTA aggregation, the exact nature of the interaction triangle between DCE, BTA, and PDMS remains to be fully elucidated.

## 5.5 Conclusions

We synthesized BTA-olefin intermediates in good yields that were readily attached to the commercially available PDMS polymers via hydrosilylation with use of Pt[0] catalyst. The polymers obtained were characterized in bulk and in solution. In bulk, the supramolecular assembly of BTAs attached to PDMS leads to phase-segregated structures. The formation of helical aggregates stabilized by threefold hydrogen bonding was confirmed by IR and CD spectroscopy. In solution, we demonstrated that proper selection of the polymeric backbone can lead to extraordinary polymer assembly properties. As observed by VT-CD, **P1-*g*-(*S*)-BTA** exhibited highly cooperative assembly of the BTAs in DCE, which was not achieved for any BTA-graft copolymers before and suggests that this unusual behaviour is connected to the synergy between BTA-backbone, BTA-solvent, and backbone-solvent interactions. Sergeants-and-soldiers experiment confirmed that the nucleation of the BTA aggregates occurs at the single polymer chain level. DLS and AFM showed that this combination leads to the thermodynamically controlled formation of multi-chain aggregates in which nearly all BTAs are aggregated. The degree of functionalization in combination with the degree of polymerization also has a significant impact on the folding characteristics, which indicates that a proper balance in BTA density is needed.

## 5.6 Experimental Section

### 5.6.1 Materials and methods

All solvents were obtained from Biosolve, Acros or Aldrich. Trimesic acid was obtained from Thermo Fischer Scientific. PDMS-co-PHMS precursor polymers were purchased from Gelest. All other chemicals were obtained from Aldrich. Dry DCM, THF, and DMF were tapped off a distillation setup which contained molsieves. $CHCl_3$ was dried over molsieves and triethylamine was stored on KOH pellets. 1,2-Dichloroethane was used as received and showed a water content of 119 ppm. Flash column chromatography was performed on Biotage SP-1 Flash Chromatography system, with KP-SILTM Silica Gel SNAP columns. The $^{1}H$ and $^{13}C$ NMR, FT-IR and CD spectra were recorded using apparatus described in Experimental Section of Chapter 2 and 3. Size exclusion chromatography (SEC) measurements were conducted on a Shimadzu Prominence-i LC-2030C 3D with a Shimadzu, using eluent flow of 1 ml min-1 (THF) and solutions were of concentration 1 mg $ml^{-1}$ were filtered through 0.2 µm Whatman Anatop 10 filters before injection. CD experiments in solution were performed at a BTA concentration of 50 µM (**P1-*g*-BTA**, 0.11 mg/mL) in a 0.5 cm Hellma quartz cell. Dynamic light scattering measurements were performed using a Malvern µV Zetasizer equipped with a 830 nm laser and a scattering angle of 90 °C at a temperature of 20 °C in a fluorescence cell with a path length of 1 cm. Samples were prepared by solubilizing the polymers in 1,2-dichloroethane previously filtered through 0.2 µm PTFE-filter (Whatman). Atomic Force Microscopy (AFM) was carried out on an Asylum Research MFP-3D mounted on an anti-vibration chamber. AFM was carried out in tapping mode using silicon probes manufactured by NanosensorsTM (type PPP-NCSTR-50 with a tip height of 10-15 µm and force constant of 1.2 – 29 N/m). Images were recorded at a resolution of 512×512 pixels and a scan rate of 1.0 Hz. The obtained images were subjected to first order flattening and removal of rastoring horizontal lines using Gwyddion software (v. 2.48). Samples were spin-coated on a silicon wafer from c = 1 mg $mL^{-1}$ solutions in 1,2-dichloroethane.

### 5.6.2 Synthetic procedures

*Undec-10-en-1-yl 4-methylbenzenesulfonate* (**2**)

Undec-10-en-1-ol (**1**) (12 mL, 59 mmol) and 4-methylbenzene-1-sulfonyl chloride (11.8 g, 62 mmol) were dissolved in dry dichloromethane (40 mL) and the solution was cooled down to 0 °C. Then pyridine (9.5 mL, 117 mmol) was added dropwise and the mixture was stirred at 0 °C for another 30 minutes. Then the mixture was allowed to warm up to room temperature and stirred overnight. The progress was monitored by TLC (*n*-heptane / EtOAc 1:1). Full conversion was observed after 24 h. On completion, the mixture was diluted with 200 mL of DCM and moved to a separatory funnel with 150 mL of 2M HCl. The organic layer was washed then with 2 M NaOH (150 mL), water and brine. The organic phase was dried over magnesium sulfate, filtered off and the solvent evaporated under reduced pressure to give the product as an orange oil (15.6 g, 78%).

$^1$H NMR (400 MHz, $CDCl_3$): δ (ppm) 7.82 – 7.73 (m, 2H), 7.37 – 7.29 (m, 2H), 5.80 (m, 1H), 4.98 (m, 2H), 4.01 (m, 2H), 2.44 (d, *J* = 3.6 Hz, 3H), 2.03 (m, 2H), 1.62 (m, 2H), 1.43 – 1.14 (m, 12H)

*11-Azidoundec-1-ene* (**3**)

Undec-10-en-1-yl 4-methylbenzenesulfonate (**2**) (15.6 g, 48.1 mmol) was dissolved in dry DMF (35 mL). Then sodium azide (4.7 g, 72.1 mmol) and potassium iodide (0.1 g, 0.5 mmol) were added to the solution and the mixture was stirred at 50 °C overnight. The progress was monitored by TLC (heptane / EtOAc 4:1). After 16 h, full conversion was observed. The reaction mixture was then moved to a separatory funnel and washed with water. The upper phase was collected. The lower aqueous layer was extracted with *n*-hexane until no more product was in the organic phase (4 x 150 mL of hexane). Then, the combined organic phases were washed twice with water and dried over magnesium sulfate. The solution was filtered off and the solvent was removed under reduced pressure to give colorless oil to give 11-azidoundec-1-ene (8.45 g, 90% yield).

$^1$H NMR (400 MHz, $CDCl_3$): δ (ppm) 5.81 (m, 1H), 4.98 (m, 2H), 3.25 (m, 2H), 2.09 – 1.99 (m, 2H), 1.60 (m, 2H), 1.29 (m, 12H).

*Undec-10-en-1-amine* (**4**)

11-Azidoundec-1-ene (**3**) (8.4 g, 43.3 mmol) was dissolved in THF (50 mL). Then triphenylphosphine (11.3 g, 43.3 mmol) and water (1.2 mL, 65.0 mmol) were added and the reaction mixture was heated up to 50 °C and stirred overnight. The progress was monitored by TLC (hexane / EtOAc 2:1). On completion, the solvent was removed under reduced pressure, the white solid was triturated with pentane and washed until no product was observed in the filtrate (10 x 50 mL). Then, the filtrate was concentrated *in vacuo* to give an orange oil as crude product. The title compound was obtained by vacuum distillation to get undec-10-en-1-amine (6 g, 81% yield) as a colorless liquid (bp. 50 °C, $3.7 \times 10^{-2}$Torr).

$^1$H NMR (400 MHz, $CDCl_3$): δ (ppm) 5.81 (m, 1H), 4.98 (m, 2H), 2.73 – 2.63 (m, 2H), 2.11 – 1.98 (m, 2H), 1.47-1.26 (m, 14H)

*5-(Methoxycarbonyl)isophthalic acid (**6a**), 3,5-bis(methoxycarbonyl)benzoic acid* (**6b**)

To a solution of benzene-1,3,5-tricarboxylic acid (**5**) (10 g, 47.6 mmol) in methanol (200 mL), sulfuric acid (2.5 mL, 47,6 mmol) was added dropwise and the mixture was heated to reflux. The progress of the reaction was monitored by TLC ($CHCl_3$ / MeOH 9:1 + drop of acetic acid). The formation of mono- di- and triester was observed. After 2 hours full conversion was observed. The reaction was cooled down to room temperature and quenched with 200 mL of saturated sodium bicarbonate. A precipitate of trimethyl ester was formed. The suspension was filtered off, the filtrate was collected and concentrated under reduced pressure to remove methanol. The remaning aqueous solution was washed with 300 mL of EtOAc (organic phase was discarded), acidified to pH 1 with aqueous 1 M $KHSO_4$ and extracted three times with 300 mL of EtOAc. The collected organic phases were dried over magnesium sulfate, filtered, and the solvent removed in vacuo. This afforded a white solid which was dried in vacuum to give 8.8 g of mixture of mono- and diester. The title compounds were isolated by means of column chromatography to give 5.6 g of 5-(methoxycarbonyl)isophthalic acid (**6a**, 49%) and 3.5 g of 3,5-bis(methoxycarbonyl)benzoic acid (**6b**, 33%). Chromatographic data is summarized in Table 5.2. Obtained acids were used as collected in further steps.

***Table 5.2***: Elution of profile of the separation of the acids **6a** and **6b**.

| Solvent composition (vol%) | | | volume permeated [L] | fraction | mass [g] |
|---|---|---|---|---|---|
| DCM | MeOH | AcOH | | | |
| 99 | 1 | 0.3 | 1.5 | F0 (refuse) | - |
| 98 | 2 | 0.3 | 1.5 | F1 acid (**6a**) | 5.6 g |
| 97 | 3 | 0.5 | 3 | F2 diacid (**6b**) | 3.5 g |

*Dimethyl 5-(undec-10-en-1-ylcarbamoyl)isophthalate* (**7a**)

3,5-Bis(methoxycarbonyl)benzoic acid (**6a**) (0.195 g, 0.819 mmol) was dissolved in $CHCl_3$ (4 mL) and cooled down to 0 °C. Then oxalyl dichloride (0.1 mL, 0.901 mmol) and a drop of DMF were added dropwise and the mixture was allowed to warm to room temperature. After an hour, the full conversion was observed (TLC, eluent: DCM / EtOAc 9:1, a drop of the reaction mixture was added to a solution of octylamine in DCM and the resulting solution of amide was spot on plate). On completion the solvent was removed *in vacuo*, the residue was redissolved in toluene and concentrated under reduced pressure (this was repeated three times). Then the residue was dissolved in $CHCl_3$ (4 mL) and added dropwise to the solution of triethylamine (0.3 mL, 2,047 mmol) and undec-10-en-1-amine (**4**) (0.152 g, 0.901 mmol) in 4 mL of $CHCl_3$ at 0 °C. After 15 minutes the reaction mixture was allowed to warm to room temperature. The reaction mixture was stirred overnight. Full conversion was confirmed by TLC (DCM / EtOAc 9:1). The solution was diluted with 15 mL of chloroform and washed twice with 20 mL of 1M HCl. Next, the organic layer was washed with water and dried over magnesium sulphate. The solvent was removed under reduced pressure to give 291 mg of a yellow solid as crude product, which was purified via column chromatography (DCM

/ acetone 98:2 to 95:5 gradient) to afford dimethyl 5-(undec-10-en-1-ylcarbamoyl)isophthalate (0.191 g, 0.49 mmol, 60% yield).

$^1$H NMR (400 MHz, $CDCl_3$): δ (ppm) = 8.78 (s, 1H); 8.60 (s, 2H); 6.27 (t, 1H); 5.80 (m, 1H); 4.97 (m, 2H); 3.97 (s, 6H); 3.49 (t, 2H); 2.03 (m, 2H); 1.62 (m, 2H); 1.28 (m, 12H).

*3,5-Bis(((S)-3,7-dimethyloctyl)carbamoyl)benzoate* (**7b**)

5-(Methoxycarbonyl)isophthalic acid (**6b**) (2 g, 8.9 mmol) was dissolved in dry DCM (50 mL) and cooled down to 0 °C. Then oxalyl dichloride (1.5 mL. 17.84 mmol) and a drop of DMF were added dropwise and the mixture was allowed to warm to room temperature. After an hour, the full conversion was observed (TLC, eluent: DCM / EtOAc 9:1, a drop of the reaction mixture was added to a solution of (*S*)-3,7-dimethyloctylamine in DCM and resulting solution of amide was used). On completion the solvent was removed under reduced pressure, the residue was redissolved in toluene and concentrated under reduced pressure (this was repeated three times). Then the residue was dissolved in $CHCl_3$ (20 mL) and added dropwise to the solution of triethylamine (3.7 ml, 26.8 mmol) and (*S*)-3,7-dimethyloctan-1-amine (2.8 g, 17.8 mmol) in 20 mL of $CHCl_3$ at 0 °C. After 15 minutes the reaction mixture was allowed to warm up to room temperature. The resulting mixture was stirred overnight. Full conversion was confirmed by TLC (DCM / EtOAc 9:1). The solution was diluted with 200 mL of chloroform and washed twice with 200 mL of 1M HCl. Next, the organic layer was washed with water and dried over magnesium sulphate. The solvent was removed under reduced pressure to give 4.3 g of orange solid as crude product, which was purified via column chromatography (DCM / acetone 98:2 to 9:1 vol/vol gradient) to afford methyl 3,5-bis(((*S*)-3,7-dimethyloctyl)carbamoyl)benzoate (3.2 g, 71% yield).

$^1$H NMR (400 MHz, $CDCl_3$): δ (ppm) = 8.51 (s, 2H); 8.39 (s, 1H); 6.31 (t, 2H); 3.96 (s, 3H); 3.49 (m, 4H); 1.69 – 1.1 (m, 20H); 0.94 (d, 6H), 0.86 (d, 12H).

*5-(Undec-10-en-1-ylcarbamoyl)isophthalic acid* (**8a**)

Lithium hydroxide (0.025 g, 1 mmol) in water (0.5 mL) was added to the solution of dimethyl 5-(undec-10-en-1-ylcarbamoyl)isophthalate (**7a**) (0.19 g, 0.490 mmol) in methanol (5 mL). The reaction was carried overnight at room temperature with extra addition of lithium hydroxide (0.025 g, 1 mmol). The progress was monitored by TLC (two tests: DCM / EtOAc 9:1 and DCM / MeOH 9:1 + AcOH to make sure that is no monoacid observed). On completion, the solvent was removed under reduced pressure, the residue was redissolved in water and washed with EtOAc. The aqueous phase was acidified with 1M HCl to pH 1 and extracted with EtOAc. The organic phase was washed with water, dried over magnesium sulfate and solvent removed in vacuo to give 5-(undec-10-en-1-ylcarbamoyl)isophthalic acid (0.142 g, 0.393 mmol, 80% yield) as white crystals, which were used straight away in the next step without further purification and analysis.

*3,5-Bis(((S)-3,7-dimethyloctyl)carbamoyl)benzoic acid* (**8b**)

Lithium hydroxide (3.4 g, 14 mmol) in water (6 mL) was added to the solution of 3,5-bis(((*S*)-3,7-dimethyloctyl)carbamoyl)benzoate (**7b**) (3.2 g, 6.4 mmol) in methanol (60 mL). The reaction was carried overnight at room temperature. The progress was monitored by TLC (DCM / EtOAc 9:1). On completion, the solvent was removed under reduced pressure, the residue was redissolved in EtOAc and washed with water. Then aqueous phase was acidified to pH 1 with 1M HCl and extracted with EtOAc. The combined organic fractions were washed with water, dried over magnesium sulfate, solvent removed *in vacuo* to

give 3,5-bis(((*S*)-3,7-dimethyloctyl)carbamoyl)benzoic acid (3 g, 6.2 mmol, 96% yield) as a white solid, which was used straight away in the next step without further purification and analysis.

*$N^1$,$N^3$-Bis((S)-3,7-dimethyloctyl)-$N^5$-(undec-10-en-1-yl)benzene-1,3,5-tricarboxamide* (**9**)

5-(Undec-10-en-1-ylcarbamoyl)isophthalic acid (**8a**) (0.14 g, 0.39 mmol) was dissolved in DMF (1 ml) and cooled to 0 °C. Then TBTU (0.3 g, 0.8 mmol) followed by (*S*)-3,7-dimethyloctan-1-amine (**4a**) (0.12 g, 0.8 mmol) and DIPEA (0.15 g, 1.2 mmol) were added. The mixture was stirred overnight at room temperature. The progress was monitored by TLC (DCM / EtOAc 9:1). On completion the mixture was diluted with DCM and washed with 1M HCl. The organic phase was washed with 1M NaOH and water, dried over magnesium sulfate and the solvent removed to give 0.75 g of crude product, which was purified via column chromatography ($CHCl_3$ to $CHCl_3$ / acetone 95:5 vol/vol gradient) to yield 0.17 g (66%) of $N^1$,$N^3$-bis((*S*)-3,7-dimethyloctyl)-$N^5$-(undec-10-en-1-yl)benzene-1,3,5-tricarboxamide as a white solid.

3,5-Bis(((S)-3,7-dimethyloctyl)carbamoyl)benzoic acid (**8b**) (3 g, 6.2 mmol) and TBTU (2.2 g, 6.8 mmol) were dissolved in DMF (12 mL) and cooled to 0 °C. Then DIPEA (3.2 ml, 18.5 mmol) and undec-10-en-1-amine (**4b**) (1.1 g, 6.8 mmol) were added. The reaction was stirred overnight at room temperature. The progress was monitored by TLC (DCM / EtOAc 9:1). On completion, the mixture was diluted with DCM and washed with 1M HCl. The organic phase was washed with 1M NaOH and water, dried over magnesium sulfate and solvent removed to give 4 g of crude product, which was purified via column chromatography ($CHCl_3$ to $CHCl_3$ / acetone 95:5 vol/vol gradient) to yield 2.5 g of $N^1$,$N^3$-bis((*S*)-3,7-dimethyloctyl)-$N^5$-(undec-10-en-1-yl)benzene-1,3,5-tricarboxamide as a white solid.

$^1$H NMR (400 MHz, $CDCl_3$): δ (ppm) = 8.33 (s, 3H), 6.50 (t, 3H), 5.80 (m, 1H); 4.97 (m, 2H), 3.46 (m, 6H), 2.03 (m, 2H), 1.73 – 1.46 (m, 8H), 1.70 – 1.09 (m, 34H), 0.93 (d, 6H), 0.86 (d, 12H).

$^{13}$C NMR (100 MHz, $CDCl_3$): δ (ppm) =165.99; 139.15; 135.30; 127.85; 114.11; 40.36; 39.22; 38.50; 37.11; 36.58; 33.78; 30.77; 29.51; 29.48; 29.43; 29.30; 29.09; 28.90; 27.92; 27.01; 24.62; 22.69; 22.58; 19.45.

*$N^1$,$N^3$-Bis(octyl)-$N^5$-(undec-10-en-1-yl)benzene-1,3,5-tricarboxamide* (**10**)

5-(Undec-10-en-1-ylcarbamoyl)isophthalic acid (**8a**) (0.5 g, 1.38 mmol) was dissolved in DMF (2.5 mL) and cooled to 0 °C. Then TBTU (1.11 g, 3.45 mmol) followed by 1-aminooctane (0.35 g, 2.77 mmol) and DIPEA (0.536 g, 4.15 mmol) were added. The mixture was stirred overnight at room temperature. The progress was monitored by TLC (DCM / EtOAc 9:1). On completion, the mixture was diluted with DCM and washed with 1 M HCl. The organic phase was washed with 1 M NaOH and water, dried over magnesium sulfate, filtered and the solvent removed to give 0.75 g of crude product. The crude product was purified via column chromatography ($CHCl_3$ to $CHCl_3$ / acetone 95:5 vol/vol gradient) to yield 0.51 g (63%) of $N^1$,$N^3$-bis(octyl)-$N^5$-(undec-10-en-1-yl)benzene-1,3,5-tricarboxamide as a white solid.

$^1$H NMR (400 MHz, $CDCl_3$): δ (ppm) = 8.34 (s, 3H), 6.62 (t, *J* = 4.4 Hz, 3H), 5.80 (m, 1H); 4.97 (m, 2H), 3.45 (q, *J* = 5.2 Hz, 6H), 2.03 (q, *J* = 5.6 Hz, 2H), 1.79 (bs, 3H), 1.40 – 1.20 (m, 31H), 0.87 (t, *J* = 5.2 Hz, 6H).

General procedure for the synthesis of **PDMS-*g*-BTA**

Calculated amounts (see below) of PDMS-co-PHMS and BTA-olefin (**9** or **10**) were placed in a 2-neck round-bottom flask and dried for 5 minutes under vacuum. Then the system was refilled with argon. The flask was then evacuated and refilled two times and next dry THF (1 mL per 0.1 g of BTA) was added.

When the starting materials were completely dissolved, a drop of Karstedt catalyst solution in xylene was added to the stirred mixture and the reaction was stirred for 2 hours. After that time no olefin protons were observed on the $^1$H NMR spectrum. On completion, over half of the solvent was removed *in vacuo* and the concentrated polymer solution was separated on a BioBeads™ column in THF and eluted to yield pure PDMS-*g*-BTA polymers.

The following **PDMS-*co*-PHMS** / **BTA-olefin** mass ratio was used:

**P1-g-BTA**: 1.95 g polymer / 1 g BTA-olefin
**P2-g-BTA**: 1.27 g polymer / 1 g BTA-olefin
**P3-g-BTA**: 0.61 g polymer / 1 g BTA-olefin

The density of BTA grafts was calculated using the following expression:,

$$f_{BTA} = \frac{1}{\frac{a}{6}+1} \cdot 100\%$$

where a = total integral of PDMS protons at 0.1 ppm. The spectrum was first normalized to the integral of Si-$CH_2$ protons at 0.5 ppm (H = 2).

## 5.7 References


[1] D. Zhu, S. Handschuh-Wang, X. Zhou, *J. Mater. Chem. A* **2017**, *5*, 16467–16497.
[2] J. Zhou, A. V. Ellis, N. H. Voelcker, *Electrophoresis* **2010**, *31*, 2–16.
[3] F. Abbasi, H. Mirzadeh, A. A. Katbab, *Polym. Int.* **2001**, *50*, 1279–1287.
[4] E. Yilgör, I. Yilgör, *Prog. Polym. Sci.* **2014**, *39*, 1165–1195.
[5] W. Roth, *J. Am. Chem. Soc.* **1947**, *69*, 474–475.
[6] E. L. Warrick, M. J. Hunter, A. J. Barr, *Ind. Eng. Chem.* **1952**, *44*, 2196–2202.
[7] F. Weinhold, R. West, *Organometallics* **2011**, *30*, 5815–5824.
[8] J. C. McDonald, D. C. Duffy, J. R. Anderson, D. T. Chiu, H. Wu, O. J. Schueller, G. M. Whitesides, *Electrophoresis* **2000**, *21*, 27–40.
[9] M. A. Unger, H. P. Chou, T. Thorsen, A. Scherer, S. R. Quake, *Science* **2000**, *288*, 113–116.
[10] J. Veres, S. D. Ogier, S. W. Leeming, D. C. Cupertino, S. M. Khaffaf, *Adv. Funct. Mater.* **2003**, *13*, 199–204.
[11] Y. Mi, Y. Chan, D. Trau, P. Huang, E. Chen, *Polymer* **2006**, *47*, 5124–5130.
[12] N. Q. Balaban, U. S. Schwarz, D. Riveline, P. Goichberg, G. Tzur, I. Sabanay, D. Mahalu, S. Safran, A. Bershadsky, L. Addadi, B. Geiger, *Nat. Cell Biol.* **2001**, *3*, 466–472.
[13] M. Galin, A. Mathis, *Macromolecules* **1981**, *14*, 677–683.
[14] J. Yang, G. Wegner, R. Koningsveld, *Colloid Polym. Sci.* **1992**, *270*, 1080–1084.
[15] L. M. Pitet, S. F. Wuister, E. Peeters, E. J. Kramer, C. J. Hawker, E. W. Meijer, *Macromolecules* **2013**, *46*, 8289–8295.
[16] M. D. Rodwogin, C. S. Spanjers, C. Leighton, M. A. Hillmyer, *ACS Nano* **2010**, *4*, 725–732.
[17] B. Van Genabeek, B. F. M. de Waal, M. M. J. Gosens, L. M. Pitet, A. R. A. Palmans, E. W. Meijer, *J. Am. Chem. Soc.* **2016**, *138*, 4210–4218.
[18] Y. Luo, D. Montarnal, S. Kim, W. Shi, K. P. Barteau, C. W. Pester, P. D. Hustad, M. D. Christianson, G. H. Fredrickson, E. J. Kramer, C. J. Hawker, *Macromolecules* **2015**, *48*, 3422–3430.
[19] Y. S. Jung, J. B. Chang, E. Verploegen, K. K. Berggren, C. A. Ross, *Nano Lett.* **2010**, *10*, 1000–1005.
[20] Y. S. Jung, C. A. Ross, *Nano Lett.* **2007**, *7*, 2046–2050.
[21] I. Bita, J. K. W. Yang, Y. S. Jung, C. A. Ross, E. L. Thomas, K. K. Berggren, *Science* **2008**, *321*, 939–943.

[22] J. W. Jeong, W. I. Park, M. J. Kim, C. a Ross, Y. S. Jung, *Nano Lett.* **2011**, *11*, 4095–4101.
[23] L. M. Pitet, A. H. M. van Loon, E. J. Kramer, C. J. Hawker, E. W. Meijer, *ACS Macro Lett.* **2013**, *2*, 1006–1010.
[24] R. P. Sijbesma, F. H. Beijer, L. Brunsveld, B. J. B. Folmer, J. H. K. K. Hirschberg, R. F. M. Lange, J. K. L. Lowe, E. W. Meijer, *Science* **1997**, *278*, 1601–1604.
[25] D. Tyagi, I. Yilgör, J. E. McGrath, G. L. Wilkes, *Polymer* **1984**, *25*, 1807–1816.
[26] N. E. Botterhuis, D. J. M. van Beek, G. M. L. van Gemert, A. W. Bosman, R. P. Sijbesma, *J. Polym. Sci. Part A Polym. Chem.* **2008**, *46*, 3877–3885.
[27] J. Zhao, R. Xu, G. Luo, J. Wu, H. Xia, *Polym. Chem.* **2016**, *7*, 7278–7286.
[28] C.-H. Li, C. Wang, C. Keplinger, J.-L. Zuo, L. Jin, Y. Sun, P. Zheng, Y. Cao, F. Lissel, C. Linder, X.-Z. You, Z. Bao, *Nat. Chem.* **2016**, *8*, 618–624.
[29] M. García-Iglesias, B. F. M. de Waal, I. de Feijter, A. R. A. Palmans, E. W. Meijer, *Chem. Eur. J.* **2015**, *21*, 377–385.
[30] R. H. Zha, B. F. M. De Waal, M. Lutz, A. J. P. Teunissen, E. W. Meijer, *J. Am. Chem. Soc.* **2016**, *138*, 5693–5698.
[31] P. J. M. Stals, M. A. J. Gillissen, T. F. E. Paffen, T. F. A. De Greef, P. Lindner, E. W. Meijer, A. R. A. Palmans, I. K. Voets, *Macromolecules* **2014**, *47*, 2947–2954.
[32] T. Terashima, T. Mes, T. F. A. De Greef, M. A. J. Gillissen, P. Besenius, A. R. A. Palmans, E. W. Meijer, *J. Am. Chem. Soc.* **2011**, *133*, 4742–4745.
[33] G. M. Ter Huurne, M. A. J. Gillissen, A. R. A. Palmans, I. K. Voets, E. W. Meijer, *Macromolecules* **2015**, *48*, 3949–3956.
[34] M. A. J. Gillissen, T. Terashima, E. W. Meijer, A. R. A. Palmans, I. K. Voets, *Macromolecules* **2013**, *46*, 4120–4125.
[35] M. Artar, T. Terashima, M. Sawamoto, E. W. Meijer, A. R. A. Palmans, *J. Polym. Sci. Part A Polym. Chem.* **2014**, *52*, 12–20.
[36] E. Huerta, B. van Genabeek, P. J. M. Stals, E. W. Meijer, A. R. A. Palmans, *Macromol. Rapid Commun.* **2014**, *35*, 1320–1325.
[37] O. Altintas, E. Lejeune, P. Gerstel, C. Barner-Kowollik, *Polym. Chem.* **2012**, *3*, 640–651.
[38] T. Mes, R. van der Weegen, A. R. A. Palmans, E. W. Meijer, *Angew. Chem. Int. Ed.* **2011**, *50*, 5085–5089.
[39] N. . Hosono, M. A. J. . Gillissen, Y. . Li, S. S. . Scheiko, A. R. A. . Palmans, E. W. Meijer, *J. Am. Chem. Soc.* **2013**, *135*, 501–510.
[40] O. Altintas, T. Rudolph, C. Barner-Kowollik, *J. Polym. Sci. Part A Polym. Chem.* **2011**, *49*, 2566–2576.
[41] E. J. Foster, E. B. Berda, E. W. Meijer, *J. Am. Chem. Soc.* **2009**, 6964–6966.
[42] P. J. M. Stals, M. A. J. Gillissen, R. Nicolaÿ, A. R. A. Palmans, E. W. Meijer, *Polym. Chem.* **2013**, *4*, 2584.
[43] O. Altintas, M. Artar, G. Ter Huurne, I. K. Voets, A. R. A. Palmans, C. Barner-Kowollik, E. W. Meijer, *Macromolecules* **2015**, *48*, 8921–8932.
[44] G. M. ter Huurne, L. N. J. de Windt, Y. Liu, E. W. Meijer, I. K. Voets, A. R. A. Palmans, *Macromolecules* **2017**, *50*, 8562–8569.
[45] Y. Ogura, M. Artar, A. R. A. Palmans, M. Sawamoto, E. W. Meijer, T. Terashima, *Macromolecules* **2017**, *50*, 3215–3223.
[46] M. M. J. Smulders, A. P. H. J. Schenning, E. W. Meijer, *J. Am. Chem. Soc.* **2008**, *130*, 606–611.
[47] O. Colombani, C. Barioz, L. Bouteiller, C. Chanéac, L. Fompérie, F. Lortie, H. Montès, *Macromolecules* **2005**, 1752–1759.
[48] P. J. M. Stals, M. M. J. Smulders, R. Martín-Rapún, A. R. A. Palmans, E. W. Meijer, *Chem. Eur. J.* **2009**, *15*, 2071–2080.
[49] M. A. Obrezkova, A. A. Kalinina, I. V. Pavlichenko, N. G. Vasilenko, M. V. Mironova, A. V. Semakov, V. G. Kulichikhin, M. I. Buzin, A. M. Muzafarov, *Silicon* **2014**, *7*, 177–189.
[50] L. Brunsveld, A. P. H. J. Schenning, M. A. C. Broeren, H. M. Janssen, J. A. J. M. Vekemans, E. W.

Meijer, *Chem. Lett.* **2000**, 292–293.
[51] Y. Nakano, T. Hirose, P. J. M. Stals, E. W. Meijer, A. R. A. Palmans, *Chem. Sci.* **2012**, *3*, 148–155.
[52] N. Hosono, A. R. A. Palmans, E. W. Meijer, *Chem. Commun.* **2014**, *50*, 7990–7993.

# Chapter 6

# *Towards sequence-defined oligomers holding supramolecular BTA-based motifs: iterative versus solid-phase synthesis*

**Abstract**:

In this chapter, we attempt to arrive at perfect-discrete and sequence-defined oligomers with the aim to study their intramolecular folding. Although it is a great challenge, a first approach is presented. Two strategies are discussed with the aim to obtain sequence-defined oligomers holding a benzene-1,3,5-tricarboxamide-based supramolecular motif: solution iterative exponential growth and step-wise growth using a solid-phase strategy. In the first strategy, discrete oligomers up to the octamer in the backbone are prepared. These oligomers comprise either alkene or alkyne pendants. Full functionalization of the octamer was achieved with use of Cu(I)-catalyzed alkyne-azide and thiol-ene "click" chemistry. The downside of the route was the decreasing solubility of the growing oligomers, which effectively hampered the backbone extension towards the hexadecamer. In the second strategy, solid phase synthesis protocol comprising thiolactone chemistry was applied. Supramolecular recognition motifs were attached via conjugated thiol-ene addition to the thiol formed *in situ*. Both oligomers showed propensity to form hydrogen bonds in bulk, however, due to structural complexity, competition between different conformations staying in dynamic equilibrium was observed. CD spectroscopy in dilute solutions confirmed the presence of helical aggregates of BTA. The mechanism of aggregation was found to be highly dependent on the backbone nature and substitution pattern. The limited solubility of the octamers constitute a major limit of the approach thus the sequence control and folding of complex macromolecular structures remain a big challenge.

This work has been performed in close collaboration with Ir. Ian Segers, Dr. Yiliu Liu (section 6.2), Dr. Steven Martens and Prof. Dr. Filip Du Prez from University of Gent (section 6.3)

## 6.1 Introduction

Technological applications of synthetic macromolecules have driven the field of polymer chemistry to a point in which seemingly every material can be synthesized.[1] Nowadays great variety in available polymerization methods combines a plethora of topologies with an immense choice of monomers, permitting unprecedented control over the functionalization density and molecular mass distribution of macromolecules.[2–4] Yet, Nature is able to build hundreds of different types of functional proteins from only 20 different monomers.[5] The secret of such diverse functionality of biomacromolecules lies in the precise control of the position of each monomer in the polymeric chain – sequence control.[6] Therefore in recent years, polymer chemists have been particularly interested in the development of methodologies that allow controlling both the sequence as well as the molar mass.[7,8] Currently, two independent methodologies are applied. The first method: solid phase synthesis (SPS) - pioneered by Merrifield[9,10] for peptide synthesis - enables the one by one build-up of monomers in a sequence-defined way to the growing chain by using iterative chemical steps. This method enables the fast synthesis and isolation of oligomers via automated process and thereby revolutionized the peptide and oligonucleotide chemistry. Later the concept of SPS evolved towards synthetic oligomers including nucleotides,[11] peptoids,[12,13] phosphodiesters,[14] and thiolactone[15,16] chemistry. However, most of the fixed solid-phase synthetic protocols approach their limits in terms of possibilities to incorporate more complex structures into the sequence-defined backbone chain. This makes it extremely challenging, for example, to maintain side groups in the monomers orthogonally active for post-functionalization. Eventually, ultimate control of the reaction kinetics[17] as well as near to quantitative yields[18] are required during the SPS to make the protocol applicable. In addition, typically a large excess of reactants is needed, making SPS mostly suitable for chemistries that rely on the use of cheap chemical building blocks.

A second approach is based on solution iterative (exponential or direct) growth strategies and has become equally attractive in recent years. While the direct growth strategy enables to attach a monomer or a short chain depending on the building blocks[19–21], in the iterative exponential strategy each coupling extends the growing chain by a factor of 2.[22] The iterative exponential growth strategy, also known as the orthogonal iterative divergent/convergent approach, makes use of bifunctional monomers with orthogonally protected end-groups. The end-groups can be separately deprotected (the divergent part) and eventually coupled with each other (the convergent part) giving an orthogonally protected dimer. The same steps can be repeated with the obtained dimer, resulting in an exponential growth of the chain. However, the required orthogonality of the protection end-groups reduces the diversity of applicable monomers. Consequently, oligomers built through this strategy contain either a stiff backbone[22] or polar groups as linkages between monomers (i.e. triazoles,[23] ester,[24,25] or amides[26,27]) which due to secondary interactions reduce the solubility as the molecular mass increases.[25] This is considered as a major drawback of this

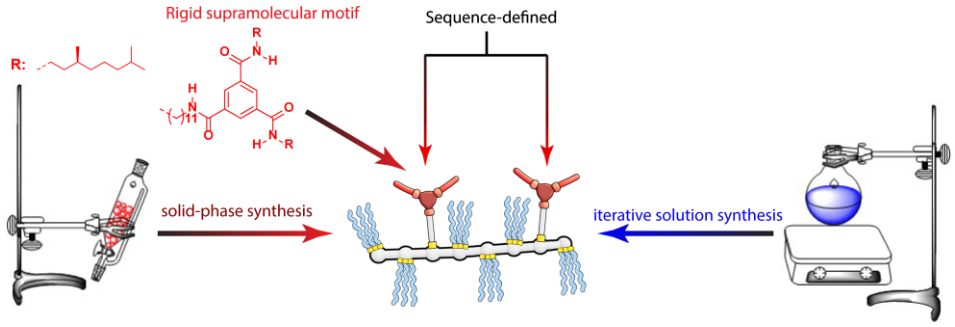


***Figure 6.1*** *Solid-phase synthesis and iterative solution synthesis for sequence-defined oligomers holding supramolecular recignition motif.*

method as it hampers not only the purification of the products but also the reactivity of the end-groups at later stages of the synthesis.

While both methods (SPS and iterative) offer attractive ways to synthesize well-defined oligomers, none were so far exploited to synthesize sequence-controlled oligomers decorated with functional arms that can contribute to the formation of secondary and tertiary structures via supramolecular interactions. In this work, we present the synthesis of two oligomers that hold a supramolecular motif – benzene-1,3,5-tricarboxamide (BTA) - via iterative exponential growth and solid-phase synthesis (Figure 6.1). The iterative synthesis approach was performed in collaboration with Dr. Y. Liu and Ir. I. Segers. We selected an L-γ-glutamamide backbone as a scaffold holding propargylamide and trisallyloxyamide units that were further orthogonally functionalized via radical thiol-ene and copper (I) catalyzed 2+3 dipolar cycloaddition with decyl and BTA pendants, respectively. This approach resulted in octamers that differed in the sequence of the BTA substitution. Additionally, in collaboration with the group of Prof. Filip Du Prez (University of Gent) we applied a protocol based on SPS-thiolactone chemistry to synthesize a heptamer directly functionalized with the BTA. The structures of all oligomers was analyzed by nuclear magnetic resonance (NMR) and mass (MS) spectroscopy. Whereas the SPS-protocol suffers from side-reactions as the number of functional groups increases, the iterative exponential growth synthesis becomes more challenging due to low solubility of the longer oligomers. This work shows that despite the need for further optimization, both methods could potentially serve as a strategy for the synthesis of functionalized sequence-defined oligomers comprising side chain supramolecular motifs.

## 6.2 Iterative synthesis towards sequence-defined L-γ-glutamamide based oligomers functionalized with chiral (*S*)-BTA and decyl groups

### 6.2.1 Monomer design

The design of the iterative synthesis strategy of the sequence-defined octamer comprises an exponential growth of the oligomer chain. To ensure efficient chain elongation, the free end-groups have to be reactive towards each other, but protected end-groups have to be protected orthogonally i.e. deprotection of one group does not affect the other. These conditions are fulfilled by a pair of carboxylic acid – amine functional groups. The free functional groups can be coupled with use of a variety of activating agents to create amide bond. The orthogonality of the deprotection is provided by the proper choice of the protecting groups. Carboxylic acid can be protected with *tert*-butoxycarbonyl (*t*BuO) which is acid-labile, but base-stable, while amines can be protected with fluorenylmethyloxycarbonyl (Fmoc) which is base labile, but acid-stable. In order to synthesize the oligomer in a sequence-specific way, multiple functional side groups have to present on the oligomer chain. These side groups have to be inert during the deprotection and coupling steps as well as orthogonal with each other (so one type of functionalization is achieved at a single step). In addition, the side groups have to be easily modified in high yields at the final steps of the synthesis (post-functionalization strategy). We select terminal alkyne and alkene groups, which enable post-functionalization via copper(I) catalyzed alkyne-azide Huisgen 1,3-dipolar cycloaddition[28] and thiol-ene "click" chemistry, respectively. Because the alkyne group is also susceptible towards radical thiol-ene click chemistry, the Huisgen 1,3-dipolar cycloaddition has to be performed first to keep the post-functionalization orthogonal. The above summarized high number of requirements significantly limits the available monomeric pool. The amino acid, L-glutamic acid, comprising two acid functions and one amine function, could serve as a monomer. L-Glutamic acid is commercially available with the amine group protected with Fmoc and the γ-carboxylic acid protected with *t*BuO. Therefore successful orthogonal post-functionalization of the final

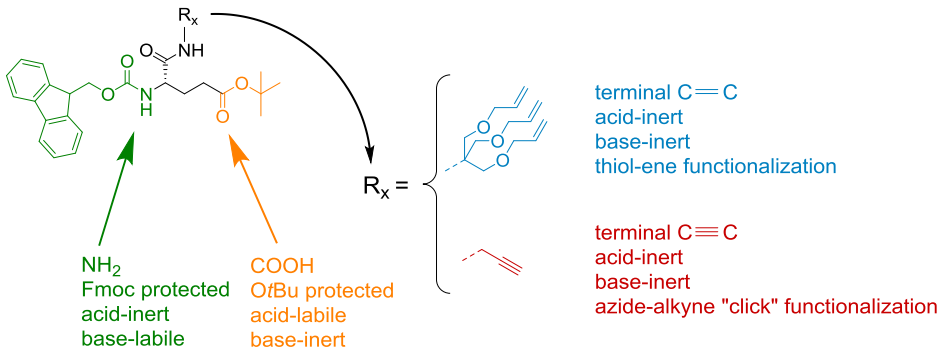


***Scheme 6.1*** *Monomer design for the synthesis of L-γ-glutamamide-based octamer.*

oligomer backbone, can be achieved via α-carboxylic acid group, which is modified with amide groups holding terminal alkene or alkyne (Scheme 6.1).

### 6.2.2 Synthesis of L-γ-glutamamide based octamers

The strategy towards sequence-defined oligomers based on L-γ-glutamamide backbone begins with the commercially available protected L-glutamic acid as explained above. The free α-COOH position can be readily functionalized via amide coupling with a terminal alkene or

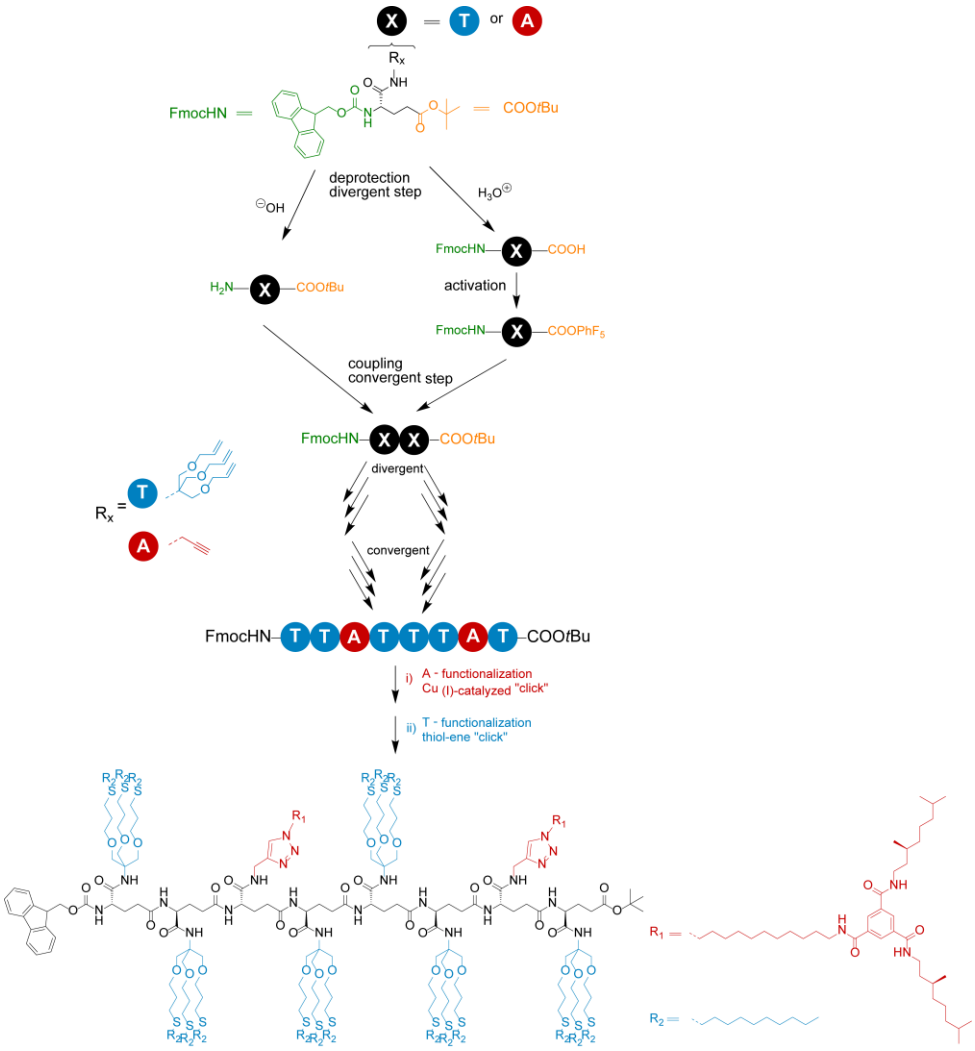


***Scheme 6.2*** *Overview of the synthesis of the BTA-functionalized L-γ-glutamamide-based octamer.*

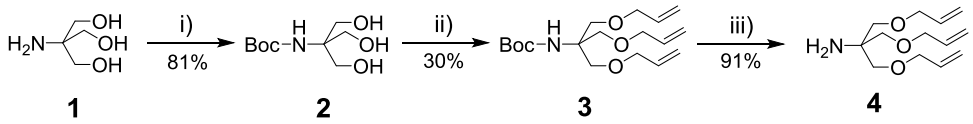


***Scheme 6.3**: Synthetic route to tris[(allyloxy)methyl]aminomethane (**4**). Reaction conditions: i) (t-BuOCO)$_2$O, MeOH/t-BuOH, r.t., O/N. ii) Allyl bromide, KOH, DMF, r.t., 3 h. iii) TFA, DCM, r.t.,*

alkyne-holding amines, which will serve as post-functionalization platforms at the last step of the synthesis. These monomers can be orthogonally deprotected in the divergent step to yield either a free acid or a free amine. The free acid derivative is subsequently activated to a pentafluorophenyl ester and coupled to the free-amine monomer (convergent step) to yield a dimer, which can be extended in the same fashion. Eventually an oligomer holding two types of reactive groups can be orthogonally functionalized with "click" chemistry (Cu(I)-catalyzed 2+3 cycloaddition followed by radical thiol-ene addition) (Scheme 6.2). Construction of L-γ-glutamamide oligomers, containing a single allyl ester side groups per monomer, was investigated by Dr. Y. Liu prior to this work. An increasing drop in solubility was experienced during synthesis of the tetramer and octamer, making purification and further elongation difficult. These solubility problems, potentially caused by intermolecular hydrogen bonds between the backbones, resulted in the use of a branched side group functionalized with 3 allyl groups. The pendant arm containing 1,2,3-tris(allyloxy) group (**4**) was synthesized in 3 steps from 2-amino-2-(hydroxymethyl)-1,3-propanediol (**1**) (Scheme 6.3). Protection with *tert*-butyloxycarbonyl protecting group (*t*-Boc), of the amine yielded **2**, which was further subjected to deprotonation of hydroxyl groups with KOH and subsequent substitution with allyl bromide to couple the allyl groups. Finally, the free amine was released with use of trifluoroacetic acid (TFA) and after removal of residual TFA and the solvent *in vacuo*, tris[(allyloxy)methyl]aminomethane (**4**) was obtained with a combined yield of 22%.

In the following step, *N*-protected and $\alpha_{COOH}$-protected *γ*-glutamic acid was modified with either the commercially available propargylamine or synthesized amine **4** to yield monomers **5** and **6**, respectively (Scheme 6.4). The activation of the *α*-positioned carboxylic acid in Fmoc-Glu(O*t*Bu)-OH was facilitated by *N*-(3-dimethylaminopropyl)-*N'*-ethylcarbodiimide hydrochloride (EDC·HCl) and 1-hydroxybenzotriazole hydrate (HOBt·x$H_2O$). The activated acid readily reacted with either propargylamine or **4** giving propargylamide (**5**) or trisallyloxy-*tert*-butylamide (**6**) as a side groups on the protected *γ*-glutamic acid. Partial undesired deprotection of Fmoc-protecting group, by *N*,*N*-diisopropylethylamine (DIPEA) was observed, leading to a decrease in the yield. Monomers **5** and **6** were purified via column chromatography in yields of 53% and 67%, respectively. Throughout this chapter the

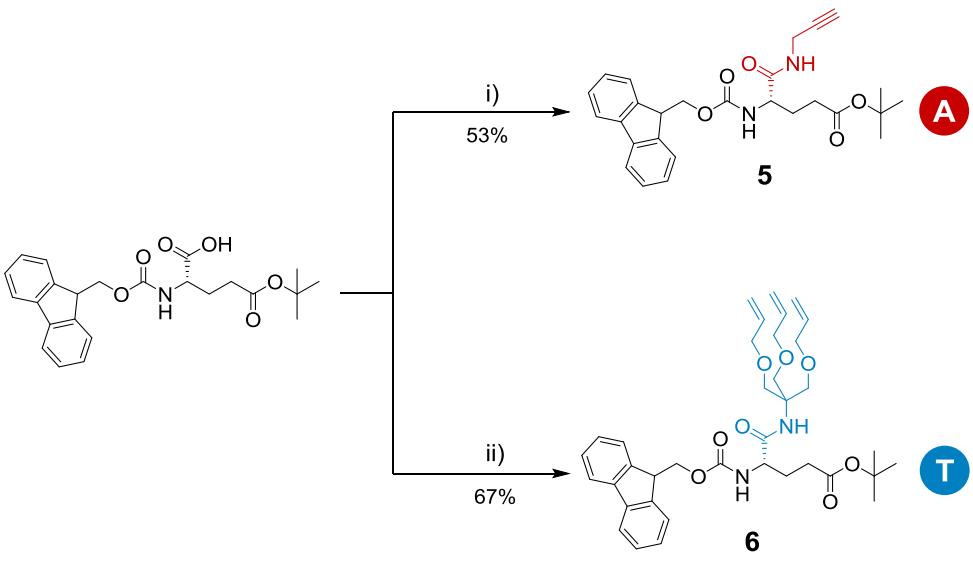


***Scheme 6.4**: Synthesis of monomers 5 and 6. Reaction conditions: i) propargylamine, EDC·HCl/HOBT·xH₂O, DIPEA, THF, r.t., O/N; ii) compound **8**, EDC·HCl/HOBT·xH₂O, DIPEA, THF, r.t., O/N.*

monomer or residue with the alkyne containing side group will be defined as an *A*, while the monomer or residue with the trisallyloxy-*tert*-butylamide side group will be defined as a *T*.

Subsequently, we synthesized octamers with varying sequence via the divergent / convergent strategy. First, the monomers **5** and **6** were selectively deprotected by removing either the Fmoc-protecting group or the *t*-butyl-protecting group (divergent part). Monomers **5** and **6** were treated with TFA to remove the *t*-butyloxy-protecting group, giving free carboxylic acids (**7a** and **9a**). Next, the addition of pentafluorophenyl trifluoroacetate to these two intermediates in the presence of DIPEA activated the acids to pentafluorophenyl esters **7b** and **9b**. In parallel to this, monomer **6** was treated with diethylamine to remove the Fmoc-protecting group and obtain monomer **8** with a terminal free amine. The isolation of free amine monomer **8** (81%) was accomplished using column chromatography. Intermediate compounds **7b** and **8**, and compounds **8** and **9b** reacted readily with each other in DMF giving dimers FmocHN-*AT*-COO*t*Bu (**10**) and a FmocHN-*TT*-COO*t*Bu (**11**) (convergent part) (Scheme 6.5). Dimer **10** (80%) and dimer **11** (74%) were isolated by column chromatography and the structures were confirmed by $^{1}$H NMR, $^{13}$C NMR, and MALDI-TOF. Subsequently, tetramer **14** was synthesized in the similar fashion from dimers **10** and **11**. During the divergent part, the dimers **10** and **11** were deprotected and activated to yield **12** and **13b**. Subsequent coupling in DMF afforded tetramer **14** (convergent part) with a yield of 60% after column chromatography.

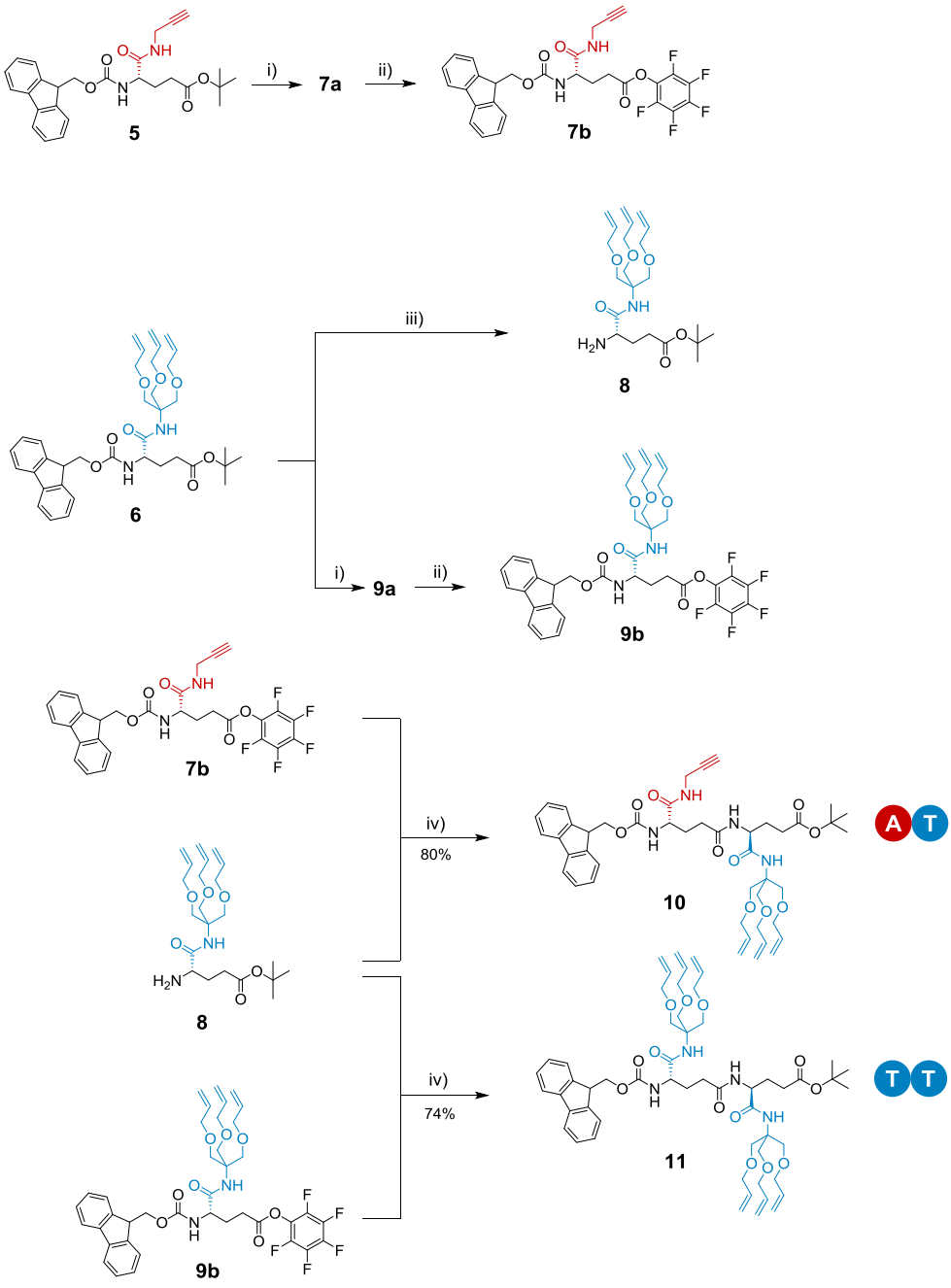


***Scheme 6.5**: Synthesis of dimers **10** and **11**. Reaction conditions: i) TFA, DCM, r.t., 3 h; ii) Pentafluorophenyl trifluoroacetate, DIPEA, $CHCl_3$, r.t., 1-3 h; iii) Diethylamine, DCM, r.t., 3 h, 81%; iv) DMF, r.t.*

Further, deprotected tetramers **15** and **16a** were obtained in a divergent part upon treatment of the tetramer **14** with either piperidine or TFA. Free acid **16a** was activated with pentafluorophenyl trifluoroacetate to yield **16b** which was subsequently coupled with **15** to yield octamer **17** (Scheme 6.6). The low yield of the final coupling (39%) was caused by the decreasing solubility of the tetramers. Octamer **17** was isolated by column chromatography and the structure was confirmed by $^{1}H$ NMR, $^{13}C$ NMR, and MALDI-TOF (Figure 6.2).

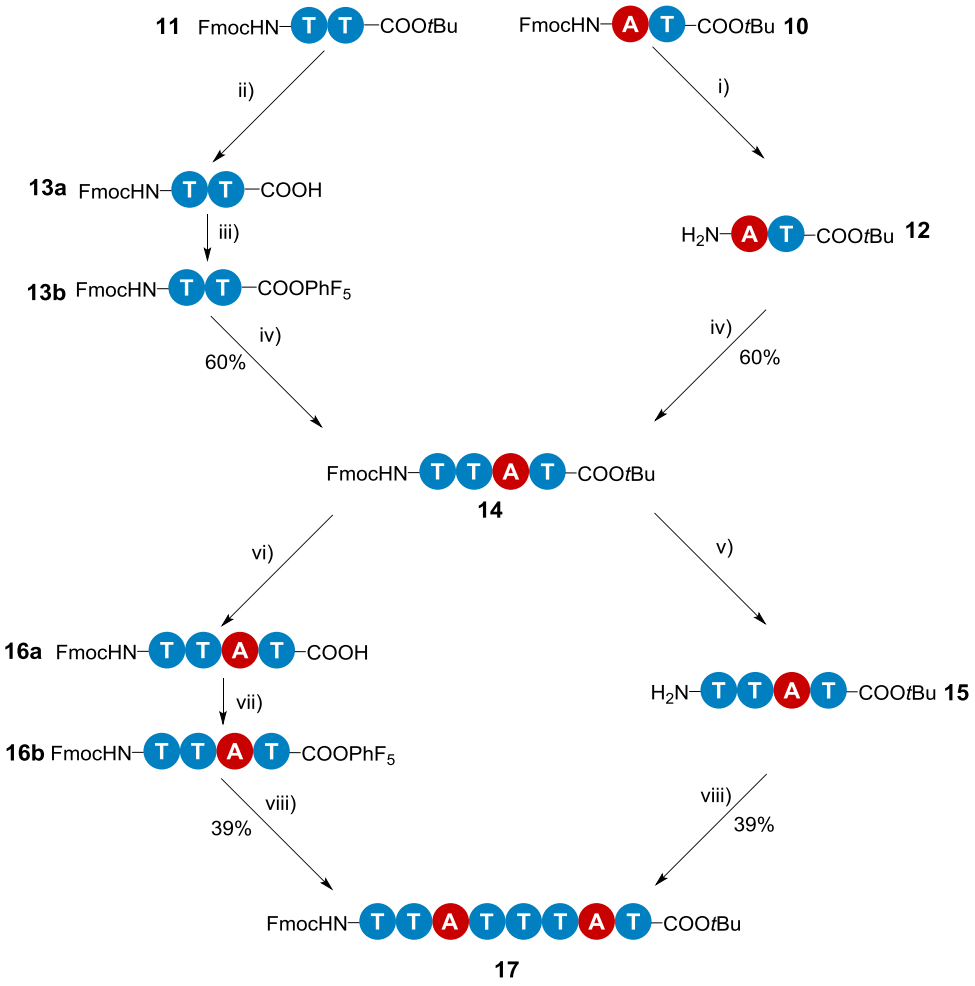


***Scheme 6.6:*** *Schematic representation for the synthesis of tetramer **14** and octamer **17**. Reaction conditions: i) Diethylamine, DCM, r.t., 3 h; ii) TFA, DCM, r.t., O/N; iii) Pentafluorophenyl trifluoroacetate, DIPEA, $CHCl_3$ r.t., 1 h; iv) DMF, r.t., 1 h; v) Piperidine, $CHCl_3$, r.t., 1 h; vi) TFA, $CHCl_3$, r.t., O/N; vii) Pentafluorophenyl trifluoroacetate, DIPEA, $CHCl_3$, r.t., 2 h; viii) DMF, r.t., 1 h.*

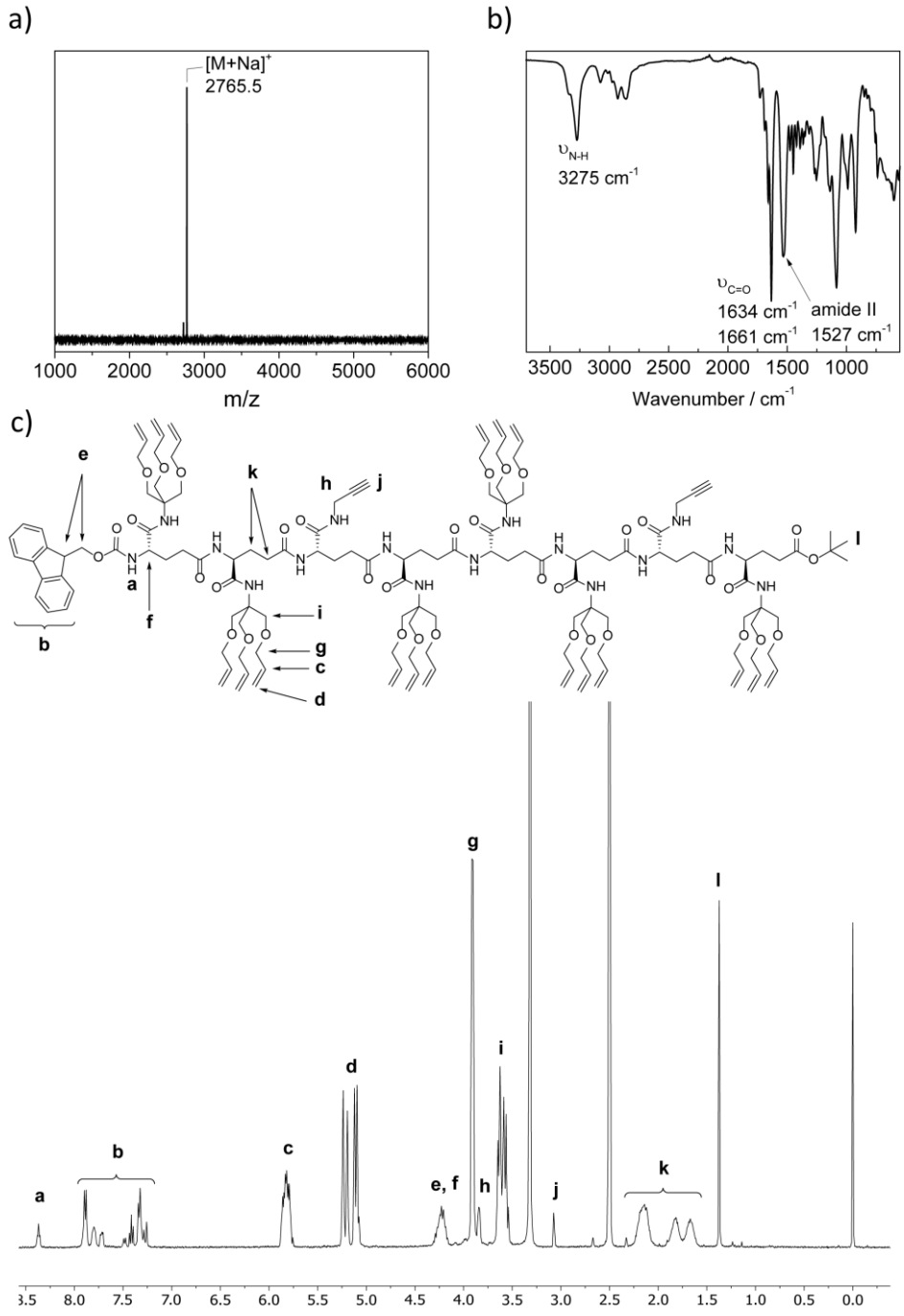


***Figure 6.2**: a) MALDI-TOF and b) IR spectra of octamer **17**; c) $^{1}H$ NMR spectrum (400 MHz, DMSO-$d_6$) of octamer **17** (Fmoc-TTATTTAT-tBu).*

Parallel to the synthesis of octamer **17**, two other octamers having different sequences (**18** and **19**) were prepared using the same synthetic procedures (Scheme 6.7). During the synthesis of all three octamers, we experienced a significant drop in the yield during the last amide coupling reaction. The conversion started to decrease during activation of the carboxylic acid group on the tetramers to the pentafluorophenylester. Increasing the chain length resulted in a decreased solubility as a result of the larger number of amide groups that enhance the propensity to form hydrogen bonds. The fact that the carboxylic acid group can also participate in the intermolecular hydrogen bonds potentially decreases its nucleophilic character and suppresses the activation to the pentafluorophenyl ester. Also, the solubility of the terminal free amine tetramers in chlorinated solvents and in DMF decreased. This, in combination with the use of not fully purified intermediates, resulted in incomplete conversion and the appearance of byproducts (for example FmocHN-*TTAT*-CO-*N*-piperidine) during the amide coupling reactions. Besides the appearance of side products, mass analysis showed the presence of unreacted substrates in the crude mixture of the amide couplings. An extensive column chromatography purification was required to purify the octamers. Due to the presence of residual amounts of base in the terminal free amine tetramer intermediate (**15**), we found by MALDI-TOF measurements that the terminal amine group was partially deprotected in octamer **18** while octamers **17** and **19** were isolated in a fully protected form.

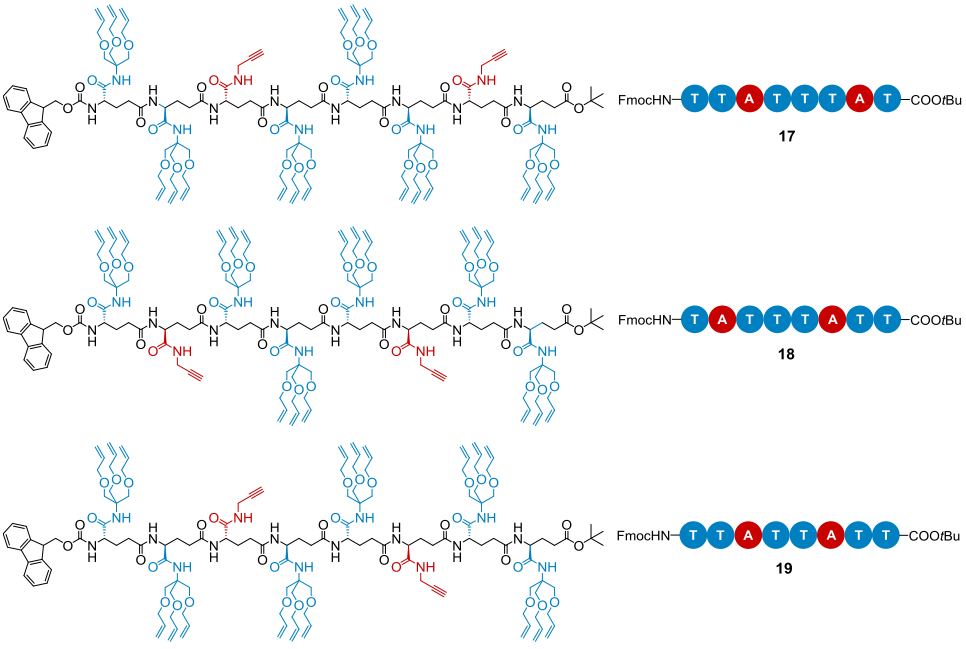


***Scheme 6.7**: Structural formulas and schematic representations of octamers **17**, **18** and **19**.*

All three octamers were obtained in moderate yields (39% and 37% for **17** and **19**, respectively), but in sufficient quantities for further synthesis. All three octamers are sparingly soluble in chlorinated solvents, such as $CHCl_3$, and the addition of polar solvents was needed for full solubility. This suggests that the extension of the backbone, and thereby the increased number of hydrogen donor and acceptor groups within the backbone, results in stronger hydrogen bonds and will reduce the solubility further upon increasing the chain length.

### 6.2.3 An attempt to synthesize sequence-defined L-γ-glutamamide hexadecamer.

To assess, where are the limits of the synthesis of the oligomer based on L-γ-glutamamide, we applied the same strategy as previously, to deprotect orthogonally the octamer **17**. The low solubility of the octamer made the deprotection difficult especially due to the hampered analysis of the reaction progress. Therefore we were not able to assess the conversion and yield of deprotected amine and acid as well as activated acid. After stirring the activated acid and the amine, we did not observe significant amounts of hexadecamer. As an alternative, we tried the elongation strategy, which comprised a TBTU-coupling, described in Chapter 2 of this thesis. This method yielded a visible amount of hexadecamer, but we could not find any reliable method to isolate it from unreacted octamers. Thus the elongation of the oligomer towards hexadecamer remains challenging. Accordingly, we focused on the post-functionalization of the octamers.

### 6.2.4 Post-functionalization of the L-γ-glutamamide octamers via "click" chemistry: copper(I)-catalyzed 2+3 dipolar cycloadditon and radical thiol-ene addition.

The preparation of the pendant bis((*S*)-3,7-dimethyloctyl)-(11-azidoundecyl)-BTA ((*S*)-BTA-azide, **23**), containing an azide group for post-functionalization, was performed by a 3 steps synthesis starting from previously synthesized (*S*)-BTA-olefin (**20**) (Scheme 6.8). The azide functionality was attached via sequence of the 3 following reactions: hydroboration of

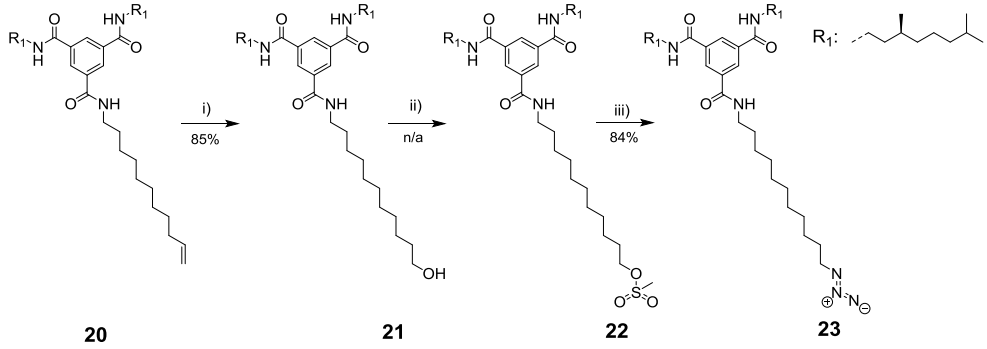


***Scheme 6.8**: Synthesis of BTA-azide **23**; reagents and conditions: i) 9-BBN, THF, argon, r.t. 2h, then aq NaOH (6 M), $H_2O_2$ (30% wt); ii) methanesulfonyl chloride, pyridine, DCM, r.t., 12h; iii) $NaN_3$, KI, DMF, 70 °C, 12h.*

the terminal alkene followed by conversion of the resulting alcohol (**21**) into corresponding mesylate (**22**) and further substitution into the azide (**23**) via $S_N2$ reaction with a combined yield of 68% after column chromatography.

To rationalize the strategy and optimize the conditions for the post-functionalization of the synthesized glutamic acid-based octamers with the BTA and alkyl pendant arms, we first carried out corresponding test reactions for the monomer **5** and Boc-protected trisallyloxy amine **3** (Scheme 6.9). The coupling of the protected propargyl amide-functionalized monomer **5** with (*S*)-BTA-azide (**23**) via Cu(I)- catalyzed 2+3 dipolar cycloaddition afforded desired functionalized monomer with 34% yield. Similarly, the tris(allyloxy)amide-functionalized monomer **6** and 3-fold excess of1-decanethiol was used in a radical thiol-ene test reaction. The functionalized monomer was isolated with a yield of 51%.

The success of the test reactions prompted us to apply the protocols for functionalization of octamer **17**. In this case the reaction sequence was important, because the free alkyne was also potentially susceptible for the free radical attack. Therefore the post-functionalization with the BTA via copper (I) catalyzed dipolar cycloaddition had to be performed first. We coupled the octamer FmocHN-$(TTAT)_2$-COO*t*Bu (**17**) with the (*S*)-BTA-azide (**23**) according to a slightly modified protocol due to low solubility of octamer **17**. After 2 days of heating the reaction mixture at 50 °C in DMSO, no azide absorption band was observed on the IR spectrum. However, MALDI-TOF showed the presence of mono- and disubstituted octamer. Calculated conversion of the terminal alkyne by the integral analysis of

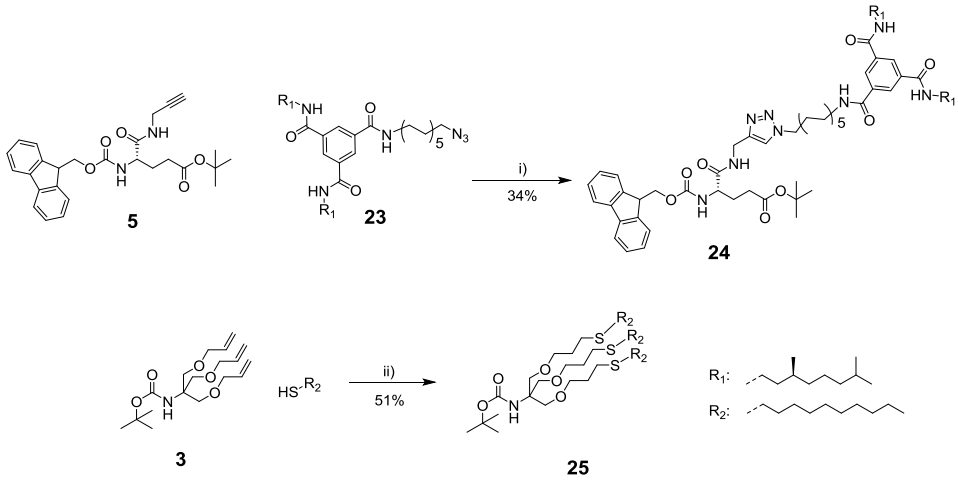


***Scheme 6.9**: Functionalization of the **6** via Cu (I) catalyzed 2+3 dipolar cycloaddition and **3** via radical thiol-ene additio; reagents and conditions: i) (1) $CuSO_4$, sodium ascorbate, DMSO, 50 °C ⟶ r.t., argon atmosphere, 2 days; ii) DMPA, THF, hv, argon, r.t., 4 h.*

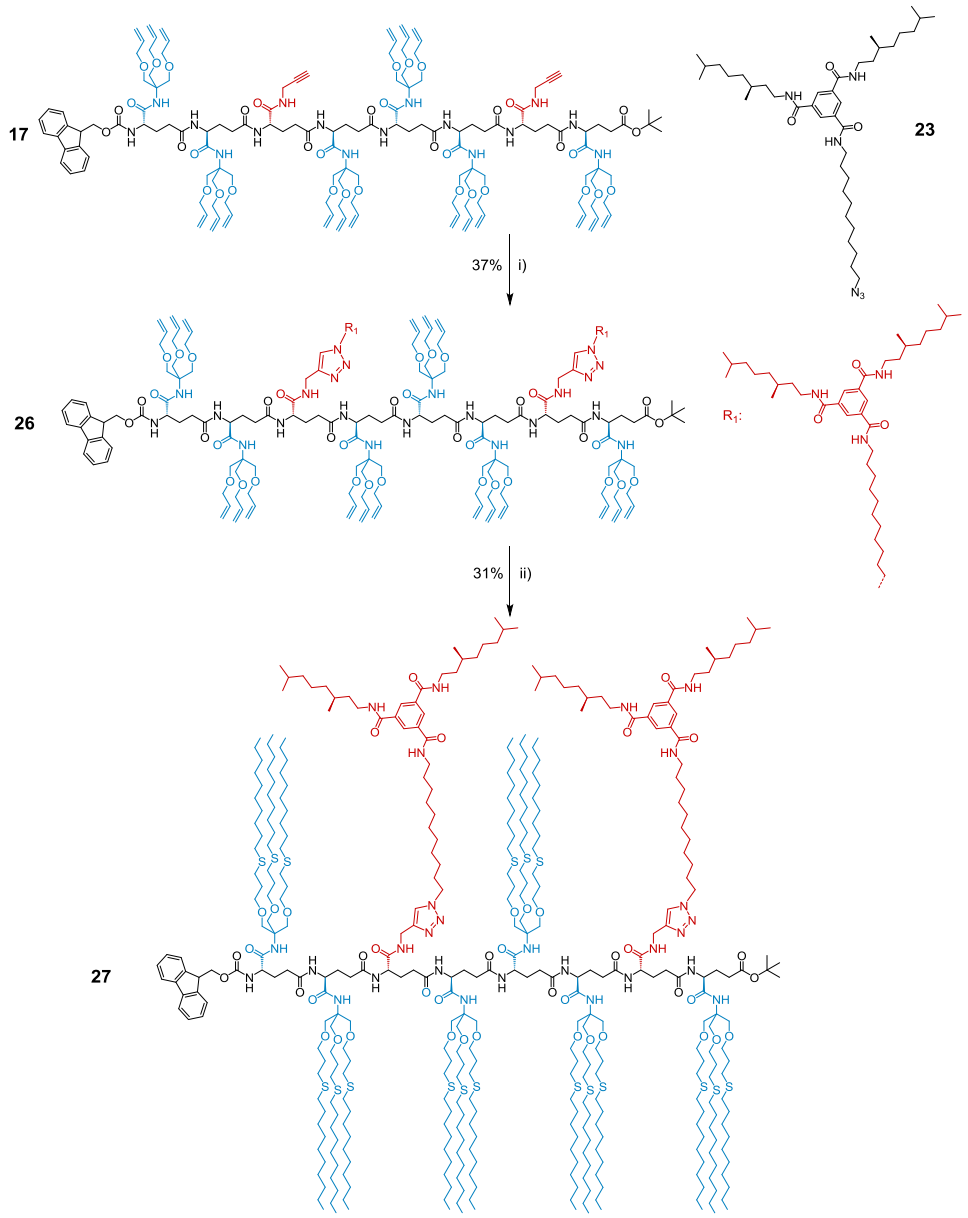


***Scheme 6.10:*** *Synthesis of bis((S)-BTA)-hexa(tris(decylallyloxy))Fmoc-(TTAT$_2$)-tBu (**27**). Reagents and conditions: i) CuSO$_4$, sodium ascorbate, DMSO, 50 °C ⟶ r.t., argon atmosphere, O/N. (2) CuSO$_4$, sodium ascorbate, DMSO, 50 °C ⟶ r.t., argon flow, 2 days; ii) 1-Decanethiol, DMPA, DMA, hν, argon, r.t., 4 h.*

the $^{1}$H NMR spectrum indicated the presence of 25% unreacted terminal alkynes. Addition of another equivalent of **23** afforded full functionalization (Scheme 6.10). The (*S*)-BTA-functionalized octamer (**26**) was isolated via column chromatography with a 37% yield with respect to the starting octamer (**17**). Subsequently, **26** was functionalized with the alkyl chains via radical thiol-ene reaction with use of 2,2-dimethoxy-2-phenylacetophenone as a photoinitiator following similar procedure as for the radical thiol-ene reaction performed on **6**.

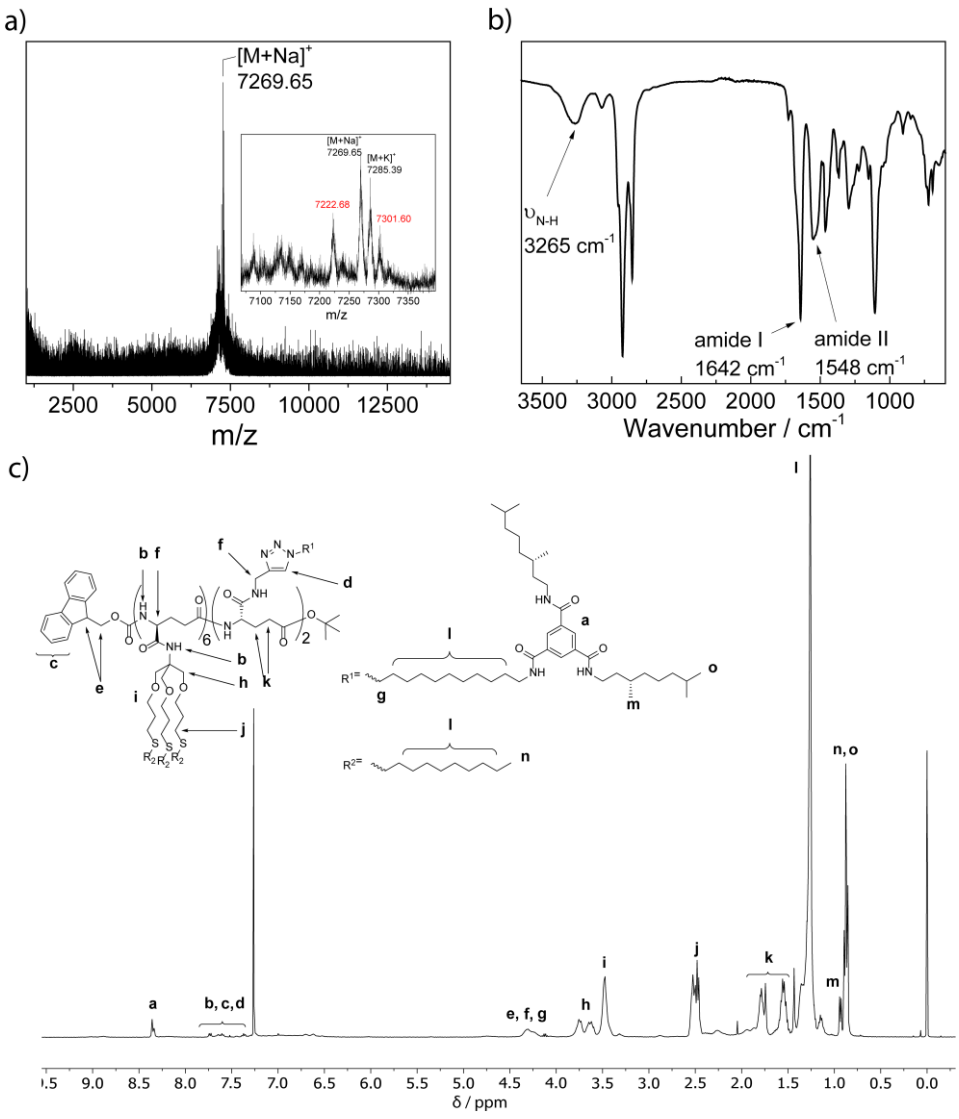


***Figure 6.3*** *a) MALDI-TOF and b) FT-IR spectrum of* ***27*** *in bulk c)* $^{1}$*H NMR spectrum of* ***27*** *(400 MHz,* $CDCl_3$*).*

Fully functionalized octamer **27** was isolated with use of column chromatography and characterized by $^{1}$H NMR, FT-IR and MALDI. All peaks present on the $^{1}$H NMR spectrum could be assigned to the structure. However, a closer look into the MALDI spectrum (Figure 6.3a), besides molecular ions M+Na and M+K reveals presence of the two additional signals atm/z = 7222.68 Da and 7301.60 Da. Since these signals are followed by additional tiny peaks at m/z + 16, probably both can be assigned to [M*+Na]+ of an unknown molecule. Lack of the additional absorption bands on the IR spectrum (Figure 6.3b) and additional signals in the $^{1}$H NMR spectrum (Figure 6.3c) suggests that either the amount of impurity is very small or its structure is very similar to that of octamer **27**. The designed orthogonal post-functionalization strategy was proven to be efficient for the coupling of the BTA and alkyl side groups in a selective fashion. However, the low yield of Cu (I)-catalyzed 2+3-dipolar cycloaddition suggests that low solubility of the octamer hampers normally excellent in yields "click" chemistry. Moreover, the radical character of the final, thiol-ene addition may lead to the formation of byproducts, which are difficult to remove. Therefore, the methodology, albeit efficient, requires further optimization.

## 6.3 Solid-phase synthesis of BTA-comprising oligourethane-amides

Parallel to the iterative approach, we designed another strategy that incorporates the solid-phase synthesis, which potentially should suffer less from low solubility of the substrates at the later stages of the synthesis. We were interested, to what extent other problems typical for SPS approach can hamper the synthesis of such complex molecules and how it can be related to the iterative approach. In other words, for practical reasons we decided to check, which methodology can be of more interest in case of applications in supramolecular chemistry. To realize the synthesis, we collaborated with the group of Prof. Filip Du Prez at the University of Gent. According to this design, the synthesis of sequence-defined oligomers is based on the 2-step iterative SPS protocol reported by group of Du Prez in 2016.[16] The strategy utilizes the thiolactone ring opening via nucleophilic attack of a primary amine followed by thiol-ene conjugate addition (Scheme 6.11, **STEP 1**, acrylate holds the desired functionality). The use of ethanolamine makes the process repeatable as the resulting terminal alcohol is reactive towards isocyanate thiolactone thereby forming a new urethane thiolactone (**STEP 2**). The new thiolactone constitutes a reactive center for another ring-opening and functionalization. After each step, part of the growing oligomer can be cleaved off the resin and analyzed using LC-MS. For this purpose 2 mg of resin is subjected to the cleavage by 1% TFA in DCM and subsequently after sample preparation submitted to the LC-MS analysis.

The synthesis was carried out with help of Dr. Steven Martens and started from the racemic thiolactone attached to the 2-chlorotrityl chloride resin which was suspended in chloroform in a glass column equipped with a teflon tap. In this setup, mixing of the components is ensured by mechanical agitation because mechanical stirring would damage the solid support. During the first step, thiolactone ring is opened via nucleophilic attack of

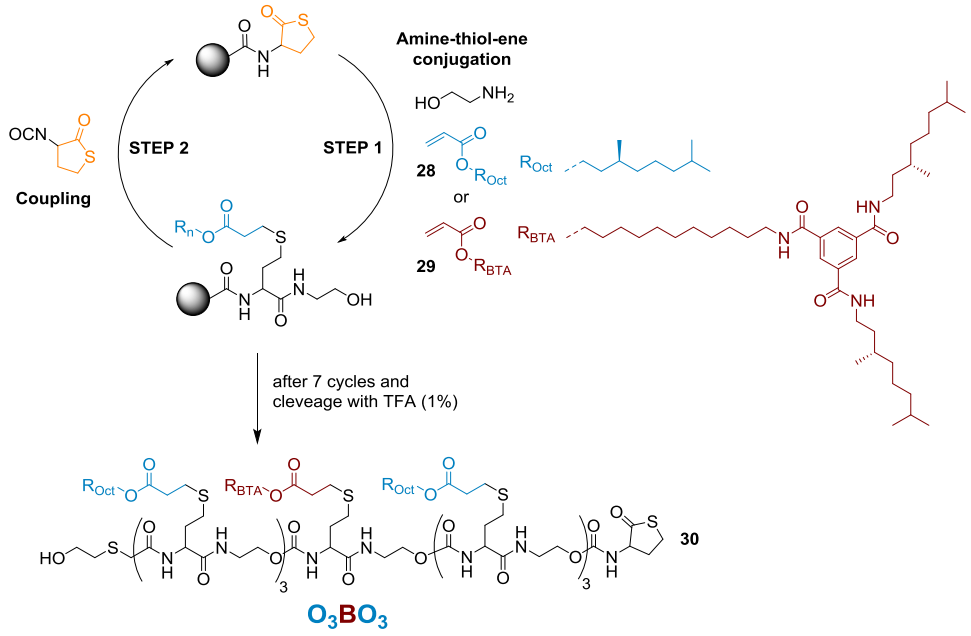


***Scheme 6.11:*** *Schematic representation of the solid-phase synthesis of sequence-defined oligourethane-amide.*

the ethanolamine which forms free thiol *in situ*. The thiol readily reacts with the acrylate that holds the functionality (here (*S*)-3,7-dimethyloctyl acrylate (**28**), or (*S*)-BTA-acrylate (**29**)). To avoid possible side reactions (aza-Michael addition and oxidation of the thiol)[17], two equivalents of the acrylate are added first as it is inert towards the thiolactone itself. Following addition of the 1 equivalent of the ethanolamine initiates the reaction. To ensure full conversion of the thiolactone, step 1 is applied twice. The thiolactone-functionalized resin with the (*S*)-3,7-dimethyloctylacrylate (**28**) and ethanolamine in chloroform is shaken for 15 minutes. Then the residual liquid is removed by filtration. Another portion of **28** and ethanolamine in chloroform are added and resulting suspension is shaken again for 15 minutes followed by removal of the liquid. The solid support is subsequently washed with DMF, methanol, chloroform and diethyl ether. Then, racemic α-isocyanato-γ-thiolactone and a catalytic amount of dibutyltin dilaurate in chloroform are added to the resin and the mixture is shaken for 1 hour. After removal of the residual liquid and washing the beads, cycle 1 is finished and yields the (*S*)-3,7-dimethyloctyloxycarbonyl-functionalized monomer-thiolactone (residue *O*). Following cycles are performed in the same manner thereby extending the oligomeric chain by one repeating unit each cycle. The only exception from this protocol was applied at the stage of attaching BTA-acrylate (**29**) to the growing oligomer (residue *B*). Due to possible aggregation of the BTAs at high concentrations in chloroform, we used here THF as a solvent instead. To achieve sequence $O_3BO_3$ (**30**), three cycles with (*S*)-dimethyloctyl acrylate were done first, followed by one cycle with the (*S*)-BTA-acrylate (**29**) and consecutive

three cycles with (*S*)-dimethyloctyl acrylate (**28**) afterwards. After seven cycles the oligomer was cleaved from the solid support by 1% trifluroacetic acid in dichloromethane to yield BTA-holding heptamer **28**.

The most convenient method to assess the purity of the oligomer is mass spectroscopy. Due to the limitation of the ESI-MS spectrometer used, only ions with m/z up to 3000 could

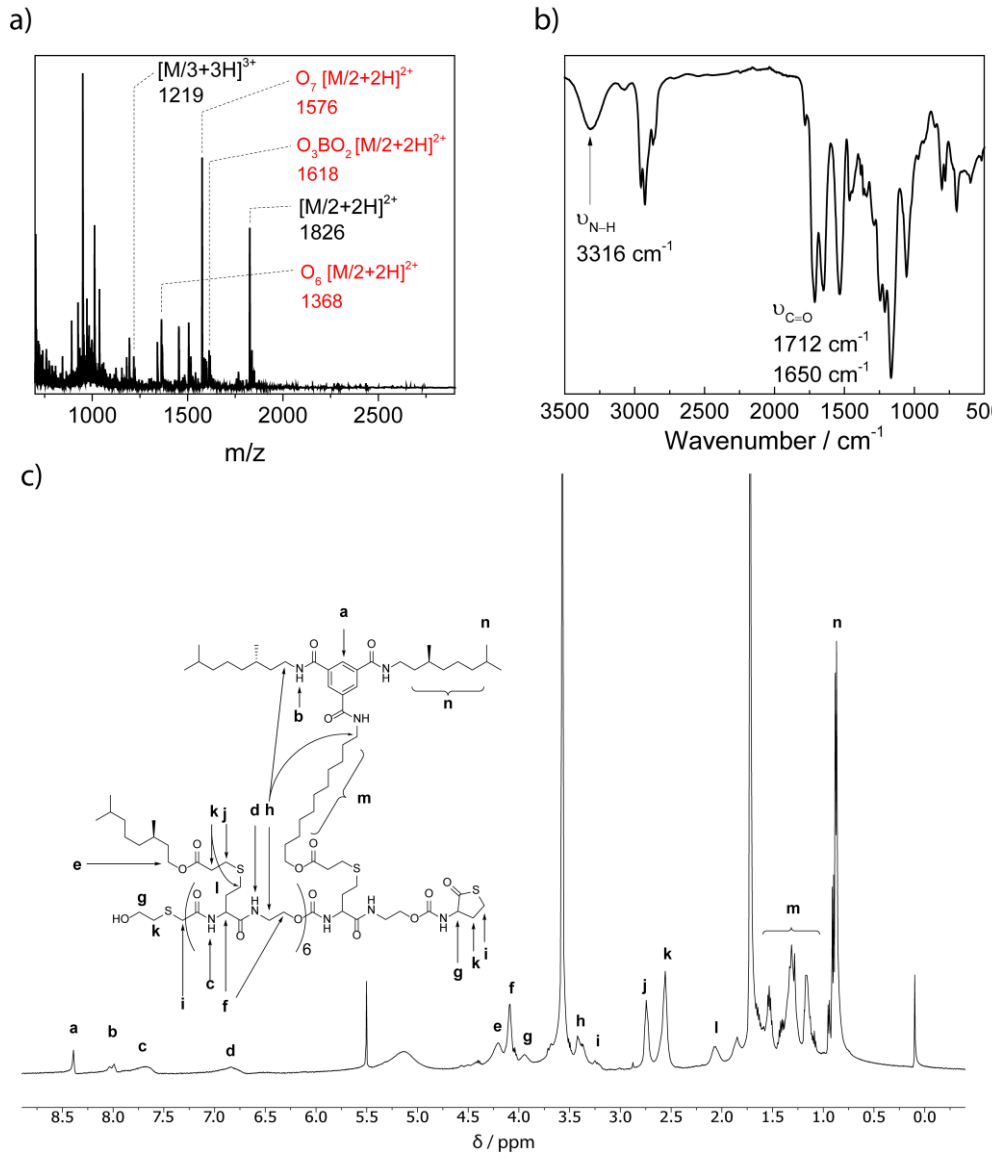


***Figure 6.4*** *a) ESI-MS spectrum of heptamer* ***30*** *with (red color indicates impurities); b) FT-IR spectrum of heptamer* ***30****. c)* $^{1}$*H NMR spectrum of heptamer* ***30*** *(500 MHz, THF-*$d_8$*).*

be observed. The molecular mass of the heptamer **30** is 3648 g mol$^{-1}$, so the primary molecular ion appears beyond this region, but the peaks corresponding to $[M/2 + 2H]^{2+}$ (1826 Da) and $[M/3 + 3H]^{3+}$ (1219 Da) are visible (Figure 6.4a). However, other peaks that can be assigned to the other variations of the (S)-3,7-dimethyloctyl-functionalized heptamer or hexamer with or without the BTA are also present. The peak at 1576 Da corresponds to the $[M/2 + 2H]^{2+}$ of a sequence *O*$_7$ (no BTA in the structure). There are also peaks corresponding to the $[M/2 + 2]^{2+}$ of sequences *O*$_6$ and *O*$_3$*BO*$_2$. The FT-IR spectrum shows characteristic bands for amides and urethanes ($\upsilon_{N-H}$ and $\upsilon_{C=O}$) (Figure 6.4b). The N-H stretching band is visible at 3316 cm$^{-1}$ and the bands corresponding to the urethane and amide I are located at 1650 cm$^{-1}$ while amide II band appears at 1530 cm$^{-1}$. The $^1$H NMR spectrum of the oligomer shows that the oligomeric backbone stayed intact during the synthesis as well as that the BTA and (*S*)-3,7-dimethyloctyl pendants are present (Figure 6.4c). However, the spectrum is rather complex and does not allow to assess the purity. The combined results of the $^1$H NMR, ESI-MS and IR spectroscopy indicate that the synthesis of the heptamer was accomplished, but also that the formation of side products occurred. These side reactions were not reported for the more simple monomers used in previous oligomer synthesis in the group of Du Prez, indicating that with an increase in complexity of the substrates, reactions conditions will require further optimizations.

## 6.4 Self-assembly of sequence-defined oligomers functionalized with BTA

The synthesized oligomers ("blank" octamer **17** and BTA-functionalized octamers **26**, and **27** and heptamer **30**) were characterized in terms of formation of the secondary structure in solid state and in solution. Infrared spectroscopy is an excellent technique to probe the formation of hydrogen bonds in amide derivatives. BTA derivatives that form helical aggregates via three-fold hydrogen bonds exhibit characteristic band pattern ($\upsilon_{N-H}$ = 3226 cm$^{-1}$, $\upsilon_{C=O}$, (amide I) = 1636 cm$^{-1}$, amide II = 1548 cm$^{-1}$).[29] On the other hand, analysis of the oligomers containing multiple amide groups in the structure is not straightforward as the IR spectrum of such oligomer is highly sensitive towards the conformation of the amides. Since in such systems multiple assembled states can be of similar energy remaining in dynamic equilibrium[30], IR spectroscopy must be supported by other experimental and theoretical techniques to fully elucidate the secondary structure. Additionally, the much higher abundance of these amides than those of the BTA results in low to no visibility of the BTA bands (Lambert-Beer law).

The IR spectrum of the octamer **26** in solid state shows the IR absorption bands at 3275 cm$^{-1}$, 1634 cm$^{-1}$ and 1537 cm$^{-1}$. The position of the bands suggests presence of the hydrogen bonds in the system,[31] however these bands cannot be assigned to the three-fold hydrogen bond in helically-aggregated BTAs. Similar bands are observed for the octamer **27**, which besides BTA, holds eighteen decyl chains ($\upsilon_{N-H}$ = 3262 cm$^{-1}$, $\upsilon_{C=O}$ = 1643 cm$^{-1}$, amide II = 1551 cm$^{-1}$). Interestingly, the presence of the long, solubilizing chains did not affect the hydrogen

bond pattern to a large extent, which may be caused by effective phase-segregation of the hard and soft segments.

The IR spectrum of heptamer **30** holding only one BTA shows absorption bands characteristic for amide group at $\upsilon_{N-H}$ = 3318 $cm^{-1}$, $\upsilon_{C=O}$ = 1650 $cm^{-1}$, amide II = 1532 $cm^{-1}$. The position of the bands suggests weaker hydrogen bonds than in case of the octamers **26** and **27**. Lack of the enantiopurity of the oligomer backbone as well as other oligomers (impurities) present in the mixture may cause defects in the supramolecular structure.

In all systems, no birefringence was observed under polarized optical microscope, suggesting that possible multiple conformations of the backbone result in a lack of long-range order in the oligomers. Despite the presence of the hydrogen bonds, DSC thermograms of the octamers showed no transitions between -50 °C and 250 °C. Interestingly, we observed a reversible transition at 220 °C in case of tetramer (**14**). However, on the basis of POM together with low enthalpy of this transition (360 J $mol^{-1}$) we assign this to an order-disorder transition. The lack of the thermal transitions in case of the octamers suggests that elongation of the oligomeric backbone significantly stabilizes the secondary structure formed. Unfortunately, due to the low amount of heptamer **30**, we did not record DSC of this sequence.

As it was clear that hydrogen bonds are formed in solid state, we examined the assembly of the oligomers in dilute solutions. Due to its intrinsic low solubility, octamer **26** could not be dissolved in methylcyclohexane (MCH). Therefore circular dichroism (CD) spectra of **26** were measured in 1,2-dichloroethane (DCE) (Figure 6.5a). On the contrary, octamer **27** holding long decyl chains and heptamer **30** were soluble in MCH. The CD spectra of all oligomers reveal the presence of a Cotton effect at around 230 nm. Remarkably, the strongest dichroic response was observed for the octamer **26** in DCE, the solvent where BTAs are normally molecularly dissolved. In analogy to Chapter 5, the aggregation of the BTA in this case is permitted by low solubility of the oligomeric backbone. The calculated molar circular dichroism Δε was -29.7 L $mol^{-1}$ $cm^{-1}$ (the value of Δε for a fully assembled (*S*)-BTA is -40 L $mol^{-1}$ $cm^{-1}$) which would suggest that a significant amount of the BTAs are incorporated in the supramolecular polymers of single handedness. However, due to the intrinsic absorption of the optically active backbone in this region (*vide infra*), the intensity of the signal was not caused by the BTA aggregation alone. Octamer **27** and heptamer **30** in MCH show much smaller values of Δε (-8.5 L $mol^{-1}$ and -13.3 L $mol^{-1}$). Similarly to octamer **26**, in case of octamer **27** the CD-effect could be affected by the inherent optical activity of the backbone.

To investigate the assembly mechanism, we also recorded VT-CD curves at 225 nm. Blank octamer **17** was soluble only in DCE at low concentrations and showed constant CD in the whole temperature regime (Figure 6.5b). Similarly, we did not observe noticeable changes in the Cotton effect of **27**, which suggested absence of helically assembled BTA. On the other hand, the increase of the CD effect of **26** below 45 °C could be assigned to the clustering of

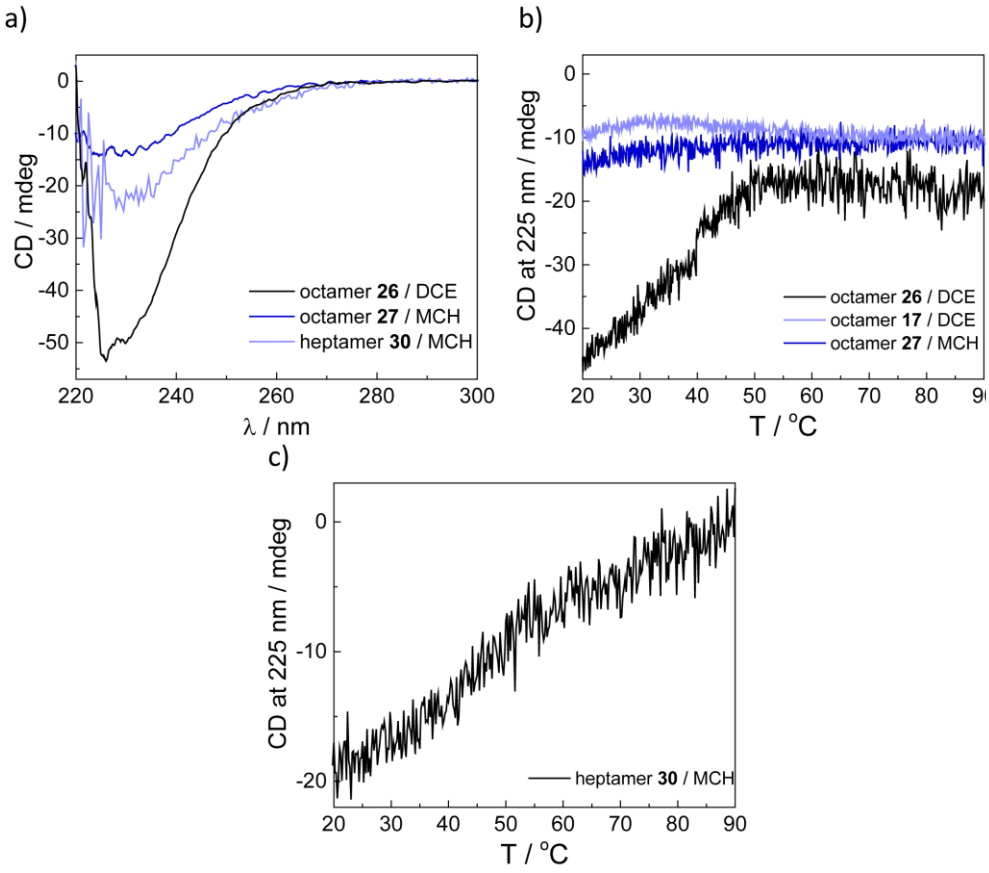


***Figure 6.5*** *a) CD spectra of the oligomers ($c_{BTA}$ = 50 µM); b) VT-CD curves of the octamers **17**, **26** and **27** in MCH or DCE ($c_{BTA}$ = 50 µM, k = 0.5 K min$^{-1}$); c) VT-CD curve of the heptamer **30** in MCH ($c_{BTA}$ = 50 µM, k = 0.5 K min$^{-1}$).*

the oligomers via BTA aggregation. Aggregation of the BTAs in the heptamer **30** takes place at high temperature, but is more gradual than in the case of octamer **26** (Figure 6.5c). Interestingly, at 55 °C the process becomes sharper showing that at lower temperatures different aggregation mechanism drives the assembly of the BTAs. We did not observe any aggregation of the backbone based on racemic monomers in alkanes. However, one cannot exclude such phenomenon when it is attached to the BTA core.

The results indicate that the aggregation of the BTAs in such complex systems is achievable. However, it becomes difficult to control the assembly process when multiple binding sites compete with each other and the interactions of all the components with the solvent are not balanced. Finally, the intrinsic absorption of the light of the similar energy by multiple parts of the molecule impedes detailed spectroscopic characterization.

## 6.5 Conclusions

We have demonstrated the successful synthesis of the orthogonally protected L-γ-glutamamide octamers, containing alkyne- and alkene-based reactive side groups via a 17-step synthesis. Increase in the chain length resulted in decreasing solubility and reactivity. This led to a significant drop in yield after an isolation of the final octamers. Nevertheless, bis((*S*)-3,7-dimethyloctyl)-(11-azidoundecyl)-BTA was successfully attached to the oligomer backbone via copper (I) – catalyzed 2+3 dipolar cycloaddition ("click" chemistry). Subsequently, full functionalization with solubilizing decyl chains was achieved upon radical thiol-ene addition. In addition we showed an approach based on solid-phase synthesis of sequence-defined heptamer functionalized with (*S*)-BTA. In both cases, presence of the side reactions caused the presence of the impurities that due to structural similarity could not be removed.

Furthermore, the herein synthesized oligomers exhibited secondary structures arising from hydrogen bond formation in bulk as well as in dilute solutions. The initial characterization showed that despite the molecular complexity, BTA aggregation is possible in these molecules, however, better molecular engineering is required to assess these system's particular assembly features. This point becomes especially apparent if one compares the solubility of octamers before and after functionalization. Before the alkyl chains were attached, the octamers were sparingly soluble in most of the solvents, therefore the interactions between the oligomers became too strong to control the assembly. On the other hand, upon functionalization with alkyl chains, the oligomer became susceptible towards the interactions with apolar solvents, thereby hampering efficient aggregation. In future experiments it is particularly important to address the interactions of all components including solvent.

The results show that synthesis of sequence-defined oligomers holding supramolecular motifs is possible. However, to become applicable in the synthesis of functional, sequence-defined oligomers, it requires major optimization and reconsideration of the strategy and supramolecular units used. Iterative approaches based on classical organic synthesis offers to synthesize sequence-defined oligomers in few steps with satisfying yields and amounts. Post-functionalization strategy does not require large excess of the reagents, therefore it is feasible to synthesize the oligomers in amounts permitting further modification and analysis. The major drawback of this method is the decreasing solubility of the backbone, which practically precludes further elongation and isolation of the oligomers longer than octamer. It is therefore necessary to adapt the nature of the backbone or the side chains to make this method useful for broader applications. This will be a challenging task due to limitations connected to the chemistry.

In this context, the major advantage of the solid-phase strategy is lack of tedious purification after each step to isolate the growing oligomer. Simplified reaction and purification setup permits quick growth of the oligomer. However, available methodology is

adapted only for the synthesis performed at small scale. The necessity of using large excess of the reactants at each step is especially troublesome, when building blocks (such as BTA-acrylate) have to be synthesized via multi-step synthesis in large amounts. Eventually, if side-products are formed, it is difficult to isolate the final product. As a way out of this situation we propose post-functionalization strategy, which would minimize the use of expensive chemicals. In this case, the growth strategy has to be optimized to exclude side reactions. In the ongoing collaboration with the group of Prof. Filip du Prez, we address these issues to arrive at optimized synthesis of functional sequence-defined oligomers.

## 6.6 Experimental Section

### 6.6.1 Materials and methods

Reagents were purchased from Sigma Aldrich, TCI chemicals, Fisher Scientific, TCI Europe, and ABCR and used as received. All solvents were purchased from Biosolve and dry solvents were obtained using MBraun solvent purification system (MB SPS-800). Thiolactone-modified solid support and α-isocyanato-γ-thiolactone were synthesized by Steven Martens (University of Ghent, Belgium) according to previously described procedures.[16] Deuterated solvents were provided by Cambridge Isotopes Laboratories. Reactions were monitored by the use of thin-layer chromatography (TLC) using 60-F254 silica gel plates (Merck) and compounds were visualized using an ultraviolet lamp (254 nm), potassium permanganate ($KMnO_4$) stain, or iodide ($I_2$) stain. Automated column chromatography was performed using a Biotage Isolera® One with Biotage Silica Cartridges and using a Grace Reveleris X2 using Reveleris Silica Flash Cartridges. $^1$H NMR and $^{13}$C NMR spectra were recorded on a Bruker ASCEND 400 MHz (400 MHz for $^1$H NMR and 100 MHz for $^{13}$C NMR). Proton chemical shifts are reported in ppm (δ) downfield from trimethylsilane (TMS) using the resonance frequency of the deuterated solvents ($CDCl_3$; 7.26 ppm & DMSO-*d*$_6$; 2.50 ppm containing TMS) as internal standards. Peak multiplicities are abbreviated as s: singlet; d: doublet; q: quartet; m: multiplet; br: broad; dd: doublet of doublets; dt: doublet of triplets and dq: doublet of quartet. Carbon chemical shifts are reported in ppm (δ) downfield from trimethylsilane (TMS) using the resonance frequency of the deuterated solvents ($CDCl_3$; 77.16 ppm & DMSO-*d*$_6$; 39.52 ppm containing TMS) as internal standards. Infrared spectra were recorded using a Perkin Elmer Spectrum Two FT-IR spectrometer equipped with a Perkin Elmer Universal ATR Two Accessory. Matrix assisted laser absorption/ionization mass time of flight (MALDI-TOF) spectra were obtained on a Bruker Autoflex Speed. α-cyano-4-hydroxycinnamic acid (CHCA) and trans-2-[3-(4-tert-butylphenyl)-2-methyl-2-propenylidene]malononitrile (DCBT) were used as matrix. All samples were dissolved in $CHCl_3$ or $CHCl_3$:DMSO (80:20). LC-MS was measured on an Agilent technologies 1100 series LC/MSD reversed phase LC-MS (liquid chromatography mass spectroscopy) system equipped with a diode array detector and single quad MS detector (VL) with an electrospray source (ESI-MS), and MS analysis. Analytic reversed phase HPLC was performed with a Phenomenex C18 (2) column (5 µ, 250 x 4.6 mm) using a solvent gradient (0 → 100% acetonitrile in $H_2O$ in 15 min) and the eluting compounds were detected via UV-detection ($\lambda$ = 214 nm). High resolution mass spectra (HRMS) were collected using an Agilent 6220 Accurate-Mass time-of-flight (TOF) equipped with a multimode ionization (MMI) source.

### 6.6.2 Synthetic procedures

#### 6.6.2.1 Iterative synthesis of γ-glutamic acid octamer

*N-(tert-Butyloxycarbonyl)tris(hydroxymethyl)aminomethane (**2**)*

2-Amino-2-(hydroxymethyl)-1,3-propanediol (**1**) (10 g, 82.0 mmol) was suspended in a mixture of MeOH (75 mL) and *t*-BuOH (175 mL). Di-*tert*-butyl dicarbonate (24 mL, 112.2 mmol) was added to the stirred mixture. The reaction was performed at room temperature overnight. The solvent was removed under reduced pressure, to yield a white residue. *N*-(*tert*-Butyloxycarbonyl)tris(hydroxymethyl)aminomethane (**2**) was isolated by precipitation in EtOAc as a white solid (14.97 g, 81%).

$^1$H NMR (400 MHz, DMSO-$d_6$): δ = 5.76 (br s, 1H, NH), 4.49 (t, 2H, OH), 3.51 (d, 6H, CCH$_2$OH), 1.37 (s, 9H, *t*-Bu).

*N-(tert-Butyloxycarbonyl)tris[(allyloxy)methyl]aminomethane (**3**)*

Compound **2** (14.1 g, 63.8 mmol) was dissolved in DMF (100 mL) and allyl bromide (31 mL, 358 mmol) was added to the mixture and cooled down to 0 °C. Crunched KOH pellets (20.1 g, 358 mmol) were gradually added and the mixture was stirred at room temperature for 3 hours. Purification was done by partitioned extraction between EtOAc and $H_2O$. After removal of the $H_2O$/DMF mixture, the organic layer was washed with brine, dried ($Na_2SO_4$) and the solvent was removed under reduced pressure. The crude product was subjected to column chromatography (heptane-EtOAc, 95:5) to give a colorless oil **3** (6.39 g, 30%), which purity was confirmed by $^1$H NMR spectroscopy.

$^1$H NMR (400 MHz, $CDCl_3$): δ = 5.88 (m, 3H, CH=CH$_2$), 5.30-5.10 (m, 6H, CH=CH$_2$), 4.96 (br s, 1H, NH), 3.98 (m, 6H, CH$_2$CH=CH$_2$), 3.70 (s, 6H, CCH$_2$O), 1.42 (s, 9H, *t*-Bu).

*Tris[(allyloxy)methyl]aminomethane (**4**)*

Compound **3** (6 g, 17.57 mmol) was dissolved in DCM (60 mL) and cooled to 0 °C. Trifluoroacetic acid (TFA) (25 mL, 326 mmol) was added to the stirred solution. The mixture was stirred at room temperature for 2 hours. The solvent and TFA were removed under reduced pressure and the residue was dissolved in EtOAc (100 ml). The organic layer was washed with $Na_2CO_3$(sat):$H_2O$ (20:80 vol%) solution (2 x 100 mL), brine (2 x 100 mL), dried ($MgSO_4$), and evaporated under reduced pressure to obtain **4** (3.86 g, 91%) as an orange liquid.

$^1$H NMR (400 MHz, $CDCl_3$): δ = 5.88 (m, 3H), 5.31 – 5.13 (m, 6H), 4.00 (dt, J = 5.5, 1.5 Hz, 6H), 3.45 (s, 6H), 2.19 (d, J = 114.2 Hz, 2H). $^{13}$C NMR (100 MHz, $CDCl_3$): δ = 134.35, 117.22, 72.43, 69.30 (d, J = 5.4 Hz), 58.44 (d, J = 5.1 Hz).

*FmocHN-Glu(COO*t*Bu)-propargylamide (**5**)*

FmocHN-Glu-(COO*t*Bu)-COOH (8 g, 18.8 mmol) was dissolved in THF (200 mL). EDC·HCl (4.32 g, 22.5 mmol), HOBt·x$H_2O$ (2.54 g, 18.8 mmol) were added before the mixture was cooled to 0 °C. Finally, DIPEA (~6.5 mL, 37.1 mmol) and propargylamine (~1.35 mL, 20.7 mmol) were added, after which the reaction was left stirring at r.t. overnight. The reaction was quenched with EtOH (20 mL), and the solvents were evaporated *in vacuo*. The residue was dissolved in EtOAc (200 mL) and washed with aq. 10% citric acid-solution (pH 3-5) (4 x 150 mL), $H_2O$ (4 x 125 mL), dried ($MgSO_4$), and evaporated under reduced pressure.

The compound was purified by column chromatography (DCM-EtOAc, 8:2) to give FmocHN-Glu(COO*t*Bu)-propargylamide (**5**) as a white solid (4.58 g, 53%).

$^1$H NMR (400 MHz, $CDCl_3$): δ = 7.77 (d, 2H, Fmoc), 7.59 (d, 2H, Fmoc), 7.41 (t, 2H, Fmoc), 7.32 (t, 2H, Fmoc), 6.52 (br s, 1H, NH), 5.71 (d, 1H, NH), 4.41 (t, 2H, Fmoc), 4.21 (m, 2H, Fmoc, Glu-H$^{\alpha}$), 4.06 (br s, 2H, $CH_2$C≡CH), 2.44 (m, 1H, Glu-H$^{\gamma}$), 2.33 (m, 1H, Glu-H$^{\gamma}$), 2.23 (t, 1H, C≡CH), 2.08 (m, 1H, Glu-H$^{\beta}$), 1.95 (m, 1H, Glu-H$^{\beta}$), 1.46 (s, 9H, *t*-Bu). $^{13}$C NMR (100 MHz, $CDCl_3$): δ = 143.72, 141.31, 127.76, 127.10, 125.08, 120.02, 81.26, 79.07, 71.83, 67.13, 47.16, 31.71, 29.25, 28.09. MALDI-TOF (m/z) calculated for $C_{27}H_{30}NaN_2O_5$, $[M+Na]^+$ = 485.21, Obs. $[M+Na]^+$ = 485.23.

*FmocHN-Glu(COOtBu)-trisallyloxyamide (**6**)*

FmocHN-Glu-(COO*t*Bu)-OH (5.14 g, 12.1 mmol) was dissolved in THF (200 mL). EDC·HCl (2.61 g, 13.6 mmol) and HOBt·x$H_2O$ (1.57 g, 11.6 mmol) were added before the mixture was cooled to 0 °C. Finally, DIPEA (~3.9 mL, 22.4 mmol) and **4** (3 g, 12.4 mmol) were added, after which the reaction was left stirring at r.t. overnight. The solvent was evaporated under reduced pressure. The residue was dissolved in EtOAc (200 mL) and washed with aq. 10% citric acid-solution (pH 3-5) (3 x 150 mL), brine (3 x 150 mL), dried ($MgSO_4$), and evaporated under reduced pressure. The compound was purified by column chromatography (DCM-EtOAc, 95:5%) to give FmocHN-Glu(COO*t*Bu)-trisallyloxyamide (**6**) (5.41 g, 67%) as a colorless oil.

$^1$H NMR (400 MHz, $CDCl_3$): δ = 7.77 (d, 2H, Fmoc), 7.60 (d, 2H, Fmoc), 7.40 (t, 2H, Fmoc), 7.32 (t, 2H, Fmoc), 6.37 (br s, 1H, NH), 5.85 (m, 3H, $CH_3CH=CH_2$), 5.71 (d, 1H, NH), 5.31-5.10 (m, 6H, $CH=CH_2$), 4.36 (t, 2H, Fmoc), 4.21 (m, 2H, Fmoc, Glu-H$^{\alpha}$), 3.96 (d, 6H, $OCH_2CH$), 3.72 (s, 6H, $CCH_2CH$), 2.38 (m, 2H, Glu-H$^{\gamma}$), 1.93 (m, 2H, Glu-H$^{\beta}$), 1.46 (s, 9H, *t*-Bu). $^{13}$C NMR (100 MHz, $CDCl_3$): δ = 172.82, 170.79, 143.80, 141.28 (d, *J* = 1.4 Hz), 134.61, 127.69, 127.06, 125.17, 119.96, 116.83, 80.77, 72.25, 68.56, 67.05, 60.39, 54.54, 47.17, 31.43, 28.82, 28.09. MALDI-TOF (m/z) calculated for $C_{37}H_{48}NaN_2O_8$, $[M+Na]^+$ = 671.33, Obs. $[M+Na]^+$ = 671.34.

*FmocHN-Glu(COOH)-propargylamide (**7a**)*

FmocHN-Glu(COO*t*Bu)propargylamide (**5**) (4.91 g, 10.6 mmol) was dissolved in DCM (50 mL) and the solution was cooled to 0 °C. TFA (50 mL, 653 mmol) was added and the reaction was stirred at room temperature for 3 hours. The solvents were evaporated under reduced pressure, where after the crude product was dissolved in DCM and dried under reduced pressure for two times to obtain FmocHN-Glu(COOH)-propargylamide (**7a**) as a soft pink/yellow colored powder.

*FmocHN-Glu(pentafluorophenylester)-propargylamide (**7b**)*

FmocHN-Glu(COOH)-propargylamide (**7a**) was suspended in $CHCl_3$ (150 mL) and became dissolved after the addition of DIPEA (6 mL, 34.4 mmol). Pentafluorophenyl trifluoroacetate (2.4 mL, 14.0 mmol) was added and the reaction was stirred at room temperature for 3 hours. The mixture was washed with aq. 10% citric acid-solution (pH 3-5) (2 x 100 mL), $H_2O$ (2 x 100 mL), brine (2 x 100 mL), dried ($MgSO_4$), and evaporated under reduced pressure to obtain FmocHN-Glu(*pentafluorophenylester*)-propargylamide (**7b**) as a solid (12.26 g).

*$H_2$N-Glu(COOtBu)-trisallyloxyamide (**8**)*

FmocHN-Glu(COO*t*Bu)-trisallyloxyamide (**6**) (7.88 g, 12.1 mmol) was dissolved in DCM (100 mL). Diethylamine (100 mL, 967 mmol) was added and the reaction was stirred at r.t. for 3 hours. On completion, volatiles were evaporated under reduced pressure and the residue was dissolved in DCM. The compound was purified by column chromatography (DCM-EtOAC, 95:5% up to DCM-EtOAc, 40:60%) to obtain $H_2N$-Glu(COO*t*Bu)-trisallyloxyamide (**8**) (4.22 g, 81%) as a yellow oil.

$^1$H NMR (400 MHz, $CDCl_3$): δ = 7.36 (d, *J* = 3.8 Hz, 1H), 5.96 – 5.81 (m, 3H), 5.34 – 5.10 (m, 6H), 3.99 (tq, *J* = 5.4, 1.5 Hz, 6H), 3.88 – 3.69 (m, 6H), 3.37 – 3.28 (m, 1H), 2.42 – 2.29 (m, 2H), 2.10 – 1.95 (m, 1H), 1.90 – 1.77 (m, 1H), 1.45 (d, *J* = 4.5 Hz, 11H). $^{13}$C NMR (100 MHz, $CDCl_3$): δ = 174.38, 172.90, 134.79, 116.67, 80.34, 72.24, 68.71, 59.46, 55.10, 31.69, 30.43, 28.10.

*FmocHN-Glu(COOH)-triallyloxyamide (**9a**)*

FmocHN-Glu(COO*t*Bu)-trisallyloxyamide (**6**) (6.74 g, 10.4 mmol) was dissolved in DCM (50 mL) and the solution was cooled to 0 °C with an ice bath. Trifluoroacetic acid (50 mL, 653 mmol) was added and the reaction was stirred at room temperature for 3 hours. On completion, volatiles were evaporated under reduced pressure, where after the crude product was dissolved in DCM and dried under reduced pressure two times to obtain Fmoc-Glu(COOH)-triallyloxyamide (**9a**) (8.31 g) as a solid.

*FmocHN-Glu(pentafluorophenylester)-triallyloxyamide (**9b**)*

Crude FmocHN-Glu(COOH)-triallyloxyamide (**9a**) (8.31 g) was dissolved in $CHCl_3$ (150 mL). DIPEA (7 mL, 40.2 mmol) and pentafluorophenyl trifluoroacetate (2.5 mL, 14.5 mmol) were added, and the reaction was stirred at room temperature for 1 hour. The reaction was washed with aq. 10% citric acid-solution (pH 3-5) (3 x 100 mL), $H_2O$ (3 x 100 mL), brine (3 x 100 mL), dried ($MgSO_4$), and evaporated under reduced pressure to obtain crude FmocHN-Glu(*pentafluorophenylester*)-triallyloxyamide (**9b**) (9.1 g).

*FmocHN-AT-tBu (**10**)*

Fmoc-Glu(*pentafluorophenylester*)-propargylamide (**7b**) (12.26 g) and $H_2N$-Glu(COO*t*Bu)-trisallyloxyamide (**8**) (2.25 g, 5.27 mmol) were dissolved in DMF (100 mL) and the mixture was stirred at room temperature for 30 minutes. EtOAc (100 mL) was added and washed with $H_2O$ (100 mL), and brine (2 x 100 mL). The organic layer was dried ($Na_2SO_4$) and evaporated under reduced pressure. The title compound was purified by column chromatography (DCM-EtOAc, 50:50%) to obtain FmocHN-AT-*t*Bu (**10**) (3.45 g, 80%) white solid.

$^1$H NMR (400 MHz, $CDCl_3$): δ = 7.76 (d, J = 7.5 Hz, 2H), 7.59 (d, J = 7.5 Hz, 2H), 7.44 – 7.27 (m, 4H), 6.72 (d, J = 7.5 Hz, 1H), 6.42 (s, 1H), 5.98 (d, J = 7.5 Hz, 2H), 5.85 (ddt, J = 17.3, 10.7, 5.5 Hz, 3H), 5.28 – 5.09 (m, 6H), 4.39 (dd, J = 18.2, 7.4 Hz, 2H), 4.26 – 4.14 (m, 3H), 4.03 – 3.90 (m, 8H), 3.83 – 3.65 (m, 6H), 2.49 – 2.26 (m, 4H), 2.24 (t, J = 2.5 Hz, 1H), 2.01 – 1.88 (m, 2H), 1.44 (s, 9H). $^{13}$C NMR (100 MHz, $CDCl_3$) δ = 172.97, 171.17, 143.84, 141.31, 134.63, 127.72, 127.10, 125.16, 119.98, 116.80, 81.04, 79.62, 72.25, 71.56, 68.56, 60.10, 53.11, 47.17, 32.45, 31.62, 28.99, 28.08. MALDI-TOF (m/z) calculated for $C_{45}H_{58}NaN_4O_{10}$, $[M+Na]^+$ = 837.41, Obs. $[M+Na]^+$ = 837.41.

*FmocHN-TT-COOtBu (**11**)*

$H_2N$-Glu(*OtBu*)-trisallyloxyamide (**8**) (4.02 g, 9.42 mmol) and crude Fmoc-Glu(*pentafluorophenylester*)-triallyloxyamide (**9b**) (9.1 g) were dissolved in DMF (100 mL). The reaction was stirred at room temperature

for 1.5 hours. EtOAc (150 mL) was added to the reaction mixture and the DMF was washed out with $H_2O$ (2 x 100 mL), and brine (2 x 100 mL) before the organic layer was dried ($Na_2SO_4$) and evaporated under reduced pressure. The compound was purified by column chromatography (DCM-EtOAc, 50:50%) to obtain FmocHN-TT-COO*t*Bu (**11**) (6.94 g, 74%) as a white solid.

$^1$H NMR (400 MHz, $CDCl_3$): δ = 7.75 (d, J = 7.5 Hz, 2H), 7.59 (d, J = 7.5 Hz, 2H), 7.35 (dt, J = 32.7, 7.5 Hz, 4H), 7.12 (s, 1H), 6.79 (d, J = 7.8 Hz, 1H), 6.39 (s, 1H), 5.86 (ddt, J = 16.9, 11.5, 5.9 Hz, 6H), 5.34 – 5.08 (m, 12H), 4.38 (q, J = 7.2 Hz, 2H), 4.32 (d, J = 7.6 Hz, 2H), 4.20 (t, J = 7.2 Hz, 1H), 3.97 (q, J = 5.0 Hz, 12H), 3.87 – 3.60 (m, 12H), 2.48 – 2.18 (m, 4H), 2.11 – 1.79 (m, 4H), 1.44 (s, 9H). $^{13}$C NMR (100 MHz, $CDCl_3$): δ = 172.55, 171.37, 171.18, 143.88, 141.25, 134.71, 134.64, 127.65, 127.07, 125.22, 119.92, 117.02, 116.71, 80.76, 72.29, 72.22, 68.51, 68.22, 60.33, 60.14, 53.07, 47.19, 31.64, 28.09. MALDI-TOF (m/z) calculated for $C_{55}H_{76}NaN_4O_{13}$, $[M+Na]^+$ = 1023.53, Obs. $[M+Na]^+$ = 1023.55.

*$H_2$N-AT-COOtBu (**12**)*

FmocHN-AT-COO*t*Bu (**10**) (3.45 g, 4.23 mmol) was dissolved in DCM (100 mL). Diethylamine (100 mL, 967 mmol) was added and the mixture was stirred at r.t. for 3 hours. Volatiles were evaporated under reduced pressure and the residue was dissolved in DCM (100 mL). The organic layer was washed with aq. 10% citric acid-solution (pH 3-5) (2 x 100 mL), $Na_2CO_3$(sat):$H_2O$ (20:80 vol%) solution (3 x 100 mL), brine (3 x 100 mL), dried ($MgSO_4$) and the evaporated under reduced pressure. The residue was precipitated in pentane. $H_2$N-AT-COO*t*Bu (**12**) (2.25 g) was obtained as a yellow sticky solid.

*FmocHN-TT-COOH (**13a**)*

FmocHN-TT-COO*t*Bu (**11**) (5.04 g, 5.03 mmol) was dissolved in DCM (50 mL) and the solution was cooled to 0 °C with an ice bath. Trifluoroacetic acid (50 mL, 653 mmol) was added and the reaction was stirred at room temperature overnight. On completion, volatiles were evaporated under reduced pressure, where after the crude product was dissolved in DCM and dried under reduced pressure for two times, to obtain FmocHN-TT-COOH (**13**) as an orange viscous liquid.

*FmocHN-TT-COOPh$F_5$ (**13b**)*

FmocHN-TT-COOH (**13a**) (4.76 g, 5.03 mmol) was dissolved in $CHCl_3$ (150 mL). DIPEA (6 mL, 34.4 mmol), pentafluorophenyl trifluoroacetate (1.3 mL, 7.57 mmol) were added, and the reaction was stirred at room temperature for 1 hour. The reaction mixture was washed with aq. 10% citric acid-solution (pH 3-5) (3 x 100 mL), $H_2O$ (3 x 100 mL), brine (3 x 100 mL), dried ($MgSO_4$), and evaporated under reduced pressure to obtain FmocHN-TT-OPh$F_5$ (**13b**) (5.44 g) as a yellow sticky solid.

*FmocHN-TTAT-COOtBu (**14**)*

FmocHN-TT-COOPh$F_5$ (**13b**) (5.44 g) and $H_2$N-AT-*t*Bu (**12**) (2.25 g) were dissolved in DMF (100 mL) and the reaction was stirred at room temperature for 1 hour. EtOAc (200 mL) was added to the reaction mixture and the DMF was washed out with $H_2O$ (3 x 100 mL), and brine (3 x 100 mL) before the organic layer was dried ($Na_2SO_4$) and evaporated under reduced pressure. The filtrate and residue were dissolved in a mixture of $CHCl_3$ and MeOH, and separated from the $Na_2SO_4$ by filtration. The residue solvents were evaporated under reduced pressure and the solid product was purified by column chromatography ($CHCl_3$-EtOAc, 50:50%, up to 100% EtOAc) to obtain FmocHN-TTAT-COO*t*Bu (**14**) (3.83 g, 60%) as a white solid.

$^1$H NMR (400 MHz, DMSO-$d_6$): δ = 8.37 (t, *J* = 5.5 Hz, 1H), 7.97 – 7.68 (m, 7H), 7.53 – 7.21 (m, 8H), 5.82 (ddq, *J* = 20.6, 9.7, 5.0 Hz, 9H), 5.35 – 4.98 (m, 18H), 4.24 (dq, *J* = 22.2, 8.8, 8.0 Hz, 7H), 3.91 (d, *J* = 5.3 Hz, 18H), 3.84 (dt, *J* = 4.9, 2.4 Hz, 2H), 3.70 – 3.49 (m, 18H), 3.08 (t, *J* = 2.5 Hz, 1H), 2.28 – 2.05 (m, 8H), 1.93 – 1.59 (m, 8H), 1.37 (s, 9H). $^{13}$C NMR (100 MHz, DMSO-$d_6$): δ = 172.09, 135.61, 135.59, 128.10, 127.54, 125.79, 120.56, 116.84, 116.77, 80.00, 79.43, 73.49, 71.96, 71.92, 68.23, 60.15, 28.19. IR ν (cm$^{-1}$) 3277 (N-H stretching), 3075 (Ar C-H stretching), 2931, 2859 (aliphatic C-H stretching), 1730 (C=O ester stretching), 1690, 1660, 1634 (C=O amide stretching), 1525 (amide II), 1448, 1252, 1150, 1084, 988, 922, 737, 598, 426. MALDI-TOF (m/z) calculated for $C_{81}H_{114}NaN_8O_{20}$, $[M+Na]^+$ = 1541.80, Obs. $[M+Na]^+$ = 1541.80.

*$H_2$N-TTAT-COOtBu (**15**)*

FmocHN-TTAT-COO*t*Bu (**14**) (1.395 g, 0.92 mmol) was dissolved in $CHCl_3$ (50 mL). Piperidine (50 mL, 506 mmol) was added and the mixture was stirred at room temperature for 1 hour. The $CHCl_3$ and piperidine were evaporated under reduced pressure and the residue was dissolved in $CHCl_3$ (150 mL). The organic layer was washed with aq. 10% citric acid-solution (pH 3-5) (3 x 100 mL), $Na_2CO_3$ (sat):$H_2O$ (20:80 vol%) solution (2 x 100 mL), brine (2 x 100 mL), dried ($MgSO_4$) and evaporated under reduced pressure. The residue was washed with pentane to partially remove the Fmoc-byproducts. $H_2$N-TTAT-COO*t*Bu (**15**) was obtained as a yellow solid.

*FmocHN-TTAT-COOH (**16a**)*

FmocHN-TTAT-COO*t*Bu (**14**) (1.395 g, 0.92 mmol) was dissolved in $CHCl_3$ (50 mL) and the solution was cooled to 0 °C with an ice bath. Trifluoroacetic acid (50 mL, 653 mmol) was added and the reaction was stirred at room temperature overnight. The volatiles were evaporated under reduced pressure, where after the crude product was dissolved in $CHCl_3$ and dried under reduced pressure for two times to obtain a product of FmocHN-TTAT-COOH (**16a**) as an orange solid.

*FmocHN-TTAT-COOPh$F_5$ (**16b**)*

FmocHN-TTAT-COOH (**16a**) was dissolved in $CHCl_3$ (150 mL). DIPEA (6 mL, 34.4 mmol) and an excess of pentafluorophenyl trifluoroacetate (0.95 mL, 5.53 mmol) were added, and the reaction was stirred at r.t. for 2 hours. The reaction mixture was washed with aq. 10% citric acid-solution (pH 3-5) (3 x 100 mL), $H_2O$ (3 x 100 mL), brine (3 x 100 mL), dried (MgSO4), and evaporated under reduced pressure to obtain FmocHN-TTAT-OPfp (**16b**) (5.44 g).

*FmocHN-TTATTTAT-COOtBu (**17**)*

FmocHN-TTAT-COOPh$F_5$ (**16b**) and $H_2$N-TTAT-*t*Bu (**15**) were dissolved in DMF (100 mL) and the reaction was stirred at room temperature for 1 hour. $CHCl_3$ (150 mL) was added to the reaction mixture and the DMF was washed out with $H_2O$ (1 x 100 mL & 2 x 150 mL), and brine (3 x 100 mL) before the organic layer was dried ($Na_2SO_4$) and evaporated under reduced pressure. The residue was washed with *n*-pentane and dried *in vacuo* (40 °C) overnight to remove the DMF. The solid product was purified by column chromatography (Acetone, 100%, $CHCl_3$-MeOH, 95:5%, up to $CHCl_3$-MeOH, 70:30%) to obtain FmocHN-TTATTTAT-COO*t*Bu (**17**) (980 mg, 39 %) as yellow solid.

$^1$H NMR (400 MHz, DMSO-$d_6$): δ = 8.42 – 7.22 (m, 24H), 5.83 (dddd, *J* = 15.6, 13.6, 6.8, 3.5 Hz, 18H), 5.16 (dd, *J* = 42.7, 13.8 Hz, 36H), 4.24 (dq, *J* = 17.6, 8.8, 8.1 Hz, 11H), 3.91 (d, *J* = 5.2 Hz, 36H), 3.84 (d, *J* = 5.5 Hz, 4H), 3.71 – 3.50 (m, 36H), 3.07 (q, *J* = 2.4 Hz, 2H), 2.16 (d, *J* = 18.7 Hz, 16H), 1.77 (dd, *J* = 74.9, 20.8 Hz,

16H), 1.37 (s, 9H). $^{13}$C NMR (100 MHz, DMSO-$d_6$): δ = 135.59, 128.11, 116.85, 116.78, 81.38, 73.48, 71.95, 71.92, 68.22, 60.13, 28.19. IR ν ($cm^{-1}$) 3273 (N-H stretching), 3075 (Ar C-H stretching), 2929, 2859 (aliphatic C-H stretching), 1729 (C=O ester stretching), 1690, 1660, 1634 (C=O amide stretching), 1533 (amide II), 1449, 1254, 1139, 1084, 989, 923, 738, 600. MALDI-TOF (m/z) calculated for $C_{143}H_{208}NaN_{16}O_{37}$, $[M+Na]^+$ = 2765.48, Obs. $[M+Na]^+$ = 2765.53.

*Bis((S)-3,7-dimethyloctyl)-(11-hydroxyundecyl)-BTA (**21**)*

Bis((*S*)-3,7-dimethyloctyl)-(undec-10-en-1-yl)-BTA (**20**) (516 mg, 0.81 mmol) was placed in a flame-dried round-bottomed flask, which was attached to the Schlenk line, evacuated and filled with dry argon. Under argon atmosphere, the substrate was dissolved in dry THF (15 mL) and the solution was placed in an ice bath and cooled to 0 °C. 9-Borabicyclo[3.3.1]nonane (5 mL, 0.5 M in THF) was added dropwise and the reaction was stirred under argon at r.t. for 2 hours. After a full conversion, the reaction was cooled back down to 0 °C and 6 M NaOH-solution (2.7 mL), and $H_2O_2$-solution (1.5 mL, 30 wt% in $H_2O$) were added. After the reaction was completed, the mixture was diluted with EtOAc (100 mL), washed with $H_2O$ (2 x 100 mL), brine (2 x 100 mL), and dried ($MgSO_4$). The crude product was purified by column chromatography (DCM, 100%, up to DCM-(10% isopropanol in EtOAc), 90:10%) to obtain bis((*S*)-3,7-dimethyloctyl)-(11-hydroxyundecyl)-BTA (**21**) (0.45 g, 85%).

Bis((*S*)-3,7-dimethyloctyl)-(11-methylsulfonateundecyl)-BTA *(**22**)*

(Dimethyloctylamide)$_2$-BTA-OH (**21**) (450 mg, 0.68 mmol) was dissolved in DCM (30 mL), and methanesulfonyl chloride (0.26 mL, 3.36 mmol) and pyridine (0.31 mL, 3.83 mmol) were added. The reaction was stirred at r.t. overnight. After the reaction was completed, the mixture was diluted with DCM (70 mL), washed with 1 M HCl-solution (2 x 80 mL), $H_2O$ (2 x 80 mL), brine (2 x 80 mL), and dried ($MgSO_4$). The solvents were evaporated under reduced pressure to obtain bis((*S*)-3,7-dimethyloctyl)-(11-methylsulfonateundecyl)-BTA (**22**).

*Bis((S)-3,7-dimethyloctyl)-(11-azidoundecyl)-BTA (**23**)*

Bis((*S*)-3,7-dimethyloctyl)-(11-methylsulfonateundecyl)-BTA (**22**) was dissolved in dry DMF (20 mL), where after sodium azide (113.3 mg, 1.74 mmol) and a potassium iodide (approximately 1 mg) were added. The reaction was stirred overnight at 50 °C. The temperature was increased to 70 °C to complete full conversion. The mixture was diluted with EtOAc (100 mL), washed with $H_2O$ (2 x 100 mL), brine (2 x 100 mL), and dried ($MgSO_4$). The solvents were evaporated under reduced pressure. The crude product was purified by column chromatography ($CHCl_3$, 100%, up to DCM-(10% isopropanol in EtOAc), 90:10%) to obtain bis((S)-3,7-dimethyloctyl)-(11-azidoundecyl)-BTA (**23**) (391 mg, 84%) as a yellow sticky solid.

$^1$H NMR (400 MHz, $CDCl_3$): δ = 8.33 (s, 3H), 6.37 (dt, *J* = 16.1, 5.6 Hz, 3H), 3.61 – 3.39 (m, 6H), 3.25 (t, *J* = 6.9 Hz, 1H), 1.81 – 1.07 (m, 42H), 0.95 (d, *J* = 6.5 Hz, 6H), 0.87 (d, *J* = 6.6 Hz, 12H). $^{13}$C NMR (100 MHz, $CDCl_3$): δ = 165.52, 135.28, 127.85, 51.49, 45.20, 40.39, 39.24, 38.53, 37.12, 36.63, 30.74, 29.55, 29.45, 29.27, 29.12, 28.84, 27.96, 26.97, 26.71, 24.63, 22.70, 22.60, 19.49. IR ν ($cm^{-1}$) 3237 (N-H stretching), 3073 (Ar C-H stretching), 2925, 2855 (aliphatic C-H stretching), 2095 (azide stretching), 1637 (C=O stretching), 1557 (amide II), 1462, 1382, 1366, 1297, 1146, 1069, 906, 799, 729, 691, 558.

*FmocHN-A-tBu-triazoleundecyl-bis((S)-3,7-dimethyloctyl)-BTA (**24**).*

FmocHN-Glu(CO*OtBu*)-propargylamide (**5**) (18.3 mg, 0.04 mmol), **23** (28 mg, 0.04 mmol) and $CuSO_4$ (1.19 mg, 0.007 mmol) were dissolved in DMSO (0.5 mL) to obtain a green colored solution. (+)-Sodium L-ascorbate (2 mg, 0.010 mmol) was added and the yellow colored mixture was stirred at 50 °C overnight under an argon atmosphere. After conversion check by TLC (DCM:EtOAc 80:20%) additional $CuSO_4$ (1.2 mg, 0.008 mmol) and (+)-sodium L-ascorbate (1 mg, 0.005 mmol) in 5 drops of $H_2O$ was added to the reaction mixture. The clouded reaction mixture, which contained red particles, was further stirred at 50 °C overnight under an argon atmosphere. After IR analysis, no absorption band of azide group (ν -$N_3$ 2095 $cm^{-1}$) was present. The reaction mixture was diluted in $CHCl_3$ (70 mL), washed with 0.1 M EDTA-solution (2 x 50 mL), $H_2O$ (1 x 50 mL), brine (1 x 50 mL), and dried ($MgSO_4$). The solvents were evaporated under reduced pressure. The product was isolated by column chromatography (DCM, 100%, up to DCM-(10% isopropanol in EtOAc) (80:20%)) to obtain FmocHN-A-*t*Bu-triazoleundecyl-bis((*S*)-3,7-dimethyloctyl)-BTA (**24**) (15.6 mg, 34%) as a white solid.

$^1$H NMR (400 MHz, $CDCl_3$): δ = 8.44 – 8.29 (m, 3H), 7.80 – 7.70 (m, 2H), 7.62 – 7.53 (m, 2H), 7.50 (s, 1H), 7.39 (tt, J = 7.8, 1.7 Hz, 2H), 7.32 – 7.27 (m, 2H), 7.18 (s, 1H), 6.79 (s, 1H), 6.58 (s, 2H), 5.91 (d, J = 7.7 Hz, 1H), 4.53 (d, J = 5.7 Hz, 2H), 4.42 – 4.07 (m, 6H), 3.47 (tt, J = 13.8, 6.4 Hz, 6H), 2.31 (ddt, J = 23.5, 16.2, 7.3 Hz, 2H), 2.17 – 1.75 (m, 4H), 1.73 – 1.47 (m, 10H), 1.43 (s, 11H), 1.38 – 1.06 (m, 28H), 0.93 (d, J = 6.5 Hz, 6H), 0.86 (d, J = 6.6 Hz, 13H). $^{13}$C NMR (100 MHz, $CDCl_3$): δ = 165.69, 144.46, 141.27, 135.33, 135.26, 128.02, 127.74, 127.08, 125.09, 122.03, 119.99, 81.03, 50.31, 47.13, 40.34, 39.24, 38.53, 37.13, 36.62, 35.16, 31.73, 30.75, 30.01, 29.38, 28.07, 28.00, 27.95, 26.71, 26.10, 24.63, 22.70, 22.60, 19.47. MALDI-TOF (m/z) calculated for $C_{67}H_{100}NaN_8O_8$, $[M+Na]^+$ = 1167.76, Obs. $[M+Na]^+$ = 1167.76.

*N-(tert-butyloxycarbonyl)tris[(allyloxy)methyl]aminomethane-tridecylsulfane (**25**)*

*N*-(*tert*-butyloxycarbonyl)tris[(allyloxy)methyl]aminomethane (**3**) (110.3 mg, 0.32 mmol) was dissolved in THF (10 mL), and 1-decanethiol (0.6 mL, 4.18 mmol) and 2,2-dimethoxy-2-phenylacetophenone (114.7 mg, 0.45 mmol) were added before the mixture was purged with argon for 10 minutes. After purging, the reaction mixture was stirred for 4 hours at room temperature under UV light (315-400 nm). The solvent was evaporated under reduced pressure and the product was isolated by column chromatography (DCM-EtOAc, 90:10% up to EtOAc, 100 %) to give *N*-(*tert*-butyloxycarbonyl)tris[(allyloxy)methyl]aminomethane-tridecylsulfane (**25**) (129 mg, 51%) as a yellow oil.

$^1$H NMR (400 MHz, $CDCl_3$): δ = 4.92 (s, 1H), 3.63 (s, 6H), 3.50 (t, J = 6.1 Hz, 6H), 2.53 (dt, J = 24.1, 7.4 Hz, 12H), 1.89 – 1.76 (m, 6H), 1.65 – 1.50 (m, 8H), 1.47 – 1.18 (m, 52H), 0.95 – 0.82 (m, 9H).

*FmocHN-(TTAT)$_2$-tBu-triazoleundecyl-bis((S)-3,7-dimethyloctyl)-BTA (**26**)*

FmocHN-TTATTTAT-CO*O*t*B*u (**17**) (48.4 mg, 0.018 mmol) and (dimethyloctylamide)$_2$-BTA-azide (**23**) (27.3 mg, 0.04 mmol) were separately dissolved in DMSO (0.5 mL). Both solutions were added to $CuSO_4$ (0.68 mg, 0.0043 mmol) and stirred at 50 °C under an argon atmosphere until $CuSO_4$ was completely dissolved. To the green colored solution, (+)-sodium L-ascorbate (1.9 mg, 0.0094 mmol) was added and the mixture was stirred at 50 °C until (+)-sodium L-ascorbate was dissolved. The reaction was consecutively stirred overnight at r.t. under an argon atmosphere. The reaction mixture was diluted in $CHCl_3$ (70 mL), washed with 0.1 M EDTA-solution (2 x 50 mL), $H_2O$ (2 x 50 mL), brine (2 x 50 mL), and dried ($MgSO_4$). The solvents were evaporated under reduced pressure. The product was isolated by column chromatography ($CHCl_3$, 100%, up to $CHCl_3$-MeOH, 95:5%) to obtain 59.4 mg of the colorless sticky solid. The analysis of the $^1$H NMR-spectrum, showed that the product consisted out of ~40% monofunctionalized octamer and ~60%

bifunctionalized octamer. IR measurements of the BTA-azide fraction (7.3 mg), obtained from column chromatography, showed no azide band. MALDI-TOF spectra showed a mixture of substrate, monofunctionalized and bifunctionalized octamer. To obtain 100% conversion, the functionalized octamer mixture and (dimethyloctylamide)$_2$-BTA-azide (**23**) (13.1 mg, 0.02 mmol) were separately dissolved in DMSO (0.5 mL). Both solutions were added to $CuSO_4$ (1.11 mg, 0.007 mmol) and stirred at 50 °C under an argon atmosphere until $CuSO_4$ was dissolved. To the green colored solution, sodium ascorbate (4.38 mg, 0.022 mmol) was added and the mixture was stirred for 2 days at r.t. under an argon flow. The reaction mixture was purified with the same procedure as earlier described to obtain FmocHN-(TTAT)$_2$-*t*Bu-triazoleundecyl-bis((S)-3,7-dimethyloctyl)-BTA (**26**) (26.9 mg, 37%) as a white solid.

$^1$H NMR (400 MHz, $CDCl_3$): δ = 8.61 (t, J = 5.7 Hz, 6H), 8.46 (s, 2H), 8.35 (s, 6H), 8.00 – 7.67 (m, 13H), 7.52 – 7.25 (m, 10H), 5.90 – 5.73 (m, 18H), 5.26 – 5.04 (m, 36H), 4.27 (dd, J = 12.0, 6.4 Hz, 18H), 3.90 (dq, J = 5.2, 1.7 Hz, 36H), 3.69 – 3.51 (m, 36H), 2.14 (s, 16H), 1.92 – 1.41 (m, 40H), 1.36 (s, 9H), 1.35 – 1.05 (m, 67H), 0.89 (d, J = 6.4 Hz, 13H), 0.83 (d, J = 6.6 Hz, 26H). IR ν ($cm^{-1}$) 3276 (N-H stretching), 3076 (Ar C-H stretching), 2926, 2854 (aliphatic C-H stretching), 1731 (C=O ester stretching), 1659, 1634 (C=O amide stretching), 1538 (amide II), 1449, 1366, 1256, 1138, 1087, 990, 923, 734, 691, 599. MALDI-TOF (m/z) calculated for $C_{222}H_{348}NaN_{28}O_{43}$, $[M+Na]^+$ = 4131.59, Obs. $[M+Na]^+$ = 4131.48.

*Fmoc-(TTAT)$_2$-tBu-triazoleundecyl-bis((S)-3,7-dimethyloctyl)-BTA-decylsulfane (**27**)*

Fmoc-(TTAT)$_2$-*t*Bu-triazoleundecyl-bis((S)-3,7-dimethyloctyl)-BTA (**26**) (15 mg, 3.65 µmol), 1-decanethiol (0.05 mL, 0.24 mmol), and DMPA (8.8 mg, 0.034 mmol) were dissolved in dimethylacetamide (1 mL) and purged with argon for 10 minutes. After purging, the colorless reaction mixture was stirred for 4 hours at r.t. under UV light (315-400 nm). The yellow colored mixture was diluted with $CHCl_3$ (70 mL), washed with $H_2O$ (2 x 50 mL), brine (50 mL), dried ($MgSO_4$), where after the organic layer was evaporated under reduces pressure. The residual liquid product was diluted in EtOAc (70 mL), washed with $H_2O$ (3 x 50 mL), brine (50 mL), dried ($MgSO_4$), where after the organic layer was evaporated under reduces pressure. The crude product was subjected to column chromatography ($CHCl_3$, 100%, up to $CHCl_3$-(10% isopropanol in EtOAc) (50:50%)) to obtain a colorless sticky solid title compound **27** (8.3 mg, 31%).

$^1$H NMR (400 MHz, $CDCl_3$): δ = 8.97 (d, J = 51.9 Hz, 1H), 8.35 (d, J = 7.9 Hz, 6H), 8.22 (s, 1H), 7.73 (d, J = 7.6 Hz, 1H), 7.62 (dd, J = 15.6, 8.2 Hz, 3H), 7.37 (t, J = 7.4 Hz, 2H), 6.79 (qd, J = 76.3, 49.0, 43.3 Hz, 17H), 4.75 (s, 2H), 4.27 (d, J = 27.4 Hz, 14H), 3.89 – 3.56 (m, 36H), 3.46 (dq, J = 13.7, 6.0 Hz, 49H), 3.32 (d, J = 5.1 Hz, 3H), 2.88 (s, 1H), 2.59 – 2.42 (m, 72H), 2.33 (d, J = 52.1 Hz, 18H), 1.80 (dt, J = 12.0, 5.7 Hz, 37H), 1.72 (s, 25H), 1.53 (dq, J = 13.3, 7.3, 6.8 Hz, 54H), 1.43 (s, 15H), 1.26 (s, 332H), 1.18 – 1.04 (m, 19H), 0.93 (dd, J = 6.6, 1.7 Hz, 13H), 0.90 – 0.83 (m, 85H). IR ν ($cm^{-1}$) 3263 (N-H stretching), 3069 (Ar C-H stretching), 2922, 2853 (aliphatic C-H stretching), 1728 (C=O ester stretching), 1642 (C=O amide stretching), 1550 (amide II), 1464, 1366, 1295, 1107, 905, 721, 692. MALDI-TOF (m/z) calculated for $C_{403}H_{744}NaN_{28}O_{43}S_{18}$, $[M+Na]^+$ = 7268.19, Obs. $[M+Na]^+$ = 7269.65, $[M+K]^+$ = 7284.9, Obs. $[M+K]^+$ = 7285.42.

### 6.6.2.2 Solid-phase synthesis based on thiolactone chemistry

***Synthesis of the building blocks:***

(*S*)-3,7-dimethyloctylacrylate (**28**)

(*S*)-3,7-dimethyloctan-1-ol (10 g, 63 mmol) and trimethylamine (12.7 g, 126 mmol) were dissolved in DCM (200 mL) and cooled to 0 °C. Then acryloyl chloride (6.29 g, 69 mmol) was added dropwise and the mixture

was stirred overnight at room temperature. On completion the reaction mixture was diluted with 300 mL of DCM, washed with aqueous 1M HCl (300 mL) water (300 mL) and brine (300 mL). Organic layer was dried over magnesium sulfate and solvent was removed under reduced pressure to give 7.1 g of brown oil as crude product. Title compound was isolated by column chromatography using gradient elution (petroleum ether 100% to petroleum ether / EtoAc 95:5 vol) to give 5.5 g of a colorless oil. The yield was 41%.

$^1$H NMR (400 MHz, $CDCl_3$): δ = 8.30 (s, 3H), 6.35 (m, 4H), 6.12 (m, 1H), 5.78 (m, 1H), 4.05 (m, 2H), 1.66 (m, 1H), 1.48(m, 4H), 1.30 (m, 3H), 1.05 (m, 2H), 0.89 (d, *J* = 6.6 Hz, 3H), 0.86 (d, *J* = 6.6 Hz, 6H).

11-(3,5-bis(((S)-3,7-dimethyloctyl)carbamoyl)benzamido)undecyl acrylate (**29**)

(*S*)-BTA-alcohol (**21**) (0.5 g, 0.76 mmol) and trimethylamine (0.15 g, 1.5 mmol) were dissolved in DCM (10 mL) and cooled to 0 °C. Then acryloyl chloride (0.76 g, 0.83 mmol) was added dropwise and the mixture was stirred overnight at room temperature. On completion the reaction mixture was diluted with 20 mL of DCM, washed with aqueous 1M HCl (30 mL) water (30 mL) and brine (30 mL). Organic layer was dried over magnesium sulfate and solvent was removed under reduced pressure to give 0.51 of yellow solid as crude product. Title compound was isolated by column chromatography using gradient elution (DCM 100% to DCM / EtoAc 9:1 vol) to give 450 mg of colorless, waxy solid with 83% yield.

$^1$H NMR (400 MHz, $CDCl_3$): δ = 6.30 (m, 1H), 6.12 (m, 1H), 5.78 (m, 1H), 4.16 (m, 2H), 3.45 (m, 6H), 1.79, 1.60 – 1.05 (m, 38H), 0.87 (d, *J* = 5.2 Hz, 6H), 0.81 (d, *J* = 5.2 Hz, 12H)

***General protocol for the manual solid-phase synthesis***

*Step 1: Aminolysis and incorporation of functionalities*

$CHCl_3$ was added to the solid support (1 mL reaction mixture per 100 mg resin). Next, the acrylate (20 equivalents relative to the thiolactone unit) and ethanolamine (10 equivalents) were added. This mixture is shaken for 15 minutes at room temperature. This procedure is repeated once more to be sure of the full conversion of the thiolactone. After this second procedure, the resin is washed with DMF (4x), methanol (4x), $CHCl_3$ (4x) and diethyl ether (4x) and dried.

*Step 2: Chain extension*

Dried $CHCl_3$ is added to the solid support (1 mL reaction mixture per 100 mg resin), then the α-isocyanato-γ-thiolactone (10 eq. relative to the resin-bound alcohol-units) and dibutyltin dilaurate (0,025 eq. relative to the resin-bound alcohol-units) are added. This mixture is shaken for 1 hour. Afterwards, the resin is washed with DMF (4x), MeOH (4x), $CHCl_3$ (4x) and diethyl ether (4x) and dried.

*Cleveage:*

Solid support was trated with 10 mL of 1% trifluoroacetic acid in DCM for 5 minutes. During cleavage, the color of the beads turns from yellow to red due to the formation of a trityl cation. The solid support was then filtered off, the filtrate was collected and concentrated under reduced pressure to yield the heptamer **30**. without further purification.

Heptamer **30** ($O_3BO_3$)

$^1$H NMR (500 MHz, THF-$d_8$): δ = 8.40 (s, 1H), 8.01 (m, 3H), 7.68 (bs, 7H), 6.84 (bs, 7H), 4.21 (m, 14H), 4.10 (m, 21H), 3.94 (m, 9H), 3.42 (m, 20H), 3.24 (m, 4H), 2.75 (m, 16H), 2.56 (m, 30H), 2.06 (m, 14H), 1.70 – 1.10 (m, 38H), o (m, 12H). IR ν ($cm^{-1}$) 3318 (N-H stretching), 1711 (C=O ester stretching), 1650 (C=O amide stretching), 1534 (amide II). ESI-MS (m/z) calculated for $C_{178}H_{316}N_{18}O_{41}S_9$ $[M+H]^+$ = 3652, Obs. $[M/2+2H]^{2+}$ = 1826.

## 6.6 References


[1] G. Polymeropoulos, G. Zapsas, K. Ntetsikas, P. Bilalis, Y. Gnanou, N. Hadjichristidis, *Macromolecules* **2017**, *50*, 1253–1290.

[2] K. Matyjaszewski, J. Xia, *Chem. Rev.* **2001**, *101*, 2921–90.

[3] S. Perrier, *Macromolecules* **2017**, *50*, 7433–7447.

[4] R. B. Grubbs, R. H. Grubbs, *Macromolecules* **2017**, *50*, 6979–6997.

[5] A. Saint-Léger, C. Bello, P. D. Dans, A. G. Torres, E. M. Novoa, N. Camacho, M. Orozco, F. A. Kondrashov, L. Ribas de Pouplana, *Sci. Adv.* **2016**, *2*, e1501860.

[6] T. N. Starr, J. W. Thornton, *Nat. Biotechnol.* **2017**, *35*, 125–126.

[7] J. F. Lutz, M. Ouchi, D. R. Liu, M. Sawamoto, *Science* **2013**, *341*, 1238149.

[8] J. F. Lutz, *Macromol. Rapid Commun.* **2017**, *38*, 1700582.

[9] B. Merrifield, *Science* **1986**, *232*, 341–347.

[10] R. B. Merrifield, *J. Am. Chem. Soc.* **1963**, *85*, 2149–2154.

[11] S. L. Beaucage, R. P. Iyer, *Tetrahedron* **1992**, *48*, 2223–2311.

[12] A. S. Knight, E. Y. Zhou, M. B. Francis, R. N. Zuckermann, *Adv. Mater.* **2015**, *27*, 5665–5691.

[13] R. N. Zuckermann, J. M. Kerr, S. B. H. Kent, W. H. Moos, *J. Am. Chem. Soc.* **1992**, *114*, 10646–10647.

[14] N. F. König, A. Al Ouahabi, S. Poyer, L. Charles, J. F. Lutz, *Angew. Chem. Int. Ed.* **2017**, *56*, 7297–7301.

[15] P. Espeel, L. L. G. Carrette, K. Bury, S. Capenberghs, J. C. Martins, F. E. Du Prez, A. Madder, *Angew. Chem. Int. Ed.* **2013**, *52*, 13261–13264.

[16] S. Martens, J. Van den Begin, A. Madder, F. E. Du Prez, P. Espeel, *J. Am. Chem. Soc.* **2016**, *138*, 14182–14185.

[17] P. Espeel, F. E. Du Prez, *Eur. Polym. J.* **2015**, *62*, 247–272.

[18] J. M. Palomo, *RSC Adv.* **2014**, *4*, 32658–32672.

[19] S. C. Solleder, M. A. R. Meier, *Angew. Chem. Int. Ed.* **2014**, *53*, 711–714.

[20] S. C. Solleder, K. S. Wetzel, M. A. R. Meier, *Polym. Chem.* **2015**, *6*, 3201–3204.

[21] M. Porel, C. A. Alabi, *J. Am. Chem. Soc.* **2014**, *136*, 13162–13165.

[22] S. Binauld, D. Damiron, L. A. Connal, C. J. Hawker, E. Drockenmuller, *Macromol. Rapid Commun.* **2011**, *32*, 147–168.

[23] S. Binauld, C. J. Hawker, E. Fleury, E. Drockenmuller, *Angew. Chem. Int. Ed.* **2009**, *48*, 6654–6658.

[24] N. Franz, L. Menin, H. A. Klok, *European J. Org. Chem.* **2009**, 5390–5405.

[25] D. Seebach, M. G. Fritz, *Int. J. Biol. Macromol.* **1999**, *25*, 217–236.

[26] S. S. Reddy, X. Dong, R. Murgasova, A. I. Gusev, D. M. Hercules, *Macromolecules* **1999**, *32*, 1367–1374.

[27] G. M. Brooke, S. Mohammed, M. C. Whiting, *Polymer* **1999**, *40*, 773–788.

[28] P. Espeel, F. E. Du Prez, *Macromolecules* **2015**, *48*, 2–14.

[29] P. J. M. Stals, M. M. J. Smulders, R. Martín-Rapún, A. R. A. Palmans, E. W. Meijer, *Chem. Eur. J.* **2009**, *15*, 2071–2080.

[30] M. Kudo, V. Maurizot, H. Masu, A. Tanatani, I. Huc, *Chem. Commun.* **2014**, *50*, 10090–10093.

[31] A. Barth, *Biochim. Biophys. Acta* **2007**, *1767*, 1073–1101.

# Summary

Ultimate functionality of biomacromolecules is provided by unparalleled control over their supramolecular structures. These highly ordered structures are regulated by multiple weak interactions, with a significant role of water as the medium for supramolecular assembly. Synthetic supramolecular systems based on the assemblies of small molecules or macromolecules permit to create new generation of functional materials. However, similarly to Nature, to arrive at *function*, the *structure* has to be controlled beforehand. Thus the interactions with solvents are equally important and have to be understood before the next step is made. In this thesis, we study the influence of solvents on the supramolecular assemblies based on helical aggregates.

In Chapter 1, the role of solvents in supramolecular polymer chemistry is introduced. For clarity, we separate the discussion on two parts. First, we highlight the assembly of oligomers and macromolecules with emphasis on how seemingly small changes in the solvent affect the supramolecular structure. Further, we discuss the assembly of small molecules into supramolecular polymers. The vital role of solvents therein is exemplified by polymorphism in the structures provided by differential interactions with solvents. In the last part, we briefly introduce the control of pathway complexity (kinetics versus thermodynamics) via interactions with solvents. Finally, application of optically active solvents in supramolecular polymer chemistry is highlighted.

In Chapter 2, we show the synthesis of novel supramolecular motif based on a $C_3$-symmetrically substituted triphenylene core decorated with amide groups. With use of robust amide coupling strategy, aliphatic, oligo(ethylene glycol), homo- and heterotelechelic oligo(dimethyl siloxane) chains are attached, affording a series of triphenylene-2,6,10-tricarboxamide (TTA) derivatives. By combination of spectroscopy, microscopy and calorimetry methods we show that TTAs assemble via hydrogen-bonds in a columnar fashion and show an increased stability compared to their benzene-1,3,5-tricarboxamide (BTA) analogues.

In Chapter 3, we study the influence of the solvent quality on the supramolecular polymerization of alkyl-TTAs in dilute solution of decalin and chloroform. With use of spectroscopy methods we confirm that similarly to the BTAs, TTAs assemble in solution in a helical fashion via three-fold hydrogen bond formation. The higher stability of the TTA-based polymers is reflected by the presence of supramolecular polymers at micromolar concentrations upon addition of chloroform up to 40%. Sergeants-and-soldiers and majority-rules experiments show that strong amplification of supramolecular chirality in TTAs is possible only by addition of chloroform. Further analysis show that high amplification of supramolecular chirality is thermodynamically favored, but in decalin the system has a strong

tendency to fall into kinetic traps. We use this property to kinetically trap achiral monomers in the aggregates of single helicity. To achieve this, we prepare supramolecular polymers of achiral monomer in a mixture of decalin and volatile optically active solvent. The latter was subsequently removed and thereby obtained polymers showed high kinetic stability illustrated by a half-life of more than 40 days.

In Chapter 4, we use optically active solvents to break the mirror symmetry between TTA enantiomers. Inspired by van't Hoff and Pasteur, we show that weak interactions of supramolecular polymers with solvents, expressed as solvation, can be exploited to control supramolecular structure. Even though no change in the amide conformation is observed, a sharp transition between two helical states is occurs. When an optically active solvent is employed, the solvation is stereospecific with respect to the helicity and favors one helicity over the other. Copolymerization of the enantiomers highlights the diastereomeric relationship in optically active solvents. This is reflected by the temperature at which any mixture of the enantiomers always polymerizes with excess of the same helicity.

In Chapter 5, we study the assembly of poly(dimethyl siloxane) decorated with the BTA-pendant grafts. We observed aggregation of the BTAs in chloroform, a solvent normally suppressing aggregation. Variable-temperature circular dichroism spectroscopy in 1,2-dichloroethane showed that high cooperativity of the BTA aggregation was achieved for the longest polymers with the lowest degree of functionalization. Extensive spectroscopic analysis showed that the nucleation of the BTA aggregates occurs at the level of single chains that is followed by further clustering of the polymers into larger particles. The cooperative aggregation is attributed to the strong phase-segregation between the PDMS backbone and the BTAs, in combination with a high propensity of these polymers to form multi-chain aggregates.

The aim of work summarized in Chapter 6 is to arrive at perfect-discrete and sequence-defined oligomers with the aim to study the intramolecular folding. Two synthetic strategies comprising solution-phase, divergent-convergent approach and solid-phase synthesis were employed. The first methodology was shown to be successful in the synthesis of a sequence-defined octamer that was functionalized with BTA via a post-functionalization strategy using "click" chemistry. Further elongation of the oligomer was hampered by the low solubility of the backbone. In the second strategy, we utilized thiolactone chemistry to synthesize BTA-functionalized heptamer on a solid support. Aggregation of the BTA pendants was studied by circular dichroism spectroscopy in dilute solutions. The mechanism of aggregation was found to be highly dependent on the backbone nature and substitution pattern. The limited solubility of the octamers constitute a major limit of the approach. As a result, sequence control and folding of complex macromolecular structures remains a challenging endeavor.

# Curriculum vitae

Marcin Ślęczkowski was born on 11-03-1990 in Kędzierzyn-Koźle, Poland. After finishing secondary education in 2009 at Drugie Liceum Ogólnokształcące in Zabrze, Poland, he studied Industrial and Engineering Chemistry at Silesian University of Technology in Gliwice, Poland. During his bachelor studies, he performed the graduation internship in 2013, under the supervision of dr. ir. Nikodem Kuźnik, where he worked on organic synthesis of Iron (III) complexes as a new class of contrast agents in MRI spectroscopy. Before completing his higher education with M. Sc. diploma in 2014 at the same university, he worked as visiting student in the groups of dr. Eugen Stulz (University of Southampton, UK, 2011), dr. Fabrice Mathevet (University Pierre and Marie Curie, Paris, France, 2012) and dr. Peter Jarowski (University of Surrey, Guildford UK, 2013). During his master research, he studied the synthesis and self-assembly of π-conjugated imine-imide systems in the group of prof. dr. Ewa Schab-Balcerzak (Centre of Polymer and Carbon Materials, Polish Academy of Sciences, Zabrze, Poland). After obtaining his master degree, he worked as Junior Synthesis Specialist at Selvita (Kraków, Poland). In September 2015, he started a PhD project under the supervision of prof. dr. E.W. (Bert) Meijer and prof. dr. ir. A.R.A. (Anja) Palmans in the Laboratory of Macromolecular and Organic Chemistry and Institute for Complex Molecular Systems at TU/e. In 2017, he worked for 1 month in the group of prof. dr. Filip Du Prez at the Ghent University, Belgium. His research focused on the pivotal role of solvents in supramolecular assembly. He studied in detail the influence of weak interactions of (supramolecular) polymers with solvents on the kinetics and thermodynamics of supramolecular polymerization. The most important results are presented in this dissertation.

# List of publications

*Cooperativity as a missing element in van't Hoff's puzzle to find a difference between enantiomers in optically active solvents*, M. L. Ślęczkowski, M. F. J. Mabesoone, A. R. A. Palmans, E. W. Meijer, *To be submitted,* **2019**

*Supramolecular Chirality of Triphenylene-2,6,10-tricarboxamides: Kinetic and Thermodynamic Control by Solvent Engineering*, M. L. Ślęczkowski, M. F. J. Mabesoone, Y. Post, E. W. Meijer, A. R. A. Palmans, *Manuscript in preparation*, **2019**

*Tuning Polymer Properties of Non-Covalently Crosslinked Poly(dimethyl siloxane) by Varying Supramolecular Interactions Strength,* B. A. G. Lamers, M. L. Ślęczkowski, F. Wouters, E. W. Meijer, A. R. A. Palmans, *Manuscript in preparation*, **2019**

*Synthesis and characterization of stereo- and sequence-defined oligomers based on thiolactone ring-opening chemistry,* C. Mertens, M. Soete, M. L. Ślęczkowski, E. W. Meijer, A. R. A. Palmans, F. Du Prez, *Manuscript in preparation*, **2019**

*Cooperative Folding of Linear Poly(dimethyl siloxane)s via Supramolecular Interactions,* M. L. Ślęczkowski, E. W. Meijer, A. R. A. Palmans, *Macromol. Rapid. Commun*. 1700566, **2017**

# Acknowledgements

Because I am quite emotional person, I have to mention many people who deserve to be acknowledged in the last words of this thesis. As such it turned out that this part became actually a separate Chapter. Herein, I am proud to introduce the longest Acknowledgements ever.

There is an universal truth that *the time catches up with everyone*. So after 4 years at MST, it caught up with me to finish this fruitful and unforgettable period. Maybe not an each day was a success, maybe many things could have been done better. But on the 1st of September 2015, I promised myself that I would enjoy every single day of my PhD. And I can proudly announce that I did it! Obviously, it could have not been possible without all of you, therefore the last words of this thesis I will address to all of the great people who made me enjoying PhD life, even when science would not favor.

At the first place, I would like to thank my promotor, prof. Bert Meijer for giving me the opportunity to become a member of the inspiring group of MST. Bert, I still remember the day in June 2015, when you would offer me a position and I remember how enthusiastic about it I was, even though having very little idea of how it might look like. I will repeat until the end that MST is one of the best places, one can consider to do science. Every meeting with you would end up with me sitting for an hour in the office, holding my head and analyzing, what we just established. The other time you would hold your head during the lunch meeting, when I came up with some of the experiments that maybe I should not have done. It's incredible that despite being busy with many other things, your office would be always open to come and talk about science or to listen endless number of anecdotes about famous scientists on conferences. Thank you for sharing the passion in my research. Thank you for your praise and criticism. You are a true leader and mentor. You helped me to become a better scientist and a better person.

I would like to thank my co-promotor, prof. Anja Palmans for everyday guidance and helping me to see my research in a broader perspective. Anja, I remember my interview and you telling me on the basis of Janus story that one carbon atom makes a go or no-go in the assembly of the BTAs. For a somebody not dedicated for such details at that time it was quite a shock. Thanks to your drive, eventually, I ended up doing research which is equally sensitive to small differences. I appreciate your impact and enthusiasm in my research and the endless number of tips on presentations and writing. Thank you for having your door always open. Thank you for being direct and straightforward, but at the same time positive. You come with a smile even, when you just arrived back from a 1 month-long holiday somewhere in Africa. I wish you a lot of the success as a well-deserved, full professor.

Also, I would like to thank prof. du Prez for the hospitality and letting me to do my secondment at the Ghent University. Dear Filip, it has been truly learning experience and I am happy that we decided to continue this collaboration with hopefully an end in a great paper.

Dear prof. Suginome, I would like to thank you for your interest and valuable remarks concerning my thesis. It is a great honor to have you in my committee. Thank you also for interesting suggestions during our first meeting at Solvay Conference in Brussels, which helped me to continue the work, described in Chapter 4. Also, thank you for taking the effort in travelling all the way from Japan and teach us an inspiring lesson on poly(quinoxaline-2,3-diyl)s.

Dear prof. Nolte, thank you for reading my thesis, your valuable comments and being a part of my committee. Dear prof. Sijbesma, thank you for your interest in my research, interesting feedback and being a part of my committee. Dear dr. Smulders, thank you for your detailed comments, suggestions to improve the quality of my thesis and being a member of the committee. Dear dr. Cantekin, thank you for reading my thesis, giving a valuable feedback and comments which made me to think about the details again. Also thank you for coming for my defense.

During my PhD I had an opportunity to work with fantastic people, who improved enormously the quality of the research output. Firstly, I spare few words to Mathijs. Jongen, thanks for your high interest in the TTAs since the very beginning, when the only people who truly believed in oncoming breakthrough were you and me. Your creativity and care for details were inspiring and I am really proud that ever since we made the TTAs big together. Brigitte, thanks for your interest and help with SAXS experiments with mentioned already TTAs. Your knowledge and excitement on completely unexpected results made Chapter 2 better. Also, thanks for keeping me involved in the follow-up of the PDMS-BTA story, it has been great to learn new things that are completely out of my original background. Yiliu, thanks for involving me in your project with sequence-defined oligomers. Your creativity, analysis and troubleshooting skills are so incredible that I know hardly anyone, who could come up with such complex and yet successful synthesis. Without you, this thesis would not have Chapter 6. Good luck with setting up your own group. I am convinced we will hear of you in scientific news soon. Also, many thanks for Steven, who was my tutor and guide in the laboratories in Ghent. Steven, thank you for your effort and drive for collaboration. Your amazing work has contributed to Chapter 6 enormously. I wish you all the best in your further steps. I also want to thank Chiel. It is a big pleasure to work with you. Thanks for keeping me involved in the activities and I hope we end up with beautiful, joint papers to reinforce the connection between Ghent and Eindhoven. I would like also to thank Chidambar for your interest in TTAs and many discussions including your critical remarks on my thoughts. Ghislaine, thank you for being so excited about the results and your endless suggestions on what we can still achieve with those molecules.

Next, I would like to thank the students, who contributed to this thesis with their hard work and dedication. Yorick, thanks for your effort in improving our understanding of the TTAs, which as you experienced yourself, sometimes can be tricky. I wish you good luck with your further career. Ian, if every student was so hard-working as you are, there would be no work in the lab for PhDs and post-docs. Thank you for your beautiful synthesis of the glutamamide oligomers (Chapter 6). It is good to know that you enjoy your new job in Leiden and I hope you will further develop. With your drive and skills you can become an outstanding chemist. Jorn, thanks for your early work with PDMS-BTA conjugates. I wish you all the best in the future. Eventually, I want to explicitly appreciate the efforts of the people joining the lunch meetings of Supramolecular Polymers and Materials, Single-Chain Polymeric Nanoparticles and Multi-Component, Non-Covalent Systems. You have to forgive me that I will not mention the names here. It has been great to have your comments and remarks on my daily progress and ideas on experiments. I enjoyed listening to every of your presentation. I would like also to thank all the rest of MST-people for joining the colloquia sharing your inspiring research as well as listening to my presentations, asking interesting questions and giving remarks.

I had a lot of luck that my PhD was a part of the Eurosequences project. I worked not only with great scientists but also great people. First of all, I thank prof. Lutz and Becer for establishing the network and creating a chance for young scientists to work in the exciting projects and thank you for constant drive to initiate collaboration between us. I would like to thank prof Leigh, prof. Borner, prof. Colquhoun,

prof. Behrends and dr. Stephane Joly for their interest in my work and all the discussions over my presentations during the project meetings. Obviously, I give also credits to all my Eurosequences brothers and sisters: Javier and Adrian, thanks for your hospitality in Manchester and good luck with finishing your PhD. Niklas, it was great to have you in Eindhoven for month. I enjoyed our bike trips and the barbeque. Yamin, you became a true member of our group after 1 day – incredible. Denise, you are great colleague, thanks for your hospitality in Strasbourg and good luck in Switzerland. Josh, thanks for our outs in Ghent and the interesting Brabants – Vlaams discussion done by two buitenlanders. Suzan, thanks for our unexpected extra shots one night in Freiburg. Also thanks to all of you: Gianni, Emmanuelle, Sensu, Marcus, Mordjane and Jeroen for all the after meeting evenings. We made the cities of Europe to live.

In the following part I would like to thank all the rest of the people, who contribute to the working atmosphere. Starting from my office-friends, STO 4.47. When I started my marriage with MST, our office would be purely PhD-based with Anneloes, Bram and Bas. Anneloes, thanks for all the discussions and your lessons of Dutch. Bram, thanks for sharing your experiences from nomad-like adventures and of course a memorable trip to Achel with Matsu. Bas, I enjoyed our discussions on chemistry. As the time passed, there would be new people joining STO 4.47. Thus many thanks Brigitte for not killing us for a hartjes on the flower on your first day at work. It was nice to have you in the office, even though short. Giulia, thanks for all our discussions on Italy and your criticism anytime I would claim that I cooked something Italian. You can hopefully find a good place to continue your career in Switzerland. Tomo, many thanks for being my first Japanese teacher. You have great sense of humor, so I did not have to explain my poor jokes. Pongphak, you are a great chemist and I learned a lot from your work.

As we now move outside the office, I would like to thank the rest of the people from Meijer group. I will start here with great Mykhailo. Misha, it was great to have you in the group and to share the experiences on Polish-Ukrainian border. I enjoyed your lessons in Ukrainian over a glass of Kwas (acid). I admire your skills in Polish! I wish you all the best with Yuliia and of course beautiful Diana. Elisabeth, I will remember long our Eurosequences trips. Thanks for all the evenings, parties and a lot of fun. You are truly people's person. Thanks for your dedication to whatever you do. Brigitte, I hope you will still win a KNVB beker – something I will not achieve. Thanks for all you have done to us outside science and especially for your amazing barbeque and help in noodsituatie (Weert mission). I hope I meet the legendary Joost once. Chidambar, besides your impact in science, I also owe you a lot for making me educated in Indian cuisine. Thank you for the amazing dinner that you organized for us one day in winter. Ghislaine, it's great to have somebody like you around. We had a lot of great time together. Thanks for taking care of one of my dear plants which otherwise would become homeless. My cousin (the brother of Gingi) also joins this acknowledgements, even though you did not want to speak to him in French at the MST Christmasafterparty 2015 at the Vooruitgang. Still we both wish you success in your further career. Bas (Robasjo), thanks for all the tips about siloxane chemistry and introducing me to amazing Dutch music such as André Hazes and Guus Meeuwis. Jolanda, thank you for all the knowledge you shared with me and for working hard on keeping the discipline, so our laboratories are still able to perform their function. Andreas (Dr Dre), Fabian and Julian, danke schön for being the German committee members and helping me to improve my skills in German. I would like also to thank José and Nic (Matsu), for all FORT- and nights-out. Bea, thank you for being so kind and making sure I would wake up on time for breakfast at our Eurosequences meetings. Jesús, thanks for being interested in developing further the TTAs. I hope, it will be a great success. I would like to thank Anjana, Cristiaan, Lafayette, Linlin, Sandra, Marle, Martin, Lu, Silvia, Hiro, Joost, Takuya, Ronald, Janus, Nate, Anindita, Helen, Andreas V, Andreas H, Simone, René, Tim,

Daan, Müge and Katja for creating fantastic and friendly environment in the group. You were always open and it was great to work with you!

In the whole MST (and outside), there are also people that have to be acknowledged. I would like to start with the Secretariat Team: Carla and Martina. Without your help, the start, the middle and the end would be undoable. Martina, thank you for your huge help at the very beginning including the list of shops and letting me know about the Woenselse Markt on Saturdays. Carla, thank you for being always so helpful with all the formal things and organization. Henk, thank you for making the best coffee in the world (even though I do not drink coffee at all) and making the common space a great place to spend breaks. You are a legend of MST and we will all miss you. Hans, ordering the chemicals (or checking why they would not arrive) with you was always an adventure! Now I would like to proceed to my 4-year long neighbor in the lab: Peter-Paul. Petro-Pablo, you are amazing guy with lots of humor and knowledge. I enjoyed all of clean and dirty jokes, music in Lab 3 and other events, including your great barbeque. You are the most unpleasant football opponent I played against. I still see you standing with a bucket held above the barbeque during the most intensive rain ever at the legendary barbeque party one Saturday in June 2016. I also want to thank my other neighbor, the Roermond-brother, Marcos. It could not have been an coincidence that we shared this great city between us. It was a short, but great time to have you there. I wish you all the best with Luiza in Terneuzen. Patri, you always added some Spanish spiciness to the events that you joined as a representative of Sijbesma group. Also thanks to Jo(dy), actually for just being yourself. Wouter, you are a great example on how big commitment to science can go along with social life. Maaike, it's surprising how small is the world of chemistry. I would meet you in Enschede one day to hear on another day in Eindhoven that *I think I know you*. Mrs Neus Fransen, you're wrong if you thought I would say nothing about you here. Thanks for all the events that we had before you sadly decided to quit MST for other job. Serge and Marcel, thanks for all the help and passion with the 500 MHz NMR machine. Anytime something would be not working, you had a ready solution. I learned a lot from you. Ralf, thanks for all the endless discussions about football and most likely most advanced analysis of specific football players skills. Timo, (even though not a MST-man), thanks for your help with setting up a high-pressure reaction that would eventually been a milestone in my research. Eventually, three chapters originate from a single reaction. I would like to thank the rest of the MST team: Luc, Maarten, René, Christian, Lech, Patricia, Margot, Jan, Lou, Joost, Paul, Dan Jing, Jingyi, Emma, Rodrigo, Antonio, Jurgen, Maarten, Olga, Pim, Glenn, Lenne, Bastiaan, Dario, Mike, Tonny, Tristan, Henk J, Eline, Eva-Magdalena, Eveline, Tom, Je, Annelore, Diederik.

I would like to spare a few words also to the supervisors of the student internships during my university course. First of all, thanks for dr Eugen Stulz, who would accept me as a summer student somewhere in 2011. At that time for me it was first contact with scientific research and laboratory work. Truly inspiring lesson of practical chemistry, which only encouraged me to follow studying organic chemistry. Practically I spent the time in the lab with dr. Gabriella Marth. Gaby, thanks for being so patient that after failing another column you would still help me out with setting up new one. Following summer I would spend in the group of dr. Fabrice Mathevet. It was a great experience to be there in Paris and exploit the field of organic liquid crystals. Since my stay in Paris I fell in love with triphenylenes and this thesis is an expression of this love. Therefore Fabrice, you deserve a special place in this hall of fame. I could not say anything about Yiming, a great chemist who was my tutor and hero in Paris. Thank you for teaching me a lot about chemistry and liquid crystals. Finally I could work more independently as a visiting student under supervision of Peter Jarowski. Peter, thank you for trusting me so much that you let me doing projects on my own while still being a master student. Thank you also for keeping me excited about

the science. I learned a lot from you and my stay at Surrey was another stimulating experience to decide to follow after the PhD. At Surrey my best labmate was Ranga. Ranga, you are a great man and I miss our common dinners and talking about the cultural differences between Poland and Sri Lanka. I wish you all the best with Dinisha and your great son.

Now we go to little bit more private matter. I will start therefore with my wróżki: paranymphs. Ik wil hartelijk mijn paranymfen bedanken. Gingi (officially known as Gijs), I remember you being frustrated at our first football game after getting another gat (canal, hole). Ever since you decided to play in a team with me. I miss our old Bier Professor Fridays and the game you never wanted to join. It was good to have you during a legendary move to Roermond. It is enough only to mention asocial behavior in the queue to Milieustraat. After moving to Roermond, your sofa was always opened for me. Thanks for all the other help you did for me since I started my life in the Netherlands including playing as somebody else for Pusphaira, for critical evaluation of batch (in)stability of home-brewed beer, for your efforts in making my Dutch communicative, for all humiliating wins in squash. Thanks for making sure I would join every weekend event. You did not change much even after becoming half-Belgian. I wish you the success in becoming CEO of Gingi&Gingi and of course a bright future with Ghislaine. Mathijs, our way of looking at and executing science is very different, which most likely was the key to the success of the whole story. You always come up with new ideas and solutions. It will remain to me a mistery, how one guy can do synthesis, measurements, calculations and even graphics and still do all of the things on time. I enjoyed our spontaneous Carnaval 2017, which would start from a hele haan from Woenselse Markt followed by watching the parade and visit at the Drinkers Pub. Thanks for organizing the legendary Stamppot 2019, a great example on how two people can feed twenty. Thanks for mediating once a great deal between your father and me. Thanks for being always proactive at any aspect. I will always remember our discussions on economy, politics and other things, where we would not agree – exactly like in science. I wish you a lot of the success with your further career and all the best with Maartje.

Obviously I missed a couple of people that are not mentioned so far. I put a separate section on the sports as sports is special part in my life. Therefore I want to thank all of the people connected with football and those who played with me for a couple of times including famous Nolte-Meijer cup. I want to thank coach Robasjo for trusting me and giving me an opportunity to score in the final Nolte-Meijer cup ever. One more time thanks to Petro-Pablo for being a tough guy on the field, even though soft in life. Gingino for being an example of typical Dutch football player: tall, strong with a good pass and shot, however with lack of high technical skills. Phil, you were a good player with potential, we could still make a serious player out of you. Thanks for all our games and for including me in the Chinese football team. Dylan, the Australian Beast, the name explains everything. I enjoyed our games, especially playing against you.

The other sport I would be involved is squash, where obviously we also had a small crew. I begin with my best coach and competitor – Romà. I enjoyed our games, some of them were quite even, others not really, yet the final result is little bit towards you. Besides squash, it was good to have a couple of tequilas with you and Marcos. I wish you success in your last months of the PhD and I am looking forward for your defense. Gingino, we had a bet that I would win something until the end of your PhD. Unluckily I have not made until the end of yours and most likely my PhD too, but that is mostly caused by you not showing up on the court for ages. Sjors, you were a strong opponent particularly difficult to play against in a physical style. Yet we had a couple of close duels with a lot of running and much less technique involved. Balu, you were one of my first true competitors. It was great to play against you as your style

was much smarter than mine. I wish you all the best back in India. Lorenzo, you are the most effective squash player I played against. It's good to have somebody to learn from.

Here we quit the university to acknowledge few people from Pusphaira. Most importantly, best coach and legend: Daan. Your passion in football and engagement was inspiring and made me to give 110% on the field. You deserve to go high as a coach and I hope you will achieve it. Rudy, thanks for being so strict coach. You put some professionalism in the very amateur team, which helped me to become better. I would like to thank a couple of people that made my first years in Eindhoven much easier so I would wait for each training or game. Stefano, you are a great defender, regardless of how many bad comments I would give on your play. Lorenzo, I never knew, where you get the energy from. Giorgio, what a memorable goal against Unitas! Alberto, I do not know other person with so many Inter Milan shirts. Edu, you are the best low-league striker ever. Matt, you did amazing job for the club (the P5 anthem). Hub, thanks for all the games together in the middle. Camiel, thanks for engaging me in the futsal team. The rest of Pusphaira: thanks for creating a fantastic environment to enjoy playing football.

The following parts will be dedicated to my Polish friends, therefore I switch now the languages. Zacznę od podziękowań wszystkim, którzy przyczynili się do mojej edukacji. Poczynając od mojej pierwszej wychowawczyni, Anny Binieckiej a dalej legendarny: Andrzej Pokrywa Elżnieta Jaruszewicz-Staniek, Agnieszka Zawalska-Lekszycka, kończąc na Krystynie Zapart – wszyscy mieliście wkład w to, kim dziś jestem. Pani Krystyna była zawsze dla mnie kimś więcej niż tylko szkolnym wychowawcą. Dziękuję za pomoc we wszystkich trudnych momentach, gdy błądziłem jako małolat. Chciałem również podziękować moim pierwszym nauczycielom chemii: Krystynie Mataczyńskiej i Agnieszce Twardowskiej za pokazanie mi, że chemia może być piękna. Dziękuję również mojemu pierwszemu naukowemu mentorowi: Nikodemowi Kuźnikowi. Nikodemie, zawsze imponowała i Twoja wiedza i cierpliwość. Wiele się od Ciebie nauczyłem, dziękuję Ci za to, że pewnego październikowego dnia w 2011 roku powiedziałeś *zrobimy z Pana chemika*. Dziękuję również promotorom mojej pracy magisterskiej: prof. Neugebauer i prof. Schab-Balcerzak. Dziękuję Marioli Siwy za pomoc w moich badaniach, które owego czasu uważałem za najważniejsze na świecie. Beata, dzięki za motywowanie mnie do działania wtedy, kiedy myślałem, że już nie będę próbował swoich sił w pracy naukowej. Dziękuję prof. Walczakowi za stworzenie możliwości studiowania na indywidualnym toku, co sprawiło, że rozpocząłem na dobre swoją przygodę z chemią organiczną.

Kolejnym ważnym etapem w moim życiu chemika była praca w drużynie Selvity. W tym miejscu szczególne podziękowania dla moich najlepszych towarzyszy z owego okresu: Siennix i Jacka. Szczególnie za nasze wszystkie najlepsze rowerowe wypady na Kraków, wliczając legendarną wycieczkę Kraków – Gierałtowice, podczas której odpadliście w Chrzanowie. Ala, dzięki za wszystkie rozmowy o sprawach ważnych i mniej ważnych. Dzięki za ugoszczenie mnie jednej nocy w najbardziej obskurnym domu w Karlsruhe. Dzięki za pokazanie mi, że nigdy nie chciałbym mieszkać w tym mieście. Jacek, dzięki za wszystkie chlorowypady i miłe słowe, Ty zawsze powiesz na mój temat coś pozytywnego. Powodzenia w byciu faryzeuszem. Tomku J, nigdy nie zapomnę naszych wyjazdów do miasta Łodzi. Z Tobą te wycieczki były zdecydowanie do przeżycia. Jeszcze bym kiedyś się chętnie tak przejechał. Życzę Ci wszystkiego dobrego razem z rodzinką! Dalej chciałbym wspomnieć o Katarzynach D i P, które niegdyś towarzyszyły mi w Krakowie a obecnie mieszkają na holenderskiej ziemii. Dobrze jest mieć Was blisko, powodzenia w dalszej karierze! Dziękuję również Uli B za to, że mogła podrzucić mnie do Krakowa z Katowic i dzięki temu została członkiem znanej grupy Ludzi Nieprzyzwoitych. Nie mogę nie wspomnieć również o twórcy pierwszego na świecie Korpo-czatu: Dżoana F. Aśka, dzięki za pozwolenie stworzenia mojej wersji Introna

na Twojej ścianie i oczywiście za słynny mikser (czy tam blender). Maciek, dzięki za wszystkie przejazdy na trasie Kraków – Gliwice przez fotoradar Bolęcin. Dziękuję również Dominice za pierwsze tygodnie i pomoc we wdrożeniu się w „standardy". Wypada wspomnieć o moim współlokatorze Dawidzie M i o wielu, którzy sprawili, że ten rok w Krakowie był niezapomniany: ekipa Novartis: Kasia C, Marta, Mateusz B, Damian i ekipa stary lab: Michał, Janek, Teresa, Rafał, Piotr, Mateusz M i Gosia. Nie mogę zapomnieć o ekipie Biznes Liga, gdzie najważniejsze role grali maestro Jacek G i Kamil vel Jodek Potasu. Dziękuję również Basi i Przemkowi za wszystkie lekcje z praktycznej chemii i wiele rozmów wykraczających poza chemię obejmującą nasze projekty.

Teraz kilka słów do moich przyjaciół i kolegów z czasów szkolnych i studenckich. Naturalnie zacznę od Mateusza vel Sielwana. Sielwan, dzięki za wszystko, co zrobiłeś. Zawsze mogłem na Ciebie liczyć, nieważne, czy były to sprawy małe, czy wielkie. Życzę Tobie i Emi wszystkiego najlepszego i żebyśmy mogli się widywać częściej, niż obecnie. Adi, niech Wam z Martą idzie jak najlepiej. Bobek, dzięki za wszystkie szopy na angielskim. Heniek, dzięki za zarażenie mnie pasją do rowerów. Mojemu towarzyszowi doktoranckiej niedoli na obczyźnie – Mateuszowi P życzę dalszych sukcesów w karierze i dużo szczęścia we wspólnym życiu z Lindą. Karolina znana jako Kocel, nie będę wspominał wszystkich imprez z Częstochowskiej, ale kto był, ten wie. Dzięki za wsparcie i wszytkiego dobrego z Leszkiem i Maksiem. Basia K, dzięki za wszystkie krokieciki i barszcz na naszych imprezach! Chomik, dzięki za współuczestniczenie we wszystkich przełomowych eksperymentach na chemii fizycznej i wkład w nasze wybitne sprawozdania. Piter, dzięki za wprowadzenie Bonkersa w nasze kręgi. Paweł, dzięki za najbardziej suche żarty obok moich na naszych imprezach. Dżeku, dzięki za pokazanie nam znaczenia imprezowych drzemek i niezapomnianą opowieść o nocnym wyjściu podczas pewnej imprezy na Konarskiego. Róża, nie wspomniałem o Tobie w poprzedniej części, bo należy Ci się specjalne miejsce tu. Pamiętam nasze pierwsze spotkanie w Eindhoven i moją zupełnie nieuzasadnioną niepewność. Zostałaś niemalże moją emigracyjną starszą siostrą. Nie zapomnę naszego „wyjścia na miasto" w Strasburgu. Miało być jedno piwko z Pawłem... Dzięki za wszystkie inne imprezy i za niezapomniany wypad na wspinaczkę. Życzę Ci powodzenia we Wrocławiu i wszystkiego dobrego razem z Dawidem i moimi najlepszymi chrześnicami! Nie mogę również pominąć mojego najlepszego współlokatora z Eindhoven – Mariusza. Mario, dzięki za te wszystkie wieczory przy Lidze Mistrzów i Johnie Tafferze. Zawsze, jak człowiek nie wiedział, co ze sobą zrobić, bo nie było treningu, mógł przyjść do salonu i tam się działo! Nigdy nie zapomnę Ciebie rozkręcającego moją domówkę. Wśród moich holenderskich znajomych jesteś legendą. Dzięki za to, że życie na obczyźnie nie było nudne i życzę Wam z Aśką wszystkiego dobrego na nowej drodze! Dziękuję również pozostałym poniżej wymienionym za wszystkie niezapomniane wyjścia i imprezy: Boczek, Feist, Smolu, Mela, Mati, Bartosz G.

Teraz przejdę do mojej rodziny. Dziękuję moim babciom: Krystynie i Hannie za opiekę i miłość, którą mnie jako wnuka obdarzyły. Pamiętam wszystkie opowieści, którym przysłuchiwałem się jako kilkuletnie dziecko. Dziękuję również najlepszej cioci na świecie – Tereni. Dziękuję za pomoc, gdy zostawałem bez dachu nad głową i najlepsze niedzelne obiady. Dziękuję za wszystkie bezpośrednie pytania, kiedy w końcu się ożenię. To już niedługo! Adamie, dzięki za wszystkie nasze partie w Siatkonogę i Naparzankę. W tym sporcie jesteśmy jak Messi i Ronaldo – nie można określić, kto jest lepszy. Dzięki też za najlepsze wypady na Mazowiecką w Wawce. Artur i Michał, dzięki Panowie za bycie czlonkami najmniej sportowej grupy rozmawiającej o sporcie. Dziękuję wujkowi Darkowi i cioci Oli za gościnność i wszystkie długie wieczory przy kominku, bądź grillu, kiedy Was odwiedzałem. Dziękuję również całej Pruszkowskiej ekipie za wszystkie śmieszne piwka, grille i wiele innych: Julia, Maciek, Kubuś, Agata, Witek, Zuzia i Bartek. Dziękuję również Warszawskiej części rodziny: Grażyna, Janusz, Artur, Kasia, Marcin i Gabryś. Dziękuję również mojej mamie chrzestnej – cioci Asi, razem z mężem Heńkiem i dziećmi: Wiktorią i Łukaszem. Specjalne słowa

należą się również cioci Krysi za wszystkie niezapomniane wakacje i wycieczki rowerowe. Niesamowite, że ciocia znalazla zawsze w sobie tyle energii, by wyjść z młodym (mną) na rower. Podziękowania kieruję również do moich przyszłych teściów – Asi i Mirka. Dziękuję za zaufanie, dzięki Wam szybko poczułem się jak członek rodziny. Nie zapominam również o niezliczonej ilości obiadów i innej pomocy, którą od Was przez te lata otrzymałem. Na koniec paragrafu zostawiłem najlepszą szwagierkę na świecie – Ewelinę. Mógłbym dziękować za wiele, ale tu podkreślę tylko Twój wkład w wybór rozmiaru pierścionka. A, że nie na ten palec był mierzony, to już inna historia. Życzę Wam szczęścia razem z Radziem i nie mogę doczekać się bycia wujkiem.

Zbliżając się do końca: Piotrek, jakiś sposobem zostałeś pierwszym fanem mojej pracy i moim najważniejszym naukowym partnerem. Mam nadzieję, że będziesz kontynuował swoją pracę z sukcesami, osiągniesz naukowe cele i rozsławisz nasze nazwisko na cały świat. Wierzę, że razem możemy jeszcze wiele zdziałać. Jesteś najlepszym starszym bratem, jakiego można sobie wyobrazić. Za bajtla broniłeś mnie przed innymi i byłeś moim pierwszym trenerem. Dzięki Tobie dostałem jedno jedyne powołanie do kadry U-6 przez Dariusza Dziekanowskiego. Życzę Tobie i Ani wszystkiego dobrego. Przedostatnie słowa kieruję do moich rodziców: Mamo, Tato, dziękuję Wam za wszystko, co zrobiliście. Dziękuję za wsparcie przez te lata i za pomoc. Bez Was, bez Waszej pomocy i motywacji ta praca by nigdy nie powstała. Dziękuję za to, że byliście przy mnie i za cały wkład w wychowanie mnie, bym został jak najlepszym człowiekiem. Ta praca jest tak Waszą zasługą, jak moją. Kocham Was!

Podziękowania zamknę oczywiście kierując specjalne słowa do mojej przyszłej żony – Mileny. Znamy się tyle lat, a Ty i tak codziennie mnie zaskakujesz. Wiele razem przeszliśmy, a to przecież ciągle początek naszego wspólnego życia. Dziękuję za to, że jesteś ze mną każdego dnia, za to, że jesteś moim najlepszym przyjacielem. Dziękuję Ci, że obdarzyłaś mnie zaufaniem i zdecydowałaś się przyjechać ze mną do Holandii. Dziękuję Ci za to, że mogłem liczyć na Twoje wsparcie i zrozumienie, pomimo wszystkiego, co wydarzyło się przez te lata. Dziękuję Ci za to, że nie miałaś pretensji o moje długie wieczory w pracy (lub poza). Dziękuję za rzeczy małe i wielkie, które razem stworzyliśmy. Dziękuję Ci za wszystkie wycieczki i wspomnienia i tak mógłbym dziękować bez końca. Życzę Ci powodzenia w spełnieniu swoich marzeń i ukończeniu doktoratu. Nie mogę się doczekać rozpoczęcia nowego etapu w naszym życiu i jestem niezmiernie szczęśliwy, że zostaniesz moją żoną. Wiem, że razem zestarzejemy się szczęśliwie i wychowamy wspaniałe dzieci, a następnie doczekamy się wnuków. Kocham Cię. Twój na zawsze Marcin.